Exploring The Receptor, Self Assembly and Photophysical Properties of Mono Formyl 5,5-Dialkyldipyrromethane Based *Cyclic* and *Acyclic* Derivatives

THESIS SUBMITTED TO
THE UNIVERSITY OF KERALA
FOR THE DEGREE OF
DOCTOR OF PHILOSOPHY
IN CHEMISTRY
UNDER THE FACULTY OF SCIENCE

BY

DERRY HOLADAY M. G.

PHOTOSCIENCES AND PHOTONICS SECTION
CHEMICAL SCIENCES AND TECHNOLOGY DIVISION
NATIONAL INSTITUTE FOR INTERDISCIPLINARY SCIENCE AND TECHNOLOGY (NIIST-CSIR), TRIVANDRUM – 695 019
KERALA, INDIA

2015

DECLARATION

I hereby declare that the Ph.D. thesis entitled "**Exploring the Receptor, Self Assembly and Photophysical Properties of Mono Formyl 5,5-Dialkyldipyrromethane Based Cyclic and Acyclic Derivatives**" is an independent work carried out by me at the Photosciences and Photonics Section, Chemical Sciences and Technology Division, National Institute for Interdisciplinary Science and Technology (NIIST-CSIR), Trivandrum, under the supervision of Dr. A. Srinivasan and Dr. M. L. P. Reddy and it has not been submitted elsewhere for any other degree, diploma or title. In keeping with the general practice of reporting scientific observations, due acknowledgement has been made wherever the work described is based on the findings of other investigators.

(Derry Holaday M. G.)

राष्ट्रीय अंतर्विषयी विज्ञान तथा प्रौद्योगिकी संस्थान
(वैज्ञानिक एंव प्रौद्योगिकी अनुसंधान परिषद्)
(पहले क्षेत्रीय अनुसंधान प्रयोगशाला)
NATIONAL INSTITUTE FOR INTERDISCIPLINARY SCIENCE AND TECHNOLOGY
(Council of Scientific & Industrial Research)
(formerly Regional Research laboratory)
इन्डस्ट्रियल इस्टेट डाक घर, तिरुवनन्तपुरम 695 019, भारत
Industrial Estate P.O., Thiruvananthapuram 695 019, India
आई एस ओ 9001 प्रमाणित
ISO 9001 CERTIFIED
MGMT. SYS. RvA C 024
DNV Certification B.V., The Netherlands

December, 01, 2015

CERTIFICATE

This is to certify that the work embodied in the thesis entitled **"Exploring the Receptor, Self Assembly and Photophysical Properties of Mono Formyl 5,5-Dialkyldipyrromethane Based Cyclic and Acyclic Derivatives"** has been carried out by **Mrs. Derry Holaday M. G.** under our supervision and guidance at the Photosciences and Photonics Section, Chemical Sciences and Technology Division, National Institute for Interdisciplinary Science and Technology (NIIST-CSIR), Trivandrum and the same has not been submitted elsewhere for a degree.

Dr. A. Srinivasan
(Thesis Supervisor)

Dr. M. L. P. Reddy
(Co-Guide)

ACKNOWLEDGEMENTS

I have great pleasure in placing on record my deep sense of gratitude to Dr. A. Srinivasan, my research supervisor, for suggesting the research problem and all his guidance support, encouragement and timely advice throughout the course of this work.

It is with immense pleasure I express my gratitude to Dr. M. L. P. Reddy, for his encouragement, discussions and support throughout the course of this work.

I thank Dr. A. Ajayaghosh, Director, NIIST-CSIR and former directors, Prof. T. K. Chandrashekar, Dr. B. C. Pai, and Dr. Suresh Das for providing me the laboratory facilities to carry out this research work.

My sincere thanks are due to:

- *Dr. K. R. Gopidas, Dr. D. Ramaiah, Dr. K. George Thomas and all the present and former Scientists of Photosciences and Photonics Section for the suggestions and discussions.*
- *Dr. Babu Varghese, IIT-Chennai, Dr. Arun Kumar, NISER-Bhubaneswar & Dr. C. H. Suresh, NIIST-Trivandrum, for their fruitful help in carrying out the single crystal X-ray structural analysis & theoretical studies.*
- *The Director and the faculty members, School of Chemical Sciences, NISER Bhubaneswar for all their help and providing me the infrastructure and facilities.*
- *Dr. S. Ramakrishnan, Dr. K. S. Anju, Dr. Ajesh P. Thomas, Dr. Gowri Sreedevi, Dr. Salini P. S, Mr. R. Sabarinathan, Mr. Gourav Tarafdar, Mr. B. Adinarayana, and all the former and present members of Photosciences and Photonics Section and chemical sciences and technology division NIIST-Trivandrum and Friends at NISER Bhubaneswar for their co-operation and timely help..*

- *Mr. Robert Philip, Mr. M. Kiran, Mr. C. Chandran, Mrs. Viji, Mrs. Soumini and Mr. Adarsh for morphological and spectral analyses.*
- *All my teachers and friends and family for their support, love and care, especially Dr. Mahesh Hariharan for helping me start my research career.*
- *I thank the entire Staff's and Faculty members of St. Teresa's College, Ernakulam, for all their love. support, and motivation especially Rev. Dr. Sr. Teresa, Rev. Dr. Sr. Vinitha, Dr. Sajimol Augustine, Dr. Geetha Andrews, Dr Ushamani M., Dr. Anu Gopinath, Dr. Saritha Chandran, Smt. Anitta Antony. Smt. Mary Lincy K. A., Smt. Divya Thomas, Dr. Navya Antony.*
- *Finally 'Jerly Sir' whom I consider my 'Gurunathan', who taught me how to love chemistry, how to be humble and passionate in life and who is my constant inspiration.*

- *CSIR, UGC and DST are highly acknowledged for the financial support.*

Above all I thank God Almighty for showering his blessings on me

Derry Holaday M. G.

Contents

List of Tables

List of figures

List of Abbreviations

AIEE	aggregation induced emission enhancement
$BF_3.OEt_2$	borontrifluoride diethyletherate
CCD	cambridge crystallographic data
CD_2Cl_2	deuterated dichloromethane
$CDCl_3$	deuterated chloroform
FAB	fast atom bombardment
FON	fluorescent organic nano particle
FT-IR	fourier transformation infra-red
NMR	nuclear magnetic resonance
TBAF	tetrabutylammoniumfluoride
TFA	trifluoroacetic acid
TLC	thin layer chromatography
TMS	tetramethylsilane
UV	ultraviolet
DSB	dragonesque Schiff base
IMR	intramolecular rotation

PREFACE

Pyrrolic supramolecular self-assemblies with cyclic and acyclic structure are of wide interest in several areas, namely in porphyrins and related macrocycles, materials, catalysis and medicine. Pyrrole exhibits a "duality" of its nitrogen moiety, as it can behave as both a hydrogen-bonding acceptor, or a metal-coordination ligand, due to the

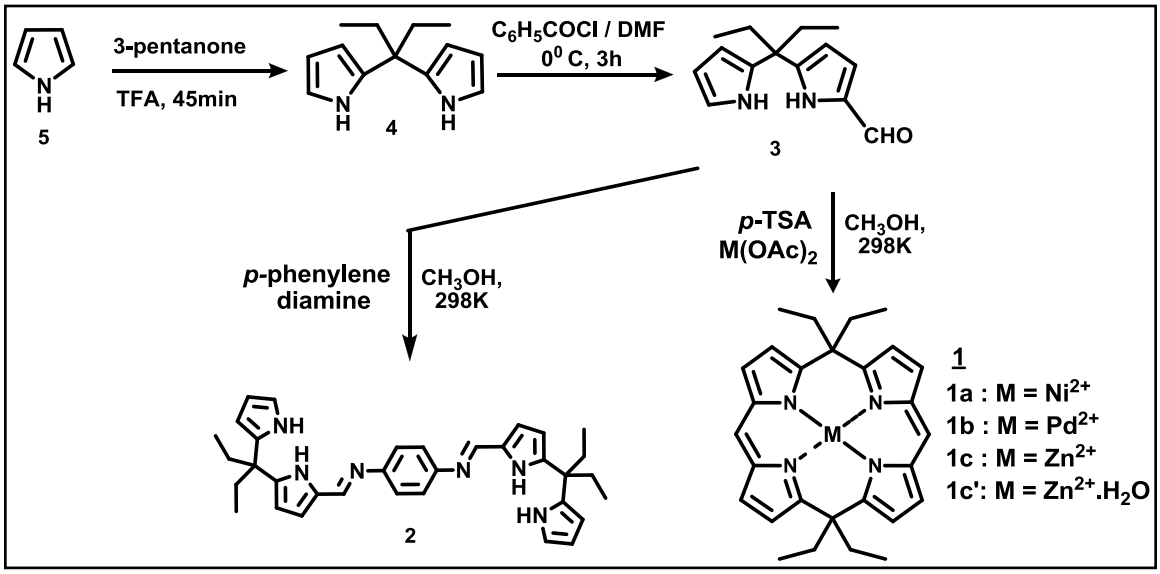

N site and a hydrogen-bonding donor due to the NH site. The main objective of our work is to study the applications of mono formyl 5,5-diethyldipyrromethane as a versatile precursor to synthesize acyclic as well as macrocyclic derivatives and explore their structural, photophysical and receptor properties.

The present thesis has been divided into four chapters. In the first chapter, a detailed literature review of dipyrromethanes and their potential applications is discussed. In the second chapter, we have demonstrated the acid-catalyzed condensation of 3-pentanone with excess of pyrrole to afford diethyldipyrromethanes (**4**), which upon Clezy-modified Vilsmeier-Haack formylation yielded mono formyl 5,5-diethyldipyrromethane (**3**). The precursor **3** was used further for the synthesis of macrocycle **1**. The synthetic methodology adopted for the synthesis of **1** is simple metal

template strategy. The synthetic route includes acid-catalyzed condensation reaction of dipyrromethane mono aldehyde in presence of metal acetates of palladium, nickel and zinc in methanol medium. The newly synthesized calixphyrin metal complexes **1a**, **1b**, **1c** and **1c′** were characterized by NMR, electronic spectral analyses and finally confirmed by X-ray single crystal analysis. The studies are mainly focused on non covalent interactions such as hydrogen bonding and anagostic interactions using 5,15-porphodimethene metal complexes as platform. The rare case of **M...H-C** anagaostic interaction is well demonstrated by variable temperature NMR spectral studies and further confirmed by single crystal X-ray analysis. Furthermore, the extra coordinated water molecule in one of the metal complexes converts the roof like conformer to planar form which is hitherto unknown in the calixphyrin metal complexes. Overall, the anagostic interactions lead to distortion, while the hydrogen bonding interaction generates dimerisation as well as array formation. (These results are published in *Dalton Trans.***2014**, *43*, 7699.

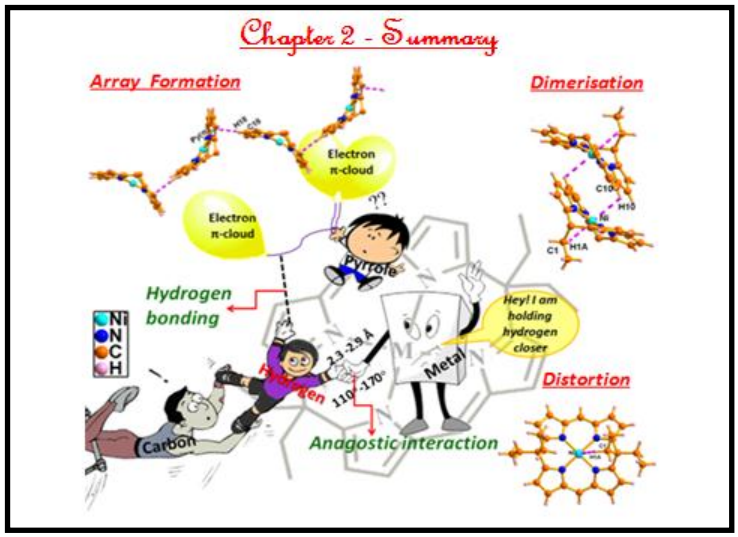

The third chapter describes two important observations; in the first part, we highlight the polymorphic nature of 5,15-porphodimethene Pd(II) complex (**1b**) and in the second part, we describe, how this complex might be used as a chemodosimetric sensor. Two polymorphs of the mentioned complex are obtained by different polar solvents and are further confirmed by single crystal X-ray analysis. The receptor properties are carried out with various anions and showed a selective affinity towards

cyanide ion. Excellent selectivity was observed even in the presence of 100 equiv. of other potentially interfering anions. We have also successfully demonstrated that the cyanide ion binds selectively at the *meso*-position of the calixphyrin skeleton and justified the chemodosimetric sensor property of the mentioned complex. To the best of our knowledge such type of cyano adduct formation is hitherto unknown in the calixphyrin chemistry and paves a new methodology for the synthesis of functionalized unsymmetrical porphomethenes and calixpyrroles (These results are published in *Chem. Commun.* **2014**, *50*, 10834).

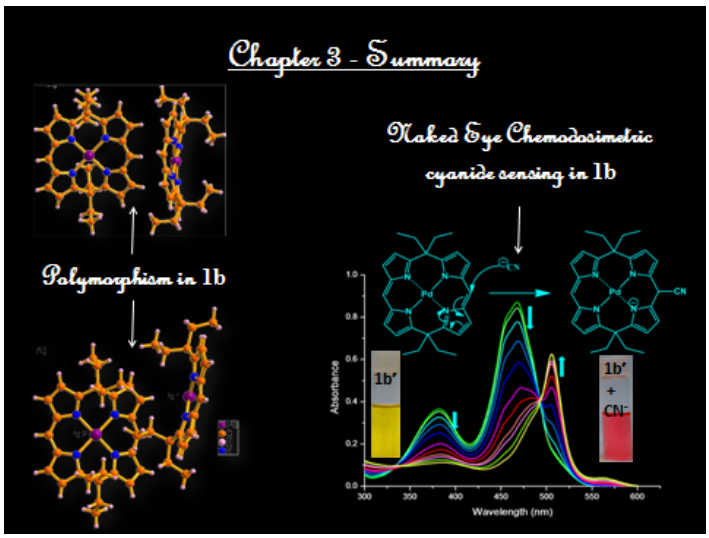

The fourth chapter deals with synthesis of acyclic compound **2** from the precursor **3**. This part mainly describes a detailed study of the aggregation induced emission enhancement (AIEE), Zn^{2+} sensing property and luminescence mechanochromic nature of '*double headed dragon*' shaped acyclic Dragonesque Schiff base (**DSB**). One pot Schiff base condensation reaction of 1-formyl-5,5-di(ethyl)dipyrromethane (**3**) with *p*-phenylenediamine in methanol at room temperature generated yellow colored ditopic dragonesque shaped ligand **DSB** in high yields. The Schiff base receptor **DSB** is soluble in common organic solvents but insoluble in water. The compound **DSB** is found to exhibit an enhanced emission in the presence of high water concentration and the aggregates form fluorescent microspheres. The molecule **DSB** selectively senses the Zn^{2+} in acetonitrile solution exhibiting 135 fold 'Turn – On' emission and also generates nano particles of different morphology depending upon the concentration of Zn^{2+} ions. At

lower concentration of Zn^{2+}, **DSB** forms greenish yellow fluorescent fibre like structures of 2:1 complexes. Increasing the concentration of Zn^{2+} ions, **DSB** forms non fluorescent, red 2:2 complexes with nano sphere like morphology. The aggregation properties and sensing studies with Zn^{2+} ion are in turn an inevitable consequence of restricted intramolecular rotation (IMR) due to intermolecular H-bonding interaction.

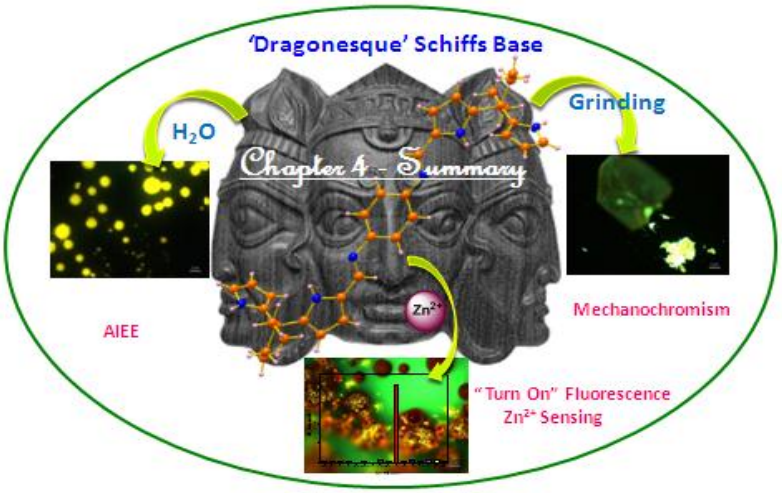

Finally, a thorough investigation of the colour and luminescence properties of the **DSB** crystal in response to mechanical stimuli revealed that **DSB** shows grinding induced luminescence mechanochromism and it reverts back to its initial state on heating or recrystallization. Thus, **DSB** is a typical '*trimurthy*' type molecule showing three characteristic properties such as AIEE, Zn^{2+} sensing and luminescence mechanochromism by single molecule, a consequence of noncovalent molecular interactions in the crystalline, amorphous and solution states.

Dedicated to Mummy, Daddy, Berry, Chettan

And

My little Aksharah

Chapter 1

Dipyrromethanes as Precursors

1.1 Introduction

Nature is the best known architect who perfected her art through millions of years of evolution by discarding the failed design, improving the worked ones and creating the new ones. Among the millions of her designs, 'Pyrrole' a π conjugated aromatic heterocyclic molecule, is a constituent of the structural skeleton of several biotic dyes like heme and chlorophyll. Porphyrins referred to as *pigments of life*, is one among the many well-crafted design responsible for the known life in this planet [Battersby *et al.* 1980; Krautler *et al.* 1987].

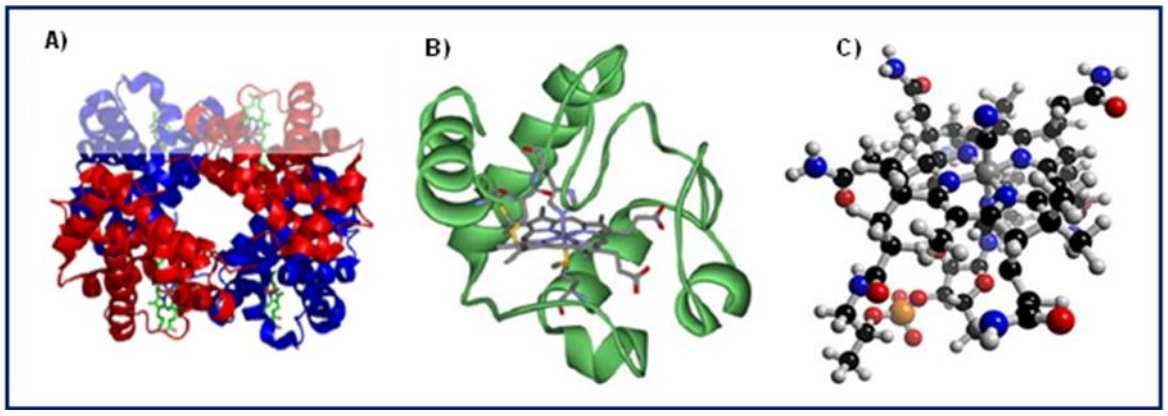

Figure 1.1 Structures of A) haemoglobin, B) cytochrome c both containing iron complexes of protoporphyrin C) vitamin B12 based on a corrin structure.

Polypyrrolic compounds are of wide interest in several areas, namely in porphyrins and related macrocycles, materials, catalysis and medicine [Tanaka *et al.* 2015, Hayashi *et al.* 2002, Polo *et al*. 2000; Rubio *et al*. 2005]. Pyrrole exhibits a "duality" of its nitrogen moiety, as it can behave as both a hydrogen-bonding acceptor, or a metal-coordination ligand, due to the N site and a hydrogen-bonding donor due to the NH site. The π-planes of the pyrrole unit

also enable effective interactions that yield stacking assemblies. Therefore, pyrrole rings can act as potential building subunits to form supramolecular architectures. To date, considerable efforts have been devoted to the development of artificial acetate and carboxylate receptors and carriers, and various binding motifs have been synthesized. Among the various artificial host molecules reported to date, macrocycles consisting of pyrroles are particularly attractive [Caltagirone *et al.* 2009].

Pyrrole is an important biologically active scaffold which possesses diverse nature of activities. Pyrrole derivatives with various pharmacophores are known to have many medicinal applications like anxiolytic, anti-cancer, anti-bacterial, anti-fungal, anti protozoal, anti-malarial etc. Pyrrole and its derivatives are ever present in nature. Pyrrole subunit has

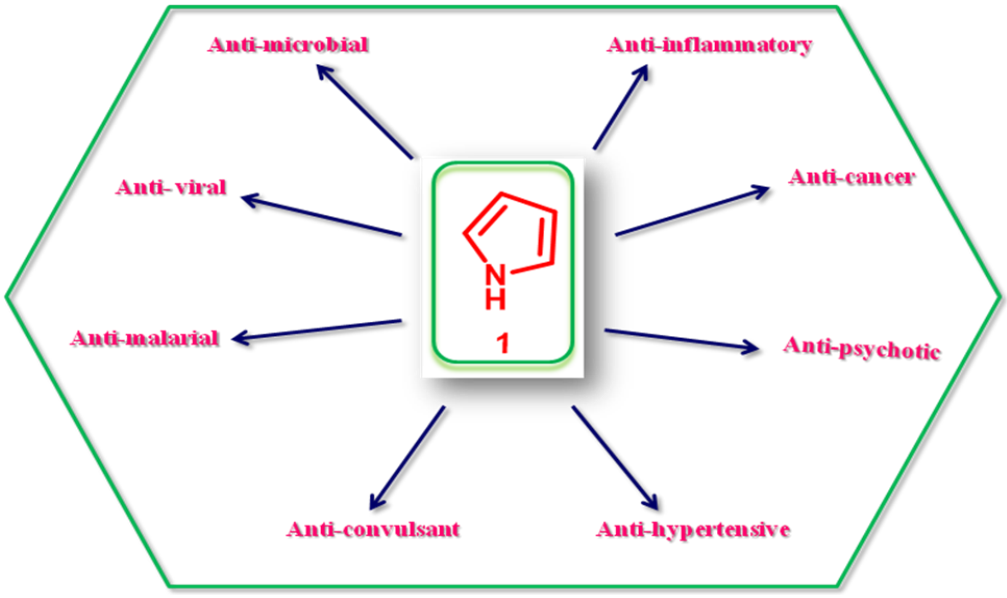

Figure 1.2 Therapeutic applications of pyrrolic compounds (Adapted from the reference Bhardwaj *et al*. 2015).

diverse applications in therapeutically active compounds including fungicides, antibiotics, cholesterol reducing drugs, antitumor agents and many more. They are known to inhibit reverse transcriptase [human immunodeficiency virus type 1 (HIV-1)] and cellular DNA polymerases protein kinases. Moreover, they are also a component of polymers, indigoid dyes and of larger aromatic rings. In catalytic reactions, pyrroles are well utilized as catalyst

for polymerization process, corrosion inhibitor, preservative, solvent for resin, terpenes, in metallurgical process, transition metal complex catalyst chemistry for uniform polymerization, luminescence chemistry and spectrochemical analysis. Furthermore, some of these compounds are useful intermediates in the synthesis of biologically important naturally occurring alkaloids and synthetic heterocyclic derivatives [Bhardwaj *et al.* 2015].

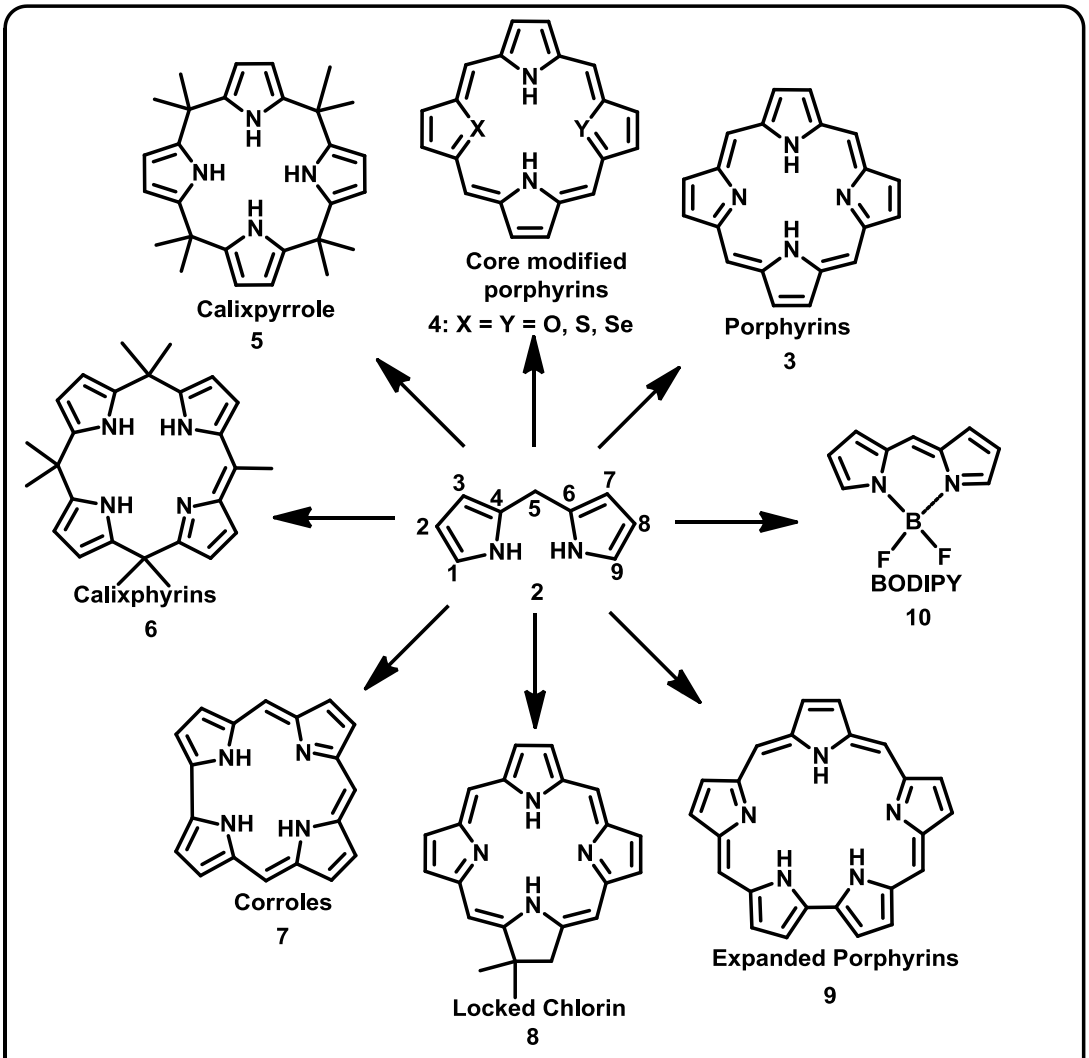

Chart 1.1 Dipyrromethanes as important precursors

Pyrrole based precursor, such as Dipyrromethanes (**2**) or dipyrranes are important building block for the syntheses of porphyrins and related compounds. It was introduced for the direct synthesis of tetraphenyl porphyrins (**3**) in 1960 [Shinohara *et al*. 1960; Woodward 1960]. Since then, it has been widely explored in the development of various synthetic core-

modified porphyrins (**4**), calixpyrrole (**5**), calixphyrins (**6**), corrole (**7**), chlorin (**8**), sapphyrin (**9**), BODIPY (**10**), etc (Chart 1.1). These are widely used as, anion, cation and neutral substrate receptors, Magnetic Resonance Imaging (MRI) contrast agents, Photodynamic therapeutic (PDT) agents, Non-linear Optical (NLO) materials etc [Wagner *et al.*1996; Jasat *et al*. 1997; Gale *et al.* 2001].

1.2 Structure and classification of dipyrromethanes

Dipyrromethanes are derivatives of methane in which two hydrogens are replaced by pyrrole rings. According to the common convention, the carbon atoms are numbered from one end to the other from 1 to 9 as shown in the Chart 1.1., where Carbon atoms 1 and 9 are referred as α-carbons, whereas 2, 3, 7 and 8 positions are referred as β-positions. The term *meso* is used to designate the bridging methyl carbon that separates the heterocyclic constituents.

Dipyrromethanes are classified broadly into four major divisions which include

(a) both β and *meso*-unsubstituted dipyrromethanes **2**,

(b) both β and *meso*-substituted dipyrromethanes **11**,

(c) β-substituted dipyrromethanes **12**,

(d) *meso*-substituted dipyrromethanes, **13** (Chart 1.2).

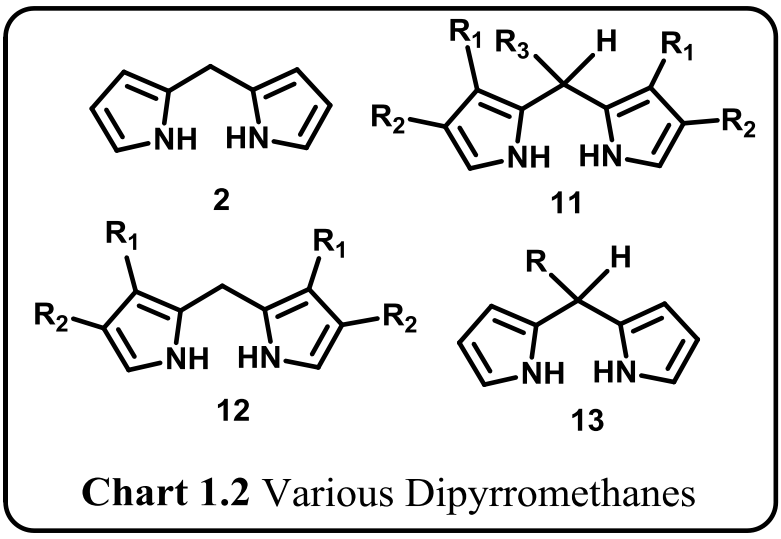

Chart 1.2 Various Dipyrromethanes

1.3 Synthetic Methods

1.3.1 Both *β* and *meso*-unsubstituted Dipyrromethanes (2)

The *β* and *meso*-unsubstituted dipyrromethanes were synthesized in 1969 by Clezy by a three-step procedure starting from pyrrole and thiophosgene with an yield of 40% [Clezy and Smythe 1969; Chong *et al.* 1969]. In 1995, Wang and Bruce reported one-step synthesis of **2** by the condensation of pyrrole with paraformaldehyde in methanol using acetic acid as catalyst at room temperature under nitrogen with 41% yield as shown in Scheme 1.1 [Wang and Bruce 1995].

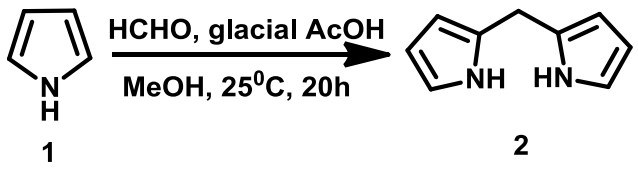

1 2

Scheme 1.1 *β* and *meso*-unsubstituted dipyrromethanes

1.3.2 Both *β* and *meso*-substituted Dipyrromethanes (11)

This dipyrromethanes are used for the synthesis of *β*-substituted porphyrins and related compounds. *β*-substituted dipyrromethanes are of two types, symmetrically substituted or unsymetrically substituted dipyrromethanes. *β*-symmetrical dipyrromethanes bearing substituent at *meso*-carbon was synthesised by the condensation of two equivalents of monopyrrole with an aryl aldehyde such as benzaldehyde **11a** (Scheme 1.2) in good yield [Fisher and Orth 1934]. Lee and co-worker's under similar reaction conditions by changing the aryl aldehydes to dimethyl acetals of aliphatic aldehydes provided **11b** in 60% yield (Scheme 1.2) [Lee and Smith 1997]. The unsymmetrical dipyrromethanes (**11c – 11g**) were prepared by the condensation of pyrrole derivatives onto N-benzylhydroxylamines in the presence of HCl in 60-70% yield [Murat-Onana *et al.* 2010].

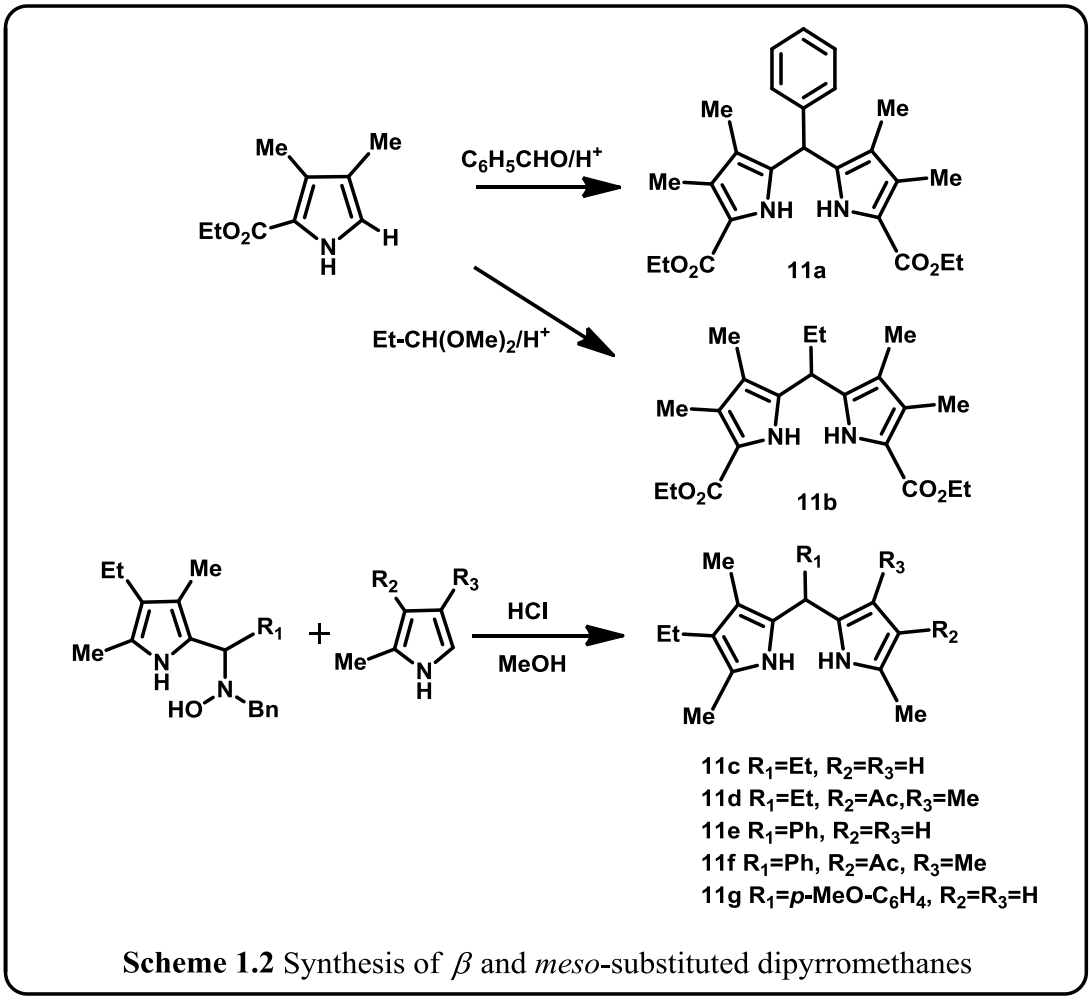

Scheme 1.2 Synthesis of β and *meso*-substituted dipyrromethanes

1.3.3 β-substituted Dipyrromethanes (12)

The β-substituted dipyrromethanes are also classified into two types with respect to meso carbon, such as symmetrical and unsymmetrical substituted derivatives. In 1973, Cavaleiro and co-workers synthesized β-substituted unsymmetrical dipyrromethanes by the condensation between 2-acetoxymethyl substituted pyrroles and 2-unsubstituted pyrroles in methanol or acetic acid to afford **12a** in 75% yield (Scheme 1.3) [Cavaleiro *et al.* 1973]. Pyridinium salts of 2-bromomethylpyrroles react with lithium salts of pyrrole-2-carbamide in polar solvents at 100°C to give **12b** in 40% yield [Hayes *et al.* 1958; Jackson *et al.* 1965]. **12c** can be readily prepared by heating 2-acetoxymethyl pyrrole in methanol-hydrochloric acid

mixture, similarly **12d** was prepared from 2-unsubstituted pyrroles on treatment with formaldehyde.

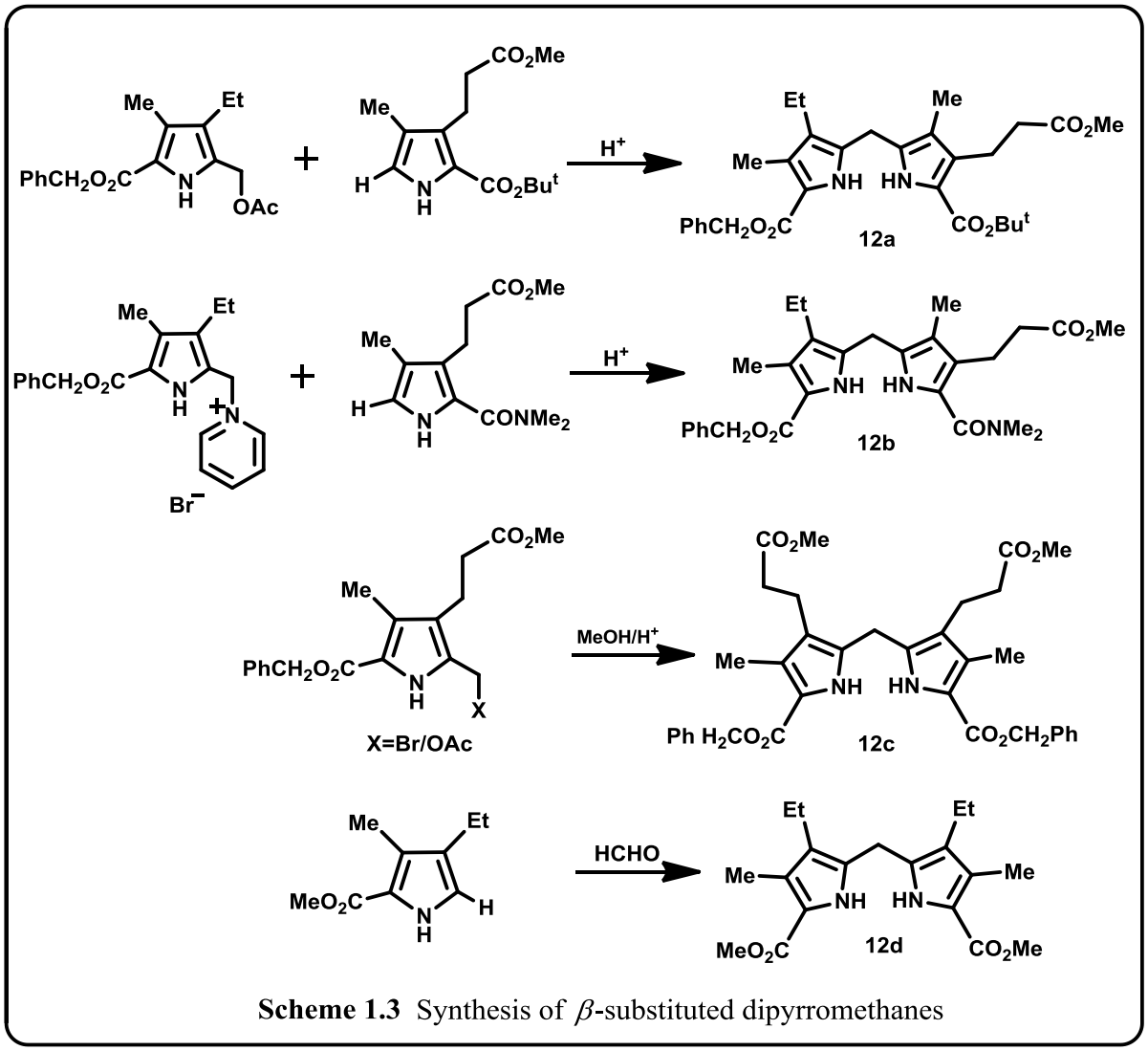

Scheme 1.3 Synthesis of β-substituted dipyrromethanes

1.3.4 *meso*-substituted dipyrromethanes (13)

The first *meso*-substituted dipyrromethanes such as pyridyl substituted dipyrromethane **13a** was synthesised by Ashley *et al.* in 1974 by the reaction of pyridine-4-carboxaldehyde with pyrrole in methanol with hydrochloric acid as a catalyst in 70% yield (Scheme 1.4) [Nagarkatti and Ashley 1974]. Later, several groups modified this procedure by varying the combination of acids and solvents [Casiraghi *et al.* 1992; Hammel *et al.* 1992] (Scheme 1.4). Important problems associated with the synthesis of *meso* substituted

dipyrromethanes were pyrrole trimer formation, scrambling, formation of N-confused dipyrromethanes etc. The synthetic procedure reported by C.-H. Lee and J. Lindsey in 1994

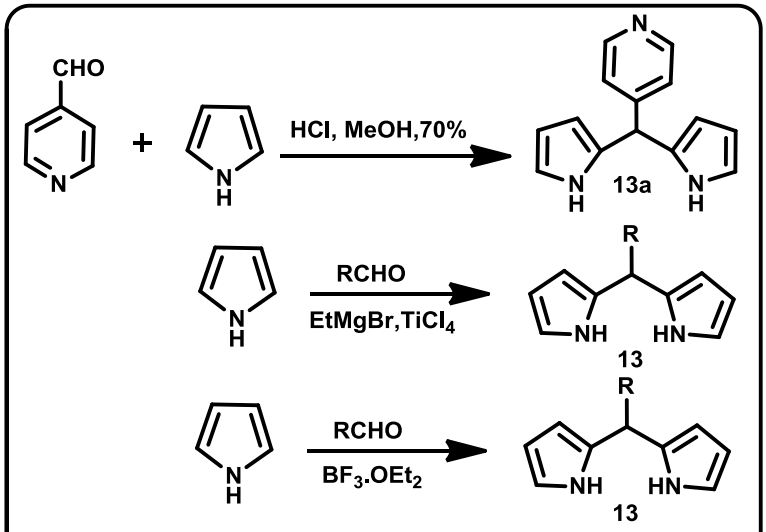

Scheme 1.4 *meso*-substituted dipyrromethanes

became a standard method for the preparation of 5-substituted dipyrromethanes bearing various functional groups. Here, an aryl aldehyde was dissolved in 40-fold excess of pyrrole with a catalytic amount of an acid at room temperature in the absence of any other solvent to avoid the formation of oligopyrromethanes (Scheme 1.5) [Lee and Lindsey 1994].

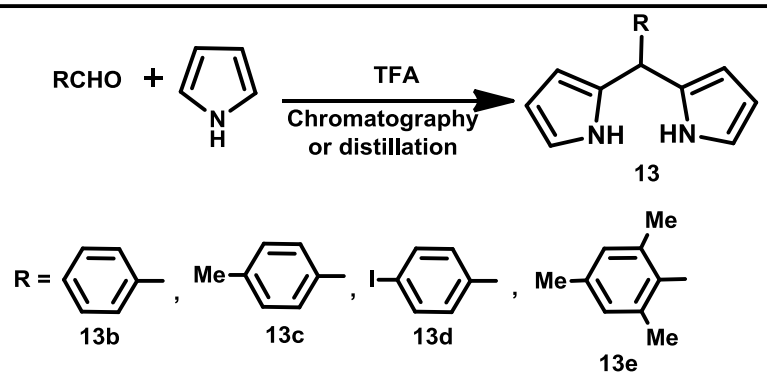

Scheme 1.5 Synthesis of *meso*-aryl dipyrromethanes from aryl aldehydes

Meso-dipyrromethanes were also prepared by other approaches including (i) reaction of pyrrole with cyclic vinyl ether and indium bromide [Yadav *et al.* 2003], (ii) reaction of

pyrrole-2-carboxaldehyde with diethyl malonate, followed by Michael-type nucleophilic addition of pyrrole in excess in presence of TFA (Scheme 1.6) [Hong *et al.* 2004], (iii) dipyrromethanes by the reaction of pyrrole, with alkynes in the presence of indium triflate [Tsuchimoto *et al.* 2003].*Meso*-diaryldipyrromethanes synthesis were well established by Eichen and co-workers where pyrrole and the ketone are mixed in an ethanol medium in 2:1 ratio in the presence of $BF_3.OEt_2$ as an acid-catalyst for a week to afford the corresponding dipyrromethanes in 15% yield [Turner *et al*. 1998]. Sreedevi and co-workers demonstrated novel two-step syntheses of *meso*-diaryldipyrromethanes **13f** from diaryl pyrrole-2-carbinols [Sreedevi *et al*. 2011]. They carried out nucleophilic addition of Grignard reagent of interest to the pyrrole-2-ester, followed by the acid catalysed condensation of these pyrrole carbinols with pyrrole yielded diaryldipyrromethane **13f** in short reaction time with good yield (Scheme 1.6).

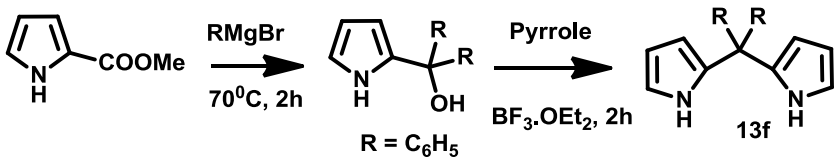

Scheme 1.6 Syntheses of diaryldipyrromethanes

1.4 Functionalisation of Dipyrromethanes

1.4.1 Acyclic dipyrromethane derivatives

The unsubstituted dipyrromethanes are unstable and undergo several side reactions like oxidation; reduction etc. therefore adequate substituents in the pyrrole rings can provide stability to the dipyrromethane precursors. Many electrophilic substitution reactions like nitration, bromination or sulfonation, with dipyrromethanes are difficult because they readily get oxidized or decomposed. Reactions such as the Mannich reaction (**14**) [Fan *et al.* 2005], the Vilsmeier reaction (**15**) [Gryko *et al.* 2003; Ptaszek *et al.* 2006], addition to electron-poor heterocycles (**16**) [Gryko and Voloshchuk 2009] etc. are possible due to high electron density

of the pyrrole unit. Recently, Dolphin and co-workers reported that it is possible to perform reaction of 5-arylsubstituted dipyrromethanes with diazonium salts to generate bis-1,9-diazodipyrromethanes (**17**) [Li and Dolphin 2011]. For selective mono-acylation, the method

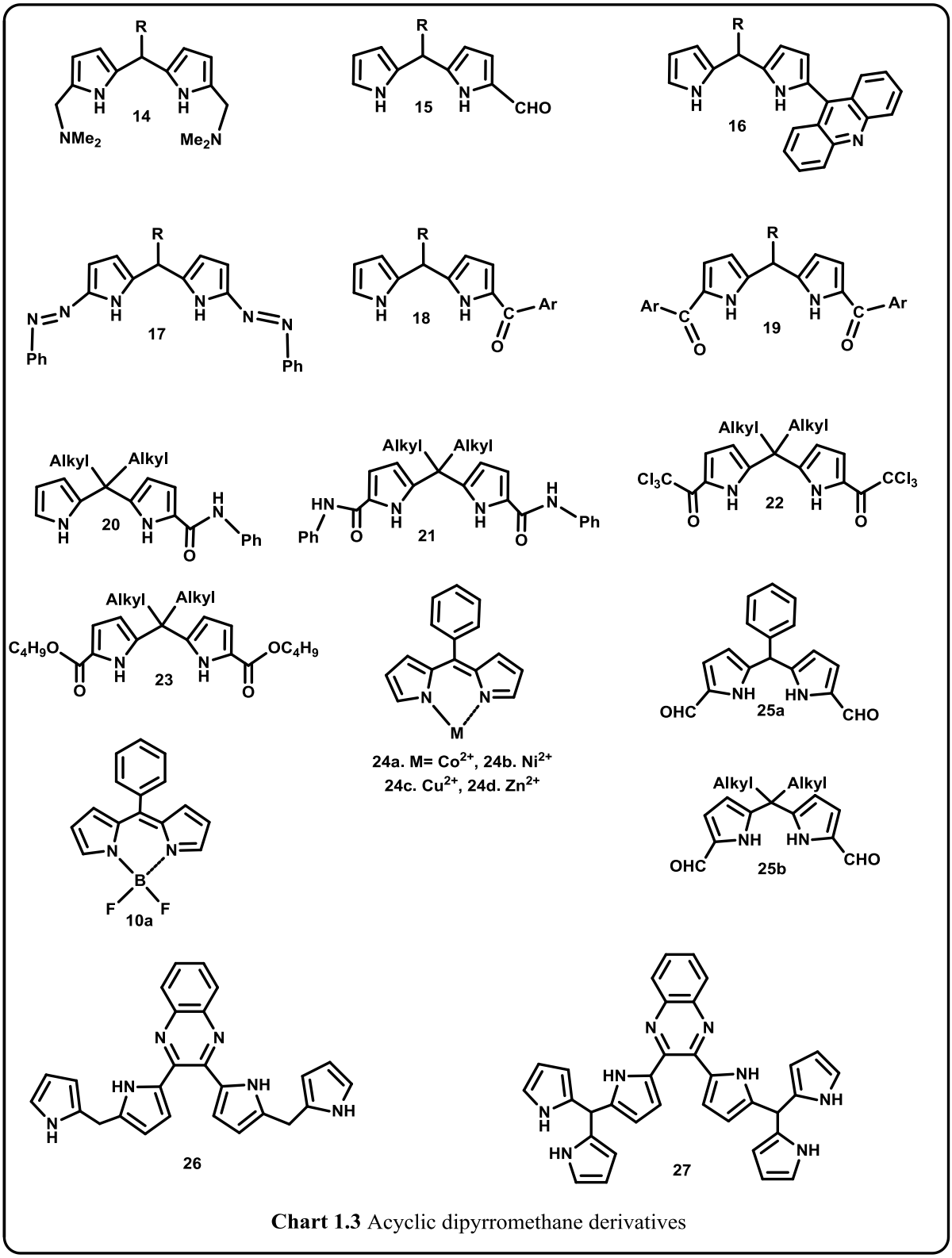

Chart 1.3 Acyclic dipyrromethane derivatives

using Grignard reagents is preferred (**18**) [Rao *et al.* 2000], whereas for bis-acylation, the Vilsmeier reaction or Friedel–Crafts reaction [Tamaru *et al.* 2004] is much more effective (**19**) Depraetere and Dehaen studied the reactivity of 5,5-dialkyldipyrromethanes [Depraetere and Dehaen 2003] and found that it reacted with phenyl isocyanate to form either mono- or diamides (**20** or **21**) and with trichloroacetyl chloride to give the corresponding diketones (**22)** which are easily transformed into esters (**23)**. Odom and co-workers proved that titanium complexes derived from 5,5-dialkyldipyrromethane are excellent catalysts for intermolecular alkyne hydroamination [Shi *et al.* 2003].

Wagner and Lindsey [Wagner and Lindsey 1994] and Bruckner *et al*. [Bruckner *et al.* 1996] were the first to report the oxidation of 5-aryldipyrromethanes (**13b)** to 5-aryldipyrromethenes. These are known to react with a variety of divalent transition metal salts to yield the corresponding dipyrrinato complexes [Wood and Thompson 2007]. The adduct formed by 5-aryldipyrromethenes with boron trifluoride is known as difluoroboraindacenes (**10**) (BODIPY), which finds its application as fluorescent dyes for biological samples [Zeng *et al.* 2006]. Sessler and co-workers prepared a series of oligopyrrolylquinoxalines **26** and **27** bearing dipyrromethane and tripyrromethane respectively, where the pyrrolic NH groups are responsible for the anion binding and colorimetric sensing property.

1.4.2 Cyclic dipyrromethane derivatives

As discussed in the introduction part, dipyrromethanes are found to be an important starting material for synthesizing various porphyrin analogues such as, normal, contracted and expanded porphyrin derivatives. For example, condensation of a dipyrromethane (**13b**) with diformyl dipyrromethane (**25a**) by MacDonald-type [2+2] method, a wide range of *meso*-substituted *trans*-porphyrins (**3a**) was synthesized [Clarke and Boyle 1998]. Similarly,

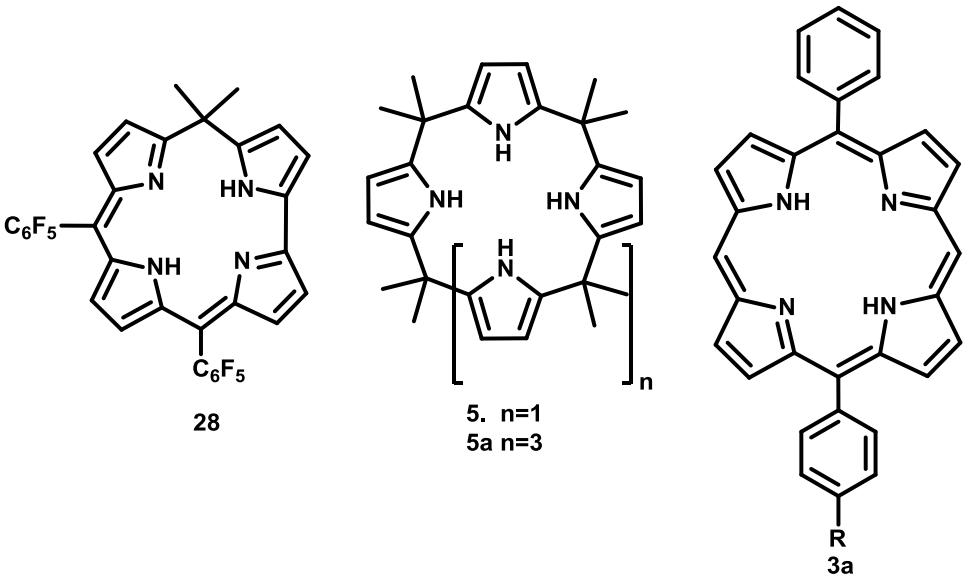

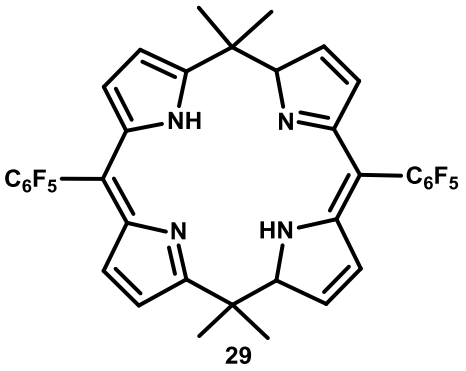

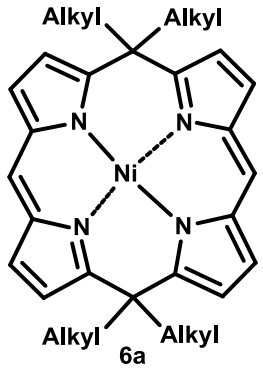

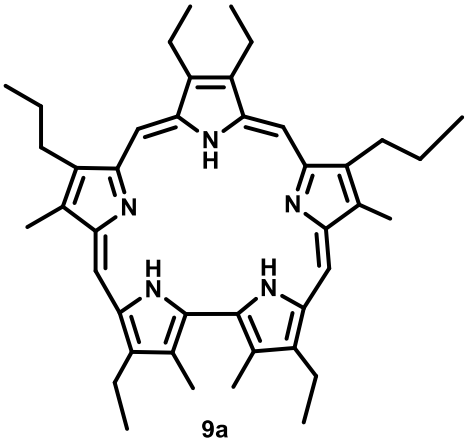

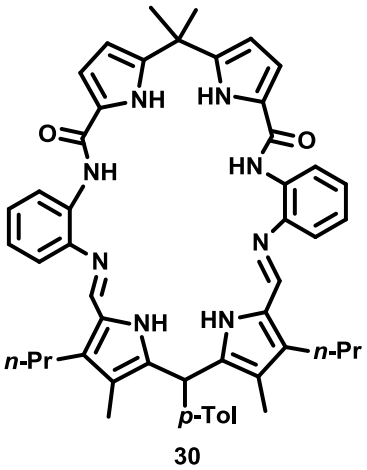

Chart 1.4 Cyclic dipyrromethane derivatives

the MacDonald condensation between diformyl dialkyldipyrromethanes such as **25b** and 5,5-dialkyl dipyrromethanes afforded *meso*-tetra alkyl calix[4]phyrins **(6a)** by templating with Ni(II) in acceptable yields [Orlewska *et al.* 2005].

Geier and co-workers investigated two complementary dipyrromethane monocarbinol routes to a *meso*-substituted 5-isocorrole (**28**) along with condensed product such as a porphodimethene (**29**) [Flint *et al*. 2010]. Sessler and co-workers synthesized a series of expanded porphyrins starting from sapphyrins (**9a**) which are used as anionic receptor in protonated state, MRI contrast agent and PDT agent [Sessler *et al.* 1990]. Calixpyrroles **(5)** are other important cyclic dipyrromethane derivatives, which are well-known for their anion binding property [Gale *et al*. 1996] [Gale *et al*. 2001] [Sessler *et al*. 2003]. Khonke and co-workers prepared higher derivatives of calixpyrrole with larger cavities like (**5a**) [Cafeo *et al.* 2002]. Sessler and co-workers synthesized an amido imine type hybrid cyclic dipyrromethane derivative (**30**) which can adjust the number of binding sites with respect to guest molecules leading to conformational changes [Katayev *et al.* 2007].

1.5. Applications of Acyclic and Cyclic Dipyrromethane derivatives

Most of the cyclic and acyclic dipyrromethane derivatives have strong absorption and emission bands and find potential application as chemosensors, chemodosimeters, labeling and imaging, and supramolecular chemistry. Due to large number of examples in the literature, in this chapter, we will discuss only the potential applications of some selected acyclic and cyclic dipyrromethane derivatives, which are pertaining to this thesis.

1.5.1 Sensing

Molecular probes or the so called "chemosensors and chemodosimeters" are the molecules of synthetic origin that are able to bind selectively and reversibly, an analyte of interest with a concomitant change in one or more properties such as absorption, emission, electrochemical, chemical reactivity and magnetic properties [Beer *et al*. 1988]. Among the

different molecular probes, fluorescence based probes have many advantages: fluorescence measurements are usually very sensitive (single molecule detection is possible), low cost, easily performed, and versatile, offering sub nanometer spatial resolution with submicron visualization and sub millisecond temporal resolution [Lakowicz *et al*. 1988]. Acyclic and cyclic dipyrromethane derivatives such as porphyrins and related tetrapyrrolic acyclic derivatives, have received attention as molecular receptors for anions and neutral substrates, as well as complexants for cations. Whereas cation coordination generally relies on the donor ability of the pyrrolic nitrogen, neutral and anionic recognition is typically achieved through hydrogen bonding through the pyrrolic N-H moiety. The selectivity of the pyrrolic host in question can be readily tuned by altering the shape and/or size of the binding cavity. Further, many expanded porphyrins possess extended π conjugation pathways, which results in unique optical features. This has made these systems attractive for use as colorimetric and fluorimetric sensors [Rambo *et al*. 2011].

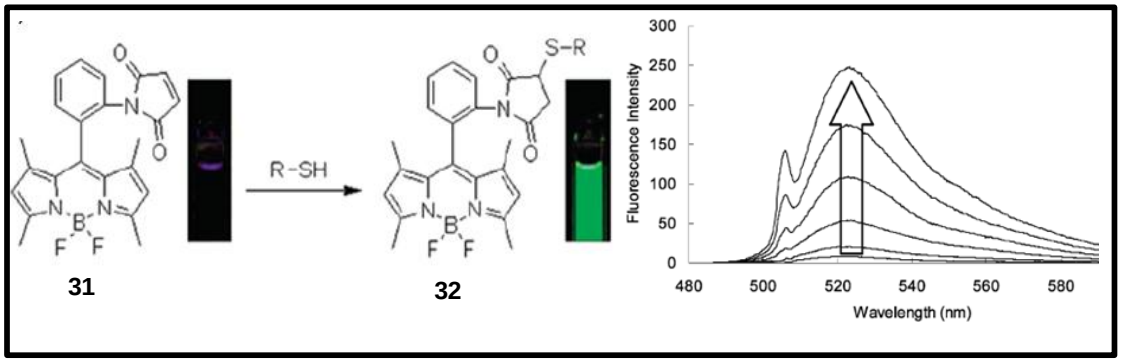

Figure 1.3 BODIPY based fluorescent sensor **31** for thiol containing amino acid (Adapted from the reference Matsumoto *et al*. 2007).

BODIPY based fluorescent probe (**31**) is used to detect thiol containing aminoacids [Matsumoto *et al*. 2007], where the emission profile is strongly quenched by photoinduced electron transfer from BODIPY to malemide moiety. However, the fluorescence of BODIPY is restored with a 350 fold enhancement in fluorescence intensity on reaction with thiols (Figure 1.3). Katayev and co-workers reported the synthesis of three new amido-imine-type

hybrid macrocycles based on substituted pyrrole units (Figure 1.4), which can act as an effective receptors for oxoanions in the solid state and in acetonitrile solution [Katayev *et al*. 2007].

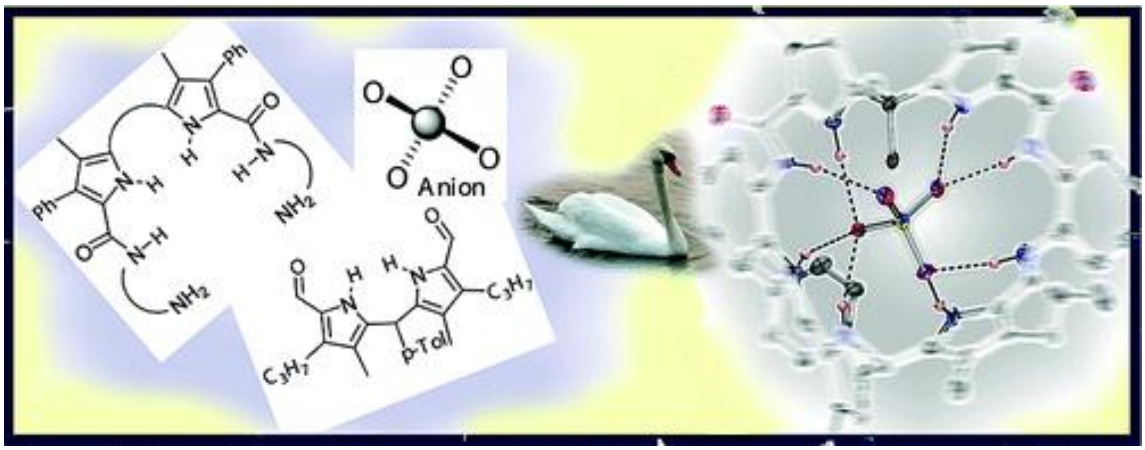

Figure 1.4 Bipyrrole and dipyrromethane based amido-imine hybrid macrocycles as receptors for oxoanions (Adapted from the reference Katayev *et al*. 2007).

Salini and co-workers synthesised a group of hybrid, core modified, expanded calix[*n*]-*m*-benzo[*m*]phyrins (*n* = 2, 3, 4; *m* = 4, 6, 8) by the acid catalysed condensation reaction of bispyrrolyl benzene with pentafluorobenzaldehyde in presence of TFA, followed by oxidation with DDQ. Among the macrocycles prepared calix[3]-*m*-benzo[6]phyrins (**33**) exhibited the property of sensing of volatile organic compound. Selective exposure of the macrocycle to volatile organic compounds (VOC) such as ketones and esters results in the

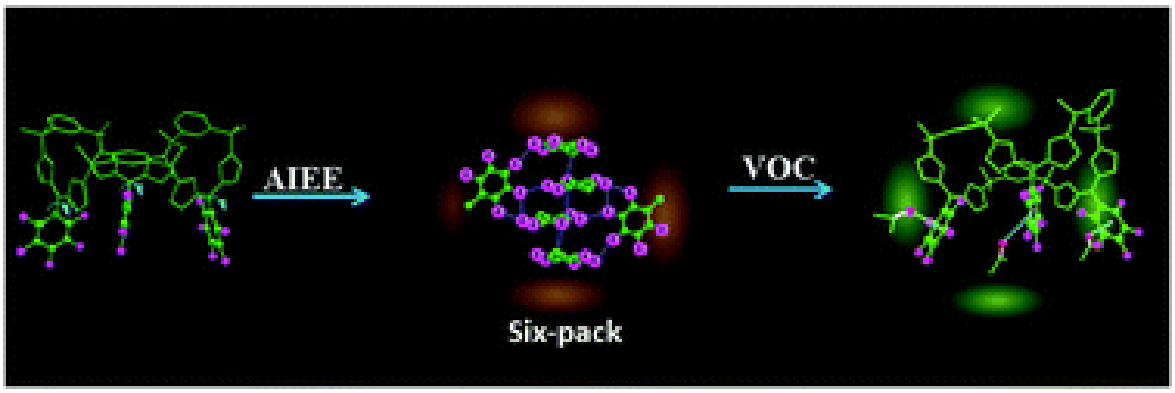

Figure 1.5 Sensing of volatile organic compound by an expanded calixbenzophyrin (**33**) (Adapted from the reference Salini *et al*. 2013).

breaking of fluorine assisted aggregate, leading to enhanced monomer emission (Figure 1.5) [Salini *et al*. 2013].

1.5.2 Photodynamic therapy

Photodynamic therapy (PDT) is a minimally invasive and promising method for the treatment of combat cancer. Three fundamental requirements for PDT are oxygen, visible light and photosensitizer. Each factor is harmless by itself but their combination can produce lethal cytotoxic agents like singlet oxygen which can eradicate tumor cells [Josefsen and Boyle 2008]. Pyrrolic macrocycles, in particular porphyrins and metalloporphyrins have large molar absorptivities in the visible region of the electromagnetic spectrum and has high affinity for tumor cells. As a result, a number of porphyrin photosensitizers have entered in clinical trials [Sternberg *et al*. 1998; Pandey 2000; Langa *et al*. 2004; Josefsen and Boyle 2008].

Several BODIPY dyes have found potential applications in the field of photodynamic therapy because of their low tendency to form aggregates, efficiency in production of singlet oxygen and high cellular uptake. He and co-workers synthesized a series of distyryl-BODIPY dyes [He *et al*. 2011] and investigated their photodynamic therapeutic properties and found that N-methyl derivative (**34**) is highly photocytotoxic with an IC_{50} value of 15nM (Chart 1.5).

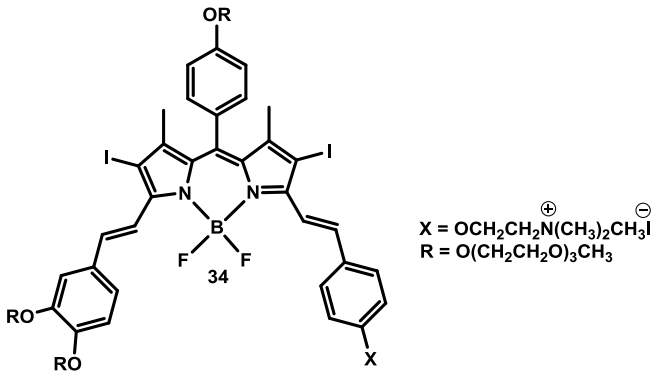

Chart 1.5 N-methylated unsymmetrical distyryl-BODIPY dye **34** with photodynamic therapeutic properties [He *et al.* 2011])

1.5.3 pH sensors and logic gates applications

The dipyrromethane derivatives are also found potential application in the field of pH sensors and logic gates. Akkaya and co-workers reported an amino group and phenolic group incorporated BODIPY fluorophore as a pH sensor both low and high pH. The protonation of

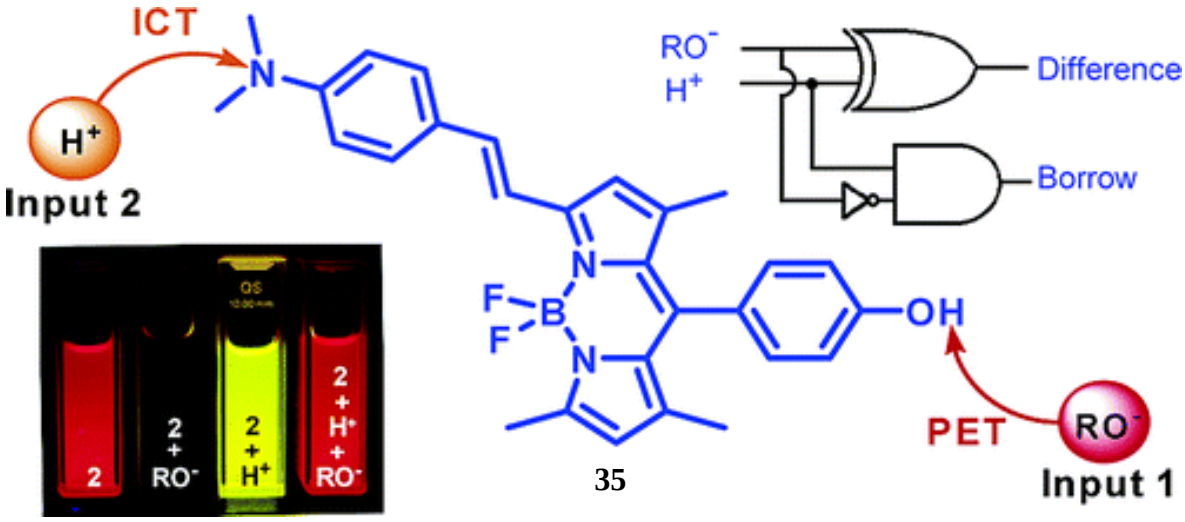

Figure 1.6 pH sensing and logic gate application of BODIPY derivative (**35)** (Adapted from the reference Coskun *et al*. 2005).

phenolic group caused quenching of fluorescence and protonation of amino group enhance the fluorescence with blue shift (Figure 1.6). An effective PET (photo induced electron transfer) and ICT (intra molecular charge transfer) switching of boradiazaindacene emission plays as reconfigurable logic gates [Coskun *et al*. 2005].

1.5.4 Molecular self-assembly

Molecular self-assembly is defined as the spontaneous and reversible association of molecules or ions to form larger, more complex supramolecular entities according to the intrinsic information from the molecules it selves. In short, self-assembly is the construction of systems without guidance or management from an outside source through noncovalent interactions. Self-assembly of molecules is one of the popular ways to create functional materials for devices in the fields like optoelectronics and photovoltaics [Li *et al*. 2003]. The

optical and electronic properties change on aggregation which finds its application in fields like organic photoconductors, markers for biological membrane systems NLO materials, PDT, superconductors etc. In the case of dipyrromethane derivatives like porphyrins, aggregation facilitates the formation of H and J aggregates with considerable change in their photophysical properties which paved the path for applications in the above fields. [Giovannetti *et al*. 2012]

Enormous number of dipyrromethane derivatives is reported in recent years which self-assemble to form molecular systems for various applications. Protoporphyrin derivatives self-assembled into a variety of nanostructures such as nanotubes and nanospheres, the helical and vesicular morphology of which depends on the substitution and solvent used from nanometer to millimetre [Bhosale *et al*. 2013]. Yin and co-workers prepared 5,5′-bisdiazo-dipyrromethane (**36**). The Quadruple N–H···N hydrogen bond driven self-assemblies of two units (Chart 1.6) of were studied by X-ray crystallography, ^{1}H NMR and DFT calculation [Yin *et al*. 2008].

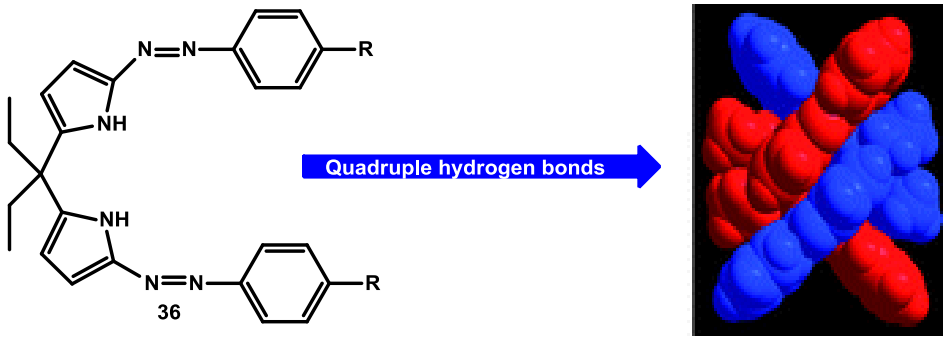

Chart 1.6 Self-assembly in 5,5-bisdiazo-dipyrromethane (**36**) via quadruple N-H···N hydrogen bond

1.5.5 Labelling Reagents

The dipyrromethane derivatives are used as labelling agents. For example the BODIPY dyes have been introduced as replacements for fluorescein and rhodamines. These

dyes are based on an unusual boron-containing fluorophore (Chart 1.7). Depending on the precise structure, a wide range of emission wavelengths are obtained from 510 to 675 nm.

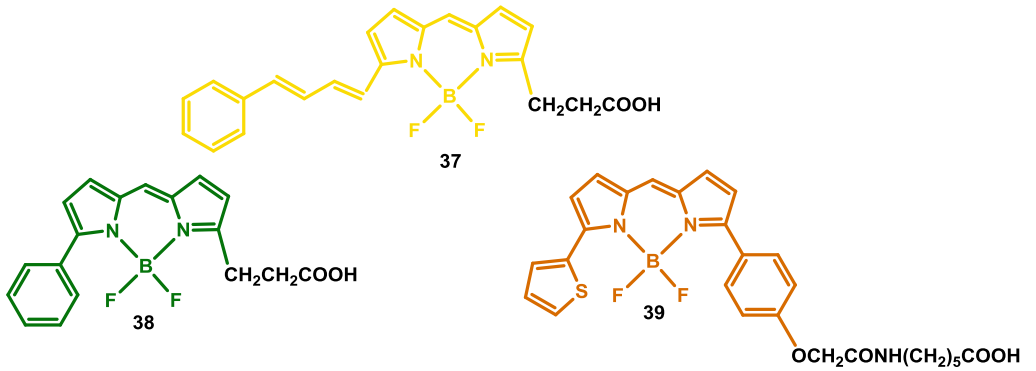

Chart 1.7 BODIPY containing fluorophores **37**, **38** and **39** with wide range of emission characteristics (Adapted from the reference [Haugland *et al.* 1991]).

The BODIPY dyes have the additional advantage of displaying high quantum yields and molar extinction coefficients near 80,000 M^{-1} cm^{-1}, insensitivity to solvent polarity and pH. The emission spectra are narrower than those of fluorescein and rhodamines, so that more of the light is emitted at the peak wavelength, possibly allowing more individual dyes to be resolved.

1.5.6 Solar Cells

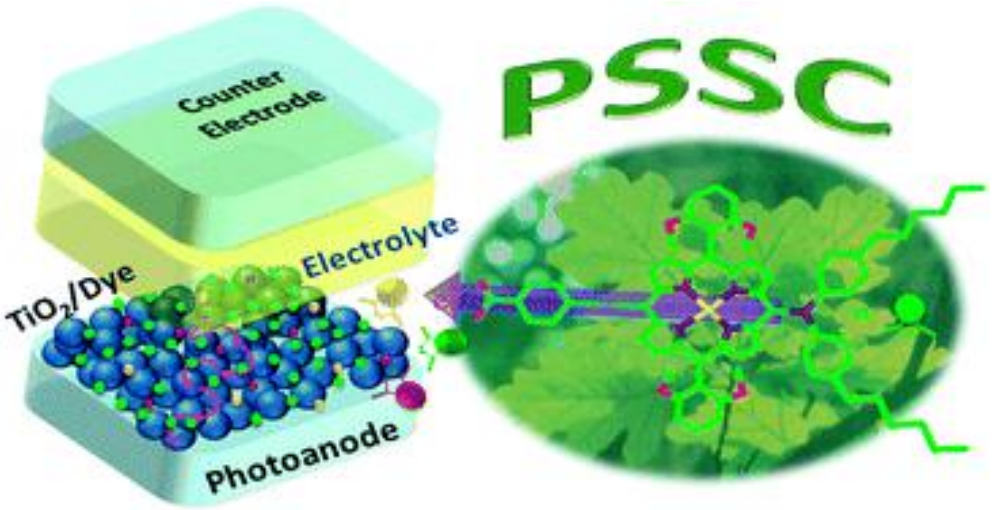

Figure 1.7 The porphyrins - as efficient centres to harvest light for solar cells sensitized with a porphyrin (Adapted from the reference Li *et al*. 2013).

Chlorophylls are the light harvesting antenna in plants. Inspired from photosynthesis, scientists utilized artificial chlorophylls -porphyrins and its derivatives as potential centres to harvest light for dye sensitized solar cells (Figure 1.7). Several numbers of Porphyrins and fused porphyrins with various linkers like thiophene etc. at *meso, β* position, functionalized with π extended chromophores finds its applications in dye sensitized solar cells [Li *et al*. 2013]**.** Several BODIPY derivatives functions as energy transfer antennas, D'Souza and co-workers developed an aza-BODIPY derivative (Chart 1.8) consisting of a zinc porphyrin part and a three dimensional electron acceptor fullerene part. This supramolecular polyads were used to build photochemical cells with an incident photon-to-current efficiency of 17% [D'Souza *et al*. 2012].

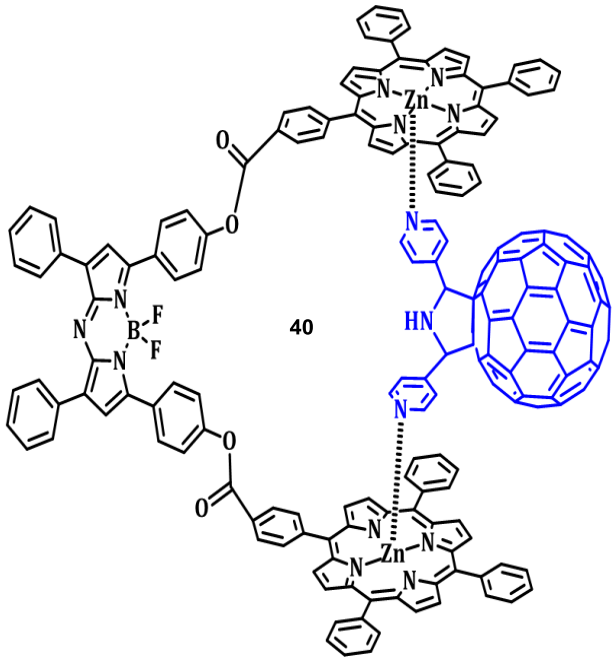

Chart 1.8 Supramolecular tetrad consisting of BF_2-chelated tetraarylazadipyrromethane covalently linked to two Zn-porphyrins, co-ordinated to bis-pyridine functionalized fullerene (**40**) (Adapted from the reference D'Souza *et al.* 2012)

1.5.7 Synthetic chemistry

Dipyrromethanes are the precursors for the syntheses of a wide range of compounds like porphyrins, dipyrrins, calixpyrroles, chlorins, calixphyrins, corroles, acyclic derivatives

etc. These are used as ligands in organometallic syntheses and catalyses. Bakavoli and co-workers reported that the dipyrromethane as new organic reagent for the synthesis of gold nano particles. They used substituted dipyrromethanes as reducing agents for $HAuCl_4$. They proposed that the formation of polydipyrromethane was acting for the synthesis of the nano particle [Eshghi *et al*. 2013].

O_2 activation by metal complexes as important applications in areas like bioinorganic chemistry and preparative organic chemistry. Several synthetic complexes have been reported that are able to activate molecular oxygen in interesting stoichiometric or catalytic reactions. Katayev and co-workers reported the use of diimino dipyrromethane complexes of Ni, Pd and Pt in O_2 activation resulting in metal dependant autoxidation of the ligand [Katayev *et al*. 2007].

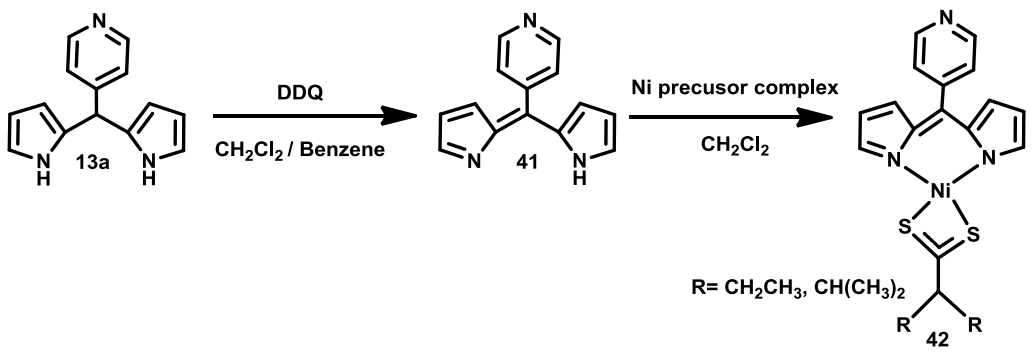

Scheme 1.7 Syntheses of dipyrrinato complexes **42** (Adapted from the reference Gupta *et al.* 2015)

Gupta and co-workers reported the syntheses of heteroleptic dipyrranato nickelcomplexes (Scheme 1.7) and utilized it as a capping agent in the preparation of silver nanoparticles. The fuctionalization and stabilization of the nanoparticles was acheieved by the availability of free pyridyl nitrogen on the dipyrrin core of the complexes. The nanoparticles obtained through this route successfully catalyzed the reduction of 4-nitrophenol to 4-aminophenol (Figure 1.8).

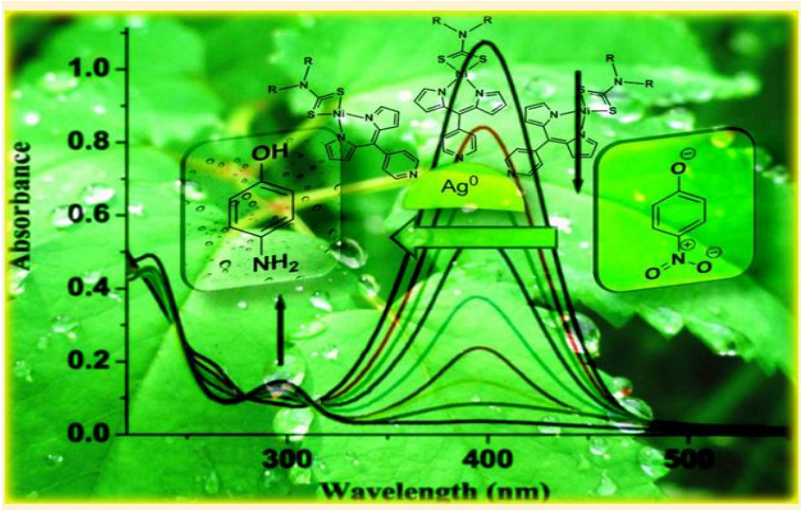

Figure 1.8 Size-Controlled syntheses of Ag nanoparticles functionalized by heteroleptic dipyrrinato complexes (Adapted from the reference [Gupta *et al.* 2015]).

1.5.8 Catalysis

Dipyrromethane derived macrocyclic systems like porphyrins occur widely in Nature, and they play very important roles in various biological catalytic processes. Heme [the iron (II) protoporphyrin-IX complex] is the prosthetic group in hemoglobins and myoglobins, which are responsible for oxygen transport and storage, respectively, in living tissues. Heme can also be found in the enzyme peroxidase, which catalyzes the removal of perilous peroxides from the same tissues. In 1979, during the studies of chemical fixation of carbon dioxide, potential utility of metalloporphyrins as catalysts for controlled macromolecular synthesis was discovered [Takeda *et al.* 1978]. Generally, several metal co-ordinated dipyrromethane derivatives like metalloporphyrins are used for catalysis of reactions of oxidation, epoxidation, hydroxylation, nitrene and carbene transfer, activation of nitric oxide and oxidative DNA cleavage. Metalloporphyrins of aluminium, zinc, manganese, cobalt and rhodium have been demonstrated to serve as excellent initiators for controlled anionic and free-radical polymerizations [Kadish *et al.* 1999; Aida *et al.* 1999]. Yadav and co-workers reported the syntheses of hetroleptic penta methyl cyclopentadienyl rhodium / iridium (III)

complexes imparting dipyrrins as co-ligands which are used as catalyst in the reduction of terephthalaldehyde to 4-hydroxymethybenzaldehyde [Yadav *et al.* 2009].

1.6 Objectives of the present thesis

Pyrrolic supramolecular self-assemblies with cyclic and acyclic structure are of wide interest in several areas, namely in porphyrins and related macrocycles, science materials, optics and medicine. Pyrrole exhibits "as either as a hydrogen-bonding acceptor, due to N site and a hydrogen-bonding donor due to the NH site. Also pyrrole can form stacking assemblies by strong π interactions. Therefore, pyrrole rings can act as potential building subunits to form supramolecular architectures. Among various artificial host molecules reported to date, macrocycles consisting of pyrrole and its derivatives are particularly attractive, where the meso-dialkyldipyrromethanes are potential building blocks for the syntheses of porphyrins and related compounds. In addition, the studies on di-formyl derivatives of meso-dialkyl dipyrromethanes are well explored, however, research on mono-formyl derivatives are less exploited in the literature. Hence, the main objective of our work is to study the applications of mono-formyl 5,5-diethyldipyrromethane as a versatile precursor to synthesize acyclic as well as macrocyclic derivatives and explore their structural, photophysical and receptor properties.

The present thesis has been divided into four chapters. In the first chapter, a detailed literature review of dipyrromethanes and their potential applications is discussed. In the second chapter, satisfies one of our objective of designing a macrocyclic system derrived from mono-formyl 5,5-diethyldipyrromethane. We achieved this goal by the design and syntheses of the macrocycle 5,15-porphodimethene. The synthetic methodology adopted for the synthesis is simple metal template strategy. It was executed by acid-catalyzed condensation reaction of dipyrromethane mono aldehyde in presence of metal acetates of palladium, nickel and zinc in methanol medium. Different spectroscopic studies including

NMR, electronic spectral analyses, X-ray single crystal analysis threw light into the struture of the synthesized calixphyrin metal complexes. Another objective of the chapter was to the study of noncovalent interactions such as hydrogen bonding and anagostic interactions using 5,15-porphodimethene metal complexes as platform. The rare case of **M...H-C** anagaostic interaction is well demonstrated by variable temperature NMR spectral studies and further confirmed by single crystal X-ray analysis. Furthermore, the extra coordinated water molecule in one of the metal complexes converts the roof like conformer to planar form which is hitherto unknown in the calixphyrin metal complexes. Overall conclusion of the studies is that, the anagostic interactions lead to distortion, while the hydrogen bonding interaction generates dimerisation as well as array formation.

The third chapter describes our interest of study of the polymorphic nature of 5,15-porphodimethene Pd(II) complex and how this complex is used as a chemodosimetric sensor. Two polymorphs of the mentioned complex are obtained by different polar solvents and are further confirmed by single crystal X-ray analysis. The receptor properties are carried out with various anions and showed a selective affinity towards cyanide ion. Excellent selectivity was observed even in the presence of 100 equiv. of other potentially interfering anions. We have also successfully demonstrated that the cyanide ion binds selectively at the *meso*-position of the calixphyrin skeleton and justified the chemodosimetric sensor property of the mentioned complex. To the best of our knowledge, such type of cyano adduct formation is hitherto unknown in the calixphyrin chemistry and paves a new methodology for the synthesis of functionalized unsymmetrical porphomethenes and calixphyrroles.

The fourth chapter demonstrates our yet another objective of design of an acyclic system using the precursor mono-formyl-5,5-diethyldipyrromethane and evaluate their ability to act molecular receptors properties for various receptor applications. We have synthesised

an acyclic Schiff base compound from the precursor mono-formyl-5,5-diethyldipyrromethane. This chapter mainly describes a detailed study of the aggregation induced emission enhancement (AIEE), Zn^{2+} sensing property and luminescence mechanochromic nature of '*double headed dragon*' shaped acyclic Schiff base. One pot Schiff base condensation reaction of 1-formyl-5,5-di(ethyl)dipyrromethane with *p*-phenylenediamine in methanol at room temperature generated yellow colored ditopic dragonesque shaped Schiff Base (**DSB**) in high yields. The compound **DSB** is found to exhibit an enhanced emission in the presence of higher water concentration and the aggregates form fluorescent microspheres. The molecule **DSB** selectively senses the Zn^{2+} in acetonitrile solution exhibiting 135 fold 'Turn-On' emission and also generates nano particles of different morphology depending upon the concentration of Zn^{2+} ions. At lower concentration of Zn^{2+}, **DSB** forms greenish yellow fluorescent fibre like structures of 2:1 complexes. Upon increasing the concentration of Zn^{2+} ions, **DSB** forms non fluorescent, red 2:2 complexes with nano sphere like morphology. The aggregation properties and sensing studies with Zn^{2+} ion are in turn an inevitable consequence of restricted intramolecular rotation (IMR) due to intermolecular H-bonding interaction. Finally, a thorough investigation of the colour and luminescence properties of the crystal of the Schiff base in response to mechanical stimuli revealed that it shows grinding induced luminescence mechanochromism and it reverts back to its initial state on heating or recrystallization. Thus demonstrating AIEE, Zn^{2+} sensing and luminescence mechanochromism characteristics of **DSB**, a typical '*trimurthy*' type molecule, a consequence of noncovalent molecular interactions in the crystalline, amorphous and solution states forms the objective of the final chapter of this thesis.

Chapter 2

Syntheses, Characterisation and Structural Properties of 5,15-Porphodimethene Metal Complexes

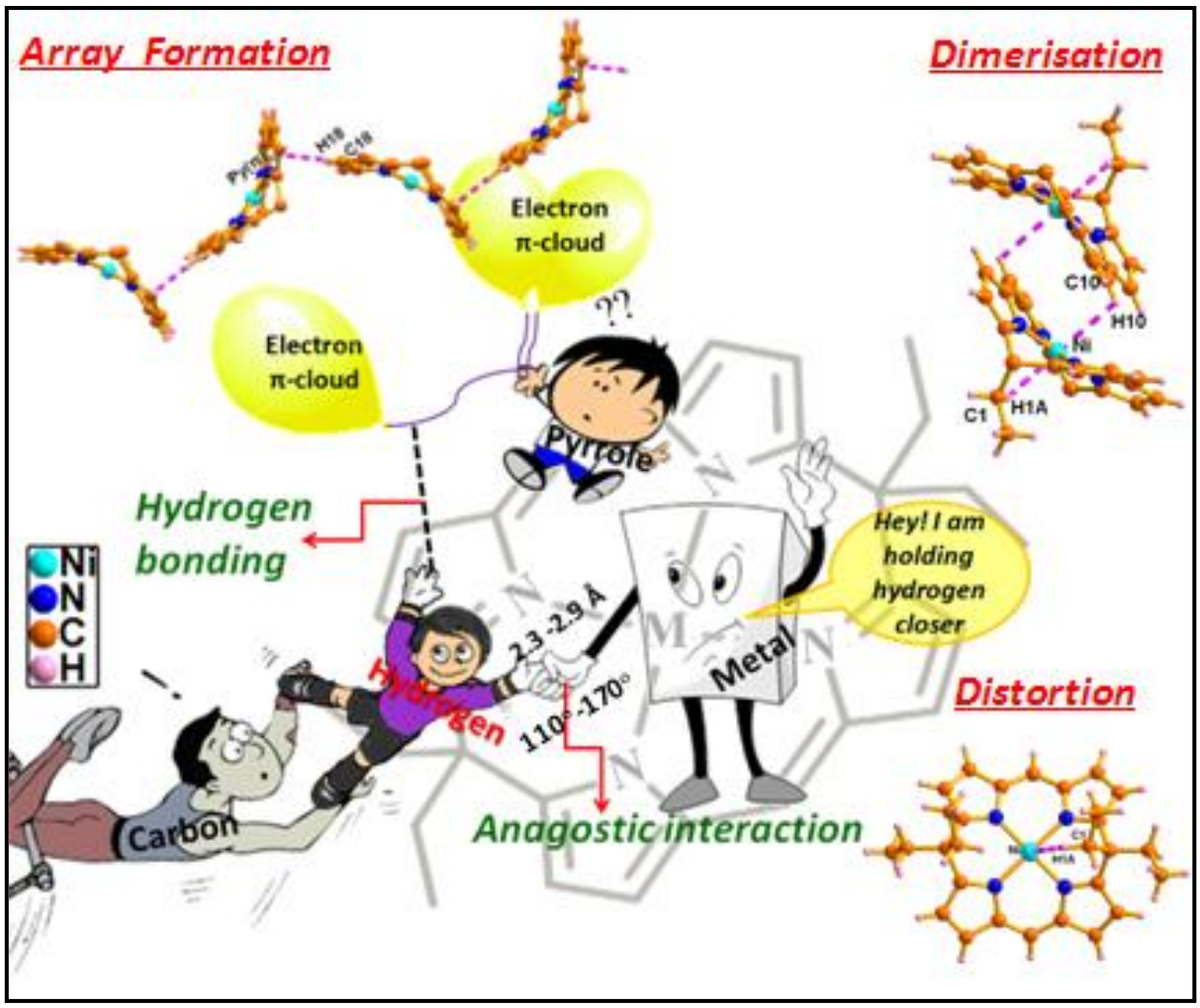

2.1 Abstract

Calixphyrins, a structural cross road between porphyrins and calixpyrroles, play as a receptor for both cations and anions. Syntheses, spectral and structural characterization of a group of 5,15-porphodimethene metal complexes ***1a-1c′*** *are described in this chapter. Metal templated synthesis has been emerged as an important strategy for the synthesis and separation of unstable calixphyrins. The synthetic route includes acid-catalyzed condensation reaction of a dipyrromethane mono-aldehyde in presence of acetates of palladium, nickel and zinc in methanol medium. The newly synthesized calixphyrin metal complexes were characterized by NMR, ESI-MS, electronic spectral analyses and finally confirmed by X-ray single crystal analysis. The research is also focused mainly on the study of noncovalent interactions such as hydrogen bonding and anagostic interactions using 5,15-porphodimethene metal complexes as platform. The rare case of* ***M...H-C*** *anagostic interaction exhibited by two metal complexes* ***1a*** *and* ***1c****, which was well demonstrated by variable temperature NMR spectral studies and confirmed by single crystal X-ray analysis. Furthermore, the extra coordinated water molecule in one of the metal complexes converts the roof like conformer to planar form which is hitherto unknown in the calixphyrin metal complexes. We have successfully explored the role of noncovalent interactions governing the structure and stability of the metal incorporated 5,15-porphodimethene synthesized via metal templated methodology. The free-base porphodimethene was also synthesized de-metallation of the metal complexes. Overall, the anagostic interactions lead to distortion, while the hydrogen bonding interaction generates dimerisation as well as array formation.*

2.2 Introduction

Coordination compounds have been the focus of interest from many decades due to their ability to be used as active elements in fields like supramolecular chemistry [Holliday *et al*. 2001], catalysis [Elsevier *et al*. 2003], medicinal chemistry [Drewry *et al*. 2011], etc. The ability of these compounds is not just as a result of their chemical composition but also imparted to them through a deliberate consequence of noncovalent interactions between the constituent molecules [Müller-Dethlefs *et al*. 2000]. Among these, hydrogen atom assisted interactions such as hydrogen bonding, agostic and anagostic interactions are highly significant. They play major role in the structural stability, reactivity and applications like hydride extraction and elimination, which highlights the need for the study of these delicate interactions [Brookhart *et al*. 2007]. However, compared to agostic interactions, anagostic interactions are not well explored in the literature. Pyrrole based macrocycles like porphyrinogens form an excellent platform for the study and utilisation of the noncovalent interaction due to their rich co-ordination chemistry and anion binding properties.

2.2.1. Calixphyrins

Porphyrinogens are partially oxidized intermediate products obtained during the acid-catalysed condensation reactions of pyrrole and aldehyde followed by oxidation which finally results in the formation of completely oxidized stable porphyrins [Dolphin 1970, Senge *et al*. 2000]. Among the different porphyrinogens, calixphyrins, which are the structural hybrids of porphyrins and calixpyrroles, provide an excellent base for exploring the anion and cation recognition properties. They form an intermediate between completely oxidized cation binding porphyrins (**6**) and completely non-oxidized anion or neutral electron rich molecule binding calixpyrroles (**7**). The recognition properties of calixphyrins

is due to its unique structural features such as presence of sp^3 and sp^2 carbons interrupting with conjugated pathway, flexible frameworks and rigid π-conjugated networks. Calixphyrins are pyrrole based macrocycles in which at least one of the *meso* carbon atoms is sp^2 hybridized in addition to sp^3 hybridized carbon atoms in the molecular framework (Chart 2.1). The macrocycles with; (i) one sp^2 hybridized *meso* carbon atom are known as porphomonomethenes (**8**); (ii) two sp^2 hybridized *meso* carbon atoms are known as porphodimethenes (**9**) and (iii) three *meso* sp^2 hybridized carbon atoms are known as porphotrimethenes (**10**).

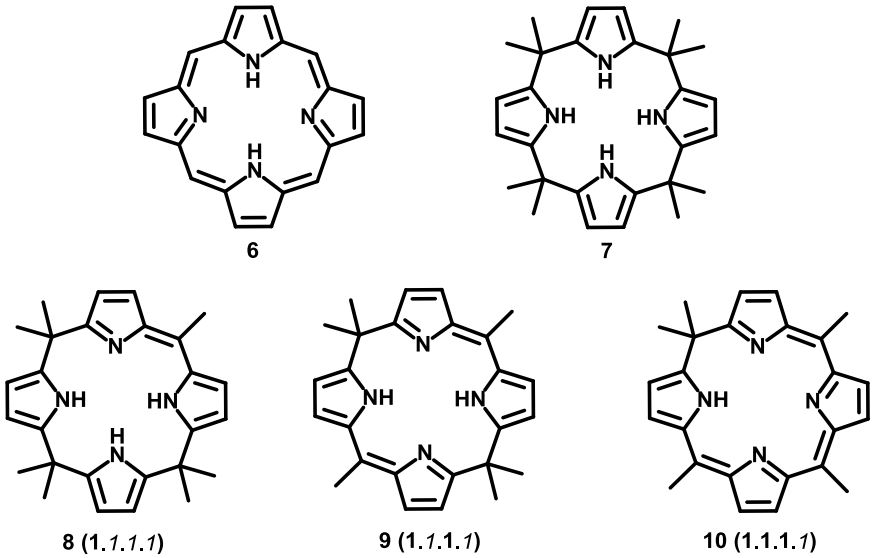

Chart 2.1 The structure of porphyrin (**6**), calixpyrrole (**7**) and various calixphyrin (**8**, **9** and **10**) derivatives

In general, the calixphyrins are orange or red-yellow colored solids, soluble in most of the organic solvents. They show broad UV-Vis absorbances ranging between 400 and 500 nm mainly due to π - π^* transition within the dipyrrin moiety. Porphomonomethene usually absorbs at 460 to 470 nm, while the porphodimethenes show absorption peak around 410 nm [Bucher *et al*. 2000] etc. ^{1}H NMR analysis of calixphyrins clearly reveals the presence of

NH protons at high down field region ranging from 11 to 15 ppm. This is mainly due to (i) the delocalization of lone pair of electron of the amine N atom and (ii) the strong intramolecular hydrogen bonding interaction between amine NH and imine N.

2.2.1.1 Nomenclature of calixphyrins:

Sessler and co-workers in 2000 proposed the systematic naming of **9** (Chart 2.1) was as calix[4]phyrin(**1**.*1*.**1**.*1*). Starting with the highest order sp^2 center, the molecule is named in the direction in which the nearest sp^2 center lies. The square bracketed number refers to the number of pyrroles in the macrocycle. The numbers in the circular bracket denotes the number of bridging *meso* centers between each pyrrole subunit. Bold numbers refer to number of sp^2 centers, and italicized numbers refer to number of sp^3 centers [Sessler *et al*. 2001].

2.2.1.2 Types of calixphyrins:

The definition of calix[4]phyrins comprehends systems with one, two, and three sp^2-hybridized bridging *meso* carbons (Chart 2.1). They are divided into three types based on the number of sp^2 hybridized *meso* carbon atom as porphomethenes (**8**) (one *meso* carbon), porphodimethenes (**9**) (two *meso* carbons), and Porphotrimethenes (**10**) (three *meso* carbons). Porphotrimethenes are further divided into two, based on the number of –NH protons,which are isoporphyrins (one NH hydrogen atom) [Barkigia *et al*. 1993] and Phlorins (three NH hydrogen atoms) [Mauzerall and Granick 1958, Mauzerall 1960].

2.2.1.3 Porphodimethenes (9):

Among the different categories of calixphyrins, 5,15-porphodimethene is an important class with partially conjugated and non-conjugated characters in its framework. These macrocycles contain two sp^2-hybridised *meso* carbon atoms. There are two types of

porphodimethenes; 5,10-porphodimethene type calix[4]phyrin-(**1**.**1**.*1*.*1*) **(9a)**, where two sp^2 hybridized *meso* carbon atoms are adjacent to each other and 5,15-porphodimethene type calix[4]phyrin-(**1**.*1*.**1**.*1*) (**9b**), where the sp^2 hybridized *meso* carbon atoms are opposite to each other (Chart 2.2).

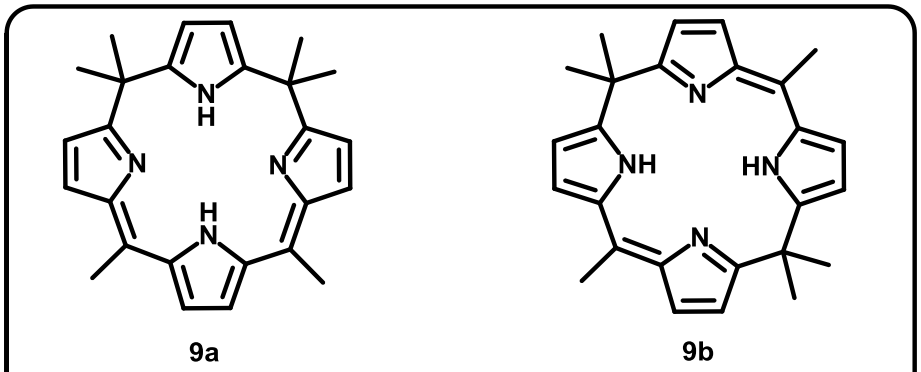

Chart 2.2. Porphodimethenes **9a (1.1.*1.1*)** and **9b (1.*1*.1.*1*)**

Porphodimethenes bearing bulky alkyl groups at the sp^3 *meso* position are stable towards oxidation. Such type of 5,10-porphodimethene (**9c**) was first isolated and characterized by Krattinger and co-workers by the alkylation of *meso*-tetraphenylporphyrin as shown in Scheme 2.1 [Krattinger and Callot 1996, Krattinger and Callot 1998]. On the

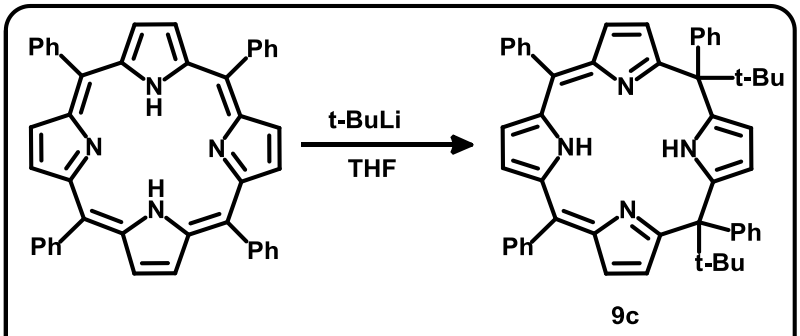

Scheme 2.1 Synthesis of 5,10-porphodimethene (**9c**)

other hand 5,15 porphodimethene with unsymmetrically substituted carbon atoms at the *meso* sp^3 centers can exist in three isomeric forms: syn-equatorial, anti and syn-axial as shown in Chart 2.3 [Inhoffen *et al*. 1968, Buchler and Puppe 1970, Dolphin 1970, Dwyer *et al*. 1974, Botulinski *et al*. 1988].

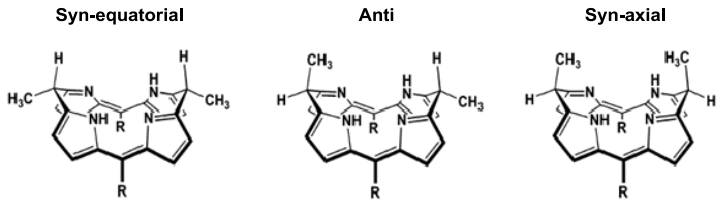

Chart 2.3 Conformations of unsymmetrically substituted 5,15-porphodimethene (**9d**)

5,15-Porphodimethene (**9d)** was synthesized by the trifluoroacetic acid (TFA) acid-catalysed condensation of 5-mesityl dipyrromethane with acetone (Scheme 2.2) followed by oxidation with 2,3-dichloro-5,6-dicyano-*p*-benzquinone (DDQ) in 44% yield [Kral *et al*. 2000]. Since, this macrocycle appears in the biosynthetic pathway towards porphyrins, thus, thoroughly researched [Nayar *et al*. 1992, Belanzoni *et al*. 2001].

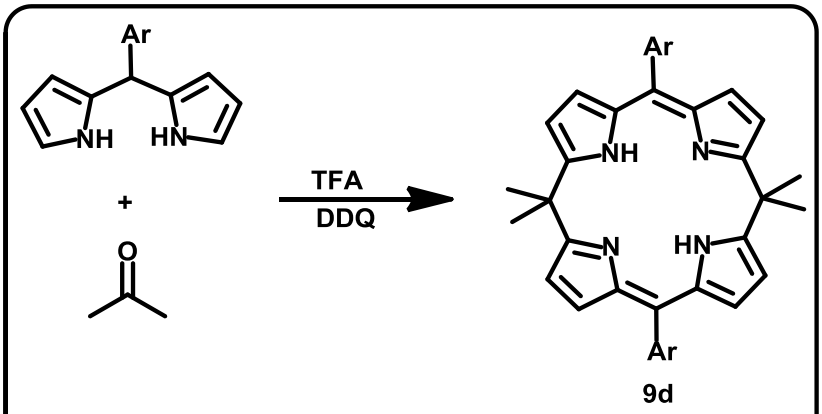

Scheme 2.2 Synthesis of 5,15-Porphodimethene (**9d**)

In general, porphodimethenes and its complexes are prepared through; (i) reductive alkylation at *meso* position of porphyrins; (ii) de-alkylation of octaalkylcalix[4]pyrrole; and (iii) acid-catalyzed condensation of oligopyrroles and acetone or condensation of sterically hindered aldehyde and pyrrole. In the methodologies (i) and (ii), the metal complexes of porphyrins / calixpyrroles are converted into respective 5,15-prophodimethene metal complex. In the methodology (iii), the metal complexes are synthesized through stepwise strategies, where the first step involves the synthesis of free-ligand followed by metal ion

insertion. In 2000, Sessler and co-workers demonstrated the synthesis of series of calix[4]phyrins (**12**) with one, two and three sp^3 hybridized *meso* carbons as shown in the Scheme 2.3 and introduced the cation complexation by using $ZnCl_2$ in presence of Et_3N [Bucher *et al*. 2000].

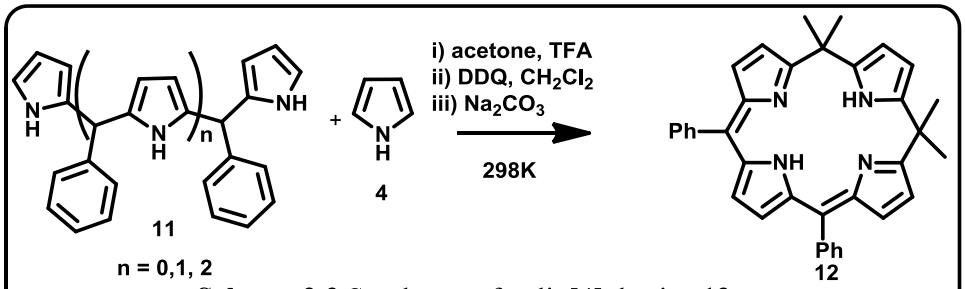

Scheme 2.3 Syntheses of calix[4]phyrins **12**

Later in 2005, Lindsey and co-workers reported the Pd complex of porphodimethene, where the 1-acyldipyrromethane afforded less than 1% of respective metal complex by metal templating strategy (Scheme 2.4).. However, through stepwise synthesis, the Pd complex was obtained in 22% yield [Sharada *et al*. 2005].

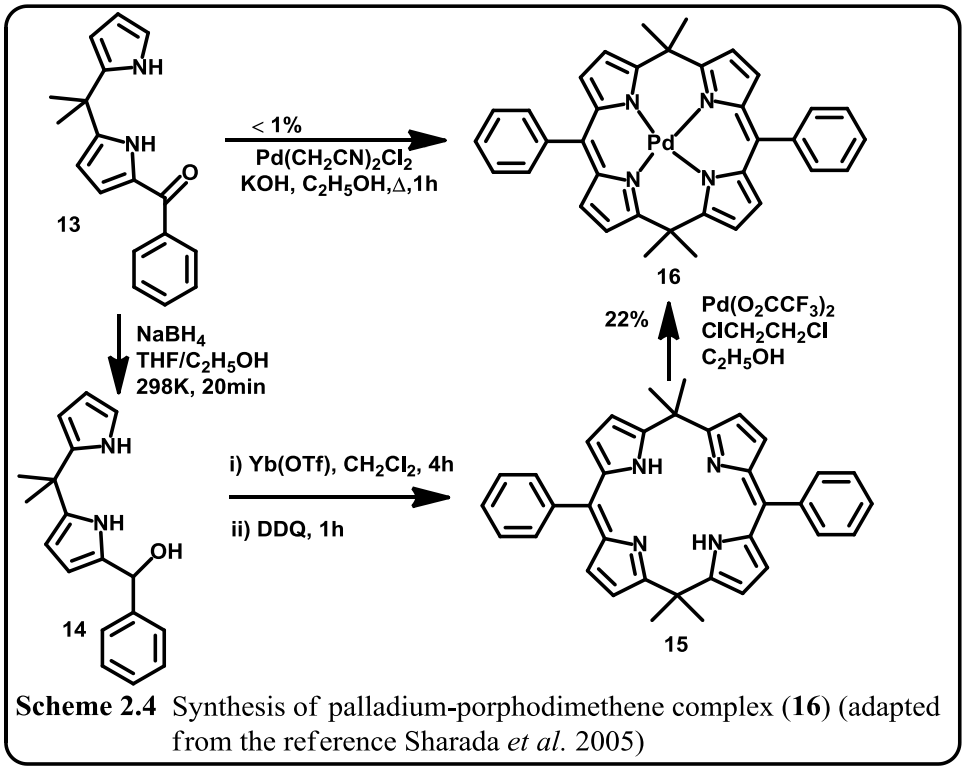

Scheme 2.4 Synthesis of palladium-porphodimethene complex (**16**) (adapted from the reference Sharada *et al.* 2005)

Same year, Wim Dehaen and co-workers adopted similar strategy, where the acid-catalyzed condensation of 1-formyldipyrromethane afforded the free-base 5,15-porphodimethene with the maximum yield of 5.5% and utilized the metal templating strategy by Ni(II) as template and obtained the respective complex in 28% yield [Orlewska *et al*. 2005]. Recently, series of core-modified porphodimethenes such as phosphole [Stępień *et al*. 2004, Matano *et al*. 2009] and benzene ring incorporated derivatives [Hung *et al*. 2008, Chang *et al*. 2009] were reported. These were synthesized as free-base followed by metal complexation or used as metal ion receptors.

2.2.2 Non Covalent Interactions and Supramolecular chemistry:

Atoms and molecules can interact together leading to the formation of either a new molecule (reactive channel) or a molecular cluster (non-reactive channel). The former is clearly again a covalent interaction; the latter one in which a covalent bond is neither formed nor broken and is termed as a noncovalent interaction. The chemistry of noncovalent intera-

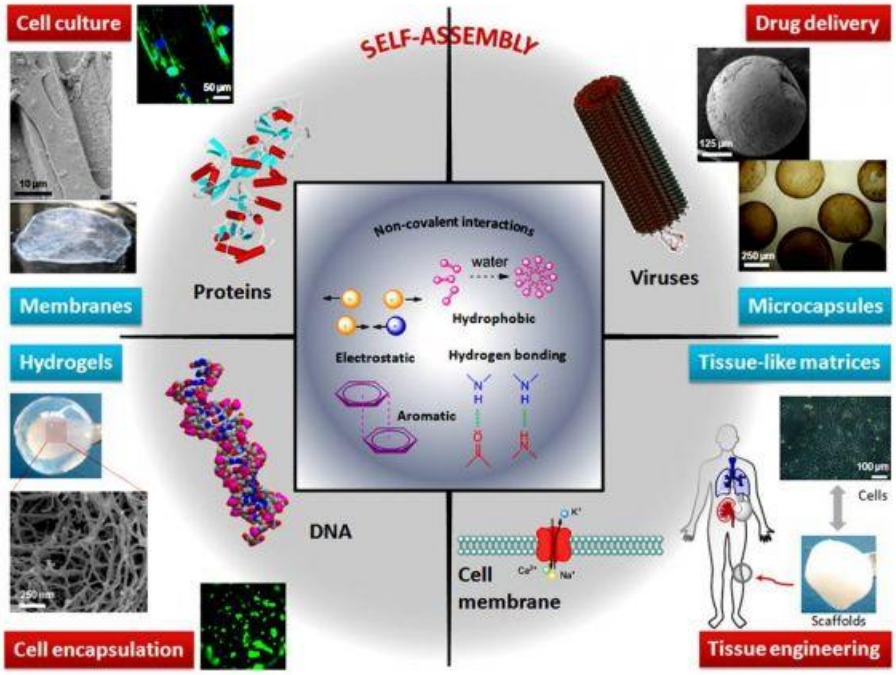

Figure 2.1 Schematic illustration of noncovalent interactions in nature and using it to create complex nanobiomaterials (Adapted from the reference Mendes *et al*. 2013).

ctions dealing with non molecular chemistry namely 'Supramolecular Chemistry' is one of the most popular and fastest growing areas of experimental chemistry. This highly interdisciplinary field has marked its signature not only in the field of chemistry but biochemistry, biology, environmental science, engineering, theoretics, physics, mathematics etc. It is actually 'the chemistry beyond molecule' [Steed *et al*. 2009]. The report by Koshevoy *et al*. that the non-covalent interactions within the ligand sphere in luminescent Au^{I}–Cu^{I} clusters can effectively determine the metal-core geometry (Figure 2.2) is one among the enormous reports in literature.

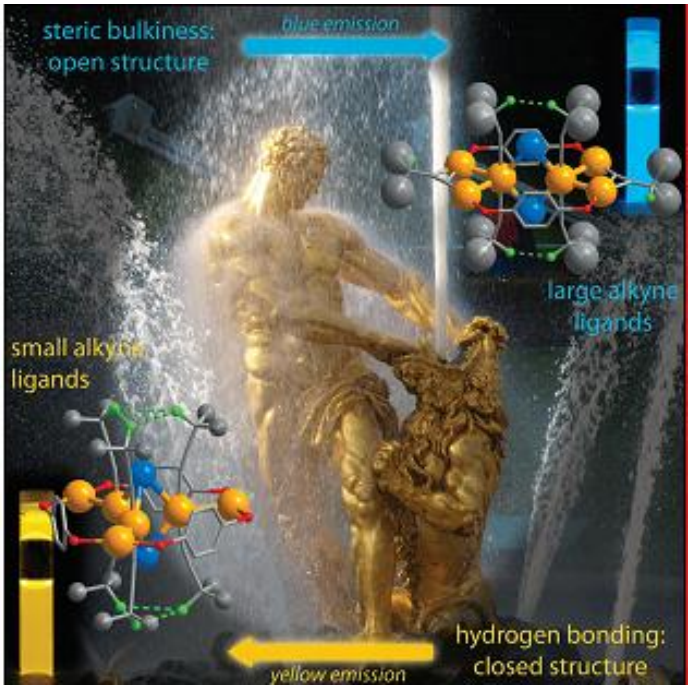

Figure 2.2 The schematic illustration of non covalent interactions in bimetallic Au^{I}–Cu^{I} clusters in an aza-BODIPY derivative. (Adapted from the reference Koshevoy *et al*. 2011).

Domination of O···H—O hydrogen bonding (lion) between the hydroxyaliphatic alkynes (oxygen atoms shown in green) facilitate an assembly of a "closed" structure (yellow phosphorescence), while increase of steric hindrance (Samson) leads to partial cluster opening and formation of a novel molecular type, which exhibit a characteristic sky-blue

emission [Koshevoy *et al*. 2011]. This noncovalent interactions encompasses an enormous range of effects both attractive and repulsive. The most important are ion-ion interactions, ion dipole interactions, dipole-dipole interactions, π interactions, π-π interactions, van der waals forces, hydrogen bonding, agostic and anagostic interactions.

2.2.2.1 Hydrogen Bonding:

A hydrogen bond can be regarded as a particular kind of dipole–dipole interaction in which a hydrogen atom attached to an electronegative atom (or electron withdrawing group) is attracted to a neighbouring dipole on an adjacent molecule or functional group. These are commonly written D–H··A, where hydrogen atom attached to an electronegative atom such as O or N as the donor (D) and interact with similar electronegative atom, often bearing a lone pair, as the acceptor (A).

	Strong	Moderate	Weak
A—H ··· B interaction	Mainly covalent	Mainly electrostatic	Electrostatic
Bond energy (kJ mol^{-1})	60–120	16–60	<12
Bond lengths (Å)			
H ··· B	1.2–1.5	1.5–2.2	2.2–3.2
A ··· B	2.2–2.5	2.5–3.2	3.2–4.0
Bond angles (°)	175–180	130–180	90–150
Relative IR vibration shift (stretching symmetrical mode, cm^{-1})	25%	10–25%	<10%
^{1}H NMR chemical shift downfield (ppm)	14–22	<14	?
Examples	Gas phase dimers with strong acids/bases	Acids	Minor components of bifurcated bonds
	Proton sponge	Alcohols	C—H hydrogen bonds
	HF complexes	Biological molecules	O—H ··· π hydrogen bonds

Table 2.1 Properties of hydrogen bonded interactions (**A–H** hydrogen bond acid, **B** hydrogen bond base, Adapted from the reference Steed *et al*. 2009).

There are also significant hydrogen bonding interactions involving hydrogen atoms attached to carbon, rather than electronegative atoms such as N and O. Because of its relatively strong and highly directional nature, hydrogen bonding has been described as the

'masterkey interaction in supramolecular chemistry'. Hydrogen bonds come in a wide range of lengths, strengths and geometries and can be divided into three broad categories, the properties of which are listed in Table 2.1. A strong interaction is somewhat similar in character to a covalent bond, whereby the hydrogen atom is close to the centre-point of the donor and acceptor atoms [Steed *et al*. 2009]. Hydrogen bonds are ubiquitous in supramolecular chemistry. In particular, hydrogen bonds are responsible for the overall shape of many proteins, recognition of substrates by numerous enzymes, and (along with π-π stacking interactions) for the double helix structure of DNA etc.

2.2.2.2 Agostic and Anagostic Interactions:

In addition to the intra molecular hydrogen bonding interactions, the other noncovalent interactions were also observed between the metal ion and C-H units. There are two types of such inteactions known in the literature, which are (i) Agostic interaction and (ii) Anagostic interaction. The Agostic interaction in transition metal complexes was first

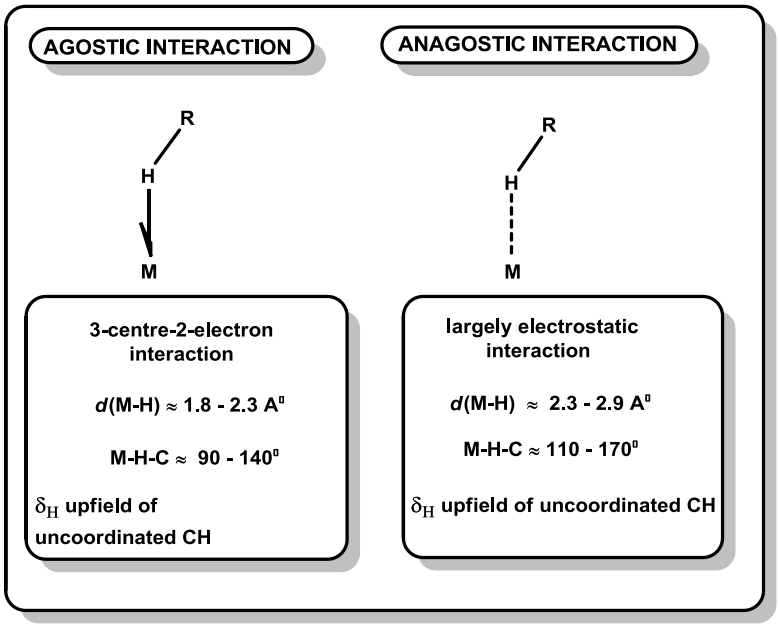

Figure 2.3 The structural and spectroscopic differences between agostic and anagostic interactions (Adapted from the reference Brookhart *et al*. 2007).

reported by Brookhart and co-workers, to describe a specific type of 3-center-2-electron (3c-2e) interaction in which a sigma C-H bond could act as a ligand to transition metal centre. The distance between the metal and the proton are 1.8 to 2.3 Å and the bond angle of M…H-C bond is between 90 and 140 degree. The interactions which are not agostic are called as called as Anagostic interaction, which is mainly of electrostatic interaction, where the bond length distance is 2.3 to 2.9 Å and the bond angle of M…H-C bond is between 110 degree and 170 degree. Furthermore, the chemical shifts of agnostic hydrogen atoms are typically observed upfield of the uncoordinated group, whereas anagostic hydrogen atoms are typically observed downfield; the latter observation is in accord with the hydrogen-bonded description of the interaction [Brookhart *et al*. 2007].

2.3 Objective of Our Work

From the initial part of the discussion it is clear that 5,15-porphodimethenes are an important class of calixphyrin with partially conjugated and non-conjugated character within its framework. The coordination and anion-binding properties of porphodimethenes, in particular, promise to be unique and different, while the structural features of these hybrid systems, containing both sp^2- and sp^3-hybridized bridging *meso* carbon atoms within their frameworks, are sure to be of interest. However, to isolate, 5,15 porphodimethene have proved to be more difficult than porphyrins due to their relative conformational and electronic instability, something that drives to oxidize to the corresponding porphyrin. Dehaen and co-workers used the metal templating strategy to synthesize *meso*-tetraalkyl or dialkylaryl-calix[4]phyrins, however which were difficult to isolate as free-base form, due to high steric strain involved in the formation of tetraalkyl or aryl porphyrinogen intermediate [Dehaen *et al*. 2005]. In this chapter, we describe the synthesis of 5,15-porphodimethene

metal complexes by a single-step metal templating strategy. In addition to the regular spectral analyses, all the complexes were confirmed by X-ray single crystal analysis. The present contribution is focused on the study of noncovalent interactions such as hydrogen bonding and anagostic interactions using 5,15-porphodimethene metal complexes as the platform. The three porphodimethene metal complexes synthesized here provide us a unique opportunity to explore the various noncovalent interactions which are highly decisive in nature when dealing with the basic properties of the complexes. The *meso* substituent was also carefully selected. Double ethyl arms were imparted to the ligand system in order to ensure solubility, flexibility and ability to interact noncovalently. Metals were also selected based on their applicability and coordination behavior. Ni(II), Pd(II), and Zn(II) ions were selected because of their wide application in the field of catalysis and biochemistry. Apart from the series of noncovalent interactions, the anagostic interaction explored here is hitherto unknown in porphyrin chemistry in general and calixphyrin chemistry in particular. Furthermore, Zn(II) and its axial water coordinated complex of 5,15-porphodimethene is not known in the literature.

2.4 Results and Discussion

2.4.1 Synthesis and characterization

The syntheses of the complexes were achieved in three steps (Scheme 2.5).The first Step involves the treatment of excess of pyrrole (**4**) with 3-pentanone (**5**) at room temperature afforded the corresponding diethyl dipyrromethane (**3**) in 55% yield. The second step involves the mono formylation of the dipyrromethane obtained. It was achieved by Clezy modified Vilsmeier Hack formylation. The purified mono-formyl dipyrromethane **(2)** is treated with the corresponding metal acetates in the third step. The final step involves

the synthesis of the complexes **1a-1c′** by metal template strategy in which stirring a methanol solution of 1-formyl-5,5-di(ethyl)dipyrromethane (**2**) [Orlewska *et al*. 2005] with acetates of nickel, palladium and zinc in the presence of *p*-toluenesulphonic acid as acid-catalyst afforded Ni (**1a**) and Pd (**1b**) in 30% and 35% yield, respectively. On the other hand, the corresponding Zn complex (**1c**) was obtained in 1% yield due to the formation of axial-water coordinated polymorph **1c′**(10%) and other higher derivatives.

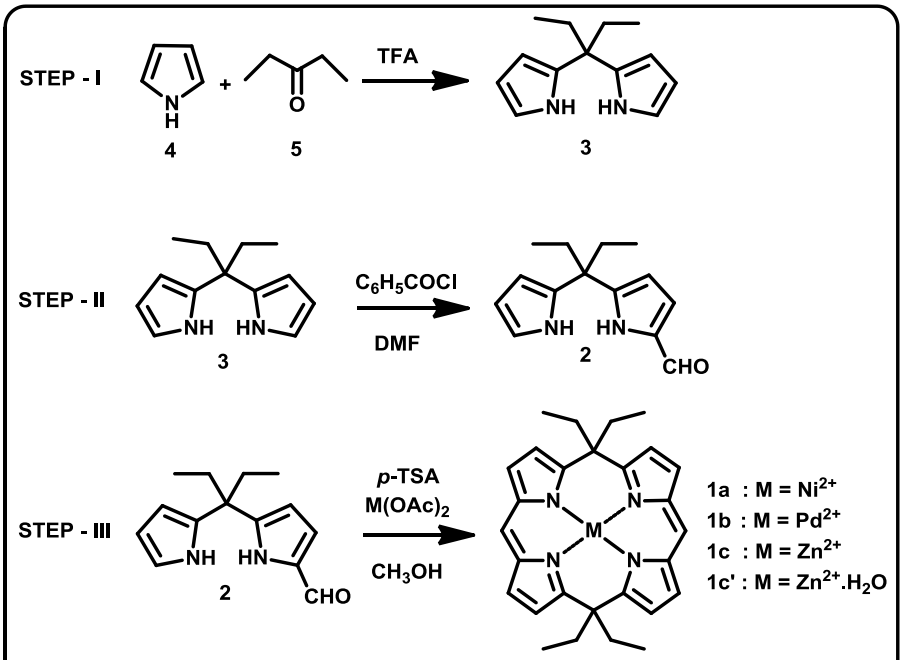

Scheme 2.5 Syntheses of porphodimethene metal complexes **1a-1c′**

The identity of the complexes were characterized and confirmed by electronic spectral studies, ^{1}H NMR spectroscopy, ESI-MS analysis and single crystal X-ray analysis. The ESI-MS spectral analyses of all the metal complexes **1a-1c′** shows the isotopically resolved signals at m/z 481.1964 (Calcd for $[(C_{28}H_{30}N_4Ni)]^+$ = 480.1823), 529.1683 (Calcd for $[(C_{28}H_{30}N_4Pd)]^+$ = 528.1505), 486.1914 (Calcd for $[(C_{28}H_{30}N_4Zn)]^+$ = 486.1761) and 487.1820 (Calcd for $[(C_{28}H_{32}N_4OZn)]^+$ = 504.1867) respectively. The single crystals of all

the complexes (**1a**, **1b, 1c, 1c′**) were grown at room temperature by vapour diffusion technique in CH_2Cl_2/n-hexane solvent combination.

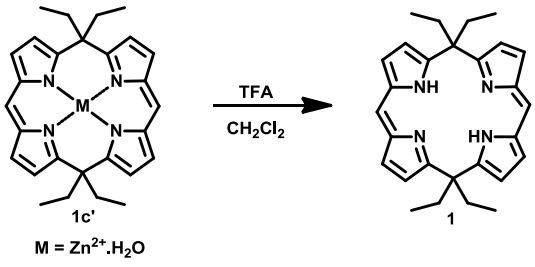

Scheme 2.6 Syntheses of 5,15-porphodimethene free base (**1**)

The free-base porphodimethene can be obtained by de-metallation of the metal complexes (Scheme 2.6). Acid catalyzed de-metallation of water co-ordinated zinc porphodimethene(**1c′**) in presence of TFA in CH_2Cl_2 yielded 5,15-porphodimethene free base (**1**). Free base (**1**) was purifed from the reaction mixture through column chromatography using basic alumina and n-hexane as elutent. The 5,15-porphodimethene free base (**1)** was characterized through ^{1}H NMR spectroscopy, ESI-MS analysis. The ESI-MS spectral analyses gave isotopically resolved signals at m/z 425.2701 the theorectically calculated m/z value for $[(C_{28}H_{32}N_4)]^+$ is 424.2627. This synthetic route for the 5,15-porphodimethene is more efficient and convenient as compared to conventional synthesis of the free base.

2.4.1.1 NMR Analyses

^{1}H NMR spectra of **1a**-**1c′** were recorded in $CDCl_3$ at room temperature and shown in Figure 2.4. The *meso* –CH protons are resonated as a sharp singlet in the range 6.71 – 6.94 ppm. The doublets centered at 6.44 to 6.78 ppm correspond to pyrrolic β-CH protons. The

ethyl protons are observed as quartet around 2.05 ppm and triplet around 0.66 to 0.84 ppm, respectively. Furthermore, as compared to 1-formyl-5,5-di(ethyl)dipyrromethane **2**, the absence of pyrrolic α-CH, NH protons which are observed at 6.91 ppm for pyrrolic α-CH and 7.80 to 8.90 ppm for pyrrolic NH signals, in addition, the upfield shift of the 1-formyl –CH signals suggests the formation of the macrocycle with metal ion insertion. The disappearance of the signals corresponding to pyrrolic α-CH, NH protons along with upfield shift of the 1-formyl –CH signals suggests the formation of the macrocycle with metal ion insertion. For example, the ^{1}H NMR spectrum of **1b** shows the *meso*-CH protons as singlet at 6.94 ppm, the pyrrolic β-CH protons resonate at 6.93 and 6.40 ppm, while the ethyl protons are at 2.05 and 0.82 ppm, respectively.

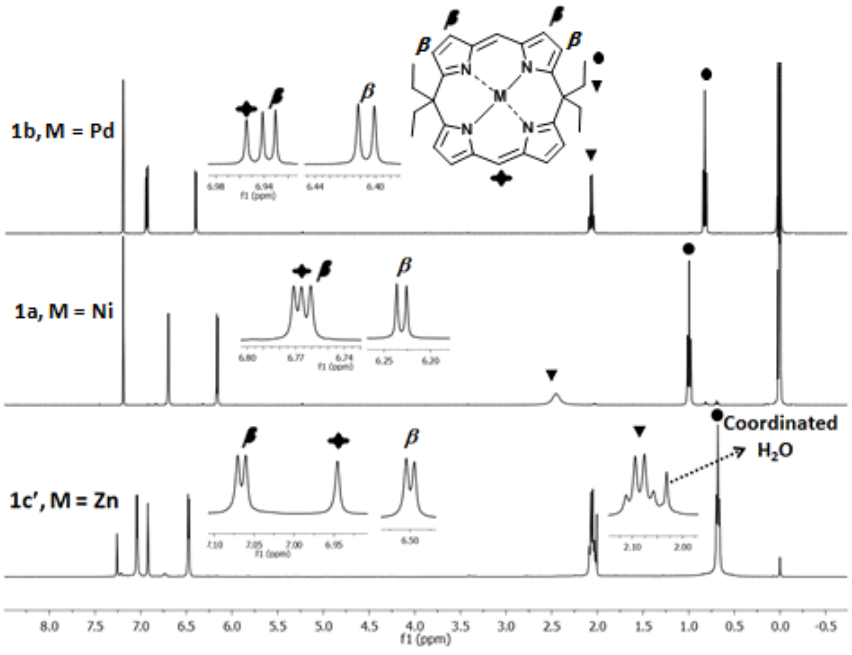

Figure 2.4 The stacked ^{1}H NMR spectra of **1a, 1b** and **1c′**

2.4.1.2 Electronic Spectral Analyses

The electronic spectral analysis of the complexes (**1a-1c′**) in $CHCl_3$ consists of a lesser and a more intense band or vice versa from 386 to 518 nm, suggesting the π–π* transition. For

example, **1a** shows an absorption maxima at 423 nm with shoulder around 518 nm; on the other hand, **1b** shows a broad band at 386 nm with an intense band at 472 nm (Figure 2.5).

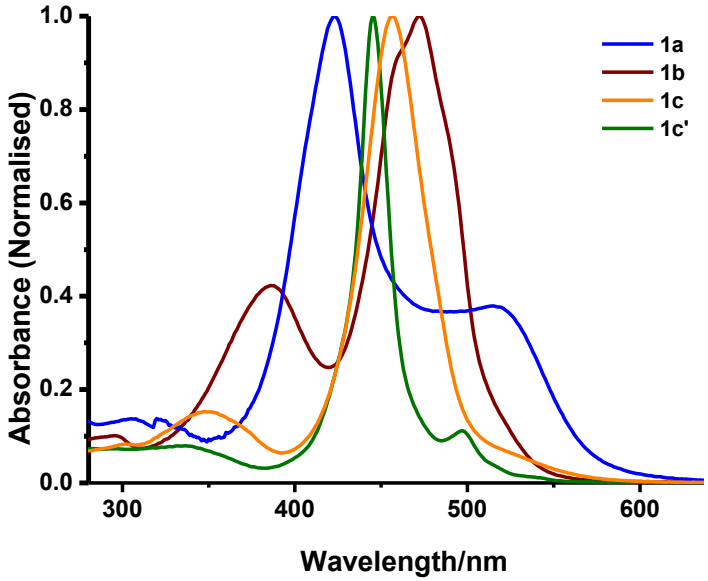

Figure 2.5 Normalized absorption spectra of **1a, 1b, 1c** and **1c′** in $CHCl_3$

The molar extinction coefficient values of the complexes are summarized in Table 2.2 suggests that the intense bands are around 2.5 fold higher than the broad ones. All the metal complexes have practically no emission.

Metal complex	**λ_1 /nm (ε/$M^{-1}cm^{-1}$)**	**λ_2 /nm (ε/$M^{-1}cm^{-1}$)**
1a	**423 (1.92 x 10^4)**	**518 (7.65 x 10^3)**
1b	**386 (2.3 x 10^4)**	**472 (5.39 x 10^4)**
1c	**349 (2.75 x 10^3)**	**456 (1.83 x 10^4)**
1c′	**445 (7.15 x 10^4**	**496 (2.88 x 10^4)**

Table 2.2 Electronic spectral data and molar absorption coefficient values of **1a-1c′**

2.4.2 Structural features of metal complexes

2.4.2.1 Structural features of Porphodimethene Nickel complex (1a)

Investigating the structural features of **1a** by ^{1}H NMR analysis and single crystal X ray analyses revealed that **1a** was found to show a rare case of **M···H–C** anagostic interactions in addition to the normal hydrogen bond interactions.

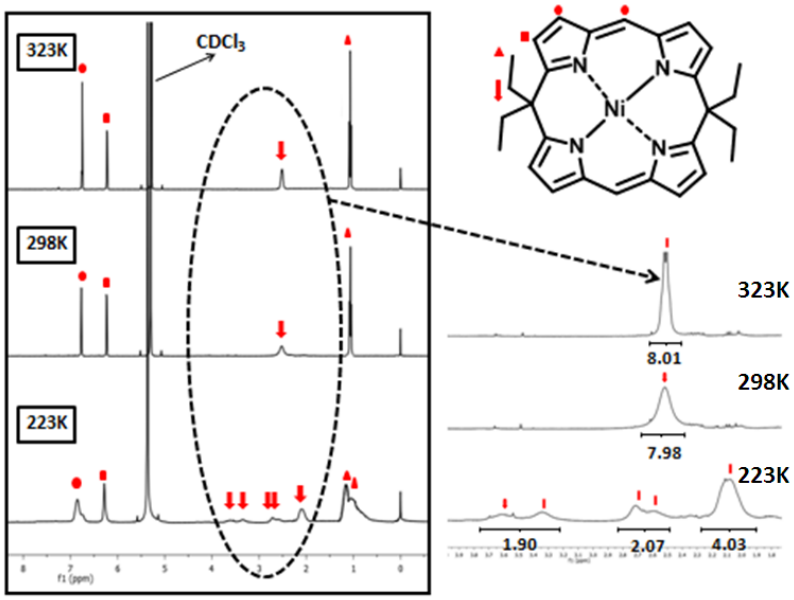

Figure 2.6 Temperature dependent ^{1}H NMR spectral changes of **1a**. The inset shows the expanded methylene proton signals.

In addition to the regular pattern as that of **1b**, where the methylene protons in the *meso*-ethyl unit appears as a quartet, however, the methylene protons in **1a** resonate as a broad peak at 2.46 ppm, which is 0.41 ppm downfield shifted as compared to **1b**, suggest that the methylene protons are involved in noncovalent interactions, which are shown in Figure 2.6 and 2.7. This was further investigated by the temperature dependent NMR measurements. Upon increasing the temperature from 298 to 323 K, the broad peak at 2.47 ppm converts into

quartet. On the other side, upon lowering the temperature from 298 to 223 K, the broad peak converts into five broad singlets from 2.07 to 3.60 ppm.

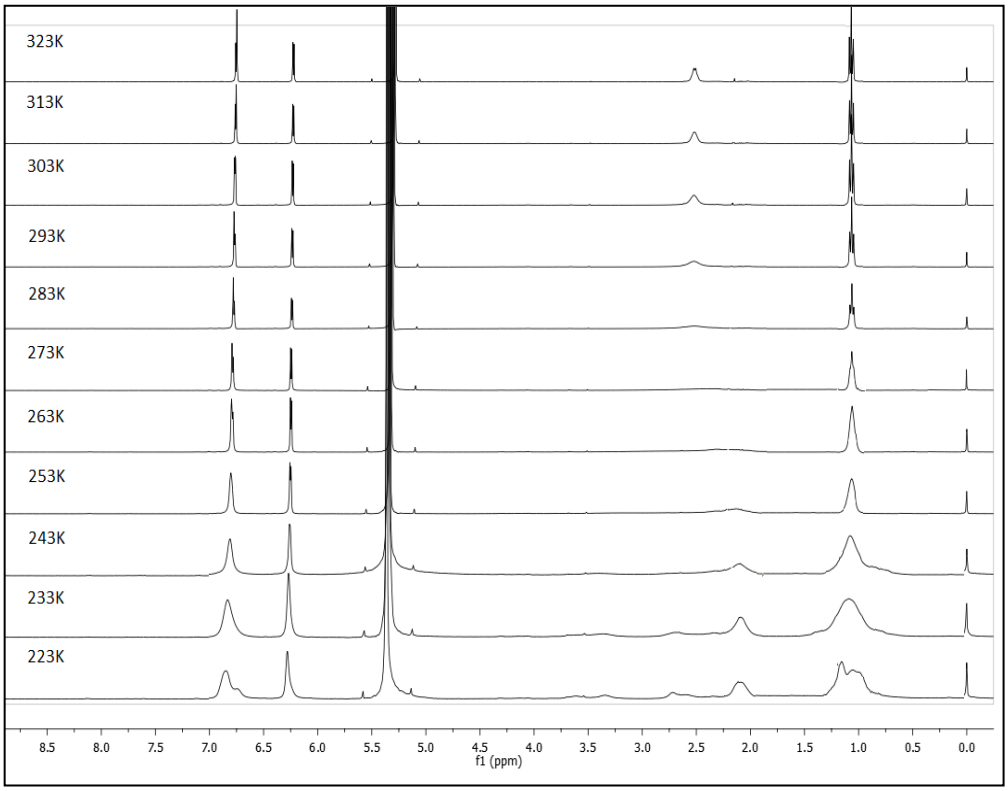

Figure 2.7 Variable temperature ^{1}H NMR spectra of **1a** in CD_3CN

While excavating the structural features of all the complexes, it was found that **1a** is embedded with multiple types of noncovalent interactions involving the hydrogen atoms. The single crystal X-ray structure of **1a** is shown in Figure 2.8 A and B, where one of the *meso*-ethyl units (C1-H1A) shows an unusual electrostatic interaction with the Ni centre. The distance and angle of C1-H1A…Ni is 2.72 Å and 130°, respectively. As evident from the literature, these interactions in which a hydrogen atom is held close to a metal centre are termed as anagostic or pre-agostic interactions. Such interactions are characterized by **M···H** distance ranging from 2.3 to 2.9 Å and **M···H–C** bond angle of 110^{o} to 170^{o} with a NMR downfield shift for the **M···H–C** proton.

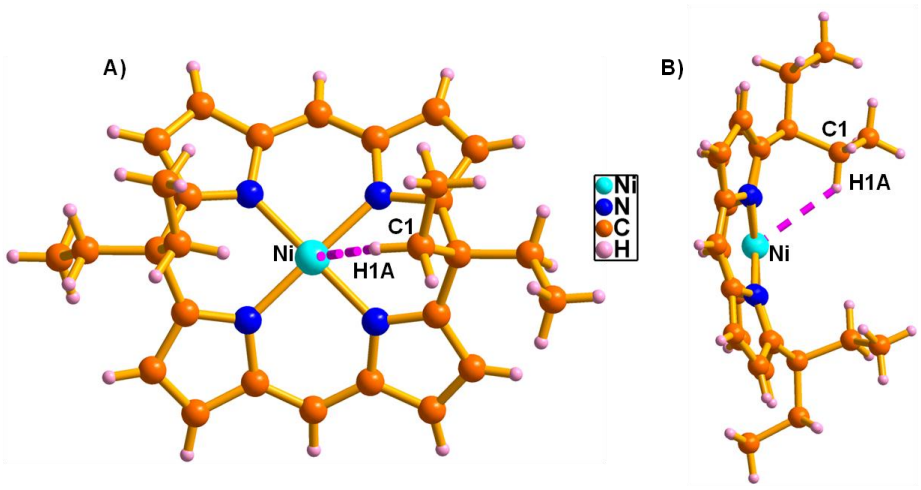

Figure 2.8 Single crystal X-ray structure of **1a**. A) **1a** top view; B) **1a** side view with anagostic interaction.

In addition to such interaction, **1a** shows strong intermolecular hydrogen bonding interactions, where *meso*-hydrogen of one unit (C10-H10) interacts with Ni of another unit to generate the self-assembled dimer (Figure 2.9A) and also generates the 1-D array, where one unit of pyrrolic β-CH (C18-H18) interacts with next unit pyrrolic π cloud.

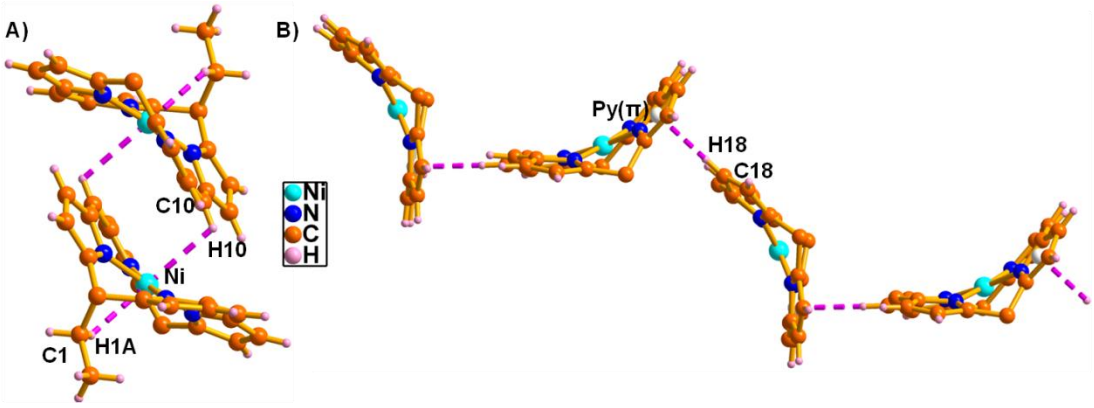

Figure 2.9 Single crystal X-ray analysis of **1a**. A) Self-assembled dimer and B) 1-D array. The *meso*-di-ethyl units are omitted for clarity.

The distances and angles of self-assembled dimer (C10-H10..Ni) and 1-D array (C18-H18…Py(π)) are 2.84 Å, 105° and 2.67 Å and 163°, respectively (Figure 2.9). Overall, the β anagostic interaction between the ethyl group and the nickel centre is leading to the

lowering of symmetry and *distortion* of the molecule as evident from the low temperature NMR and crystal structure analysis of **1a**. The hydrogen bonding interaction leads to *dimerisation* as well as self-assembled 1-D *array formation* of **1a**.

2.4.2.2 Structural features of porphodimethene Zinc complex (1c)

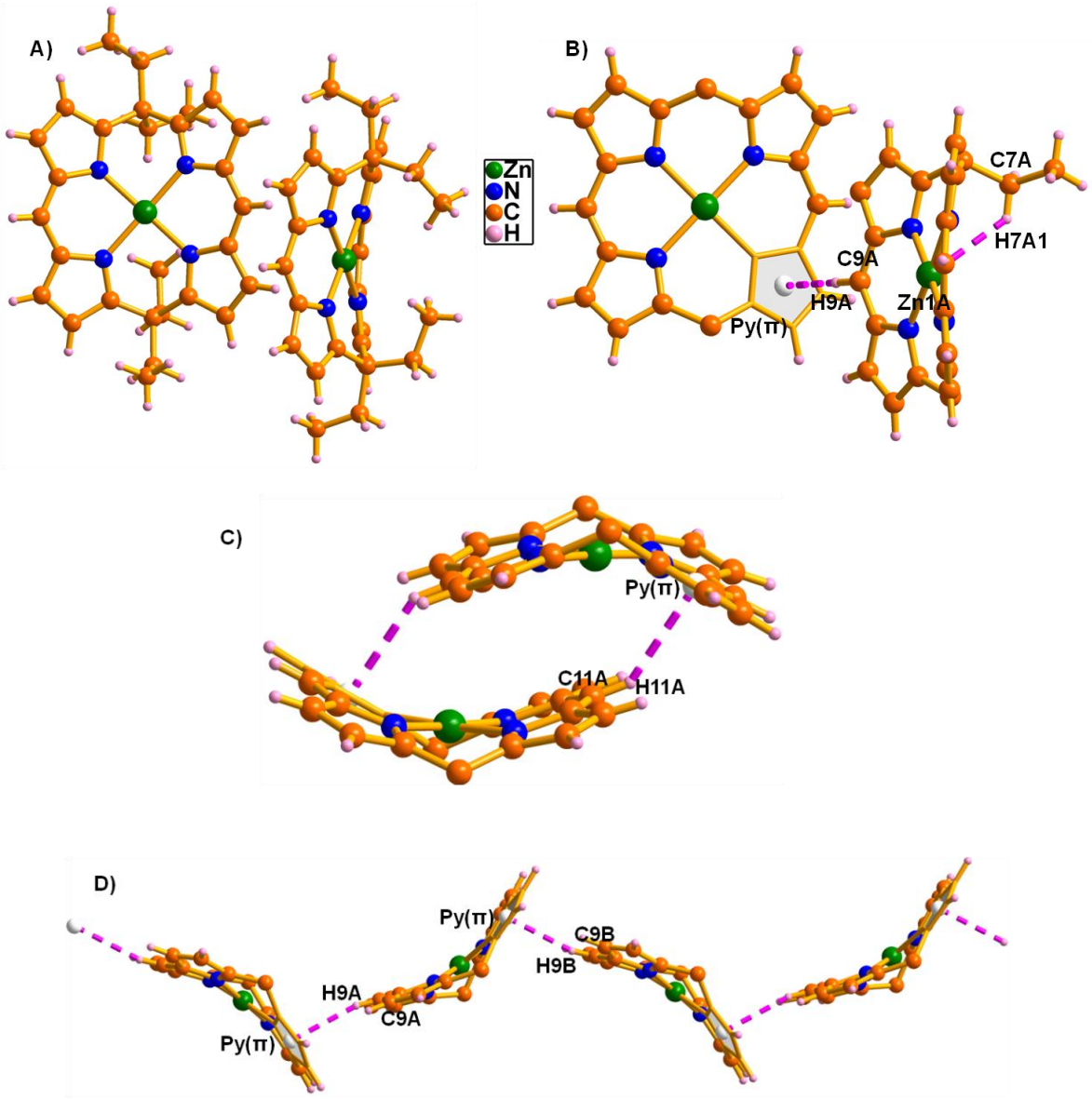

Figure 2.10 Single crystal X-ray structure of **1c**. A) Top view; B) side view with intra- and intermolecular hydrogen bonding interactions; C) self-assembled dimer and D) 1-D array. The units which are not involved in the hydrogen bonding interactions are omitted for clarity.

The single crystal X-ray structure of **1c** is shown in Figure 2.10. As observed in **1b**, the unit cell of **1c** also contains two units of respective metal complexes, which are perpendicular to each other (Figure 2.10A). These two units are connected through intermolecular hydrogen bonding interaction, where *meso*-hydrogen (H9A) of the second unit interacts with pyrrolic π cloud of the first unit and generates the dimeric complexes. In addition, there is an intramolecular hydrogen bonding interaction in the second unit between one of the *meso*-ethyl unit (C7A-H7A) with Zn1A. The distances and angles of C9A-H9A…Py (π) and C7A-H7A…Zn1A are 2.84 Å, 165° and 2.84 Å and 130°, respectively (Figure 2.10B). The latter interactions are well within the anagostic or pre-agostic interaction as observed in **1a**. The single crystal analysis of **1c** also generates the self-assembled dimer as well as the one-dimensional array. The self-assembled dimer is formed from one of the two metal complexes from the unit cell, where *meso*-hydrogen (H11A) are in intermolecular hydrogen bonding interaction with the pyrrolic π cloud, the distance and angle (C11A-H11A…Py (π)) is 2.78 Å, 141° (Figure 2.10C).

On the other hand, both the metal complexes present in the unit cell combinedly generate the 1-D array through the intermolecular hydrogen bonding interaction, where *meso*-hydrogen (C9B) of the first unit interacts with the pyrrolic π-cloud of the second unit. The distance and angle of C9B-H9B…Py (π) is 2.82 Å and 165°, respectively. Thus in short, the hydrogen bond interactions in **1c** play a key role in dimerisation and 1-D array formations as in the case of **1a**.

2.4.2.3. Structural features of Porphodimethene Palladium complex (1b)

The single crystal analysis of **1b** reveals that two units of metal complexes are present in the unit cell (Figure 2.11A), where both the units are perpendicular to each other and are

connected through the strong intermolecular hydrogen bonding interactions, where one unit *meso*-hydrogen (C5-H5) and the pyrrolic β-hydrogen (C7-H7) interact with the second unit Pd metal (Pd2) and pyrrolic π-cloud Py(π) and generate the dimeric complexes with the distances and angles of C5-H5…Pd2 and C7-H7…Py(π) are 2.89 Å, 157° and 1.70, Å, 162° respectively, as shown in Figure 2.11B. The distance between two Pd in **1b** is 7.07 Å. Unlike **1a**, **1b** lacks the formation of self-assembled dimer and 1D array interaction. As evident from the crystal structure and the NMR spectral analyses, due to the absence of anagostic interaction, **1b** generates a more symmetric structure.

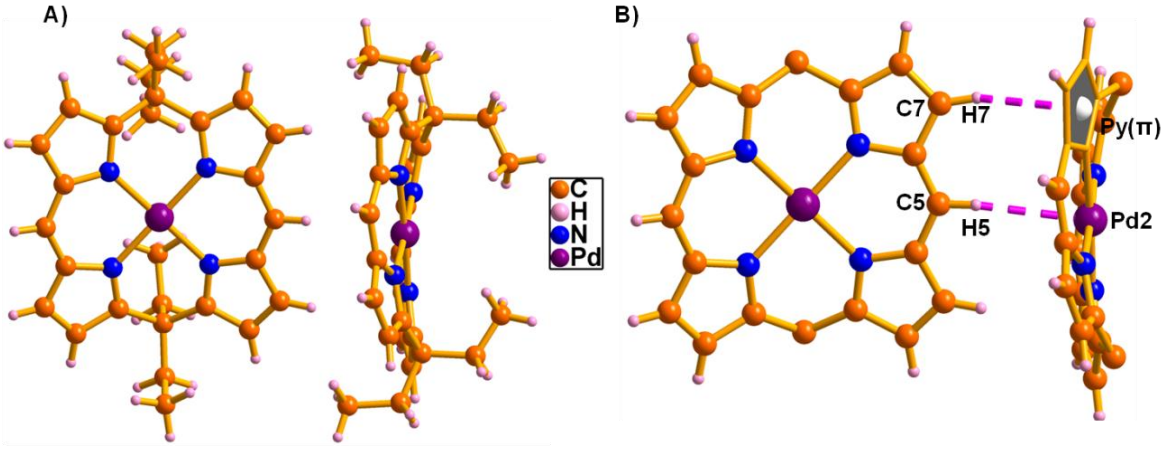

Figure 2.11 Single crystal X-ray structure of Single crystal X-ray structure of **1b** by slow evaporation of CH_2Cl_2 / *n*-Hexane. A) Top view and B) side view with intermolecular hydrogen bonding interactions. The units which are not involved in the hydrogen bonding interactions are omitted for clarity in the side view.

2.4.2.4. Structural features of 1c′

NMR analyses of **1c′** shows the regular pattern as that of **1b** and the axial water protons are resonated as a broad singlet at 2.01 ppm, which is further confirmed by D_2O exchange experiment. The single crystal X-ray structure of **1c′**, its 1D-array and 2D-array is shown in Figures 2.12, 2.13 and 2.14.

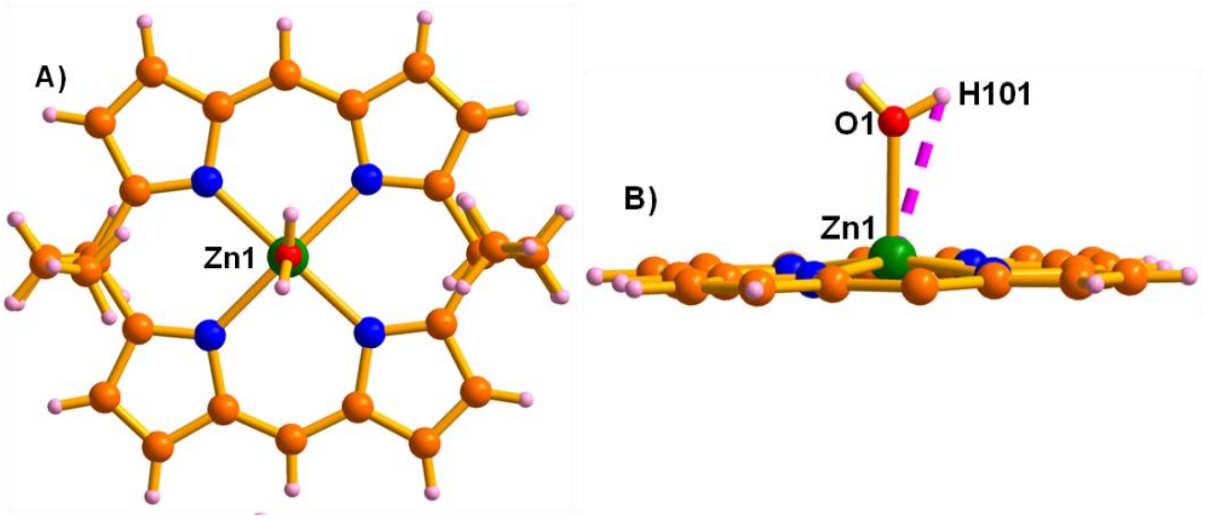

Figure 2.12 Single crystal X-ray structure of **1c′** . A) Top view; B) side view, where the *meso* di-ethyl groups are omitted for clarity.

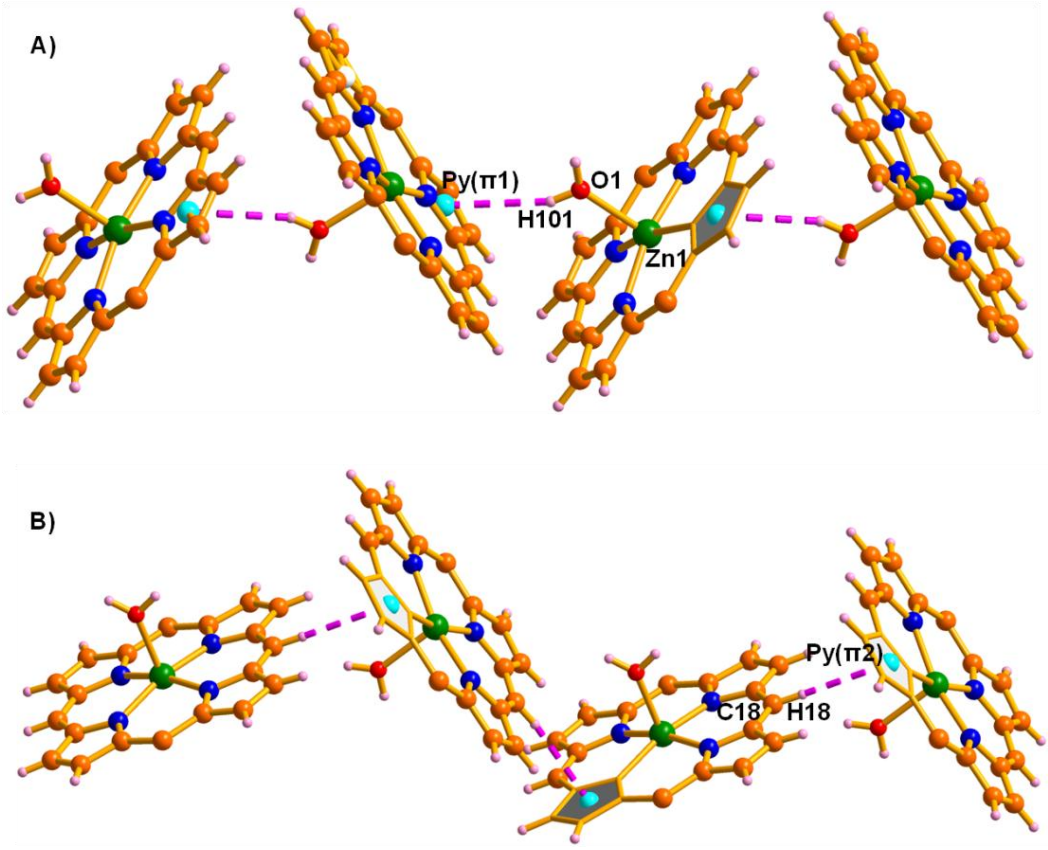

Figure 2.13 1-D arrays of **1c′**. The units which are not involved in the hydrogen bonding interactions are omitted for clarity.

As predicted from the NMR spectral analysis, Zn1 in **1c** is further coordinated to the H_2O molecule to generate **1c′**. One of the hydrogens in the H_2O molecule is in intramolecular hydrogen bonding with Zn1 with a distance of 2.71Å which is shown in Figure 2.12B. Unlike **1c**, the coordinated H_2O molecule pushes the Zn1 to center of the cavity and generates a planar structure which is unprecedented in the calixphyrin coordination chemistry. Zn1 is 0.23Å above the plane of the four nitrogens and 0.26Å above the mean plane of the macrocyclic ring. The crystal analysis of **1c′** generates two 1D-intermolecular hydrogen bonding interactions (Figure 2.13), which are between; (i) one of the hydrogen atoms (H101) in the coordinated H_2O molecule with one of the pyrrolic-π [Py1(π)] clouds (Figure 2.13A), and (ii) one of the *meso*-CHs (C18-H18) with another pyrrolic-π (Py2(π)] cloud. The distances and angles of O1-H101…Py1(π) and C18-H18…Py2(π)] are 2.81, 2.88 Å and 161°, 171°(Figure 2.13B) respectively.

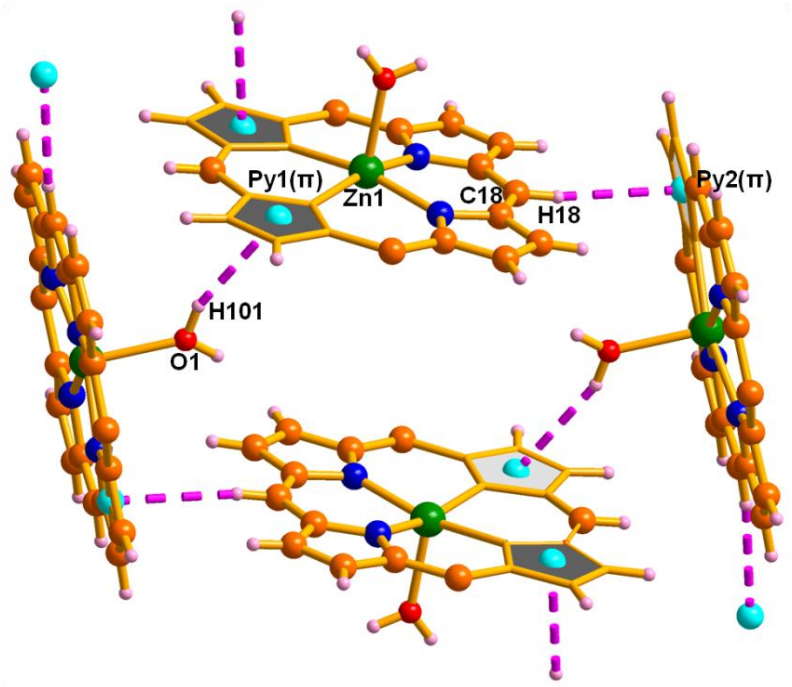

Figure 2.14 2-D supramolecular assembly of **1c′**. The *meso* di-ethyl groups are omitted for clarity.

Combining the two 1D- arrays, **1c′** generates two dimensional supramolecular assembly in the solid state which is shown in Figure 2.14. As evident from the NMR and crystal structure, **1c′** lacks any type of anagostic interactions due to the stronger interaction of the Zinc metal centre with the coordinated apical water molecule.

2.5 Conclusion

In summary, transition metal complexes (Ni, Pd, and Zn) of 5,15-porphodimethene have been successfully synthesized through a single-step metal templated synthetic strategy. All the metal complexes have been well characterized through NMR, ESI-MS and single crystal X-ray analysis XRD. The free base porphodimethene has been obtained by demetallation of the metal complexes is an efficient and simple way as compared to conventional methods for the synthesis of the free base.

The structural features of the metal complexes have been closely studied. In summary, the noncovalent interactions, like hydrogen bonding and anagostic interactions, play a decisive role in the structure, geometry and properties of metal complexes. We have successfully explored the role of the noncovalent interactions governing the structure and stability of metal incorporated 5,15-porphodimethene. Investigation of the crystal structure revealed that **1a** and **1c** were found to show a rare case of **M···H–C** anagostic interactions in addition to the normal hydrogen bonding interactions for the first time. The extra coordinated water molecule in **1c′** converts the roof like conformer to a planar form which is hitherto unknown in calixphyrin metal complexes. Overall, the anagostic interaction leads to structural distortions while the hydrogen bonding interactions lead to dimerisations and array formations. These interactions may find potential application in H-activation, catalytic applications and the receptor properties of these complexes.

2.6 Experimental Section

2.6.1 General Information

The reagents and materials for synthesis were used as obtained from Sigma - Aldrich chemical suppliers. All solvents were purified and dried by standard methods prior to use. NMR solvents were used as received. The NMR spectra were recorded with Bruker 400 MHz spectrometer with TMS as internal standard. ESI mass spectra were recorded on Bruker, microTOF-QII mass spectrometer. FAB mass spectra were obtained on a JEOL SX-120/DA6000 spectrometer using argon (6 KV, 10 mA) as the FAB gas. Electronic absorption spectra were recorded with Perkin Elmer – Lambda 750 UV-Visible spectrophotometer and data analyses were done using the UV-winlab software package. X-ray quality crystals for the compounds were grown by the slow diffusion of *n*-hexane over CH_2Cl_2 solution of the metal complexes. Single-crystal X-ray diffraction data of **1a**, **1c** and **1c′** were collected on a Bruker KAPPA APEX-II, four angle rotation system, MoKα radiation (0.71073 Å). The single crystal X-ray diffraction data of **1b** was collected on a Bruker AXS Kappa Apex 2 CCD diffractometer at 293(2) K. All experiments were carried out at room temperature (25 ±1°C), unless otherwise mentioned.

2.6.2 Synthesis

2.6.2.1 Synthesis of 5,5-di(ethyl)dipyrromethane (3)

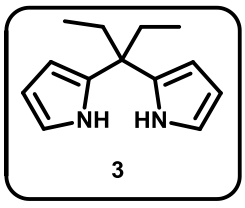

3

Pyrrole **4** (15.5 g, 0.23 mol) and 3-pentanone **5** (1 g, 0.01mol) were stirred under nitrogen atmosphere for 10 min at room temperature. Trifluoroacetic acid **TFA** (0.177 mL, 2.3 mmol) was added to the above mixture and the solution was stirred at room temperature for 45 min. After removal of

the solvent, the crude product was purified by silica gel column chromatography (100–200 mesh). Column eluted with ethyl acetate : petroleum ether (1:99) gave colourless crystalline solid identified as **3**. Yield: 55%. ^{1}H NMR (400 MHz, $CDCl_3$, 298 K): δ = 7.6 (brs, 2H, pyrrolyl NH), 6.57 (s, 2H, α-pyrrolyl CH), 6.11 (s, 4H, β-pyrrolyl CH), 1.95-1.91 (q, 4H, CH_2 H), 0.7-0.67 (t, 6H, methyl H). FAB mass (m/z): Calcd for $C_{13}H_{18}N_2$: 202.15; Found : 202.77.

2.6.2.2 Synthesis of 1-formyl-5,5-di(ethyl)dipyrromethane (2)

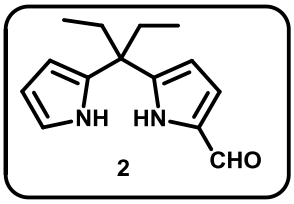

2

To a stirred solution of dipyrromethane **3** (1.15 g, 5 mmol) in 10 mL of dry DMF cooled with ice-water bath was added dropwise a solution of benzoyl chloride (0.75 g, 5.4 mmol) in 2 mL of DMF under Ar. The mixture was stirred for 30 min at 0^{o}C, and then allowed to warm to room temperature for 1.5 h. The solution was then diluted with Et_2O (50 mL) and extracted with water (3 x 15 mL), washed with Et_2O (1 x 10 mL), adjusted to pH 8 with Na_2CO_3 solution, left overnight, cooled and the yellow precipitate was filtered off. The crude product was purified by silica gel column chromatography eluted with ethyl acetate: petroleum ether. The solvent was evaporated by rotary evaporator gave 0.75g (58%) of compound **2** as cream-white crystals. Spectral data for **2**: ^{1}H NMR (400 MHz, $CDCl_3$, 298 K): δ =9.3 (s, 1H, aldehyde CH), 8.9 (brs, 1H, pyrrolyl NH), 7.8 (brs, 1H, pyrrolyl NH), 6.91-6.90 (q, 1H, α-pyrrolyl CH), 6.69-6.68 (m, 1H, β-pyrrolyl CH), 6.24-6.22 (q, 1H, β-pyrrolyl CH), 6.15-6.11 (m, 2H, β-pyrrolyl CH), 2.06 -1.94 (q, 4H, CH_2 H), 0.75-0.71 (t, 6H, methyl H). FAB mass (m/z) : Calcd for $C_{14}H_{18}N_2O$: 230.30. Found : 231.70.

2.6.2.3 Synthesis of the metal complexes of 1 (1a - 1c′)

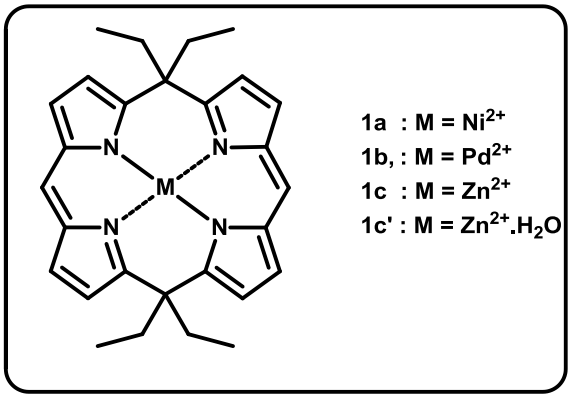

A solution of monoformyldipyrromethane **2** (100 mg, 1 mmol) in 15 mL of methanol was degassed with nitrogen gas and stirred at room temperature for 30 min, then a solution of *p*-toluenesulfonic acid (38 mg, 0.2 mmol) in 2 mL of methanol was added and stirring continued for 5 min. A solution of $M(OAc)_2 \cdot 4H_2O$ (1.0 mmol) in 10 mL of methanol was added and the mixture was stirred for 8 h, then 40 mL of water was added and the mixture was extracted with CH_2Cl_2 (40+20 mL), the combined organic layers were washed with $NaHCO_3$ solution, water, brine and dried over Na_2SO_4. The solvents were evaporated and the residue was purified by silica gel column chromatography (hexane–CH_2Cl_2) to afford corresponding metal complexes. The nickel **1a** and palladium **1b** calixphyrin complexes gave 30% and 35% yield, respectively. The yield of **1c** and **1c′** were 1% and 10%, respectively.

2.6.2.4 Synthesis of free base calix[4]phyrin (1)

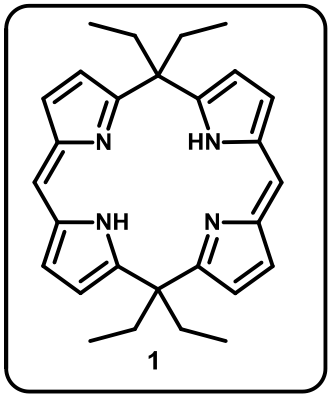

A solution of **1c'** (5 mg, 9.9 mmol) in 10 mL of CH_2Cl_2 was degassed with nitrogen gas and stirred at room temperature for 5 min. Then, a solution of trifluoroacetic acid (1 mL, 1.29 mmol) was added and stirring continued for an hour. The reaction mixture was queched with triethylamine (5 mL) and water (15 mL). The reaction mixture was extracted with CH_2Cl_2 and the combined organic layers were washed with $NaHCO_3$ solution, water, brine and dried over

Na_2SO_4. The solvents were evaporated, purified through column chromatography using basic alumina and n-hexane as eluent, afforded **1** in quantitative yield as yellow colored compound.

2.6.3 Spectral Data

Spectral data for **1a**: ^{1}H NMR (400 MHz, $CDCl_3$, 298 K): δ = 6.71 (s, 2H, meso CH), 6.71 - 6.70 (d, J = 4 Hz, 4H, pyrrolic β CH), 6.18 - 6.16 (d, J = 4 Hz, 4H, pyrrolic β CH), 2.46 (brs, 8H, methylene H), 1.02 – 0.99 (t, 12H, methyl H). ^{13}C NMR (100 MHz, $CDCl_3$, 298K, TMS): δ =164.13, 135.24, 130.64, 128.47, 116.20, 47.38, 29.71, 9.92. MS (ESI): m/z Calculated for $[(C_{28}H_{30}N_4Ni)]^+$ = 480.1824; found = 481.1964.

Spectral data for **1b**: ^{1}H NMR (400 MHz, $CDCl_3$, 298K): δ = 6.94 (s, 2H, meso CH), 6.93-6.92 (d, J = 4 Hz, 4H, β pyrrolic H), 6.40-6.39 (d, J = 4 Hz, 4H, pyrrolic β CH), 2.09 – 2.04 (q, 8H, methylene H), 0.84 – 0.80 (t, 12H, methyl H). ^{13}C NMR (100 MHz, DMSO-d_6, 298K): δ = 160.31, 133.22, 131.90, 130.26, 116.75, 50.15, 35.38, 10.46. MS(ESI): m/z calculated for $[(C_{28}H_{30}N_4Pd)]^+$ = 528.1505; found = 529.1683.

Spectral data for **1c**: MS (ESI): m/z calculated for $[(C_{28}H_{30}N_4Zn)]^+$ = 487.1762; found = 486.1914.

Spectral data for **1c′**: ^{1}H NMR (400 MHz, $CDCl_3$, 298 K): δ = 7.06 – 7.04 (d, J = 4 Hz, 4H, pyrrolic β CH), 6.92 (s, 2H, meso H), 6.48 - 6.47 (d, J = 4 Hz, 4H, pyrrolic β CH), 2.09 – 2.03 (q, 8H, methylene H), 2.01 (s, 2H, axial H_2O molecule), 0.70 – 0.66 (t, 12 H, methyl H). MS(ESI): m/z Calculated for $[(C_{28}H_{32}N_4OZn)]^+$ = 504.1867 ; observed = 487.5171.

Spectral data for **1**: ^{1}H NMR (400 MHz, $CDCl_3$, 298 K): δ =13.114 (brs, 2H, NH), 6.91 - 6.90 (d, J = 4Hz, 4H, pyrrolic β CH), 6.79 (s, J = 2H, meso CH), 6.39 - 6.38 (d, J = 4 Hz, 4H, pyrrolic β CH), 2.12 - 2.09 (q, 8H, methylene H), 0.77 - 0.74 (t, 12H, methyl H). MS (ESI): m/z Calculated for $[(C_{28}H_{32}N_4)]^+$ = 424.2627; found = 425.2701.

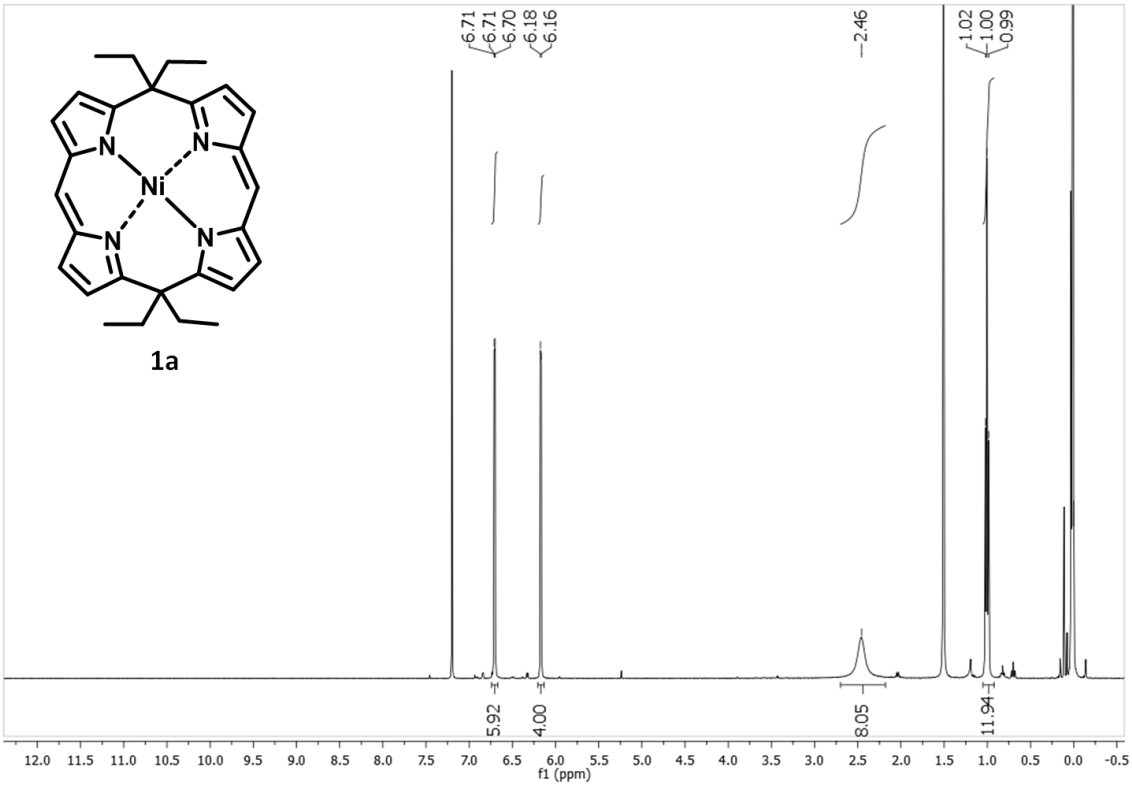

1a

Figure 2.15 ^{1}H NMR spectrum of **1a** in $CDCl_3$

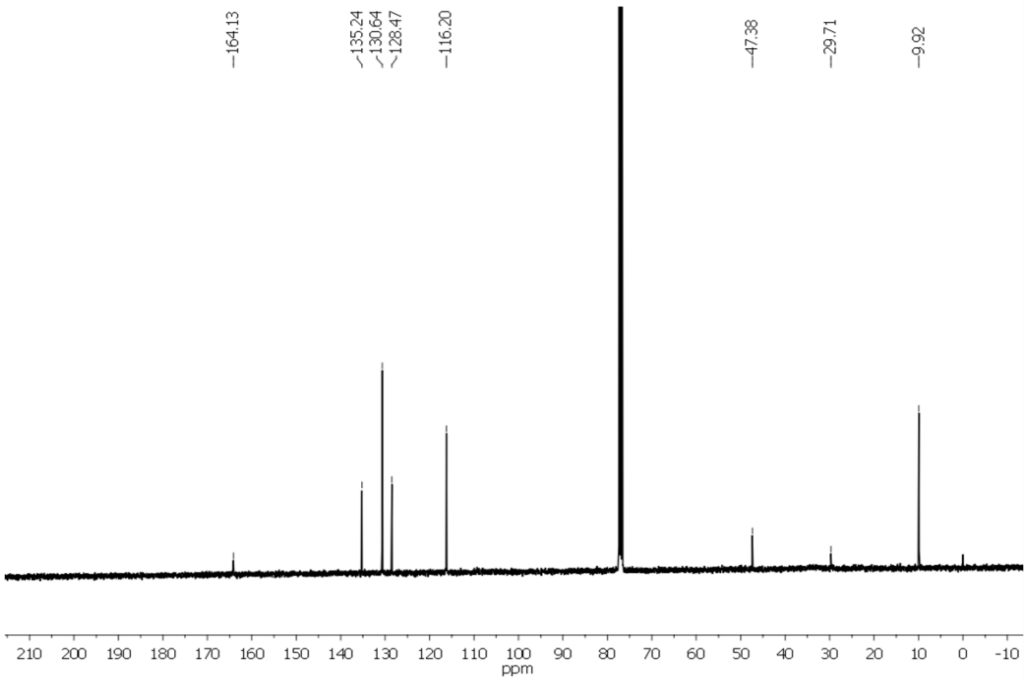

Figure 2.16 ^{13}C NMR spectrum of **1a** in $CDCl_3$

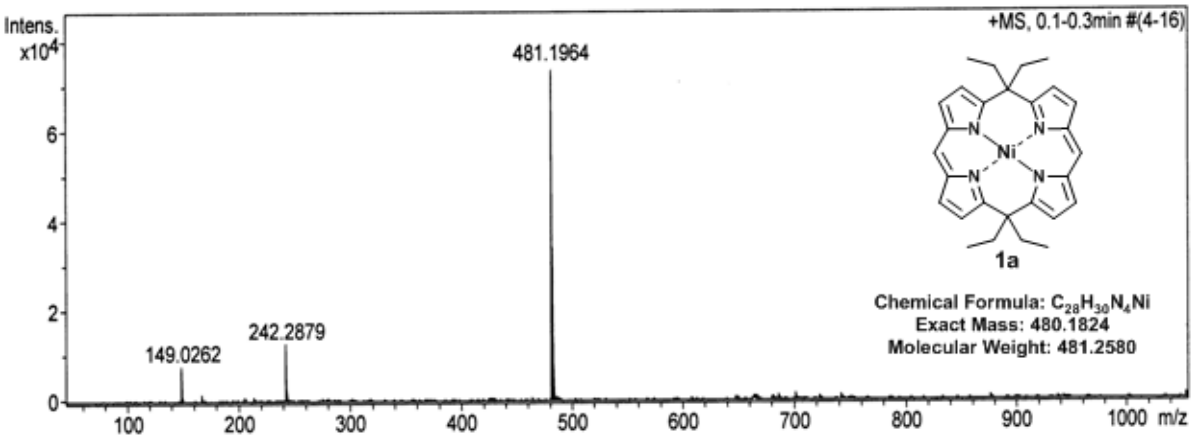

Figure 2.17 ESI-Mass spectrum of **1a**

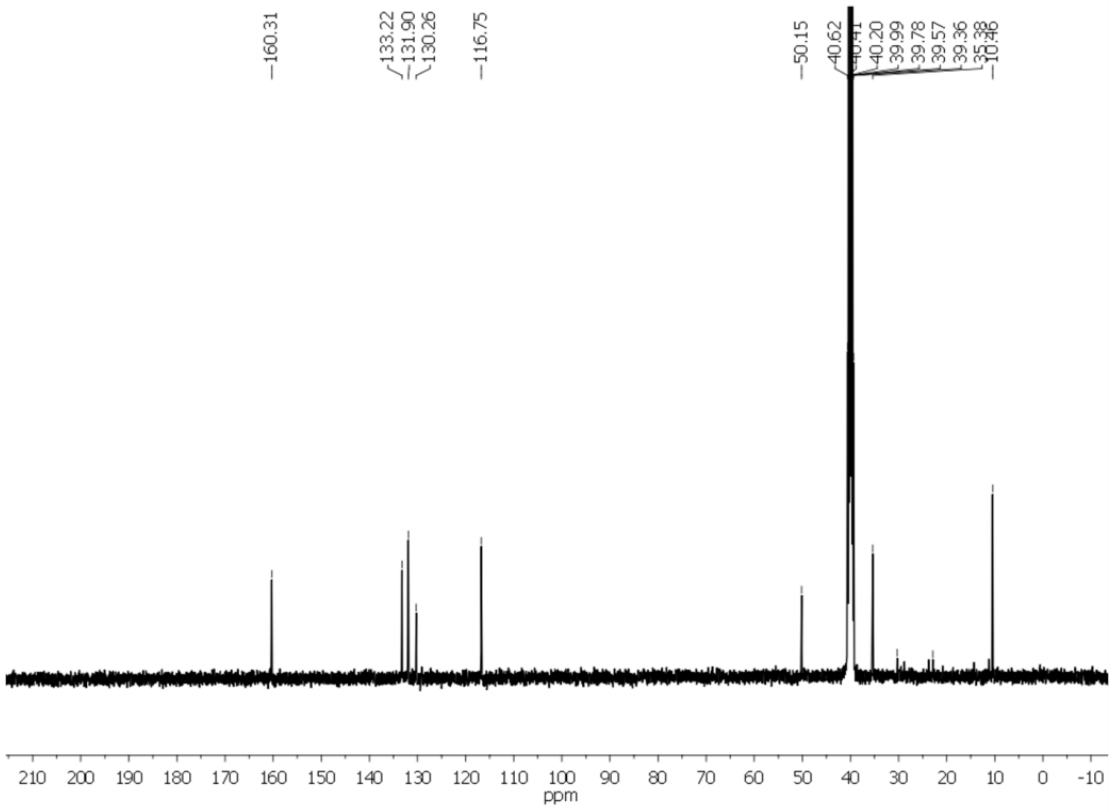

Figure 2.18 ^{13}C NMR spectrum of **1b** in DMSO-d_6

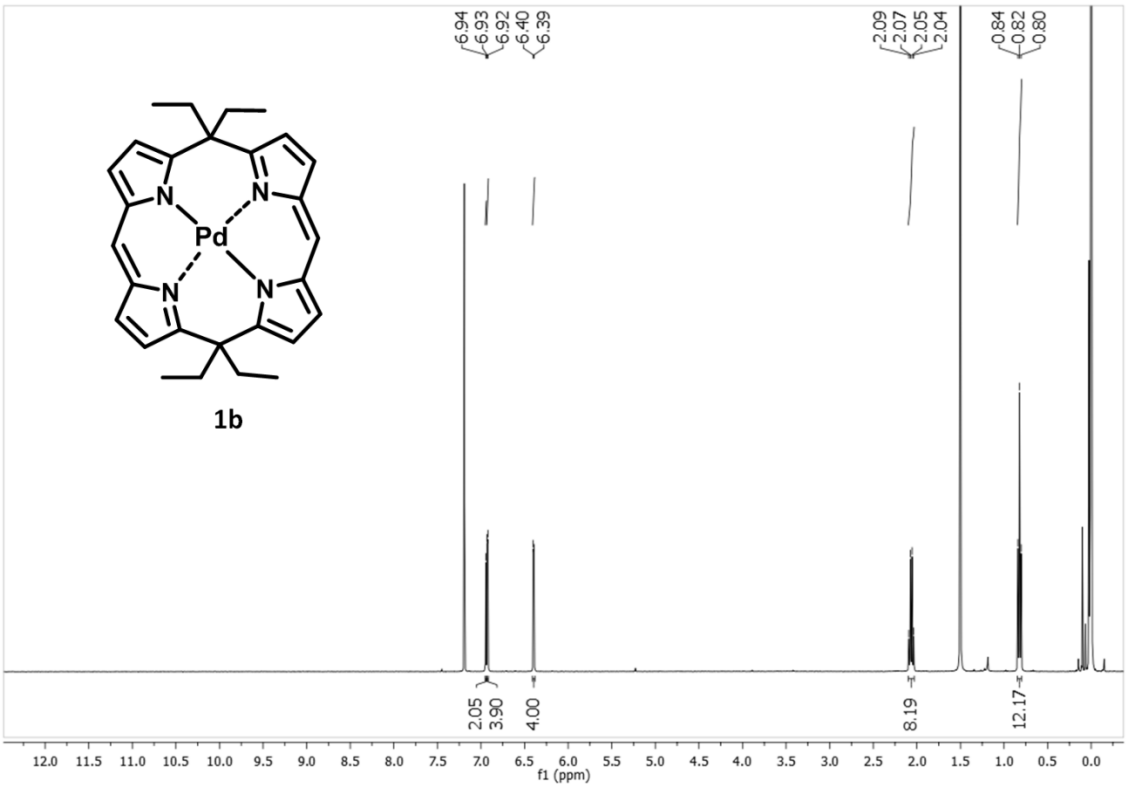

Figure 2.19 ^{1}H NMR spectrum of **1b** in $CDCl_3$

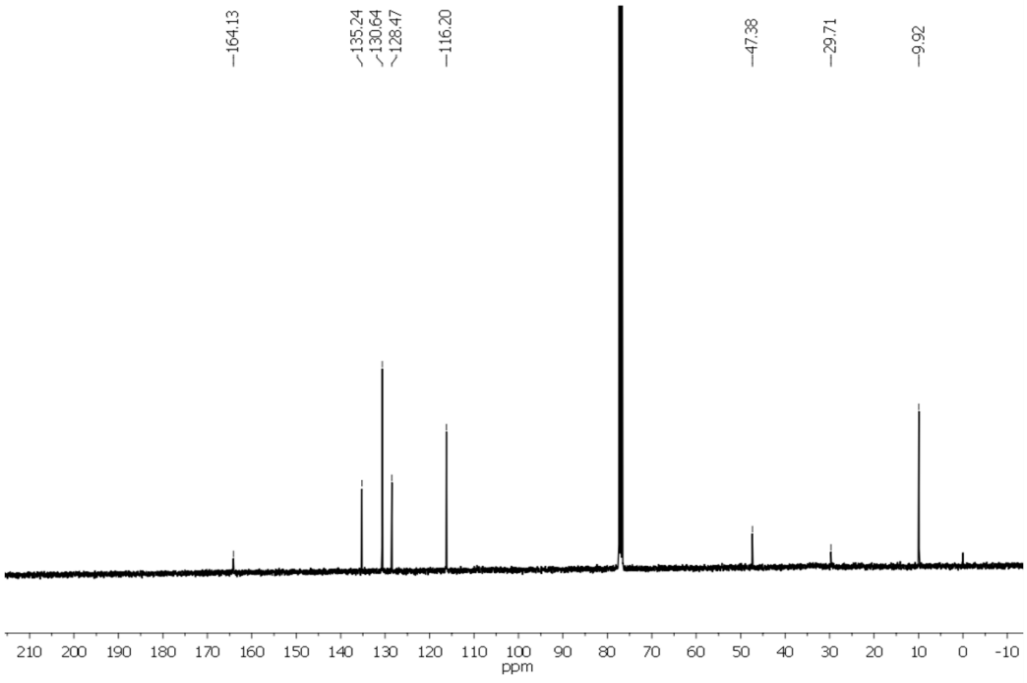

Figure 2.20 ^{13}C NMR spectrum of **1b** in $CDCl_3$

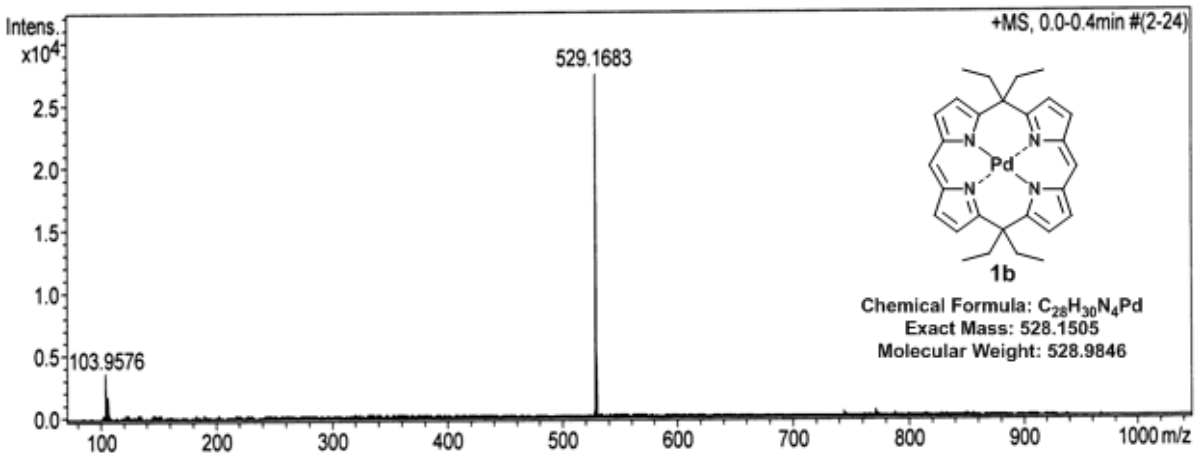

Figure 2.21 ESI-Mass spectrum of **1b**

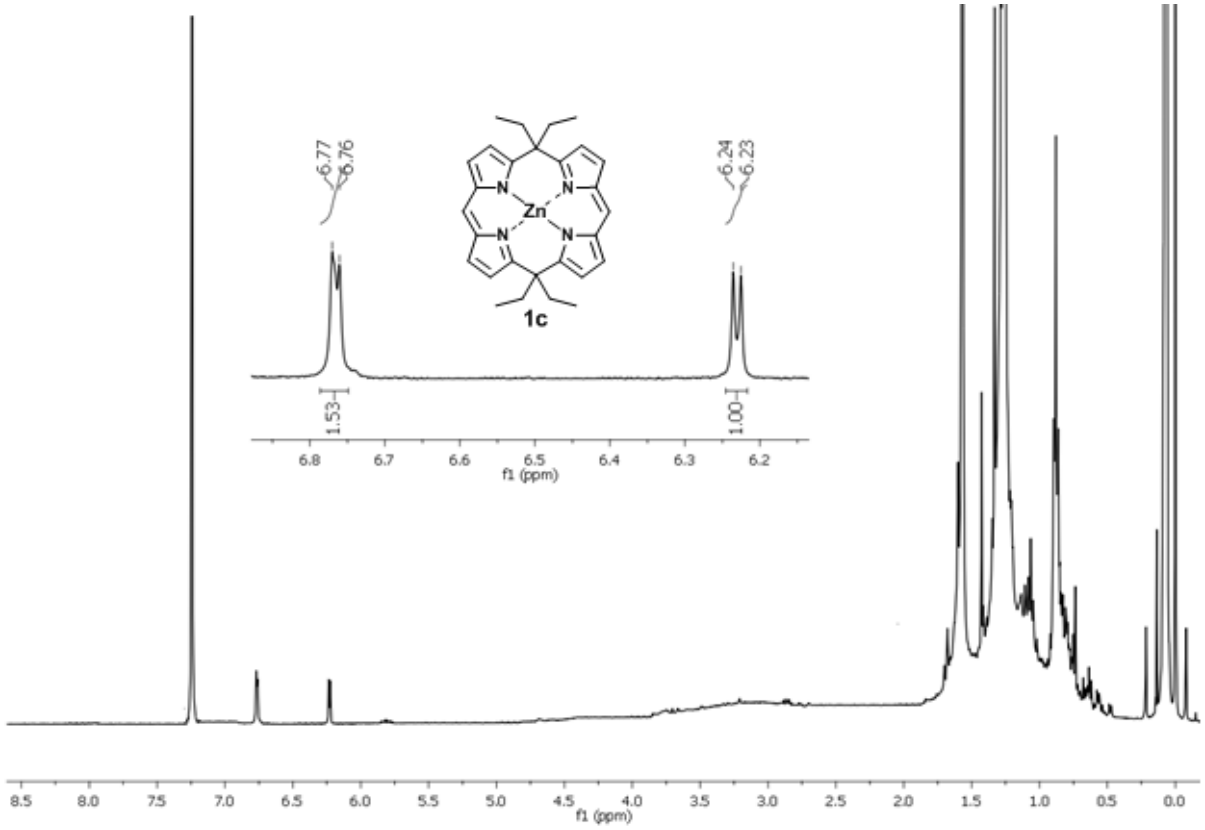

Figure 2.22 ^{1}H NMR spectrum of **1c** in $CDCl_3$. The aliphatic protons are obscured by the solvent peaks.

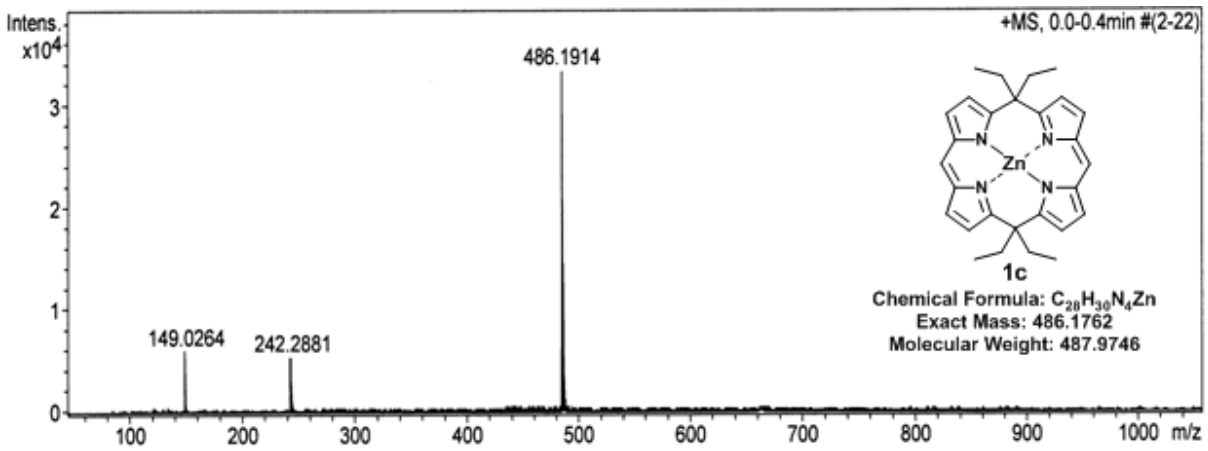

Figure 2.23 ESI-Mass spectrum of **1c**

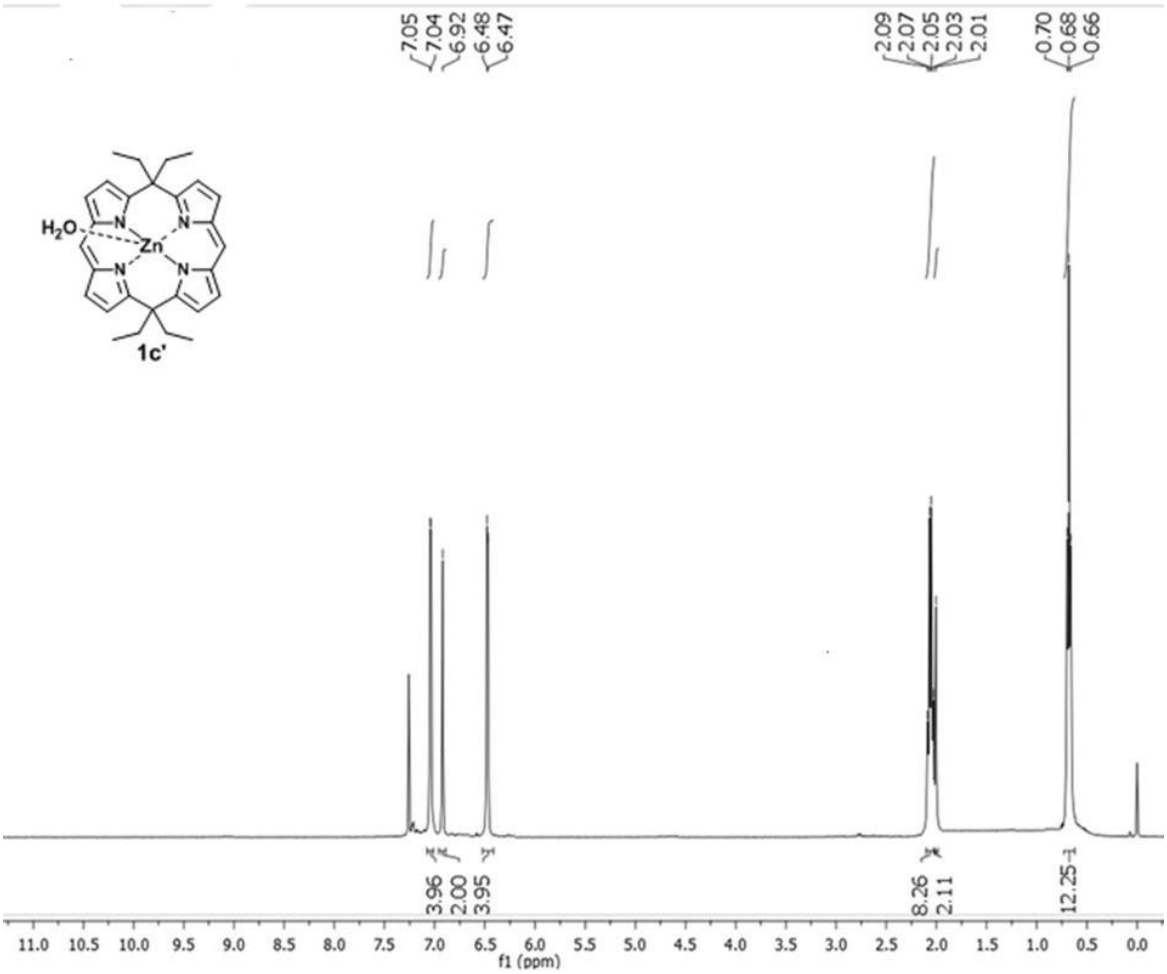

Figure 2.24 ^{1}H NMR Spectrum of **1c′** in $CDCl_3$

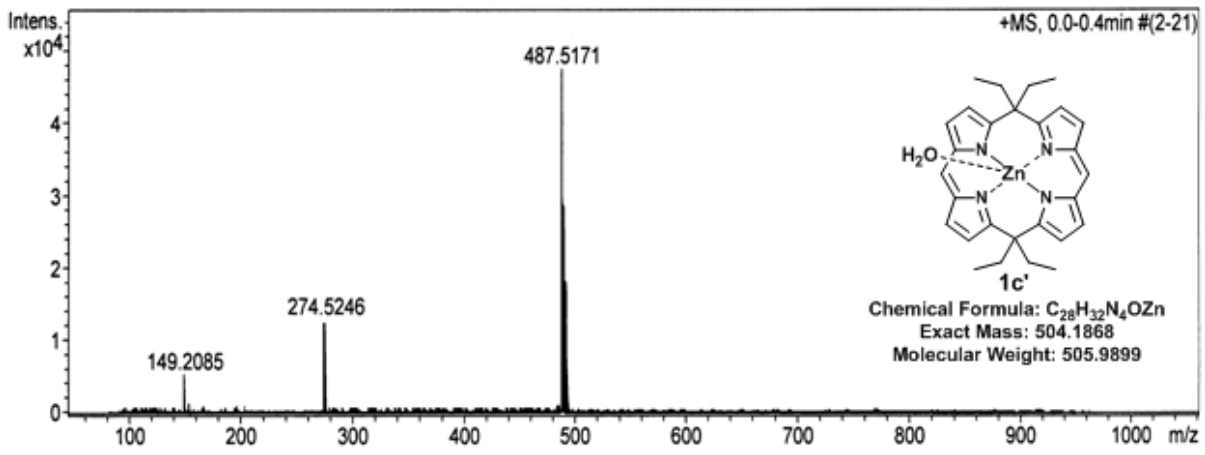

Figure 2.25 ESI-Mass spectrum of **1c′**

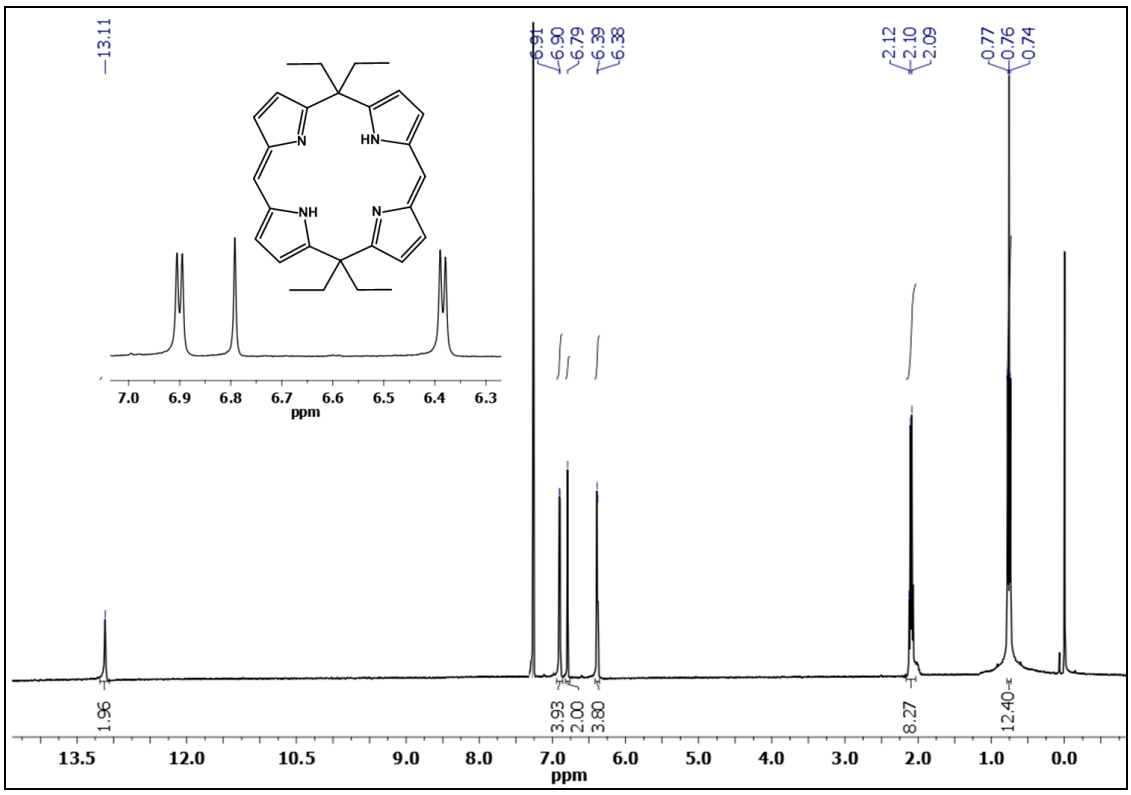

Figure 2.26 ^{1}H NMR spectrum of free base of **1 in $CDCl_3$**

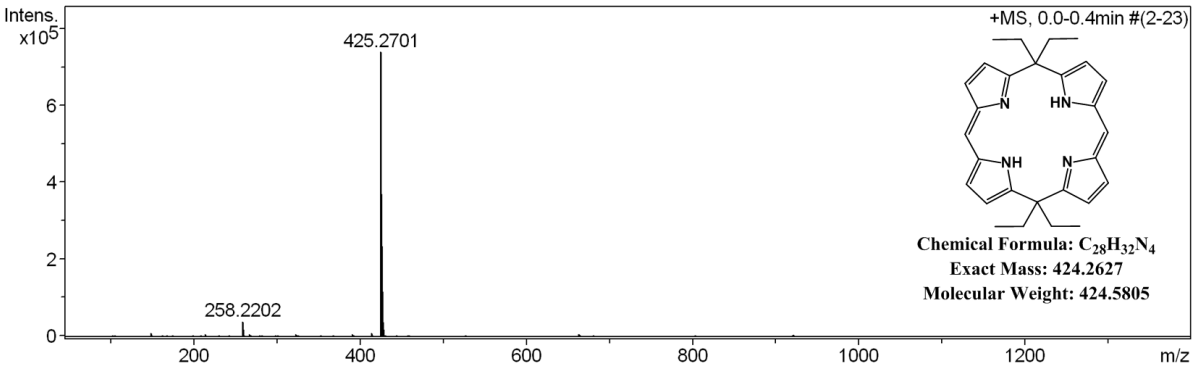

Figure 2.27 ESI-Mass spectrum of free base of **1**

2.7 Crystal data

	1a	**1b**	**1c**	**1c′**
Formula	$C_{28}H_{30}N_4Ni$	$C_{56}H_{60}N_8Pd_2$	$C_{28}H_{30}N_4Zn$	$C_{28}H_{32}N_4OZn$
M/g mol^{-1}	481.27	1057.92	487.93	505.95
T/K	296(2)	293(2)	296(2)	296(2)
Crystal dimensions/mm^3	0.12 x 0.09 x 0.07	0.20 x 0.05 x 0.05	0.11 x 0.09 x 0.07	0.13 x 0.11 x 0.09
Crystal system	monoclinic	monoclinic	triclinic	monoclinic
Space group	P21/c	P21/n	P-1	P21/c
a/Å	12.010(5)	16.5817(15)	12.1113(5)	11.925(5)
b/Å	14.987(5)	14.4709(12)	12.3679(6)	13.851(5)
c/Å	13.483(5)	20.188(2)	16.5343(7)	15.547(5)
α/°	90.000(5)	90.00	90.498(3)	90.000(5)
β/°	103.165(5)	99.123(5)	103.219(3)	103.945(5)
γ/°	90.000(5)	90.00	103.893(3)	90.000(5)
V/Å^3	2363.1(15)	4783.0(8)	2335.23(18)	2492.3(16)
Z	4	4	4	4
ρ_{calcd}/mg m^{-3}	1.353	1.469	1.388	1.348
μ/mm^{-1}	0.845	0.799	1.076	1.013
F(000)	1016	2176	1024	1064
Reflns. collected	9161	7299	8506	7591
Indep.reflns.[R(int)]	7236 [0.0447]	8420[0.0517]	8506 [0.0475]	7591 [0.0651]
Max/min transmission	0.9432 and 0.9054	0.922 and 0.801	0.9285 and 0.8909	0.9143 and 0.8796
Data/restraints/parameters	7236/0/298	8420/0/604	8506/1/595	7591/2/319
GOF on F^2	1.042	1.090	1.120	1.028
Final R indices[$I > 2\sigma(I)$]	R1 = 0.0462, wR2 = 0.1348	R1 =0.0399, wR2 = 0.1004	R1 = 0.0758, wR2 = 0.2315	R1 = 0.0384, wR2 = 0.0861
R indices (all data)	R_1=0.0705	R_1=0.0707	R_1=0.0994	*R_1=0.0703*
Largest diff peak and hole [e Å^{-3}]	1.628 and -0.414	0.787 and -0.707	1.742 and -0.741	0.533 and -0.255

Table 2.3 Crystallographic data for **1a-1c'**

Chapter 3

Study of Polymorphism and Chemodosimetric Cyanide Sensing of 5,15-Porphodimethene Palladium Complex

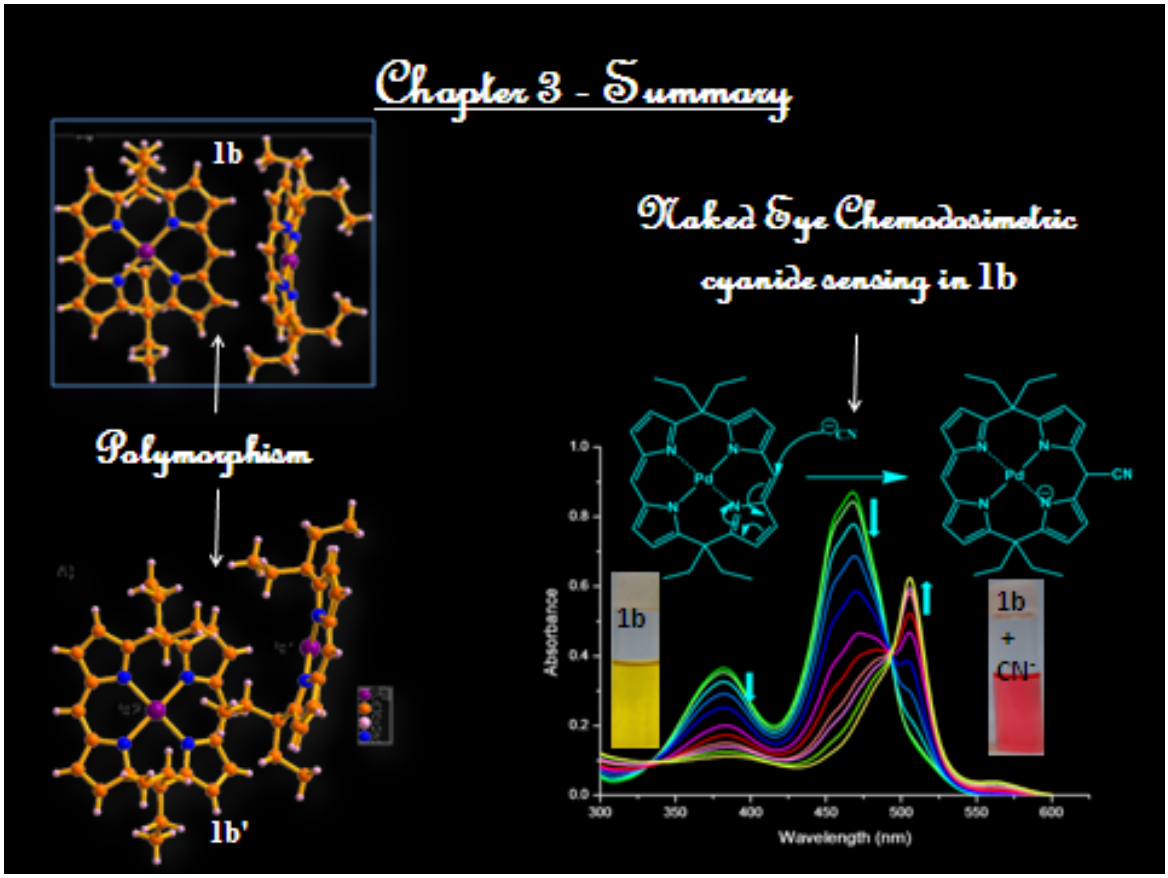

3.1 Abstract

*This chapter describes two important observations; in the first part, we highlight the polymorphic nature of 5,15-porphodimethene Pd(II) complex (**1b**) and in the second part, we describe, how this complex might be used as a chemodosimetric sensor. Two polymorphs of the mentioned complex are obtained by different polar solvents and are further confirmed by single crystal X-ray analysis. The receptor properties are carried out with various anions and showed a selective affinity towards cyanide ion. Excellent selectivity was observed even in the presence of 100 equiv. of other potentially interfering anions. We have also successfully demonstrated that the cyanide ion binds selectively at the meso-position of the calixphyrin skeleton and justified the chemodosimetric sensor property of the mentioned complex. To the best of our knowledge, such type of cyano adduct formation is hitherto unknown in the calixphyrin chemistry and paves a new methodology for the synthesis of functionalized unsymmetrical porphomethenes and calixpyrroles.*

3.2 Introduction

3.2.1 Importance of Anions in the Modern World

Anions are ubiquitous in the natural world, for example chloride in sea water, nitrate and sulphate in acid rain, phosphates and nitrates in agriculture and other human activities constitute major pollutants in our environment. Every conceivable biochemical operation involves recognition, transport and transformation of anions, hence they play critical role in the maintenance of life [Bianchi *et al.* 1997]. It is essential for the formation of majority of enzyme–substrate and enzyme–cofactor complexes as well as interaction between proteins and RNA or DNA. ATP and other high-energy anionic phosphate derivatives are at the centre of power processes as diverse and important as biosynthesis, molecular transport and muscle contraction. They also serve as the energy currency for a host of enzymatic trans-formations.

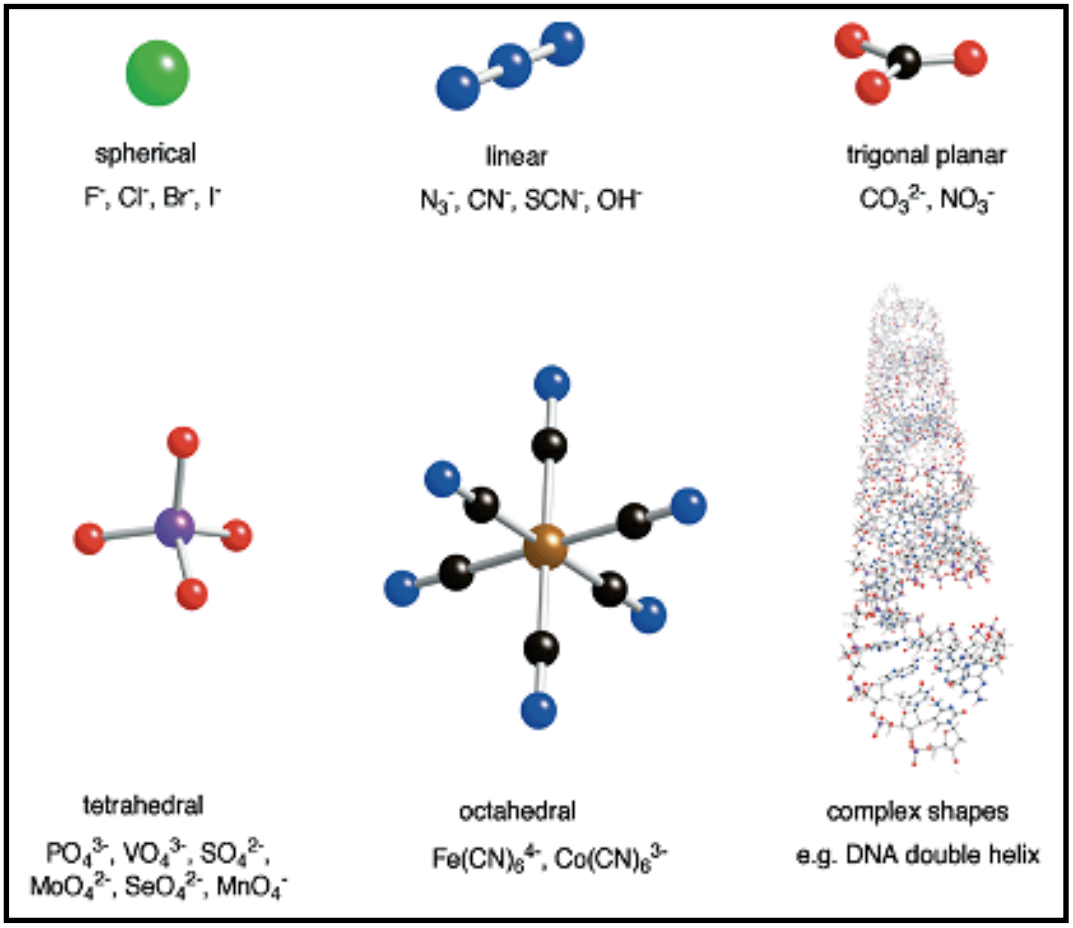

Figure 3.1 The schematic representation of various anions (Adapted from the reference *Sessler et al. 2006*).

Anion channels and carriers are involved in the transport of small anions such as chloride, phosphate, and sulphate and thus serve to regulate the flux of key metabolites in and out of cells while maintaining osmotic balance. Disturbing the different biological operations involving anions results in serious conditions like cystic fibrosis, multidrug resistance. In another level, the presence of toxic anions like cyanide, oxalate, arsenate, nitrite may cause chronic toxicity resulting in renal failure, heart attacks, stroke etc. This dichotomy underscores the complexity and importance of anion recognition in biology; it also highlights the need for and potential utility of synthetic anion receptor chemistry [Sessler *et al*. 2006].

3.2.2 Anion sensors

Anion recognition is one of the fastest growing sub disciplines within supramolecular

chemistry because of the various roles played by them in environmental and biological processes [Bianchi *et al.* 1997].

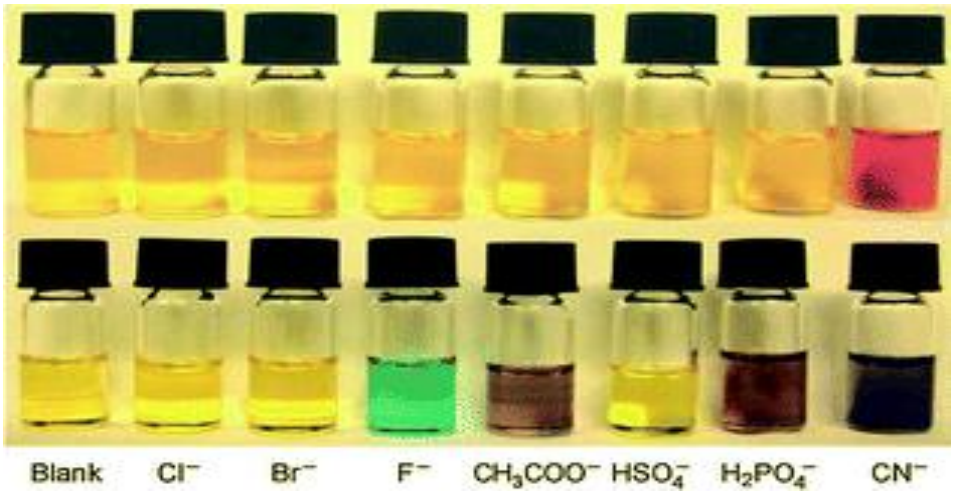

Figure 3.2 The Solutions of thiourea dye (0.5 mM) with different anions (30 equiv.) in methanol (top) and DMSO (bottom). (Adapted from the reference Gimeno *et al*. 2008).

It is often difficult to control selectivity and sensitivity among anions because of their wide range of geometries, low charge to radii ratios, sensitivities to pH, and high solvation energies. Gimeno *et al.* reported the synthesis of two azo phenyl thiourea dyes whose solution state studies in methanol indicate that the cyanide ions induces a colour change from pale orange to red which is not observed in the case of various other anions. They also observed that the dyes when dissolved in DMSO show reponses in color not only in the case of cyanide ions, but also to fluoride, acetate and dihydrogen phosphate as shown in Figure 3.2. thus the thiourea based receptors shown in Figure 3.2 binds with various anious in DMSO solvent systems, however, binds selectively with CH_3OH solvent. Considerable interest has been focused to produce a variety of new selective charged and neutral, cyclic and acyclic, inorganic and organic anion receptors for the remarkable advances in this field. Over the past decade, various examples of hydrogen-bond donors such as urea [Cho *et al.* 2005], thiourea [Liu *et al.* 2008], amine [Thiagarajan *et al.* 2007], amide [Kang *et al.* 2006], pyrrole [Lee *et al*. 2008], imidazole [Chellappan *et al.* 2005], and indole [Gale 2008] moieties have been shown to be effective anion receptors in organic solvents. Among various heterocyclic

receptors, pyrrole played an important role, because it exhibits 'duality' where the N moiety acts as a hydrogen bonding acceptor or hydrogen bonding donor due to the NH site.

The use of pyrrole as an anion receptor moiety was pioneered by Sessler in the early 1990s with expanded porphyrins such as sapphyrin **2** which binds strongly with halide anions [Sessler *et al.* 1990]. The complex between **2** and HF in CH_2Cl_2 is proved by single crystal X-ray analysis and the stability constant is found to be $>10^8$ M^{-1} for F^- ion (Chart 3.1).

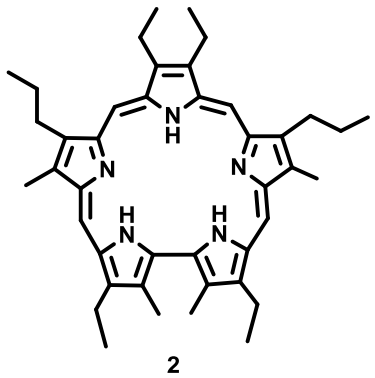

2

Chart 3.1 Pyrrole based macrocyclic anionic receptor

Another important class of pyrrole containing anionic receptors are the calixpyrroles. These are widely used as receptors for various anions both in solution and in the solid state. It possess conformational flexibility adopts 1,3-alternate conformation in the absence of an anion, however change to cone-like conformation in the presence of an anionic guest during the binding event [Gale *et al*. 1996; Gale *et al*. 2001]. In most of the macrocycles, the pyrrole rings undergo preorganization wherein their multiple NH-sites efficiently bind with desired anion in a cooperative fashion to form anion-receptor complexes [Sessler *et al*. 2003].

In sharp contrast to closed systems, pyrrole ring strongly determines the characteristics of acyclic oligopyrrolic systems which may find application in functional supramolecular materials. Linear receptors often experiences temporal preorganization with a particular anion and also, the steric and electrostatic interferences from the peripheral

substituents. Pyrrole itself can form stable complex with anions as shown by the pyrrole-chloride complex [Coles *et al*. 2001]. The binding affinity of pyrrole can be further enhanced by functionalizing the molecule in the second and fifth positions.

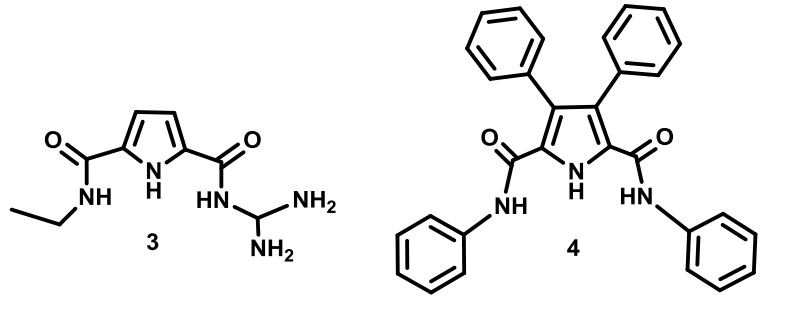

Chart 3.2 Pyrrole based acyclic anionic receptors **3** and **4**

In the literature, a wide range of acyclic pyrrole receptors are reported to date. Schmuck and co-workers have shown that positively charged guanidinio-carbonyl pyrroles (**3**) are excellent carboxylate receptors [Schmuck 1999]. Camiolo and co-workers reported the syntheses of a series of 2,5-diamide-substituted pyrroles selectively bind oxo-anion. For example selective binding of receptor **4** towards $C_6H_5CO_2^-$ ions in CD_3CN was confirmed by ^1H NMR spectroscopy [Camiolo *et al.* 2003] (Chart 3.2).

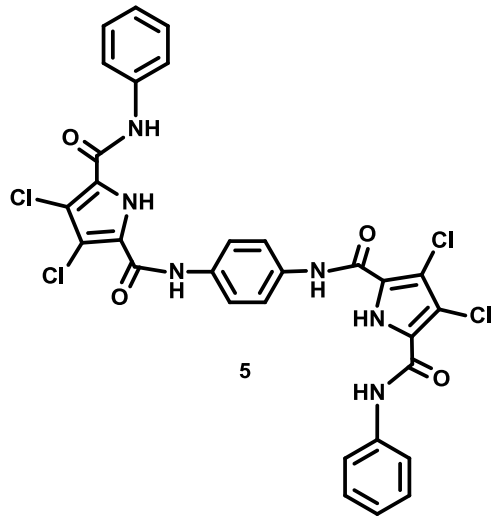

Chart 3.3 Phenelynediamine based pyrrolic receptor **5**

Gale and co-workers designed receptor **5** by attaching pyrrole moieties to phenylene diamine skeleton which binds chloride ions selectively (Chart 3.3). Receptor **5** binds two chloride ions through three NH-hydrogen bonds each [Gale *et al.* 2002]. Later, Gale and co-workers exploited dipyrromethanes as platform for syntheses of a series of anion receptors (**6**-**9**) among which **6** was selective for oxo and fluoride anions, where as **7**-**9** were shown unusually high affinities towards dihydrogen phosphate ions. Chauhan *et al.* reported the syntheses of a series of 1-Arylazo-5,5-dimethyl dipyrromethanes (**10**-**13**) (Chart 3.4) which act as chromogenic anion probes [Chauhan *et al.* 2009].

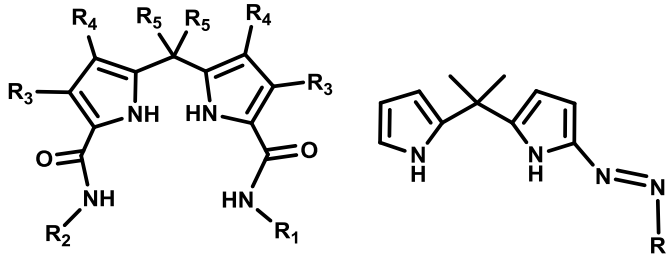

6 R_1=R_2=*n*-Bu, R_3=Me,R_4=Et,R_5=H
7 R_1=R_2=Ph, R_3=R_4=R_5=Me
8 R_1=R_2=*n*-Bu, R_3=R_4=R_5=Me
9 R_1=Ph, R_2=*n*-Bu, R_3=R_4=R_5=Me

10 R=C_6H_4Br
11 R=$C_6H_4OCH_3$
12 R=C_6F_5
13 R=$C_6H_4NO_2$

Chart 3.4 Dipyrrolylmethane Receptors

3.2.3 Cyanide Sensing

Cyanide is of particular interest, because it is widely used in various industrial applications like metallurgy, mining, electroplating, polymer synthesis, and also involved in separating metal ions like, gold, silver and copper from platinum [Young *et al.* 2001]. The cyanide anion consists of a carbon and nitrogen atom connected by a triple bond and carries an overall molecular charge of negative one which executes interesting bonding properties. Cyanide ion can act as an effective bridging ligand because both carbon and nitrogen has a lone pair of electrons, allowing either side of the molecule to bind metal centers by donating electrons as a Lewis base. Furthermore, it is very compact and capable of not only sigma

interactions by direct lone pair donation from the highest occupied molecular orbital (HOMO), but also π-acceptance of electrons into the vacant π^*- lowest unoccupied molecular orbital (LUMO), which is described as π-backbonding.

Detection of anions is of great importance considering the effects of anions on biological, environmental and physical processes. The anions are an intergral part of the biological system but they can be lethal at concentrations exceeding the optimum level. Cyanide is one of the most toxic anions and can prove fatal for humans at concentrations of 0.5-3.5 mg kg^{-1} body weight. Cytochrome c, one of the respiratory enzymes present in the mitochondria is mainly targeted by the cyanide ion. This anion blocks the active site of the enzyme which in turn blocks the electron transport chain, thus inhibiting cellular respiration [Vennesland *et al.* 1981; Baskin *et al.* 2008]. However cyanide is used in various industrial process like gold mining, electroplating and plastic production [Young *et al.* 2001]. As a result, the effluent from these industries can pose serious environmental hazards. The permissible concentration in drinking water is 2 μM to 20 μM and beyond this level is lethal. On the other side, the cyanide levels in industrial wastes need to be continuously monitored. Considerable efforts have been made in the development of cyanide sensors. Though cyanide can be detected by electronic absorption and emission, titrimetric, voltammetric, potentiometric, electrochemical methods and ion chromatography, the initial two methods is often used to detect in the case of trace amount of cyanide ions [Ma *et al.* 2010; Banica *et al.* 2012; Chen *et al.* 2012; Yang *et al.* 2013]. Optical sensing of cyanide, involving change in color or fluorescence, is the most convenient approach.

The various strategies employed to design optical sensors for cyanide anion can be broadly grouped into three classes as shown schematically in the Figure 3.3. In the first approach, the sensors have the binding and the signaling parts covalently bonded. In this case

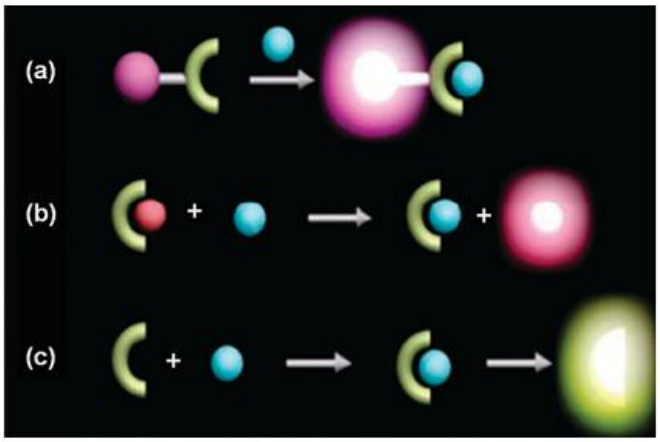

Figure 3.3 The Three approaches for chemosensors: (a) chemosensor bearing a signalling subunit as well as a binding site; (b) displacement approach; (c) chemodosimeter. (Adapted from the reference Xu *et al*. 2010).

cyanide interacts with the binding site and causes a change in the colour or fluorescence of the signaling subunit. In the second approach, the sensor consists of a coordinated complex, which on interaction with cyanide undergoes a displacement mechanism resulting in a spectroscopic regeneration of the uncoordinated species. The above two approaches are reversible, the third method of sensing is through an irreversible chemical reaction of cyanide with the sensor. Such type of sensors are called chemodosimeters. These sensors show high selectivity for cyanide compared to other anions [Xu *et al.* 2010]. This is more specific and minimizes the effect of interfering anions. Due to the nucleophilic nature, the cyanide ion has strong affinity towards carbonyl carbon, electrophilic carbon and boron, which leads to cyanide imparting absorption and emission spectral changes. Hence, the chemodosimeters utilizing visible color change are highly useful for naked eye detection of cyanide ions. The functioning mechanisms of chemodosimeters, particularly the optical properties depend on the structure of the π-conjugation and reactive subunits of the sensors. Coumarin, calix[4]pyrrole, BODIPY, oxazine, hemicyanine and cyanine moieties have been used as the π-conjugated system [Xu *et al.* 2010]. Wei Guo *et.al* reported a chemodosimeter based on the nucleophilic attack of CN^- toward the indolium group of a hybrid coumarin–hemicyanine dye **14** (Figure 3.4) [Lv *et al.* 2011]. Upon the CN- ion interaction, the red emission is gradually

changed into blue, where the intramolecular charge transfer (ICT) is restricted during interaction.

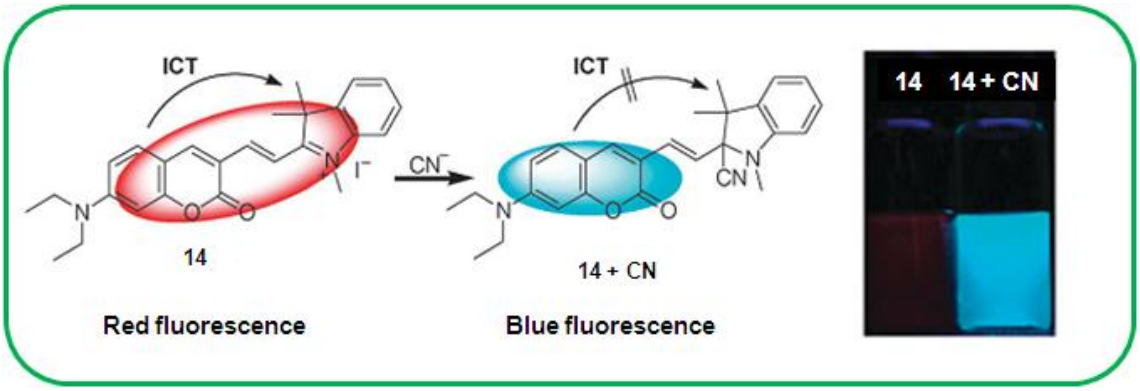

Figure 3.4 The design concept of ratiometric fluorescent probe **14** (Adapted from the reference Lv *et al*. 2011).

In 2009, Lee *et al.* reported a calix[4]pyrrole system as a chemodosimetric cyanide sensor, which showed selective color bleaching with cyanide (Figure 3.5) [Hong *et al.* 2009]. The receptor **16** contains a calix[4]pyrrole anion binding site and a dicyano-vinyl group as putative cyanide-dependant reactive subunit. The sensor **16** was synthesized by the condensation of *β*-monoformyl calix[4]pyrrole **15** and malononitrile. The yellow color of the receptor is lost by the nucleophilic addition of the Cyanide ion at the *α*-position of the dicyano-vinyl group generating stabilized anionic species **17** (Figure 3.5).

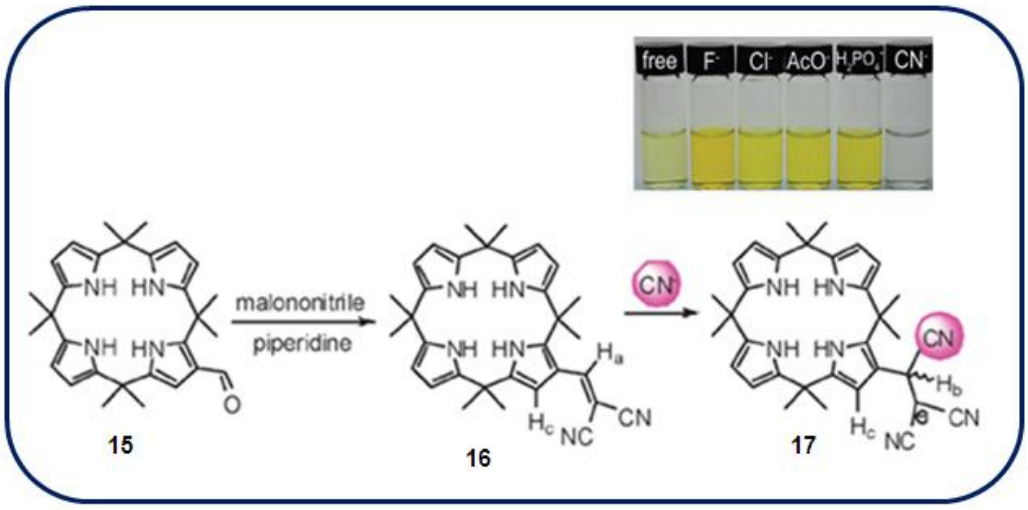

Figure 3.5 Calix[4]pyrrole based cyanide chemodosimeter **16** (Adapted from the reference Hong *et al*. 2009).

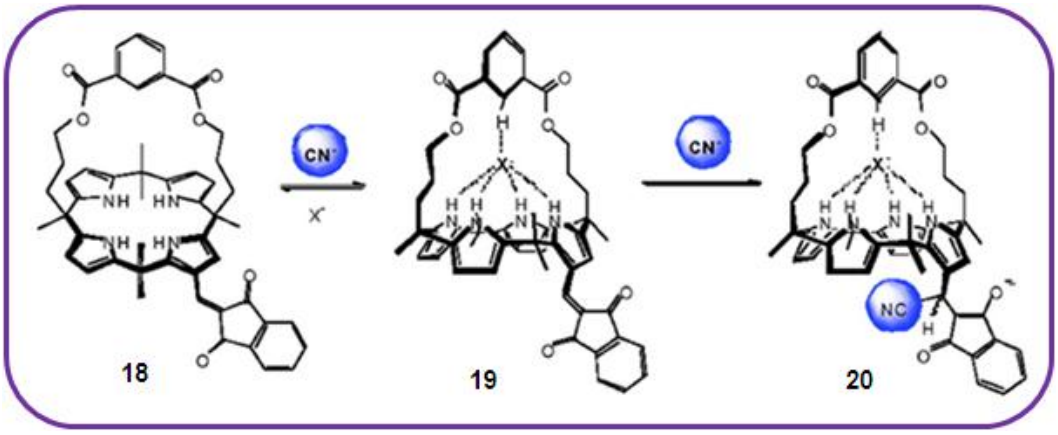

Figure 3.6 Strapped Calixpyrrole **18** as cyanide chemodosimeter (Adapted from the reference Kim *et al.* 2009)

In the same year, Sessler and co-workers reported the synthesis of a strapped calix[4]pyrrole (**18**) bearing a 1,3-indanedione group at a β-pyrrolic position, which acts as a ratiometric cyanide selective chemosensor [Kim *et al.* 2009]. A concentration-dependent bleaching of the initial yellow color of the receptor **18** was observed exclusively upon addition of cyanide ions, even in the presence of other anions. The mechanism suggested is that the cyanide ion forms a complex **19** with the receptor **18** through a fast equilibrium as shown in the Figure 3.6, which is followed by slow nucleophilic addition to the *β*-position of the 1,3-indanedione group resulting in the formation of the adduct **20** (Figure 3.6).

Woo-Dong Jang and co-workers synthesised a BODIPY based chemodosimeter **21** consisting of a boradiazaindacene unit conjugated with a dicyano-vinyl group and utilised it for the selective and sensitive detection of cyanide ions by strong fluorescence enhancement in aqueous media [Lee *et al.* 2012]. Compound **21** exhibited strong absorption at around 320 and 500 nm. However, fluorescence emission of the receptor was negligible compared to other types of BODIPY-based dyes due to the photoinduced intramolecular charge transfer (ICT) from the BODIPY unit to the dicyano-vinyl unit group. The nucleophilic attack of cyanide on the olefinic carbon results in the interruption of π-conjugation between the phenyl

and dicyano-vinyl group, in turn preventing ICT from occurring, resulting in enhanced fluorescence emission at 520nm from BODIPY units.

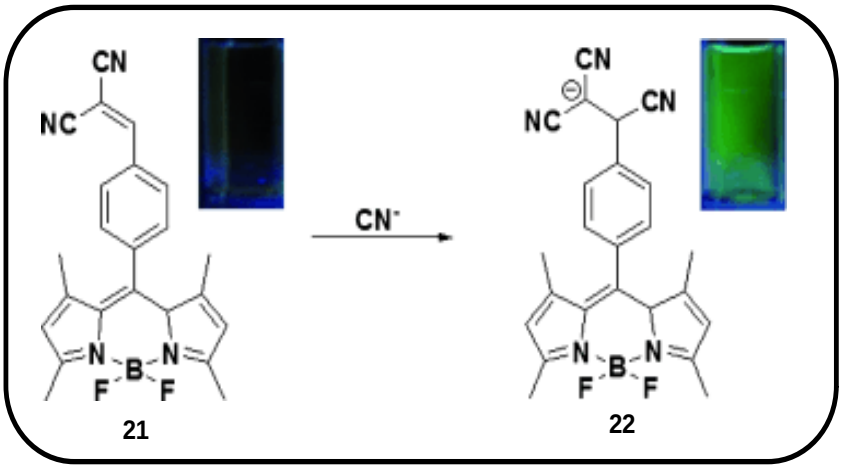

Figure 3.7 Boradiazaindacene-based turn-on fluorescent probe **21** for cyanide detection in aqueous media (Adapted from the reference Lee *et al.* 2012)

Recently, Yang and co-workers reported the synthesis of two alkyl-substituted phenazine derivative based chemodosimeters for cyanide, namely **23** and **24** (chart 3.5). Both of them can be used as a highly selective and sensitive probe for detecting nanomolar levels of CN^- ions. Probe **23**, with two dicyano-vinyl groups as the reactive site, exhibited an intramolecular charge transfer (ICT) absorption band at 545 nm and emission band at 730nm,

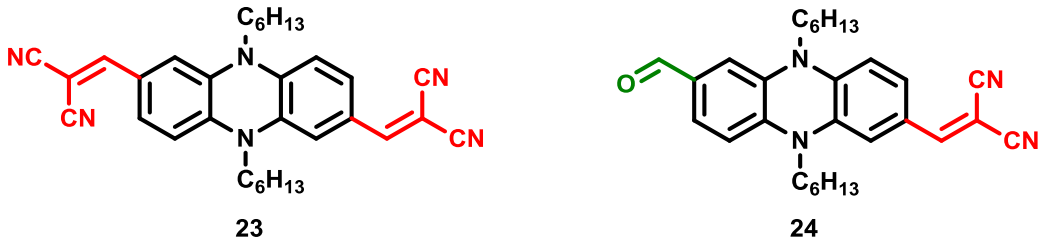

Chart 3.5 Phenazine derivative based chemodosimeters **23** and **24** for cyanide ions

respectively. The receptor **23** showed an ICT block process upon reaction with cyanide anions in CH_3CN resulting in an On-Off NIR fluorescence emission change with a remarkable detection limit of 5.77 x 10^{-8} M. There is also a dramatic color change from deep

purple to colorless enabled detection by the naked eye. The probe **24** carrying a formyl group and adicyano-vinyl group, exhibited an impressive ratiometric NIR response at 720 and 630 nm upon addition of aqueous cyanide anion, thus giving a more sensitive chemodosimeter with highly selectivity and lower detection limit of 2.31 x 10^{-8}M [Yang *et al.* 2013].

Recently Boucekkine *et.al* reported luminescence turn-on sensing of cyanide by a dicyanovinyl-substituted acetylide Pt(II) complex **25**, which primarily relies on the nucleophilic addition reaction of cyanide anions to the α-position of the dicyanovinyl group in a 1:1 manner. The strategy used for designing this cyanide-selective sensor takes advantage of a switch of charge transfer from ML′CT to MLCT/L′LCT in this acetylide Pt(II) sensor (**25**). As a result, this chromophore exhibits almost no basal luminescence displays observable changes in its UV-visible spectrum and acquires strong phosphorescence upon addition of cyanide anions. TD-DFT calculations were used to explain the switching of luminescence upon cyanide (Figure 3.8) [Fillaut *et al.* 2013].

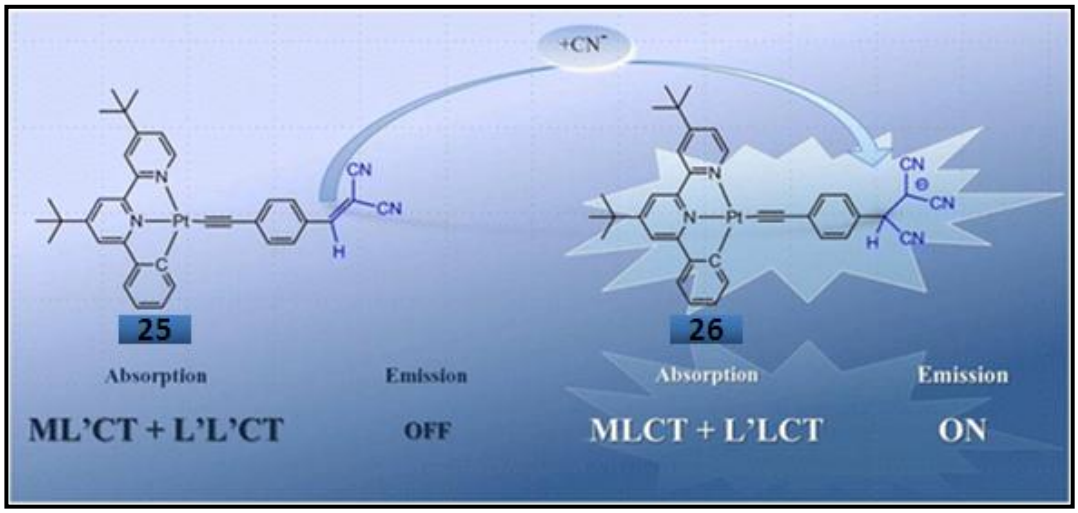

Figure 3.8 Dicyanovinyl-substituted acetylide Pt(II) complex acting as OFF-ON phosphorescent chemodosimeter for cyanide detection (Adapted from the reference Fillaut *et al.* 2013)

Calixphyrins, binds effectively with cations; the anion binding abilities rare [Sessler *et al*. 2001; Sessler *et al*. 2003]. Even though chemosensor for cyanide ions is well known

among porphyrin and phthalocyanine derivatives, only two methods are known for chemodosimetric sensors, namely (i) Chang - Hee Lee and co-workers recently reported the synthesis of a new calix [4]-pyrrole derivative which is used as a cyanide selective indicator (Figure 3.5 and 3.6). (ii) The boron incorporated subphthalocyanine dye was reported by Palomares and *et al.*, which selectively detects the cyanide ion and fluoride ions by a colori-

Figure 3.9 Carboxy-subphthalocyanine derived colorimetric and fluorometric molecular probe **27** for cyanide ions (Adapted from the reference Palomares *et al*. 2006)

metric and fluorometric technique. As shown in the Figure 3.9 the pink colour of the receptor **27** vanishes upon binding with fluoride and cyanide ions [Palomares *et al*. 2006]. However, the metal co-ordinated calixphyrin based chemodosimetric sensors are not known in the literature.

3.3 Objective of Our Work

As the chemodosimetric cyanide sensors are scarcely reported in the literature, this chapter mainly focus on the calixphyrin based chemodosimetric sensor. Herein, we report two important observations of calixphyrin derivatives such as a 5,15-porphodimethene Pd(II) complex (**1b**); in the first part, we highlight the polymorphic nature of **1b** and in the second part, we describe how this complex might be used as a chemodosimetric sensor. The sensor properties are monitored through electronic spectral analysis and identified by the naked eye.

The possible binding mechanism is also proposed based on the ^{1}H NMR analyses. Two polymorphs of the mentioned complex are obtained by using different polar solvents and further confirmed by single crystal X-ray analyses. The selective binding of CN^- at the *meso*-position of the calixphyrin skeleton causes colour change from yellow to pink which justifies the chemodosimetric sensor property of the mentioned complex. To the best of our knowledge, such a type of cyano adduct formation is hitherto unknown in calixphyrin chemistry. Moreover the nucleophilic attack at the unsubstituted *meso* position of the porphodimethene provides a new methodology for synthesis of functionalized unsymmetrical porphomethenes and calixpyrroles.

3.4 Results and discussion

3.4.1 Polymorphism in the palladium metal complexes 1b and 1b'

In chapter 2, we reported the synthesis of a series of 5,15-porphodimethene metal complexes through metal templated strategy. Among those metal complexes, the palladium complex when crystallised from two different solvent systems gave two different polymorphs **1b** and **1b'**. In the first part of this chapter, we highlight the polymorphic nature of the palladium metal complexes of **1b** and **1b'**.

Initially, the crystals of **1b** were obtained by slow evaporation of a CH_2Cl_2 solution in *n*-hexane and the compound crystallized in the monoclinic lattice with a $P2_1/n$ space group. There were two metal complexes present in the unit cell and the distance between the two metal centers was 7.07 Å. The *meso* ethyl units were oriented away from the metal centers and both the units were almost perpendicular to each other and connected by strong intermolecular hydrogen bonding interactions. To our surprise, when 5,15-porphodimethene palladium complex crystallized by slow evaporation of a CH_3CN solution in *n*-hexane (**1b′**), we observed

that the complex crystallizes in the triclinic lattice with the space group *P*-1.

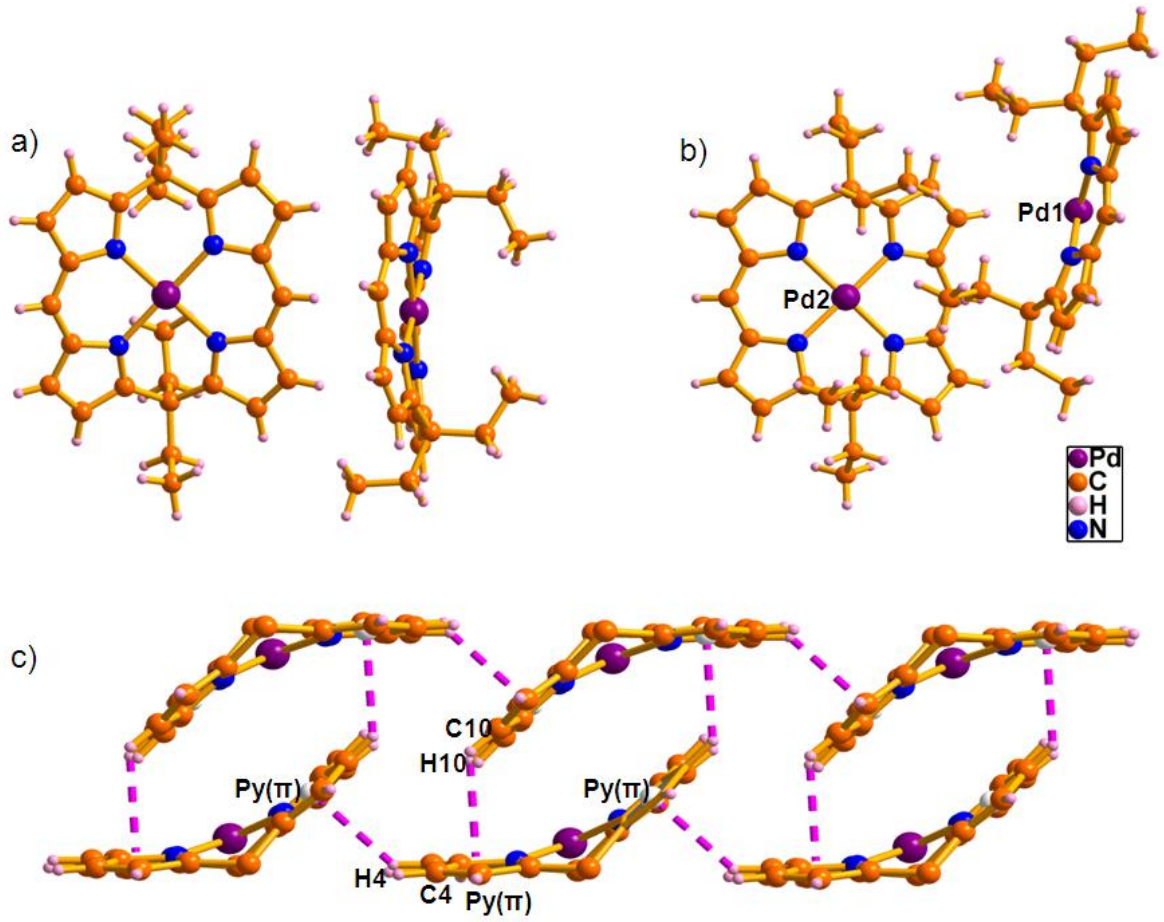

Figure 3.10 Single crystal X-ray structure of (a) **1b** by slow evaporation of CH_2Cl_2 / *n*-Hexane (b) **1b'** by slow evaporation of CH_3CN / *n*-Hexane (c) 1D array in **1b'**.

The structural features of the polymorphic crystal (**1b'**) are largely different from the one as observed in CH_2Cl_2. As observed earlier, two metal complexes are present in one unit cell. The distance between the two metal centers (Pd1 and Pd2) is 7.56Å, where one of the *meso*-ethyl units is in between the metal centers and increase the distance between them. The intermolecular hydrogen bonding interactions, as observed in the case of CH_2Cl_2, are absent in CH_3CN. However, out of two metal centers, one of the complex present in the unit cell (Pd1) forms a self-assembled dimer and a 1-D array. There are two π-clouds generated in the Pd1 unit, where the pyrrolic *β*-CH (C10–H10) and *meso*-CH (C4–H4) of the second units interact with the pyrrolic π-clouds through hydrogen bonding interactions. The distances and angles of

C10–H10·····Py(π) and C4–H4·····Py(π) are 2.86 Å, 132° and 2.80 Å, 135° respectively. The self-assembled dimer and array combine together to generate a 1-D supramolecular assembly in the solid state. However, similar hydrogen bonding interactions are absent in other complexes present in the unit cell (Pd2).

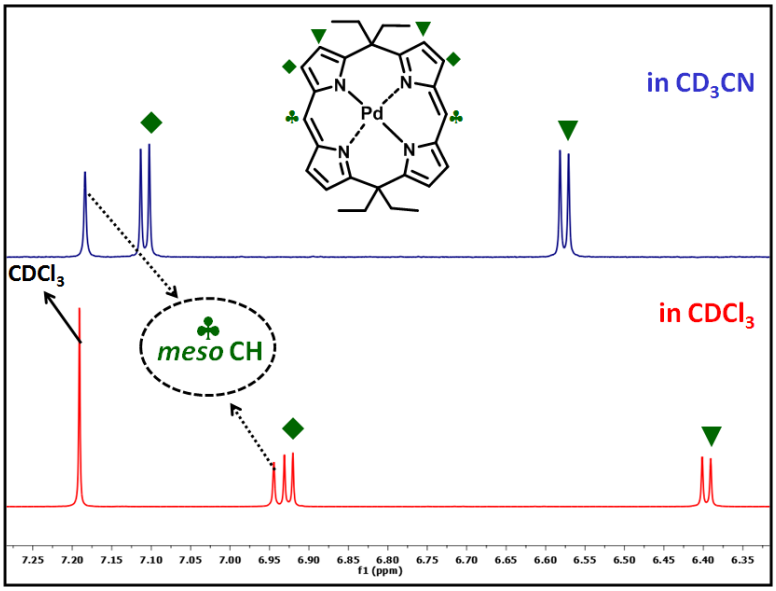

Figure 3.11 ^{1}H NMR spectrum with expansion in the aromatic region of **1b** in $CDCl_3$ and CD_3CN.

The ^{1}H NMR spectra of the palladium calixphyrin metal complex was recorded in solvents $CDCl_3$ and CD_3CN. The results fully agrees with the X- ray crystal data of the two complexes (**1b**, **1b′)** and throws light the effect of solvent polarity on the structure of the polymorphs (Figure 3.11). In the ^{1}H NMR spectrum of the Pd (II) metal complex **1b** in $CDCl_3$ the aromatic region consists of three set of peaks with the two *meso* protons resonating as a singlet around 6.94 ppm and *β*-pyrrolic CH are observed as two set of doublets at 6.93-6.92 ppm and 6.40- 6.39 ppm respectively. When the solvent is changed from $CDCl_3$ to CD_3CN in contrast to the above observations, all the peaks in the aromatic region are shifted downfield. The *meso*-hydrogen is resonated as singlet at 7.2 ppm. The Δδ value is 0.255 ppm (the Δδ is the chemical difference between **1b** and **1b'** for a particular proton). The shift is mainly due to the intermolecular hydrogen bonding interactions as evident from the crystal structure of **1b'**.

Consequently the peaks corresponding to the four pyrrolic *beta*-CH also downfield shifted and resonated as two doublets at 7.12-7.10 and 6.58-6.57 ppm (Figure 3.11). The aliphatic protons exhibited approximately same chemical shift both in $CDCl_3$ and CD_3CN, where the ethyl group protons are resonated as a triplet around 0.82 ppm and as a quartet around 2.09-2.03 ppm, respectively.

The electronic spectral analysis of **1b** in $CHCl_3$ shows absorption band centered approximately at 473 nm, suggesting the π–π* transition. The band due to n–π* transition was observed at 386 nm. The absorption spectrum of the **1b** depends upon the solvent polarity, where 6nm blue shift was observed when the solvent polarity was increased from $CHCl_3$ to CH_3CN.

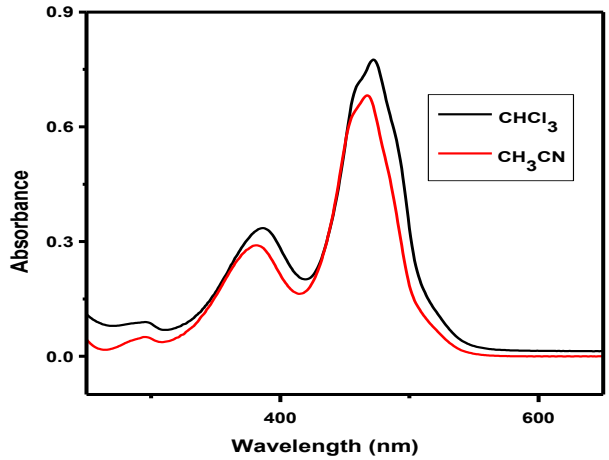

Figure 3.12 Absorption spectra of **1b** ($CHCl_3$), **1b′** (CH_3CN)

3.4.2 Anion Receptor studies of the porphodimethene palladium complex

In order to investigate the anion binding ability, a preliminary qualitative experiment was performed by using a dilute CH_3CN solution of **1b** with 10 equiv. of various anions such as F^-, Cl^-, NO_3^-, OAc^-, Br^-, I^-, NO_2^-, SCN^-, ClO_4^-, $H_2PO_4^-$, CN^- in the form of tetrabutylammonium (TBA) salts. Out of 11 anions used, no noticeable colour change was observed in the case of 10 anions (Figure 3.13). However, the colour of the solution changes

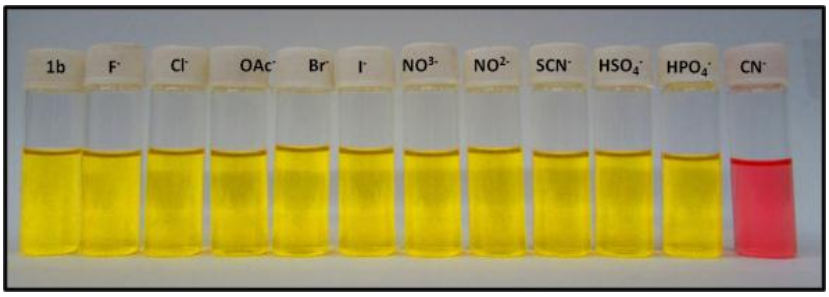

Figure 3.13 Color of the CH_3CN solution of **1b** (20 mM) in the absence and presence of different anions as seen through the naked eye.

from yellow to red upon addition of CN^-. The electronic spectral analysis of **1b** shows intense absorption bands at 467 nm and 386 nm. Upon addition of different anions other than CN^-, there was no observable change in the absorption spectra. However, on the addition of CN^-, the absorption maximum was red-shifted by about 43 nm and observed at 510 nm (Figure 3.14).

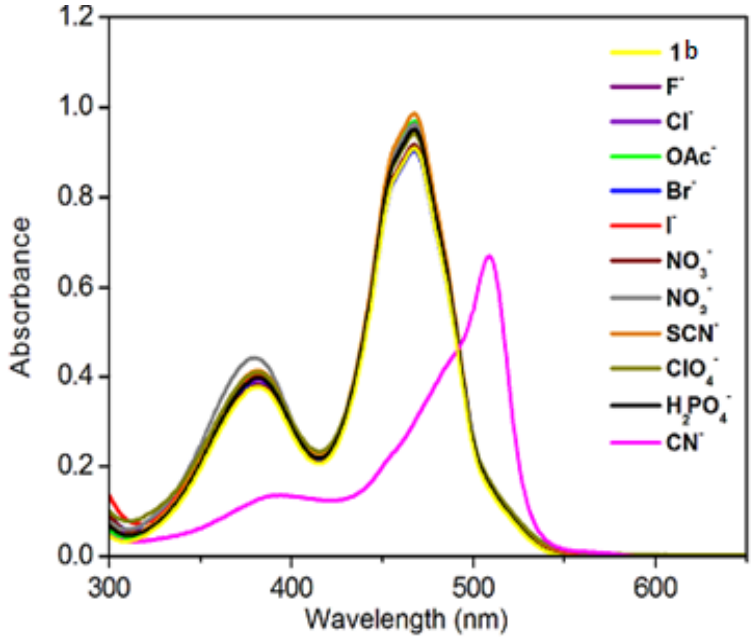

Figure 3.14 The electronic absorption spectra of **1b** in CH_3CN upon addition of various anions

To get a quantitative idea of the sensing, the experiment was further performed by using CN^- alone. The Figure 3.15 shows the changes in absorption spectrum of **1b** in CH_3CN upon increasing concentrations of CN^- ions. It is clear from the Figure 3.15 that as the

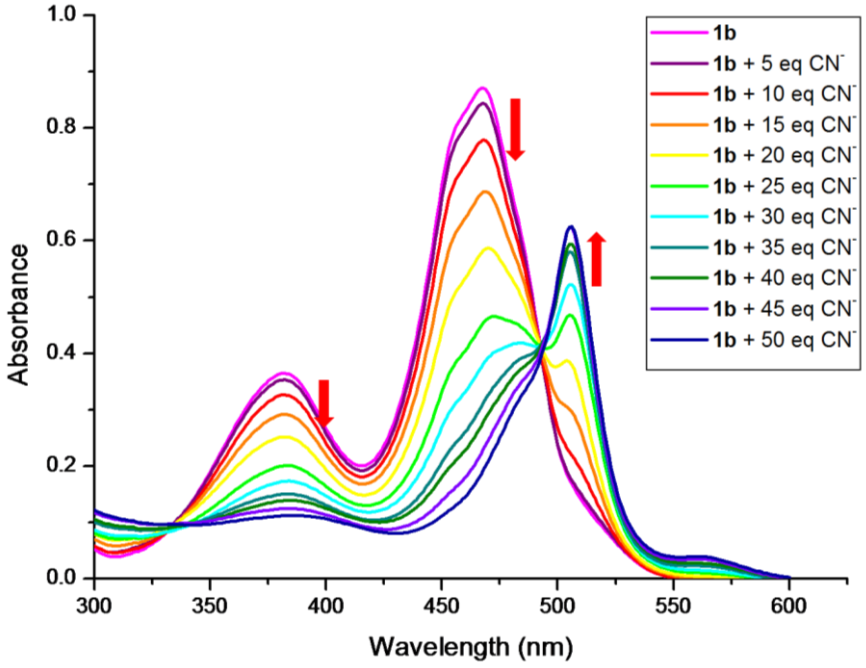

Figure 3.15 The changes in the absorption spectra of 20 μM solution of **1b** in CH_3CN upon addition of different equivalents of tetrabutylammonium cyanide.

concentration of cyanide is increased the intensity of band at 467 nm and 386 nm gradually decreased and a new band was formed at 510 nm, with two isosbestic points at 330 and 490 nm. The isosbestic points suggest the presence of equilibrium between **1b** and the **1b.**anion complex. The binding constant value is found to be 1.65 x 10^3 M^{-1} from the Benesi–Hildebrand plot (Figure 3.16).

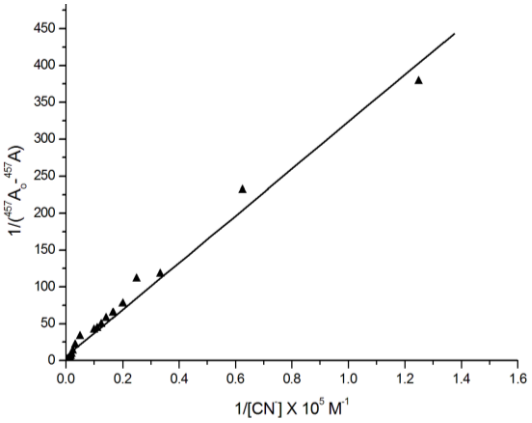

Figure 3.16 Benesi - Hildebrand plot for the absorption spectral changes of **1b** upon addition of cyanide ions. Fit details: Y = A + B * X, A = 5.25258, B = 318.39245; K = 1.65 X 10^3 M^{-1}

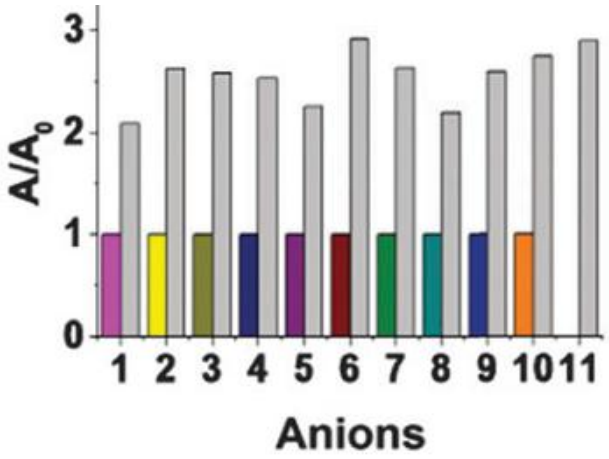

Figure 3.17 Competitive binding studies between CN^- over 100 equiv. of other anions

Furthermore, the competitive binding of the cyanide ion over the other anions was tested by studying the changes in absorption spectrum of **1b** on adding CN^- ions in presence of 100 equiv. of other anions recorded after 10 minutes of addition. The colour bars in the Figure 3.17 represent the change in absorption intensity of **1b** (20 μM) at 510 nm upon addition of 100 equiv. of anions: (1) Br^-, (2) Cl^-, (3) ClO_4^-, (4) F^-, (5) $H_2PO_4^-$, (6) I^-, (7) NO_2^-, (8) NO_3^-, (9) OAc^-, (10) SCN^- and (11) CN^-. Corresponding grey bars represent the change in absorption intensity at 510 nm upon addition of 25 equiv. of CN^- in the presence of anions. It was found that **1b** selectively senses cyanide ions even in presence of 100 equiv. of other anions (Figure 3.17). The detection limit was found to be 0.3 ppm, which is higher compared to that of other porphyrin derivatives [Hong *et al.* 2009].

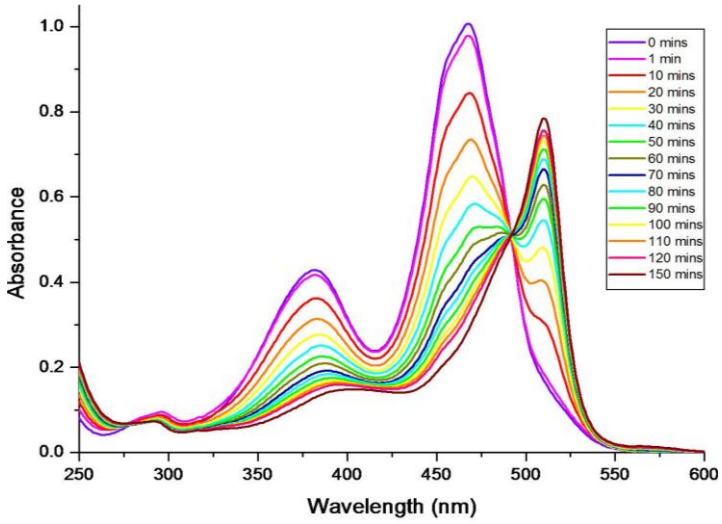

Figure 3.18 Time dependent changes in absorption spectra of **1b** (20 μM) in CH_3CN on addition of 25 eqiuv. of CN^-.

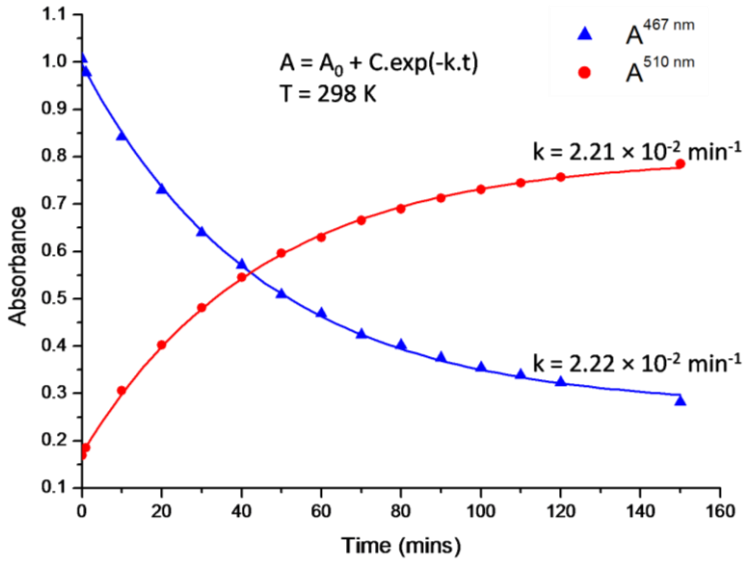

Figure 3.19 Kinetics of [**1b**-CN]$^-$ adduct formation. Changes in the absorption of **1b** (20 μM) in CH_3CN at 467 nm and 510 nm, after addition of 25 equiv. of CN^-, with time was fitted using an exponential function considering a first order rate of reaction with respect to **1b**.

It is clear from the absorption spectral studies shown in Figure 3.15 that as concentration of cyanide is increased the intensity of band at 467 nm corresponding to **1b** gradually decreases and intensity of the band at 510 nm corresponding to [**1b.CN**]$^-$ adduct increases. The time dependence of this spectral changes is further investigated by measuring the spectral changes, upon addition of 25 equiv. of CN^- to **1b** (20 μM) in CH_3CN, and monitored over time. Though there is no immediate colour change, over a period of time the colour of the solution gradually changes from yellow to red. The overall outcome is depicted in Figure 3.19 where the band at 467 nm and 510 nm is monitored at different time intervals. The saturation was observed after 150 min. The changes in the absorption intensity at 467 nm and 510 nm could be fitted perfectly considering a pseudo first order kinetics with respect to the concentration of **1b**. The rate constant for the conversion was calculated to be 2.2 x 10^2 min^{-1}.

In order to get a clear insight into the binding mechanism and the interaction of CN^- with **1b**, the ^{1}H NMR titration experiments were conducted by gradual addition of tetrabutyl

ammonium cyanide salt with 2.5 mM of **1b** in CD_3CN (Figure 3.20). The three sets of peaks initially observed in **1b** at 7.2 ppm, 7.1 ppm and 6.58 ppm, gradually decreased upon increasing the concentration of CN^-. At 1 equiv. of CN^-, the respective

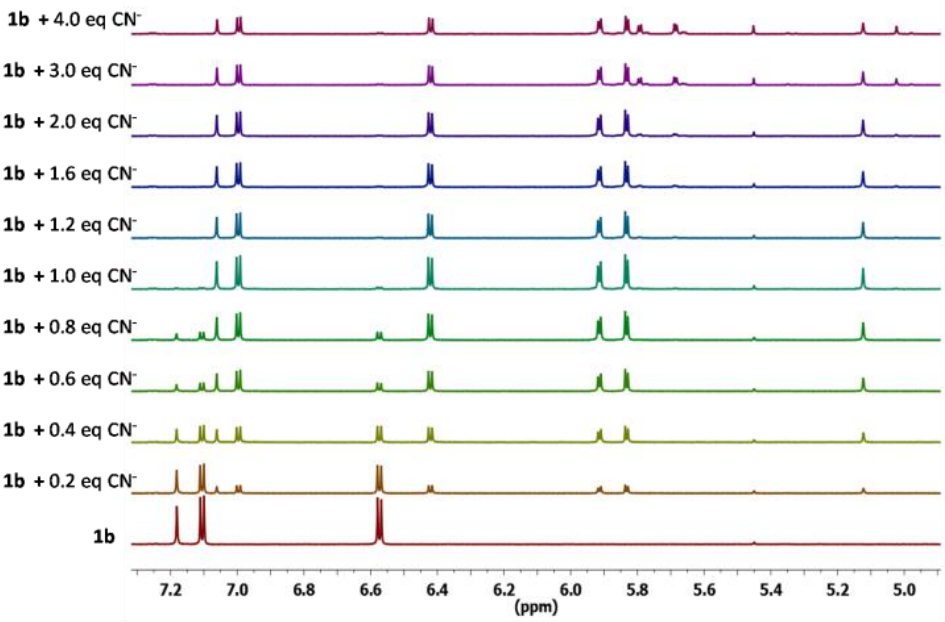

Figure 3.20 ^{1}H NMR titrations of **1b** in CD_3CN upon increasing concentration of tetrabutyl ammonium cyanide (TBACN) in CD_3CN, expansion from 5.0 to 7.2 ppm.

signals disappeared and six new peaks were observed between 5.1 ppm and 7.1 ppm, which suggests formation of a 1 : 1 adduct. Upon further increasing CN^- concentration, no appreciable change in the spectra was observed (Figure 3.20).

Efforts to crystallize the [**1b.CN**]$^-$ adduct have been unsuccessful. Nevertheless, the observations from the ^{1}H NMR titrations have been rationalized and a possible mechanism of formation of the adduct is depicted in Figure 3.22. The splitting of the aromatic peaks indicates a lowering of symmetry upon the addition of cyanide to either of the *meso* carbon of **1b** forming the [**1b.CN**]$^-$ adduct. As a result, one of the *meso*-CH is converted to a saturated carbon and the corresponding ^{1}H NMR signal is shifted upfield, where the *meso*-CH (sp^2) signal resonates at 7.1 ppm, while the *meso*-CH (sp^3) is observed at 5.1 ppm. The remaining four pyrrolic β-CH protons are resonated as doublets between 5.8 ppm and 7.0 ppm, respectively.

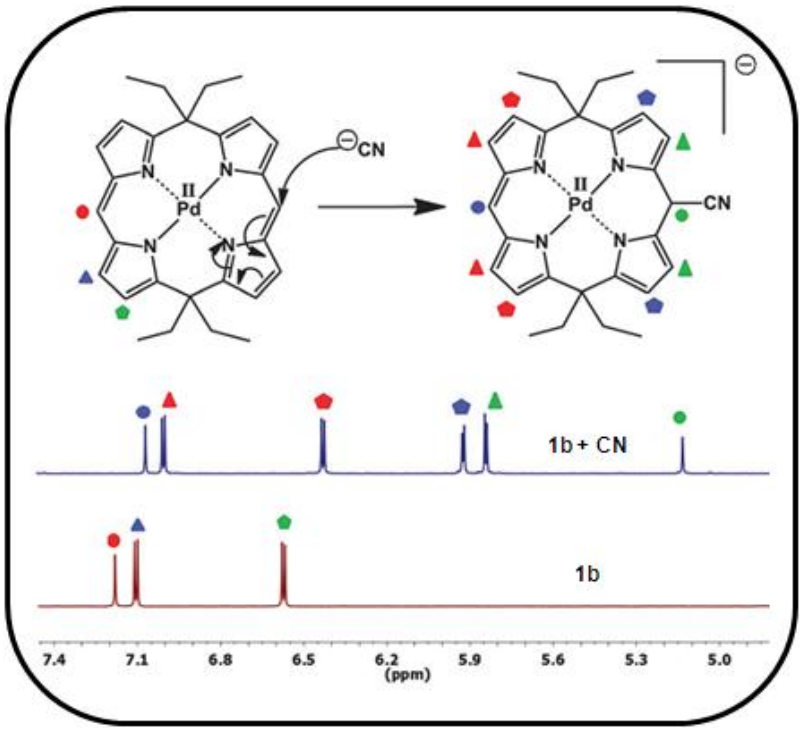

Figure 3.21 Proposed mechanism of formation of a [**1b.CN**]$^-$ adduct.

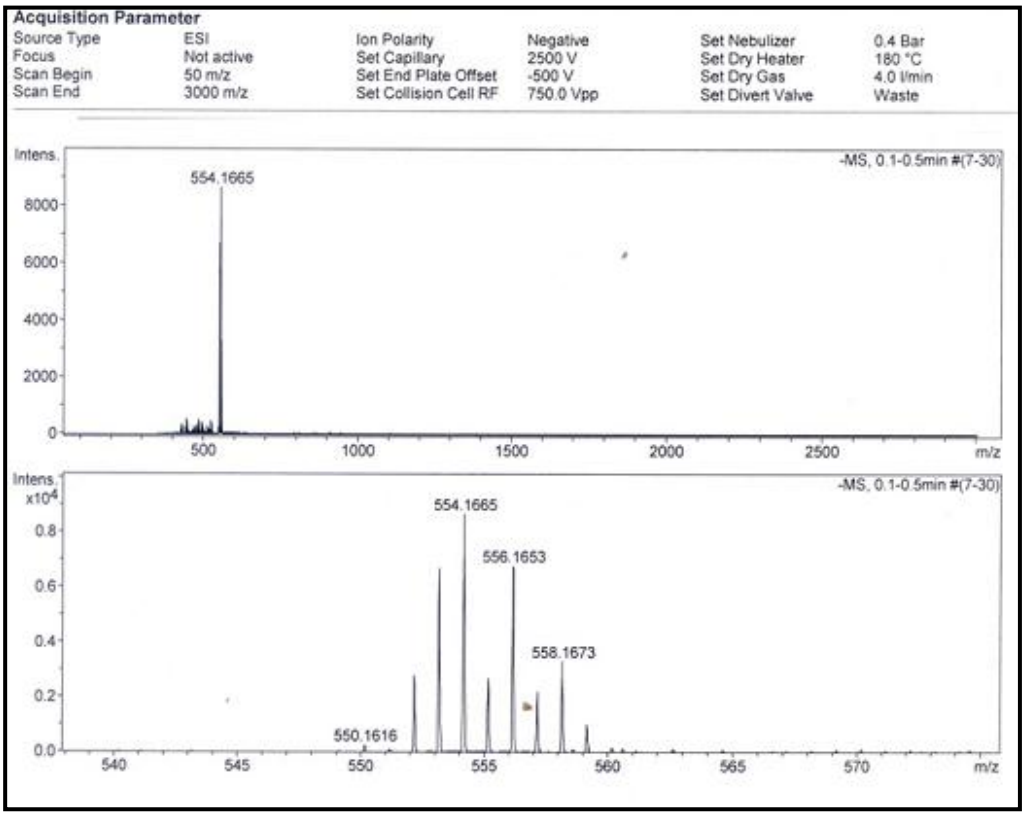

Figure 3.22 ESI-Mass spectrum of [**1b**.**CN**]$^-$ adduct in the negative mode

The 1:1 adduct is further confirmed by ESI mass spectrometry analysis, where the adduct shows the molecular ion signal at m/z = 554.1665 (calculated = 554.1542) in the negative mode (Figure 3.22).

3.5 Conclusion

In summary, we have discussed the polymorphism observed in a 5,15-porphodimethene Pd(II) complex by using polar solvents. The results are confirmed unambiguously by single crystal X-ray analysis. We have also successfully demonstrated the selective binding of CN^- at the *meso*-position of the calixphyrin skeleton and justified the chemodosimetric sensor property of the mentioned complex. To the best of our knowledge, such a type of cyano adduct formation is hitherto unknown in calixphyrin chemistry. Moreover the nucleophilic attack at the unsubstituted *meso* position of the porphodimethene provides a new methodology for synthesis of functionalized unsymmetrical porphomethenes and calixpyrroles.

3.6 Experimental Section

3.6.1 General Information

The reagents and materials for synthesis were used as obtained from Sigma - Aldrich chemical suppliers. All solvents were purified and dried by standard methods prior to use. NMR solvents were used as received. The NMR spectra were recorded with Bruker 400 MHz spectrometer with TMS as internal standard. ESI mass spectrum was recorded on Bruker, microTOF-QII mass spectrometer. Electronic absorption spectra were recorded with Perkin Elmer – Lambda 750 UV-Visible spectrophotometer and data analyses were done using the UV-winlab software package. The irradiation experiment was performed with Newport, 1918-C model, Xenon source with 135 W power supply. X-ray quality crystal for **1b** was

grown by the slow diffusion of *n*-hexane over CH_2Cl_2 solution of the metal complex, similarly slow diffusion of *n*-hexane over CH_3CN solution of the metal complex yielded the polymorph of **1b′**. Single-crystal X-ray diffraction data of **1b** and **1b′** were collected on a Bruker KAPPA APEX-II, four angle rotation system, MoKα radiation (0.71073 Å). All experiments were carried out at room temperature (25 ±1◦C), unless otherwise mentioned.

3.7 Crystal data for 1b and 1b′

	1b (CH_2Cl_2/*n*-Hexane)	**1b' (CH_3CN/*n*-Hexane)**
Formula	$C_{56}H_{60}N_8Pd_2$	$C_{56}H_{60}N_8Pd_2$
M/g mol^{-1}	1057.92	1057.92
T/K	293(2)	293(2)
Crystal dimensions/mm^3	0.20 x 0.05 x 0.05	0.13 x 0.07 x 0.06
Crystal system	Monoclinic	Triclinic
Space group	$P2_1/n$	*P*-1
a/Å	16.5817(15)	8.250(5)
b/Å	14.4709(12)	14.764(5)
c/Å	20.188(2)	19.582(5)
α/°	90.00	88.932(5)
β/°	99.123(5)	89.487(5)
γ/°	90.00	74.757(5)
V/Å^3	4783.0(8)	2300.8(17)
Z	4	2
ρ_{calcd}/mg m^{-3}	1.469	1.527
μ/mm^{-1}	0.799	0.831
F(000)	2176	1088
Reflns. Collected	7299	2704
Indep.reflns.[*R*(int)]	8420[0.0517]	10568[0.0855]
Max/min transmission	0.922 and 0.801	0.9518 and 0.8997
Data/restraints/parameters	8420/0/604	10568/0/595
GOF on F^2	1.090	1.002
Final R indices[$I > 2\sigma(I)$]	R1 =0.0399, wR2 = 0.1004	R1 =0.0493, wR2 = 0.0908
R indices (all data)	R_1=0.0707	R_1=0.0967
Largest diff peak and hole [e Å^{-3}]	0.787 and -0.707	0.783 and -0.827

Table 3.1 Crystallographic data for **1b** and **1b'**

Chapter 4

Study of Luminescence Mechanochromism, Aggregation Induced Emission Enhancement and 'Turn-On' Fluorescence Zn^{2+} Sensing in Dipyrromethane Derived 'Dragonesque Schiff-Base'

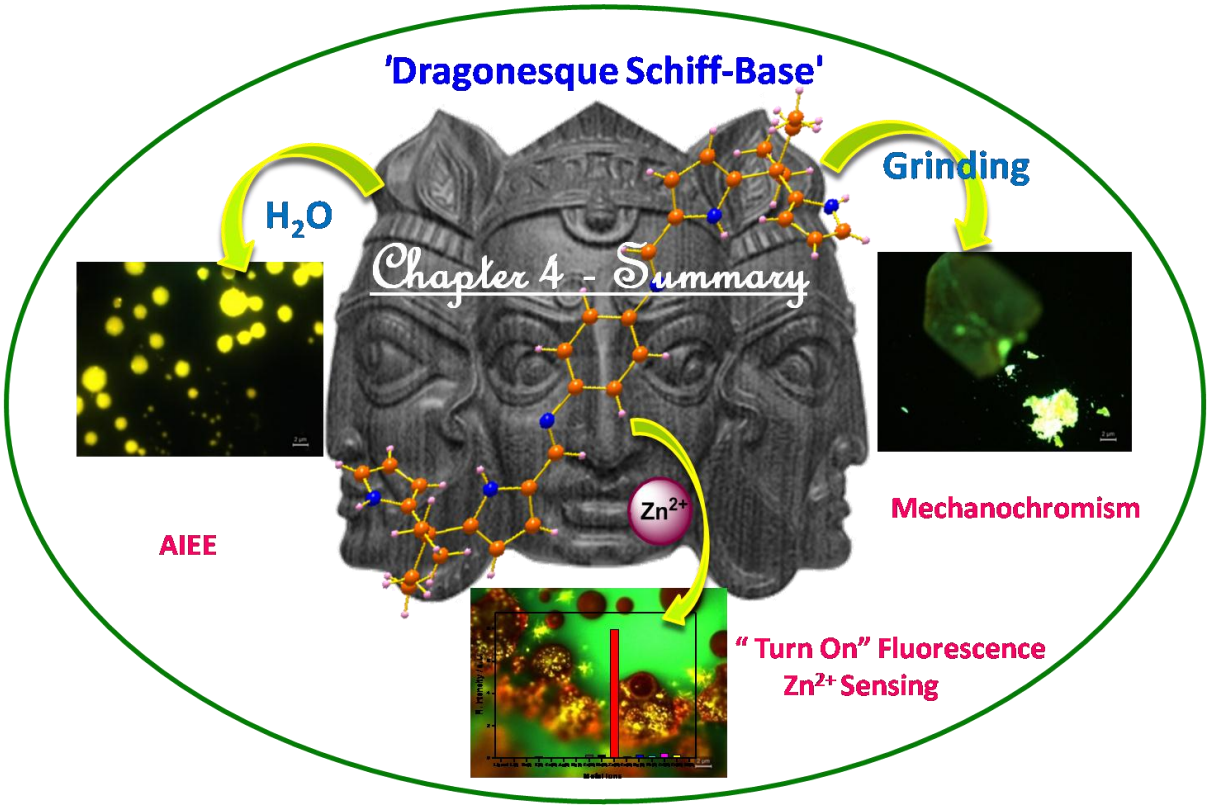

4.1 Abstract

*This chapter discloses the synthesis of novel acyclic pyrrole receptor, such as, double headed dragon shaped acyclic Schiff base, named as Dragonesque Schiff base (**DSB**) and describes three interesting properties; (i) Aggregation Induced Emission Enhancement (AIEE); (ii) Mechanochromism and (iii) Zn^{2+} ion sensing. Due to the strong intermolecular H-bonding interactions, **DSB** aggregates supramoleculerly and forms fluorescent organic nano spheres in CH_3CN solution. It aggregates further as the water content in CH_3CN increases from 80 to 95% affords fluorescent microspheres, which is highlighted in the first part of this chapter. In the second part, a thorough investigation of the colour and luminescence properties of the **DSB** crystal in response to mechanical stimuli revealed that **DSB** shows grinding induced luminescence mechanochromism and reverts back to its initial state on heating or recrystallization which is a consequence of the imine-enamine tautomerism existing in **DSB**. The last part of this chapter mainly focus on the Zn^{2+} sensing properties, where **DSB** selectively senses the Zn^{2+} ion in CH_3CN solution and exhibits 135 fold 'Turn - On' fluorescence. The ligand generates nano particles of different morphology depending upon the concentration of Zn^{2+} ions. At lower concentration of Zn^{2+}, **DSB** forms greenish yellow fluorescent fibre like structures of 2:1 complexes. Upon increasing the concentration of Zn^{2+} ions, **DSB** affords red non-fluorescent 2:2 complexes with nano sphere like morphology. The aggregation induced emission followed by FON generation and the dual fluorescence response in the presence of Zn^{2+} ion concentration are in turn an inevitable consequence of unique packing in the solid state and restricted intramolecular rotation (IMR) due to intermolecular H-bonding interaction. Thus, **DSB** is a typical 'trimurthy' type molecule showing three characteristic properties such as AIEE, luminescence mechanochromism and Zn^{2+} sensing by single molecule, a consequence of noncovalent molecular interactions in the crystalline, amorphous and solution states.*

4.2 Introduction

Nature is the biggest inspiration for many scientists for designing smart molecules. In natural supramolecular systems like enzymes, the metal ions are held closer in a flexible cavity by heterocyclic nitrogen rich ligands including imine functionality [Veauthier *et al*. 2005]. Simple dipyrromethanes can bind only anions. This can be converted into cation binding receptors by functionalising it. Thus, one can easily tune the binding properties of these dipyrromethanes by functionalising into corresponding Schiff bases, amides, carboxylic acids etc. So, Schiff base functionalisation of dipyrromethane can be an interesting strategy for construction of bi - nuclear ligands for various photophysical applications.

4.2.1 Schiff bases

Schiff bases are named after Hugo Joseph Schiff one of the founders of modern chemistry. Schiff bases are formed when any primary amine reacts with an aldehyde or a ketone under specific conditions. Structurally, a Schiff base (also known as azomethine or

Figure 4.1 Hugo Schiff, 24 April 1915, (Adapted from the reference Qin *et al*. 2013).

imine) is a nitrogen analogue of an aldehyde or ketone in which the carbonyl group (CO) has been replaced by an imine or azomethine group. Schiff bases are vigorously studied because of their attractive chemical and photo-physical properties. The imine group present in Schiff bases have been shown to exhibit a broad range of biological activities, including antifungal, antibacterial, antimalarial, antiproliferative, anti-inflammatory, antiviral, and antipyretic properties [Siji *et al*. 2011]. Imine or azomethine groups are present in various natural, natural-derived and non-natural compounds. Their photophysical properties are used in molecular self-assembly in electro luminescent devices, dyes and pigments, catalysts, intermediates in organic synthesis, polymer stabilizers, medicinal chemistry, NLO devices, chemical sensors, drug delivery devices, bioreactors, biosensors, nanotechnology [Gupta *et al*. 2008; Cozzi *et al*. 2004; Borisova *et al*. 2007, Kumar *et al*. 2009, Qin *et al*. 2013, Jia *et al*. 2015].

4.2.1.1 Syntheses of Schiff bases

The original reaction discovered by 'Hugo Schiff' for the preparation of Schiff bases consists of the reaction of an aldehyde (respectively a ketone) with a primary amine and elimination of one water molecule (Scheme 4.1). This reaction can be accelerated by an acid-

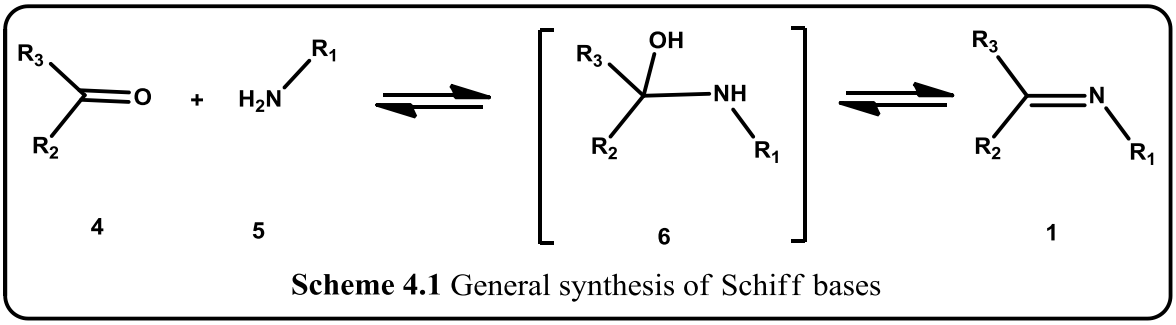

Scheme 4.1 General synthesis of Schiff bases

catalysis and is generally carried out by refluxing a mixture of a carbonyl compound **4** and an amine **5**, in a Dean Stark apparatus for removing water. This removal is important because conversion of **6** into the imine **7** is reversible (Scheme 4.1). Several dehydrating de-hydrating

agents have been successfully used including sodium sulphate and molecular sieves. Some *in situ* methods, involving dehydrating solvents such as tetramethyl orthosilicate or trimethyl orthoformate, have been reported as well. Acid-catalyst used, which includes mineral acids, like H_2SO_4 or HCl, organic acids such as *p*-toluene sulphonic acids or pyridinium *p*-toluenesulphonate, acid resin, montmorillonite or even Lewis acids like $ZnCl_2$, $TiCl_4$, $SnCl_4$, BF_3Et_2O, $MgSO_4$, and $Mg(ClO_4)_2$ [Qin *et al*. 2013].

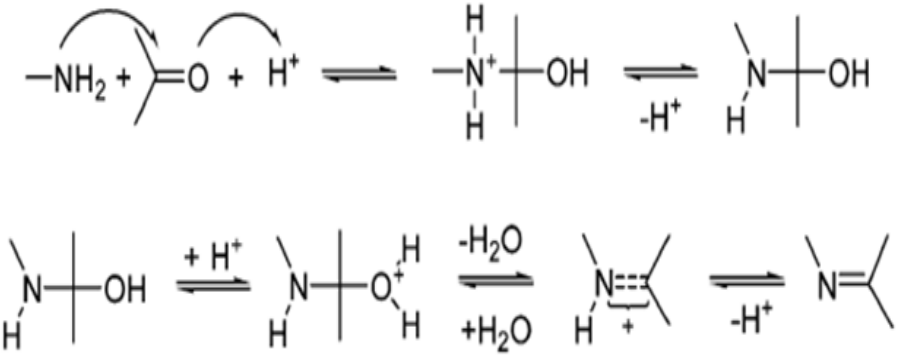

Scheme 4.2 Mechanism of Condensation of Carbonyl Compounds with Amines

The mechanism of the classical Schiff base condensation reaction is given in the Scheme 4.2. All steps in this reaction sequence are reversible. Therefore, the Schiff condensation under thermodynamically controlled conditions can be used for generating dynamic combinatorial libraries if several different amines or carbonyl compounds are used as starting compounds simultaneously [Borisova *et al*. 2007]. Some of the other methods of preparation of Schiff bases include aerobic oxidation syntheses from alcohols and amines, addition of organometallic compounds like Grignards reagents to alkyl and aryl cyanides, reaction of phenols and phenol ethers with nitriles, reaction of metal amides from ketals, reaction of amino acids with sodium hypochlorite etc. [Qin *et al*. 2013].

4.2.1.2 General properties of Schiff bases

Structurally, the presence of a lone pair of electrons in an sp^2 hybridised orbital of nitrogen atom of the azomethine group in a Schiff base is of considerable chemical importance and impart excellent chelating ability when used in presence of donor atoms near the azomethine group (Chart 4.1).

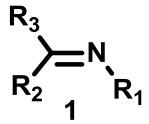

1

Chart 4.1 General structure of Schiff bases, R_1, R_2, R_3 are alkyl or aryl group.

The IR stretching frequency of the CH═N falls in the range of 1600-1700cm^{-1}, ^{1}H NMR peak lies in the range of 8.56-9.48 ppm and UV-Visible absorption spectrum shows a band around 225-335nm. CH═N bond in Schiff bases imparts autofluoresence to the molecule due to n-π* transition. More over CH═N bond is considered as a dynamic covalent bond. All these properties of Schiff bases are utilised a large range of application listed below. Schiff bases and its complexes are used as catalysts in numerous organic reactions like oxidation, epoxidation, hydrogenation etc. Large number of Schiff bases and its complexes are reported as sensors for various analytes due to the dramatic variation in ^{1}H NMR chemical shift, colour, absorption spectra, fluorescence property etc upon binding with the analytes. They can be used as building blocks for various supramolecular architectures, nano structured materials [Sessler *et al*. 2006, Ustynyuk *et al*. 2007, Kumar *et al*. 2009, Akila *et al*. 2013, Zoubi *et al*. 2013, Qin *et al*. 2013, Jia *et al*. 2015].

Among the various Schiff bases, pyrrole based derivatives are found to be particularly attractive. Jason B. Love and co-workers reported the acid-template synthesis of the compartmentalised diiminodipyrromethane macrocycle H_4[**L**] (**9**) and its Pd(II) complex **10.**

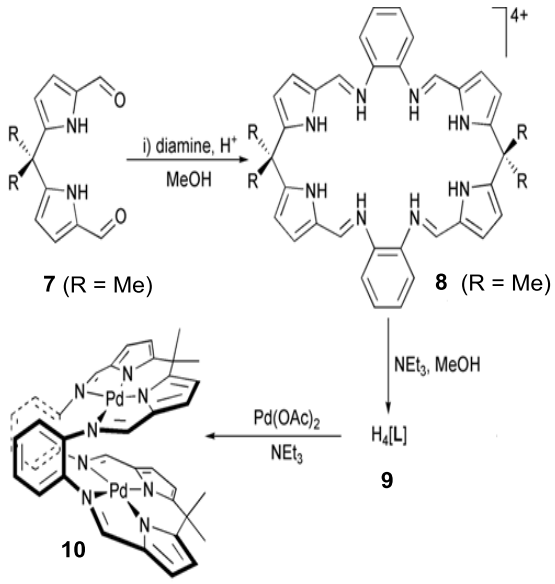

Scheme 4.3 Acid-template synthesis of diiminodipyrromethane macrocycle **8** and its Pd(II) complexe **10**.

The addition of *p*-toluenesulfonic acid to a stirred mixture of dialdehyde (**7**) and 1,2- diamino benzene in methanol generates the [2+2] Schiff-base condensation products **9**, in high yield as orange, microcrystalline solids [Givaja *et al*. 2003] (Scheme 4.3).

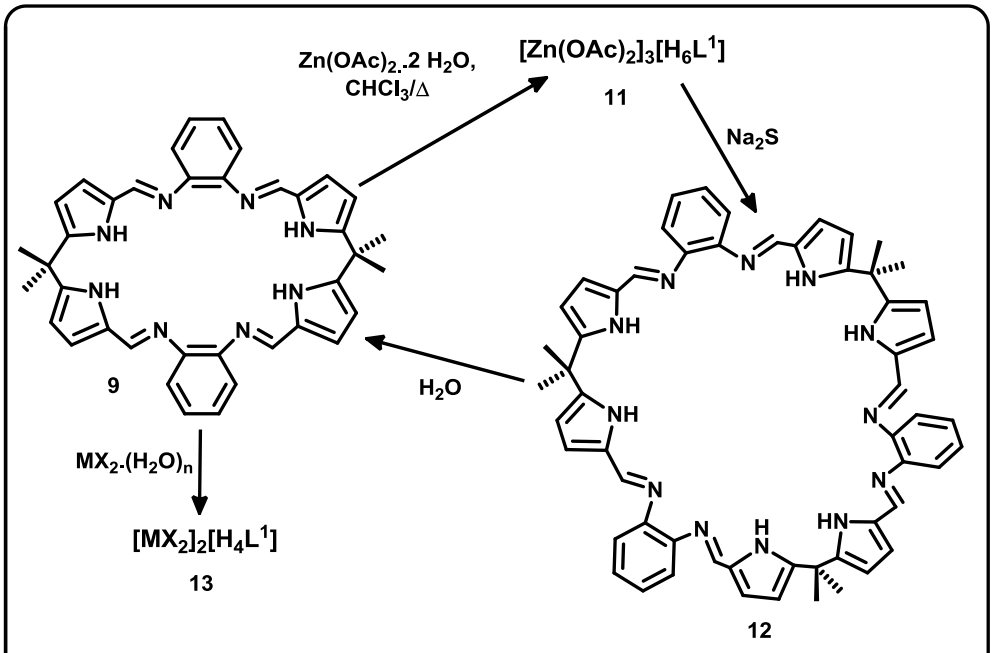

Scheme 4.4 Ring expansion, contraction and complexation reactions in Schiff base macrocycles **9, 11** and **12**.

The effect of metal complexation on the size of the ring has been studied by the same group and found that the reaction between a [2 + 2] Schiff-Base porphyrin analogue **9** and $Zn(OAc)_2$ results in the unusual formation of an enlarged [3 + 3] macrocycle that is stabilised by metal coordination and intramolecular hydrogen-bonding interactions (Scheme 4.4). The formation of expanded product (**12**) was confirmed by single crystal X-ray analysis. Expanded product undergoes ring contraction on reaction with water to yielding back the contracted macrocycle **9** which undergoes complexation with the corresponding metal hydrate yielding the metal complex **13** [Givaja *et al*. 2005]. Jin-Shi Ma and co-workers reported the syntheses of Zn^{2+} complexes **16** and **17**. The metal complexes were prepared by the co-ordination of Zn^{2+} ions with the acyclic ligands **14** and **15** of which **14** is simple dypyrrin ligand and **15** is an acyclic Schiff base ligand (Scheme 4.5) [Yang *et al*. 2003].

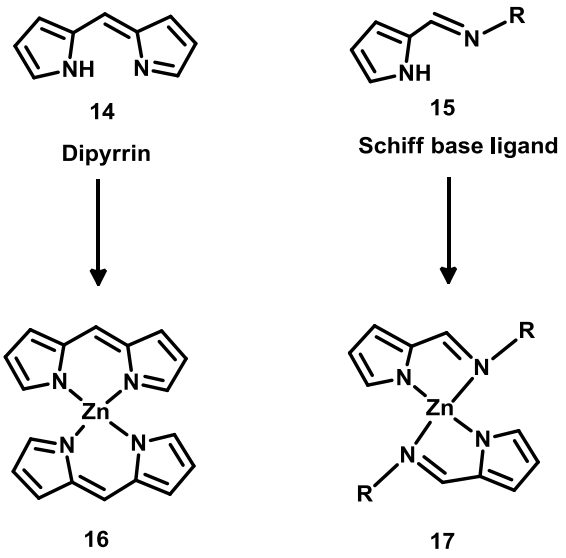

Scheme 4.5 Acyclic ligands **14**, **15** and their Zn^{2+} complexes **16**, **17** respectively.

4.2.2 Zn^{2+} ion sensing

Zinc being second most abundant transition metal ion in the human body, it plays important roles in both intra and extracellular functions [Que *et al*. 2008]. Zn^{2+} is present in a

large number of proteins and enzymes and. it is identified in recent researches to be responsible for neurological disorders such as alzheimer's disease, amyotropic lateral sclerosis (ALS), parkinson's disease and epilepsy [Cuajungco *et al*. 1997]. Zinc also plays a crucial role in insulin secretion, apoptosis, and immunity. The World Health Organisation estimates that limited dietary zinc is the reason for stunted growth in 40% of the children in the under developed countries [Onis *et al*. 2000]. This is because it is difficult to determine the amount of zinc in different biological samples due to lack of suitable biochemical markers for zinc ions. The wide range of physiological roles of biological zinc demands for highly sensitive techniques in real-time detection and imaging of zinc ions. The relative concentration of free Zn^{2+} within biological cells varies from 1nM to 1mM [Lippard et *al*. 1994]. The estimation of free zinc has proved to be difficult with classical methods because the concentration of free zinc (not strongly bound to proteins) is very low. All these facts leads to the need for developing selective and efficient molecular probes for Zn^{2+} ions. But Zn^{2+} is a difficult analyte to monitor owing to its closed shell $3d^{10}4s^{0}$ electronic configuration and the absence of oxidation-reduction activity within biological environments. The conventional techniques such as NMR, EPR and Electronic absorption spectroscopy are largely ineffective in the case of Zn^{2+} ions. Therefore Zn^{2+} ion is called spectroscopically silent metal ion. Atomic absorption spectroscopy (AA) is one of the sensitive and selective method for Zinc detection [Assaf *et al*. 1984]. However, this technique has limited spatial resolution and is destructive to the sample.

As Zn^{2+} is invisible to most analytical techniques, fluorescent technique can be used to visualize zinc ions [Kimura *et al*. 1998]. This method utilizes a probe molecule that recognizes Zn^{2+} and emits a specific wavelength upon binding, which used to track zinc ions in live cells with the help of a fluorescence microscopy. A fluorescent molecular probe consists of a fluorophore attached to a chelating agent or an ionophore with or without a

spacer group which on binding with the analyte results in either enhancement or change in the emission intensity of the probe [Silva *et al*. 1997]. Effective fluorescent probes for imaging metal ions in living cellular systems must meet several strict requirements. Most importantly, the probe should be selective for a specific metal ion over other biologically abundant cations, including those that exist at much higher cellular concentrations (for e.g. Na^{+}, K^{+}, Mg^{2+} and Ca^{2+}). Principles of co-ordination chemistry, including preferred donor numbers and ligand field geometries, as well as hard soft acid base (HSAB) considerations, are critical for designing and obtaining metal selective is preferred over a turn-off emission quenching response to maximize spatial resolution using light microscopy. Because, a metal responsive probe is inherently involved in complex equilibria with endogenous ligands within the cell, probes must be matched with dissociation constants (K_d) appropriate to the system under study. Furthermore, high optical brightness values can lower the amount of dye needed for cellular applications, which minimises the potential for altering endogenous cellular distribution. Dyes that have visible light excitation and emission are desirable in order to minimize sample damage and reduce auto fluorescence. Finally probes must be water soluble or water compatible. Addressing the challenge of meeting both chemical and biological constraints is critical to develop useful tools for cellular applications [Domaile *et al*. 2008].

In the past decade, chemosensors for Zn^{2+} ions has attracted great attention mainly due to the biological significance discussed above. A wide range of chemosensors are reported till date which includes derivatives of di-2-picolylamine (DPA), Quinoline based receptors like 8-hydroxyquinoline, bipyridine derived receptors, acyclic and cyclic polyamines, iminodiacetic acid and its derivatives and finally Schiff bases.The nitrogen of a Schiff base also exhibits a strong affinity for zinc. Therefore, the Schiff base has also been used to develop zinc chemosensors. The C=N isomerization is the predominant decay process of the excited states for compounds with an unbridged C=N structure so that those compounds are often

nonfluorescent. In contrast, the fluorescence of its analogues with a covalently bridged C=N structure increases dramatically due to the suppression of C=N isomerization in the excited states. Therefore the C=N isomerization can be applied in the design of chemosensors for metal ions. The binding of metal ions by the C=N group would stop the isomerization, and a significant fluorescence enhancement could be achieved. The appeal of C=N based fluorescent chemosensors is the large fluorescence enhancement induced by metal ion chelation. Compounds apply the C=N isomerization to act as zinc chemosensors with turn-on fluorescence signals. However, the main drawbacks of Schiff-base type receptors are the poor solubility, the instability of the Schiff-base in aqueous solutions and poor selectivity [Xu *et al*. 2010].

4.2.3 AIEE

Solid-fluorescent materials have variety of applications in diverse fields, such as fluorescent biological labels, sensors, and light-emitting diodes [Deans *et al*. 2000, Jenekhe *et al*. 1994]. Generally organic luminophores exhibit strong luminescence in dilute solutions; however, in the aggregated state, the formation of delocalized excitons or excimers often quenches the emission, which is known as "Aggregation Caused Quenching" (ACQ) of light emission in the condensed phase (Figure 4.2).The excited states of the aggregates often decay via non-radiative pathways thereby quenching the light emission in the condensed phase [Hong *et al*. 2009].

ACQ effect was an important obstacle in the development of efficient environmental sensors, biological probes, and light-emitting diodes.To eliminate or reduce this ACQ effect, various chemical and physical approaches have been developed. For example, the introduction of branched chains or bulky groups, covalently attached aromatic rings are known to hamper aggregate formation [Yang *et al*. 2008]. The best approach to the problems

above is to develop new luminophoric materials, whose aggregated state could emit more than that in solution state [Jakubiak *et al.* 1999,Chen *et al.* 2004, Thomas *et al.* 2007].

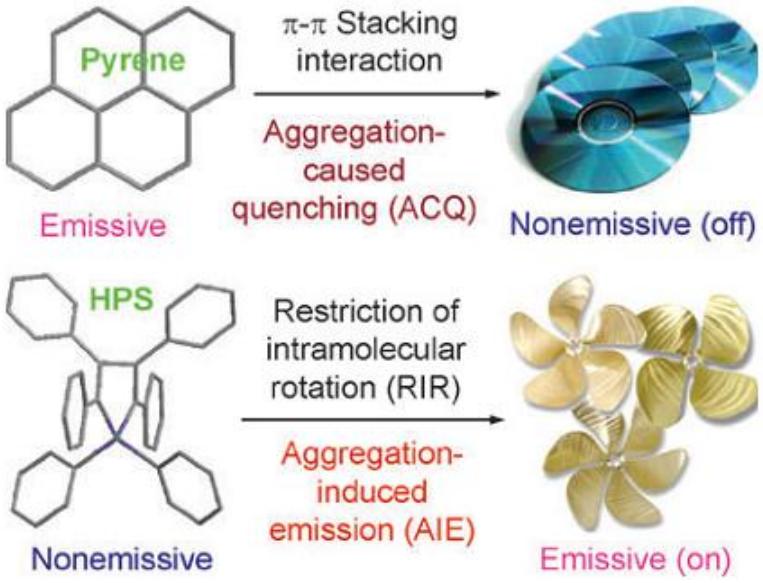

Figure 4.2 Planar luminogens pyrene tend to aggregate just as discs pile up due to strong π-π stacking interactions, which commonly turn ‘‘off’’ light emission, whereas nonplanar propeller-shaped luminogens such as hexaphenylsilole (HPS) behave oppositely, with their light emissions turned ‘‘on’’ by aggregate formation, due to the restricted intramolecular rotation in the aggregates of Luminescence mechanochromism [adapted from the reference Hong *et al*. 2009]

It seemed to be impossible to develop luminescent materials that can emit intense light in the solid state and, thereby, overcome the aggregation quenching problem. Luo and co-workers discovered such a system, in which luminogen aggregation played a constructive, instead of a destructive, role in the light-emitting process: a series of silole molecules were found to be non-luminescent in the solution state but emissive in the aggregated state (as nanoparticle suspensions in poor solvents or as thin films in the solid state). They coined the term 'aggregation-induced emission' (AIE) for this novel phenomenon, because the non-luminescent silole molecules were induced to emit by aggregate formation (Figure 4.3). Hexaphenylsilole (**HPS**) is among the first silole derivatives, from which the AIE phenomenon was unearthed [Luo *et al.* 2001]. The AIE effect has enabled silole molecule to emit efficiently in the solid state and the emission efficiency of a thin film of **HPS** (Φ_{film}) is as

high as 78%. Indeed, a few rare compounds have been found recently that show significant enhancement of their light-emission upon aggregation or in the solid state. Since then, AIE

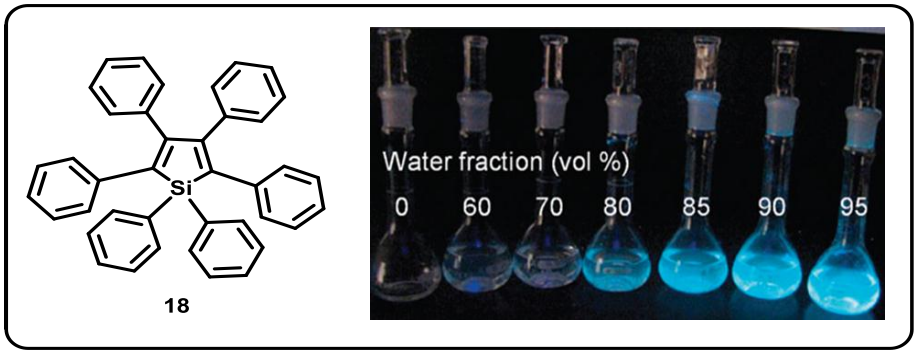

Figure 4.3 Solution of hexaphenylsilole in CH_3CN-water mixtures containing different volume fractions of water [Adapted from the reference Luo *et al.* 2001].

materials have been found to be promising emitters for the fabrication of highly efficient electroluminescent devices and stimuli-responsive materials for use in multifunctional switches. But, discoveries of AIE materials are limited and most of them are silole-based compounds. In the past decade, many research groups have enthusiastically worked on developing new AIE mechanisms, design of new AIEgens, manipulation of their morphology, and exploration of their technological applications. The dynamic research has resulted in the collection of a wealth of mechanistic insights, development of a variety of new AIEgens, and demonstration of a number of practical applications [Mei *et al*. 2014].

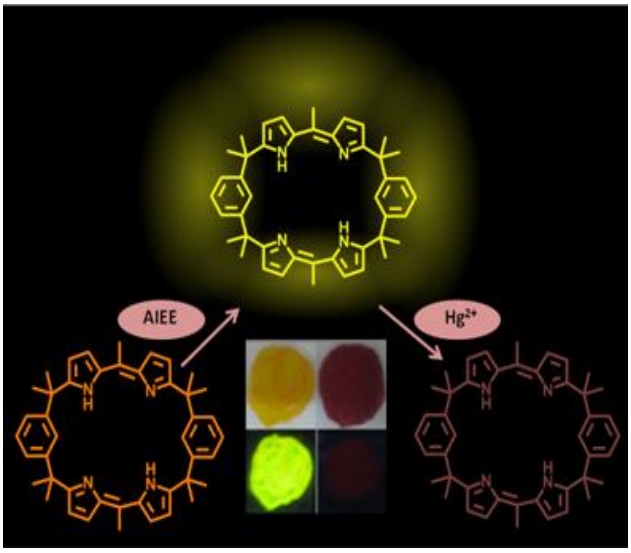

Figure 4.4 Aggregation-induced emission enhancement phenomenon in core-modified, expanded calixphyrin [adapted from the reference Salini *et al*. 2011]

Salini and co-workers reported the synthesis of a hybrid, core-modified, expanded calixphyrin, confirmed by single-crystal X-ray analysis, and found to exhibit aggregation-induced emission enhancement (AIEE) characteristics (Figure 4.4). The aggregate formation was confirmed by HR-TEM analysis. The efficient emission in aqueous solution and in the solid state was utilized for metal-ion-sensing studies, which concluded a potential application for selective detection of Hg^{2+} ions (Figure 4.4) [Salini *et al*. 2011].

4.2.4 Luminescence mechanochromism

The chromism refers to a process that imparts change in colour of compounds by a reversible process. If chromism is induced by heat it is termed as thermochromism, that induced by irradiation with light is termed as photochromism. The Figure 4.5 shows the respose of various mechanochromic materials to external stimuli like grinding or scratching

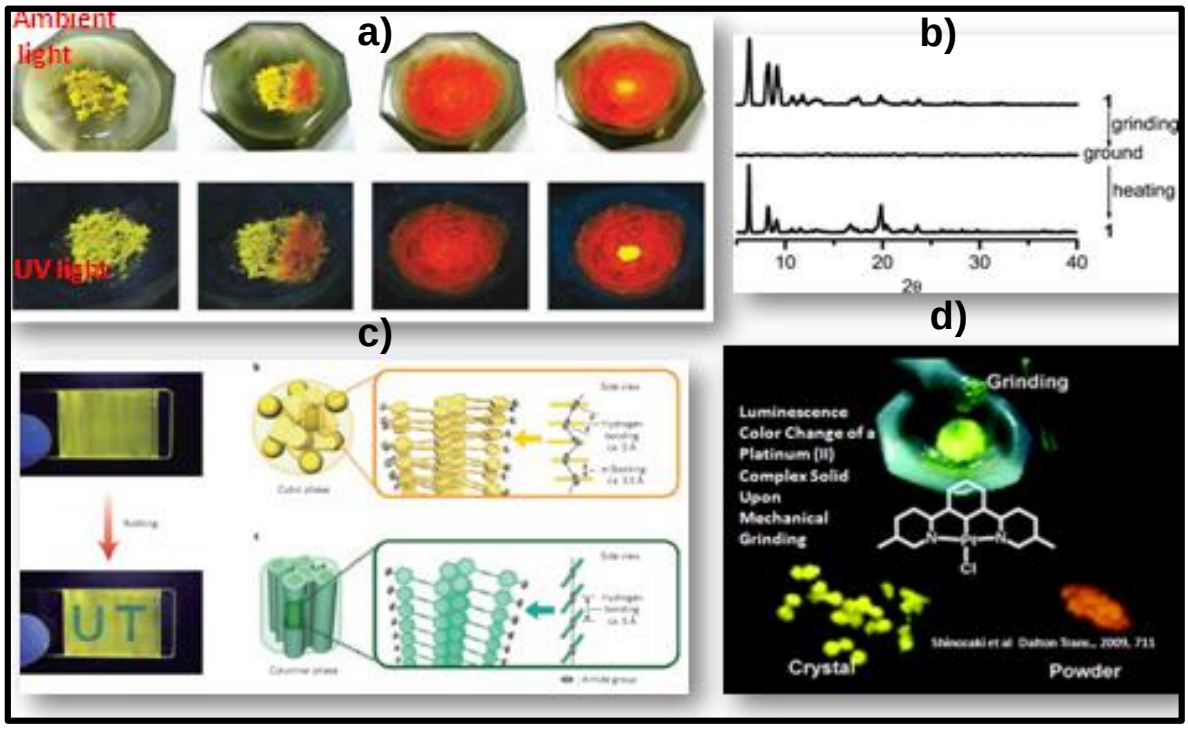

Figure 4.5 Phenomenon of Luminescence mechanochromism.

reverting back to the original form on heating or re-crystallisation. The Figure 4.5a shows unusual, reversible, and reproducible mechanical stimuli-responsive color and luminescence

switching in a Planar platinum (II) complex of 5-trimethylsilylethynyl-2,2'-bipyridine. When crystalline form of the complex is ground, bright yellow-green emitting is immediately converted to red luminescence. The crystalline state is transformed to an amorphous phase that can be reverted to the original crystalline state by organic vapor adsorbing or heating, along with red luminescence turning back to yellow-green emitting. The reversibility and reproducibility of luminescence mechanochromic properties have been dynamically monitored X-ray diffraction patterns (Figure 4.5b). The drastic grinding-triggered emission red shift is likely involved in the formation of a dimer or an aggregate through Pt-Pt interaction, resulting in a conversion of the ^{3}MLCT/^{3}LLCT emissive state in the crystalline state into the ^{3}MMLCT triplet state in the amorphous phase (Ni *et al*. 2011).

The Figure 4.5c shows that the thin film of a pyrene derivative on a glass substrate was obtained by casting from hexane solution (top), and the text 'UT' (below) was formed by rubbing the substrate with a glass rod at room temperature. The yellow emitting part is in the cubic phase, and the blue-green emitting part is in the shear-induced columnar phase. The emission images were taken under UV irradiation (365 nm) [Sagara *et al*. 2009]. The mechanochemical behavior of Pt complex of a pyridyl derivative is highlighted in the Figure 4.5d. The yellow luminescence of the crystalline complex changed to orange red when grinding into fine powder on a glass substrate with a spatula. A broad emission band, which was not detected for the crystal, was observed at around 670 nm for the powder [Abe *et al*. 2009].

Wang and co-workers investigated whether proton transfer will happen under external stress in a twisted, conjugated, amphoteric para nitro indole derivative. The molecule exists in neutral crystalline form with bright yellow color, when subjected to external stress the yellow colored compound **19** turned into red with an absorption shift from 450 nm to 550 nm as a result of zwitter ionic transformation. The red color of the ground sample **20** reverted back to

original yellow form with wetting with ethanol. Thus Stress has been proved to acidulate amphoteric molecules and promote an intermolecular proton transfer, which results in a significant absorption and emission change. The stress acidulated amphoteric molecules open a new avenue for developing mechanochromic materials and anticipate many broad applications such as stress/pressure sensors and rewritable media (Figure 4.6) [Wang *et al*. 2013].

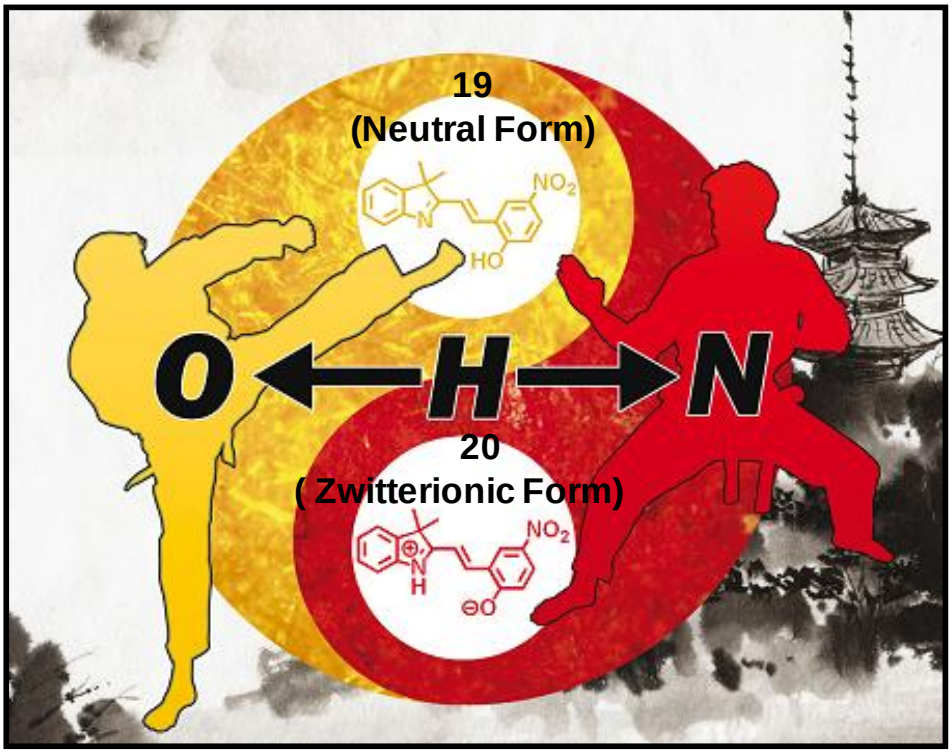

Figure 4.6 Phenomenon of mechanochromism via reversible intermolecular proton transfer in stress acidulated amphoteric molecules [adapted from the reference Wang *et al*. 2013]

In short, Luminescence mechanochromism is a reversible light-emitting or colour switch triggered by mechanical stimuli, such as grinding, crushing, rubbing, extruding, or pressing, and is useful in mechanical sensing, stress monitoring, damage detecting, optical recording, memory, and display [Sagara *et al*. 2009]. The change in fluorescence characteristics of the molecules with response to external stimuli like grinding, light or heat, may be due to various reasons and photochemical mechanisms. For example Sreedevi and co-workers reported light triggered enolization in diformyl diaryl dipyrromethane by excited

state dual proton transfer (ESDPT) induces "turn on" fluorescence (Figure 4.7). The UV-Vis absorption spectrum of **21** in acetonitrile showed an absorption maximum at 300 nm with a very weak emission band at around 560 nm. **21** in acetonitrile was exposed to UV irradiation absorption band at 300 nm decreased gradually with the appearance of a new broad band around 390 nm. UV irradiation was accompanied by a color change from colorless to bright yellow exhibited a clear isobestic point at 316 nm (Figure 4.8b), also the fluorescence intensity of the band at 560 nm enhanced with bright green emission (Figure 4.8c, inset). The role of diaryl and diformyl groups in the enolization process was confirmed by photophysical and theoretical studies [Sreedevi *et al*. 2014].

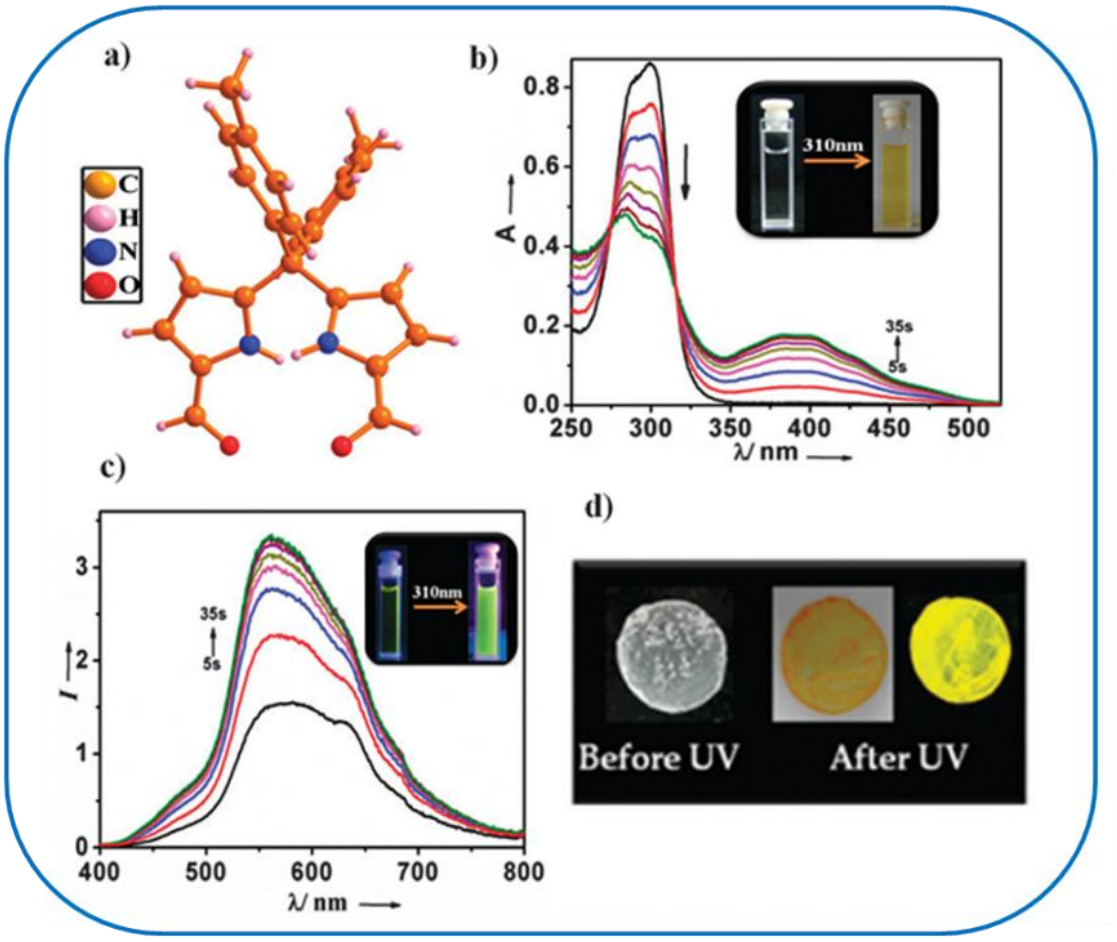

Figure 4.7 (a) Single crystal X-ray structure of diformyl diaryl dipyrromethane (**21**), (b) absorption and (c) emission changes of **21** upon UV irradiation along with visible color and emission changes (inset). (d) The solid state color change of **21** before and after UV irradiation under visible and UV light [adapted from the reference Sreedevi *et al*. 2014].

Organic fluorophores with properties like AIEE, Stimuli induced reversible solid state fluorescence is always a hot area of research due to their wide variety of application potentials in the field of optoelectronic devices, biotechnology, memory devices. Mechanochromic material which turns on emission on external force stimuli like pressure or grinding has promising application in optical data storage, pressure storage, rewriting data, security ink etc. Different mechanisms are responsible for this stimuli induced change in luminescence property. Solid state luminescence of a compound can be varied without chemical modification through non covalent routes such as polymorphism (through conformational/packing changes), phase transition (structural changes while maintaining the molecular integrity), amorphization (disrupting the long-range molecular ordering) and preparation of multi-component systems (controlling fluorophore aggregation) [Varughese *et al*. 2014].

Overall, the organic fluorophores with tunable optical properties like AIEE characteristics, 'turn-on' emission by external stimuli like pressure or grinding and material and sense exclusively the Zn^{2+} ions over the biologically interfering metal ions are quiet rare. Most of the materials have either combination two or mostly single property. Thus, the material with mentioned all these properties find suitable for developing optically smart materials.

4.3 Objective of our work

Dipyrromethane occupy the centre place in porphyrin chemistry due to rich co-ordination and anion recognition property. While Schiff bases are considered as privileged ligands due to their co-ordination, metal ion recognition and relative ease of formation. From the literature survey, it is clear that dipyrromethanes and Schiff bases are coupled to prepare a variety of macrocyclic systems. Enormous number of *Salen* and *Salphen* type Schiff bases are synthesised and properties are exploited to date but acyclic Schiff bases derived from simple

dipyrromethanes are rare. This chapter discloses the details of the synthesis of a novel acyclic Schiff base receptor. The structural design of the Schiff base will pave the way to new class of dipyrromethane based Schiff bases which can be abbreviated as *dipyrroen* and *dipyrrophen* Schiff bases. Exploiting the properties of both dipyrromethanes and Schiff base the design of the ligand was carefully done. The double ethyl groups were imparted to the ligand system at the *meso* positions of the dipyrromethane in order to ensure solubility, flexibility and ability to interact non-covalently, imine nitrogen for cation binding and hydrogen bonding, pyrrolic NH as anion binding and hydrogen donor sites, while the phenyl ring for π-π interaction. Former part of the chapter deals with synthesis of '*double headed dragon*' shaped acyclic Schiff base termed as dragonesque Schiff base (**DSB**) from the precursor **2** and latter part describes a detailed study of the aggregation induced emission enhancement (AIEE), Zn^{2+} sensing property and luminescence mechanochromic nature of **DSB**. The compound **DSB** was found to exhibit an enhanced emission in the presence of higher water concentration and the aggregates form fluorescent microspheres. The molecule **DSB** selectively senses the Zn^{2+} in acetonitrile solution exhibiting 'Turn-On' emission and also generates nano particles of different morphology depending upon the concentration of Zn^{2+} ions. Finally, the mechanochromic nature of **DSB** is also explored by grinding, which reverts back to its initial state by heating or recrystallization. Thus, **DSB** is a unique material with all the three mentioned characteristic properties, a consequence of noncovalent molecular interactions.

4.4 Results and Discussion

4.4.1 Synthesis of DSB

The synthesis of acyclic *meso*-di(ethyl)dipyrromethane based Schiff base **DSB** is summarized in Scheme 4.6. The synthesis of **DSB** was achieved in three steps. The first two steps which involves the syntheses of 1-formyl-5,5-di(ethyl)dipyrromethane (**2**), which has been already discussed in chapter two. The final step is the Schiff base condensation reaction

of 1-formyl-5,5-di(ethyl)dipyrromethane (**2**) with *p*-phenylenediamine (**3**) in methanol at room temperature generating yellow colored ditopic dragonesque shaped ligand **DSB** in 60% yield. The Schiff base receptor **DSB** is soluble in common organic solvents but insoluble in water. Schiff base **DSB** was fully characterized by electronic, FAB-MS, NMR spectral studies and finally confirmed by single-crystal X-ray diffraction analysis.

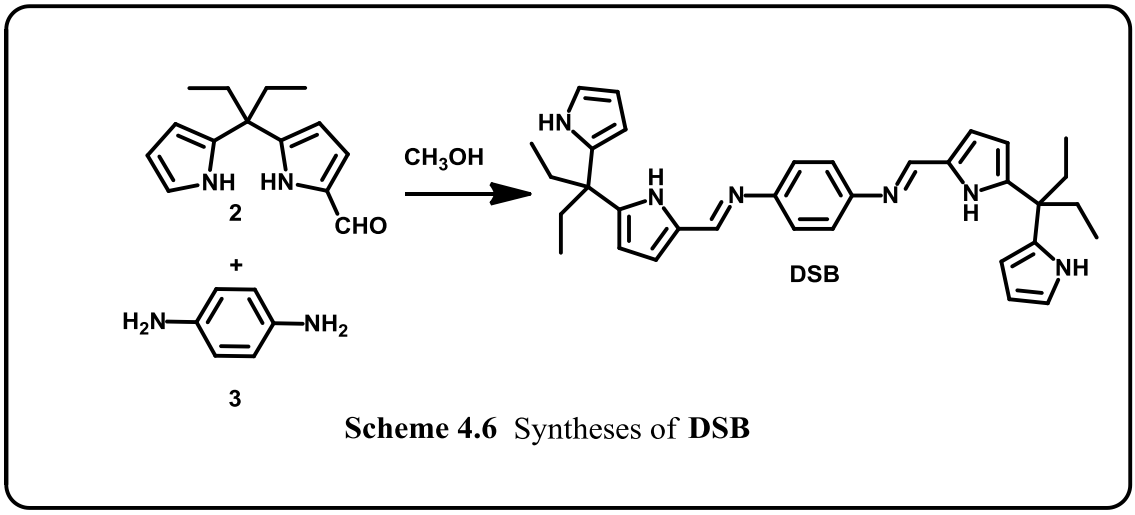

Scheme 4.6 Syntheses of **DSB**

4.4.2 Structural features of DSB from single crystal X- ray analysis

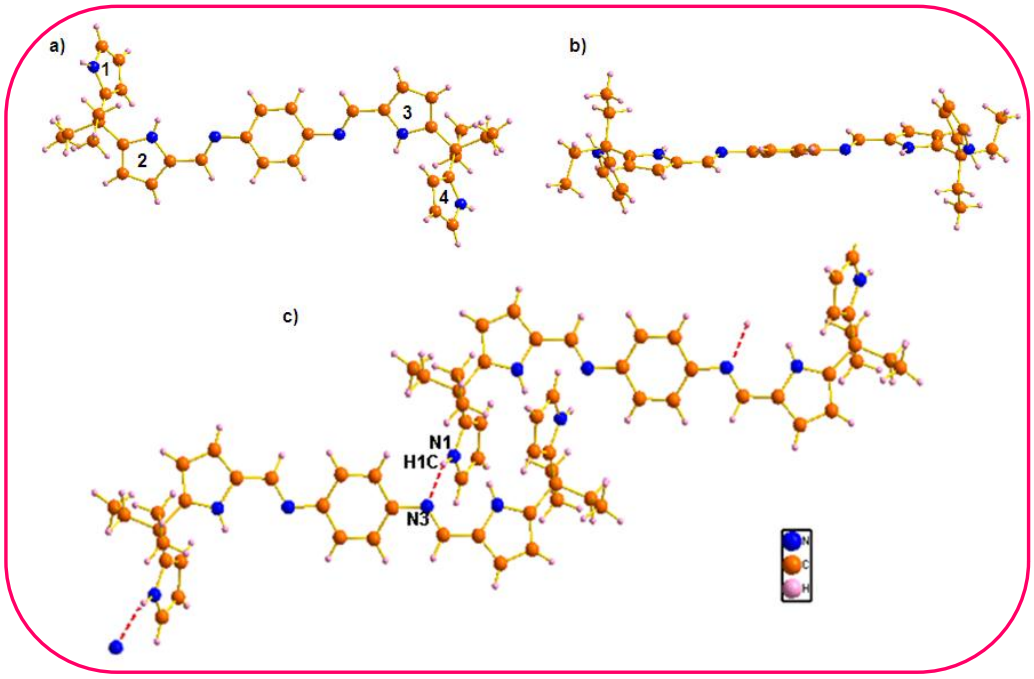

Figure 4.8 a) Single crystal X-ray structure of **DSB** a) top view, b) side view and c) 1-D array.

The single-crystal X-ray analysis of **DSB** is shown in Figure 4.8. Good quality single crystals were grown by the slow diffusion of *n*-heptane into the $CHCl_3$ solutions of Schiff base. The molecule crystallizes in monoclinic system with two molecules per unit cell. The molecule has a centre of symmetry and one half is generated using diamond software. Schiff base contains 1,4-substitued phenyl part, four pyrrole rings, four ethyl moiety, two C=N linkage and two meso sp^3 hybridized carbons. The **DSB** adopts a non-planar, *double headed dragon* like (*dragonesque*) shape in which the two dipyrromethane units linked through C=N linkage to the phenyl ring in *trans* fashion to it. From the crystal structure, it is clear that NH protons of the pyrroles which are connected to the CN bond and terminal pyrroles are pointing in opposite directions. The dihedral angle between the pyrrolic planes 2 and 3 which are linked to CN bond is zero which clearly shows that they are in one plane. The dihedral angles between the pyrrolic planes 1 and 4 are also zero which clearly shows that they belong to parallel planes. One dimension array of the Schiff base is formed by the intermolecular hydrogen bonding interaction between imine N (N3) and terminal pyrrolic N (N1-H1C)) ie. (N1-H1C….N3) interaction with bond distance and angle of 2.17Å, 152.86º respectively.

4.4.3 Photophysical properties of DSB

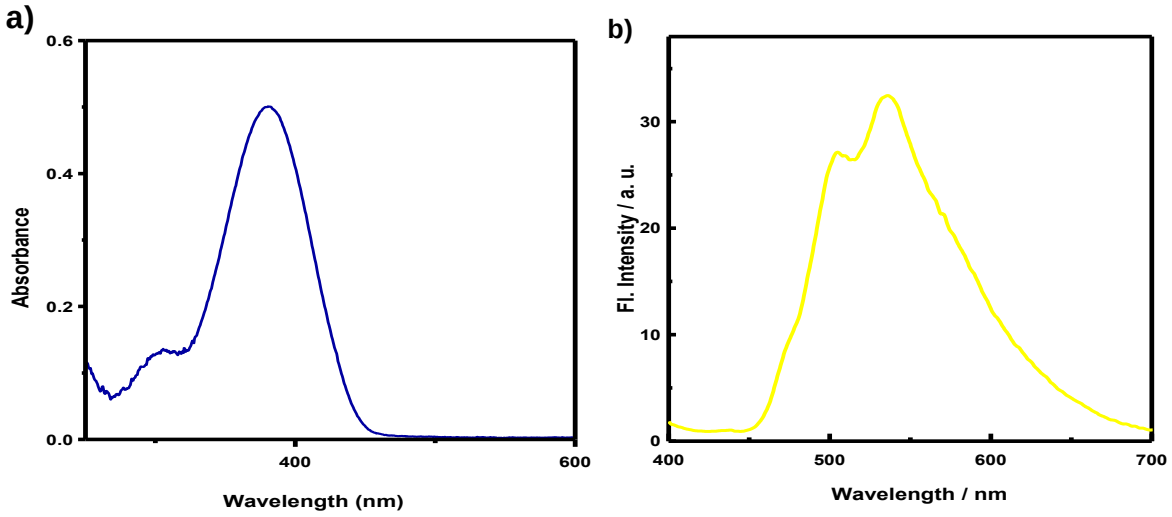

Figure 4.9 a) UV- Visible absorption spectrum of **DSB** and b) solid state fluorescence emission spectrum of **DSB**

The Schiff base receptor **DSB** is soluble in common organic solvents but insoluble in water. When dissolved in good solvents like ACN, **DSB** shows an absorption maximum at 380nm (Figure 4.9a) and with practically a very weak emission band around 480nm. But the molecule shows strong emission in the solid state (Figure 4.9b). The reason for no emission in solution state is a kind of tautomerism existing in **DSB** molecule, which is discussed later in this chapter. As observed from the single crystal x-ray structure, a single **DSB** molecule is forming four intermolecular H- bonds which restricts the tautomerism and IMR which in turn rigidifies the molecular conformation leading to solid state fluorescence.

4.4.4 AIEE characteristics of DSB

To get a clear picture of the AIEE characteristics, the ligand **DSB** was dispersed in CH_3CN (solvent) – water (non solvent) mixture systems with the concentration being kept at 15μM. The UV-Visible absorption spectra and PL spectra of **DSB** were measured in water/ CH_3CN mixtures with different volume fractions of water. The absorption spectrum of **DSB** when dissolved in 100% CH_3CN shows an intense peak at 380 nm and a weak band at 310 nm

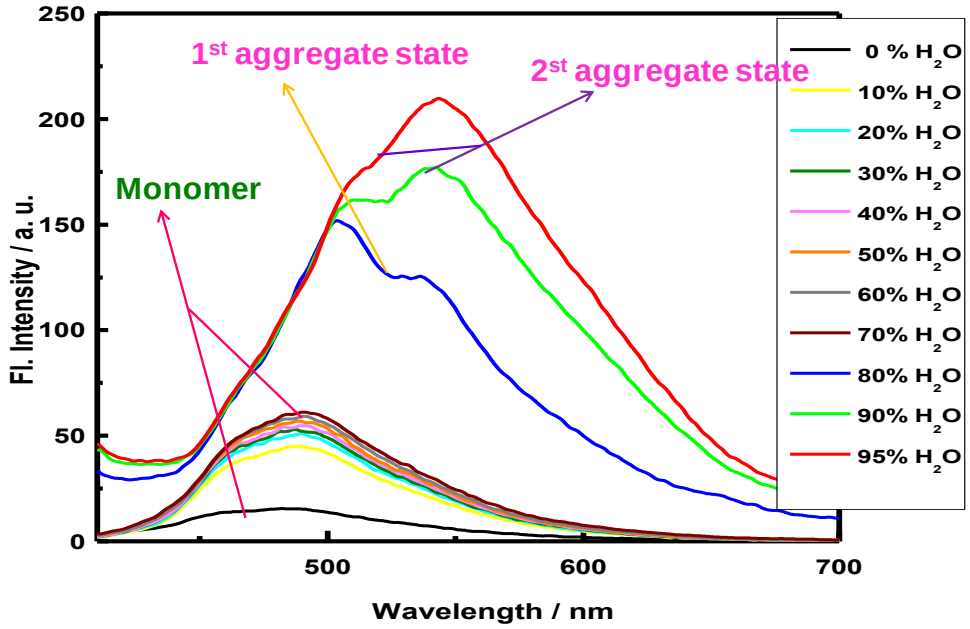

Figure 4.10 Emission spectra of DSB (15μM) in CH_3CN / water mixtures (f_w=0-95 vol%).

which is one third less intense as compared to the primary band (Figure 4.9a). The absorption band arises due to n-π* and π-π* transitions. For excitation at 380 nm, **DSB** shows a very weak broad emission band with emission maximum at 480 nm which corresponds to the monomer emission (Figure 4.10). As the water percentage increases from 0 to 70, there is a gradual increase in the monomer emission intensity. When the percentage of water reaches 80%, the emission intensity increases dramatically and appears as two distinct bands at 500 nm and 540 nm, where the band at 500nm has higher intensity than band at 540 nm (Figure 4.10). Further, when the water percentage is increased from 80% to 95%, the intensity of the peak at 540 nm increases. The Fluorescence intensity of DSB in 95% water-CH_3CN mixture is 32 fold higher than monomer emission of **DSB** in 100% CH_3CN solvent. This result is clearly reflected from Figure 4.11, where F/F0 is ploted against percentage of water. It confirms the fact that the emission observed here is from the aggregates. The spectral data reveals the presence of two type of aggregate formation depending on the percentage of water.

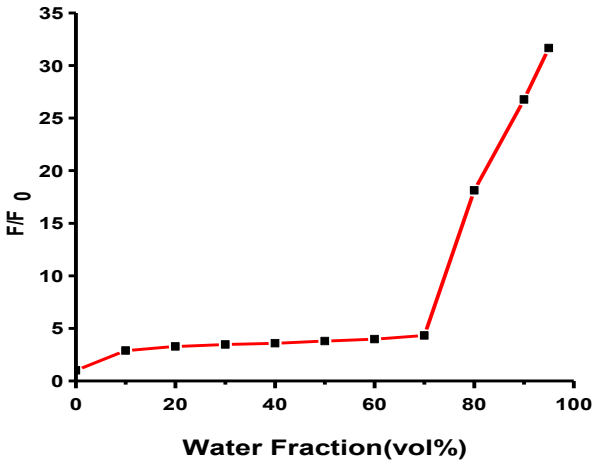

Figure 4.11 Plot showing the changes in the emission intensities of **DSB** with the water contents in the CH_3CN/water mixtures**.** $\mathbf{I_0}$= intensity in pure CH_3CN solution.

The emission spectra of the aggregate state and the solid state are almost same indicating the existence of same type of supramolecular assembly in both solid state (Figure 4.9b) and aggregate state (Figure 4.10). The results are further reflected from the electronic spectral analysis which is shown in Figure 4.12. The band at 380 nm in pure CH_3CN solution

is red shifted at 390 nm with increase in absorption intensity by 50:50 CH_3CN-water mixture. When the water percentage reaches 80% and above the absorption spectra is bathochromically shifted with large decrease in absorption intensity. It is accompanied by the observation of a light scattering tail in the long wavelength region suggesting the formation of nano aggregates (Figure 4.12). The formation of these nano particles decreases the solution concentration which is the reason for reduced absorption intensity. At this point the absorption depends on the solution concentration while the emission comes from the nano aggregates and quantum yield calculated by reference has no meaning therefore PL peak intensity versus solvent composition is used for the comparative study.

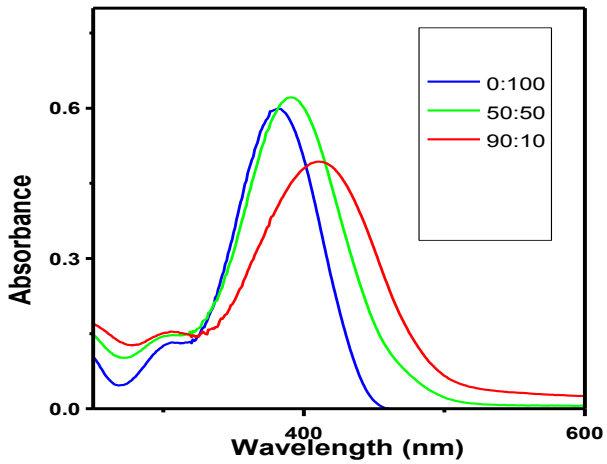

Figure 4.12 Absorption spectra of **DSB** (15µM) in CH_3CN and CH_3CN /water mixture.

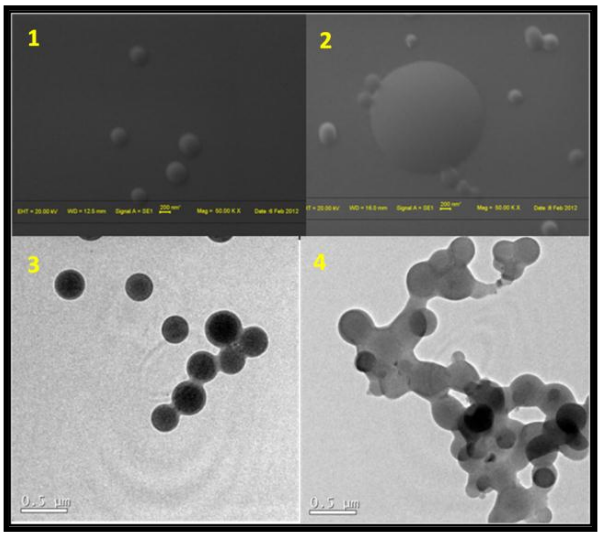

Figure 4.13 The SEM (1 & 2) and TEM (3 & 4) images obtained by drop casting of **DSB** in 100% acetonitrile (1 & 3) and 90% water/CH_3CN (2 & 4).

Finally the aggregate formation is confirmed by the SEM, TEM and OPM analysis. The morphological studies reveals the fact that the nano spheres of diameter ranging from 100 to 350nm in CH_3CN (Figure 4.13, 1 & 3) aggregates to form microspheres of diameter approximately 1.5 μm in presence of water through hydrogen bonding interaction (Figure 4.13).

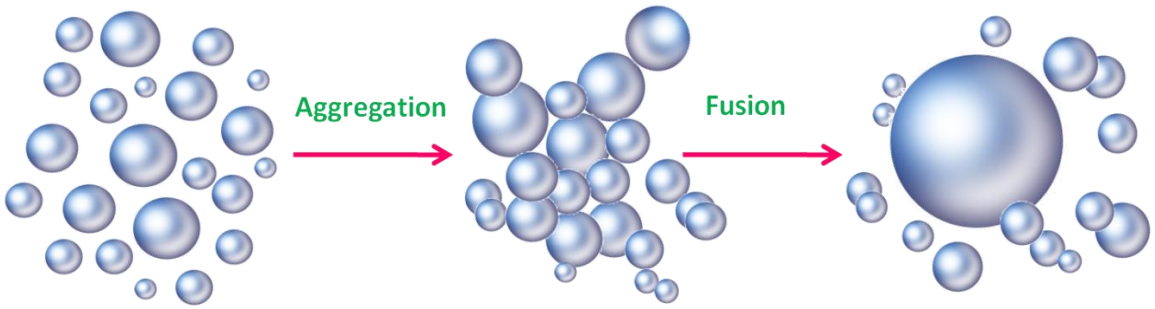

Figure 4.14 Schematic representation of conversion of nano spheres to micro spheres on aggregation.

The results are further confirmed by OPM images, where the images are obtained by drop casting DSB in 100% CH_3CN and 90% water/CH_3CN mixture on a glass slide and viewed through an optical polarisation microscope illuminated by UV light of wavelength 380nm (Figure 4.15). The images show a visual comparison of the solid state fluorescence and AIEE of **DSB**. In 100% CH_3CN the molecule forms nano spheres which in presence of water aggregates to form microspheres (schematically represented in Figure 4.14).

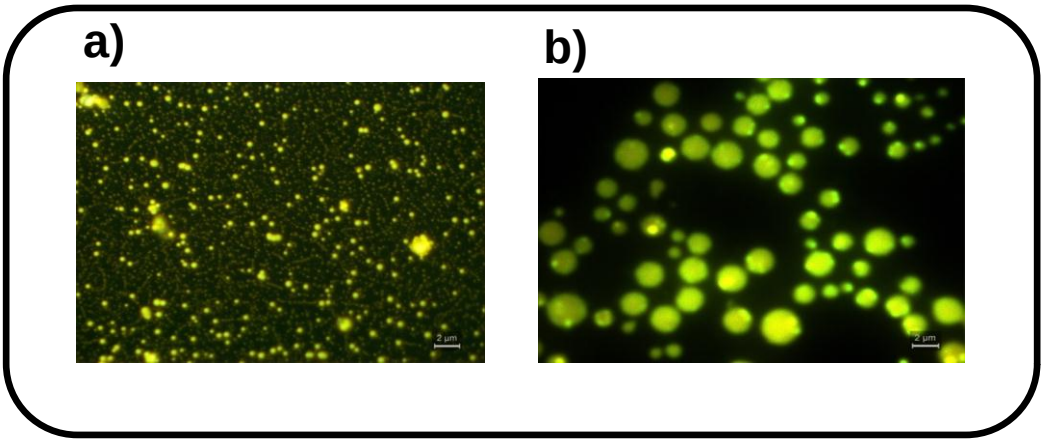

Figure 4.15 The OPM image of the **DSB** in a) 100% CH_3CN b) 90% water/CH_3CN mixture.

Finally the influence of temperature on the fluorescence spectra of **DSB** in 95% water / CH_3CN was studied in the temperature range between 288K to 358K (Figure 4.16). As the temperature increases from 288 K to 308 K, the emission intensity of the band at 545 nm decreases gradually. As the temperature reaches 308K there is an increase in intensity of the

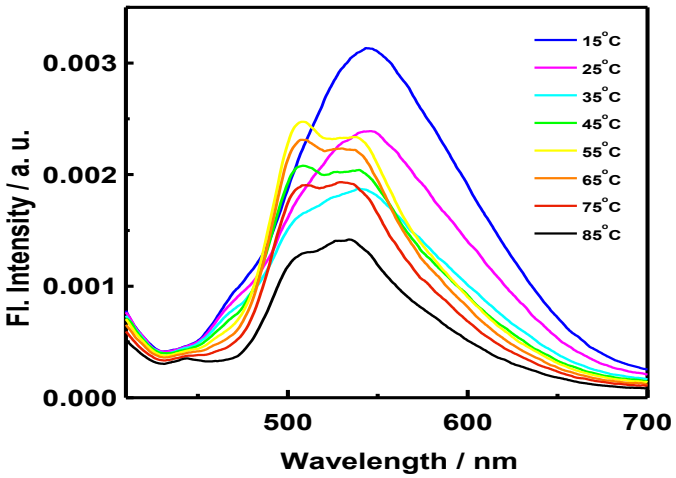

Figure 4.16 The variation of emission spectra of **DSB** with temperature.

peak at 500nm. When the temperature is increased beyond 328K quenching in emission is observed. These results suggest that the aggregated state of the compound breaks into monomer like state at high temperature causing quenching of emission. The temperature dependant studies validate the speculations that the aggregation through the inter- molecular H-bonding interaction of **DSB** molecule restricts IMR and tautomerism thus forming supramolecular assemblies similar to that of solid state enhancing the emission intensity. The increase in temperature causes breaking of aggregates which in turn causes increase in IMR and tautomerism causing quenching of emission.

4.4.5 Luminescence mechanochromism in DSB molecule

The color and luminescence properties of **DSB** were investigated with response to mechanical stimuli. The red colored crystal of **DSB** with very weak emission upon mechanical grinding produces highly luminescent yellow powder. There is a visible change of color from red to yellow (Figure 4.18). The fluorescence spectrum of both red crystal and the

yellow ground form consists of a band at 540 nm shouldered at 500 nm (Figure 4.17). The photoluminescence (PL) quantum yield of the yellow powder form is found to be 0.017 which is approximately 9 fold higher than that of the red crystalline form whose value is 0.002. Surprisingly the ground yellow form reverts back to the red form with quenching in emission upon spraying acetone or heating (Figure 4.19) or by recrystallisation.

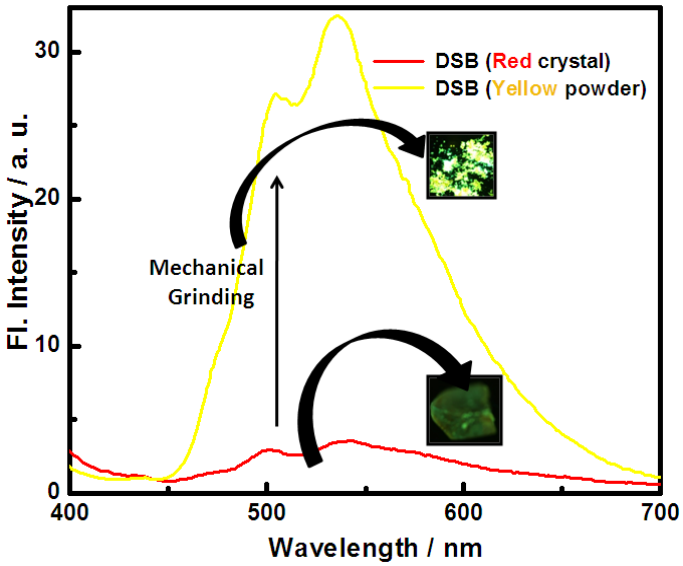

Figure 4.17 The Solid state fluorescence spectra of the red crystal and yellow powder form the inset consists of the fluorescence images of the red crystal and yellow powder illuminated by UV light of λ_{ex}=380 nm.

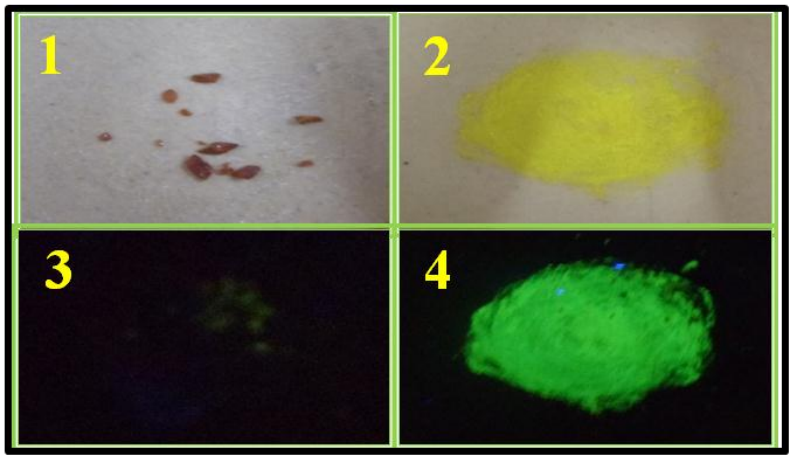

Figure 4.18 The Fluoresence microscope images of the crystalline **DSB** red form (1 & 2) and yellow powder form (3 & 4). Where 1) and 3) represents ambient light, 2) and 4) represents the UV light irradiation (λ_{ex}=380 nm).

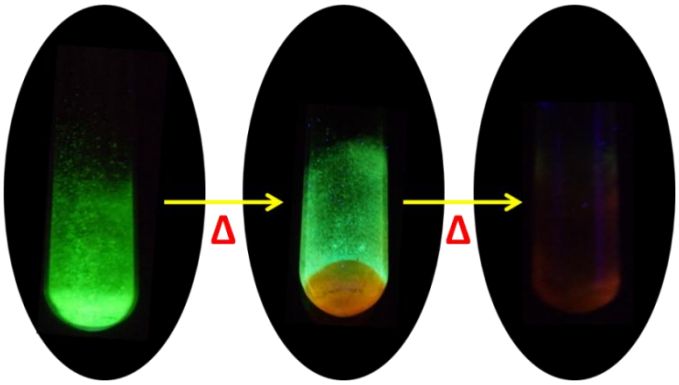

Figure 4.19 The Photographic images of the conversion of the emissive yellow powder to non-emissive red form on heating viewed under UV light (λ_{ex}=380 nm).

The results are further reflected in fluorescence microscope images of **DSB**, when illuminated under UV light of wavelength 380 nm when subjected to different stimuli like temperature, grinding and spraying of acetone (Figure 4.20). When the temperature was gradually increased from 25 ℃ to 200 ℃, the yellow form of **DSB** converted into red form with quenching in emission. The red form when further grinded re-converted into emissive yellow form 'turning-on' the emission. This yellow powder reverted back to non-emissive red form upon spraying acetone as a result of crystallization to red form of **DSB**.

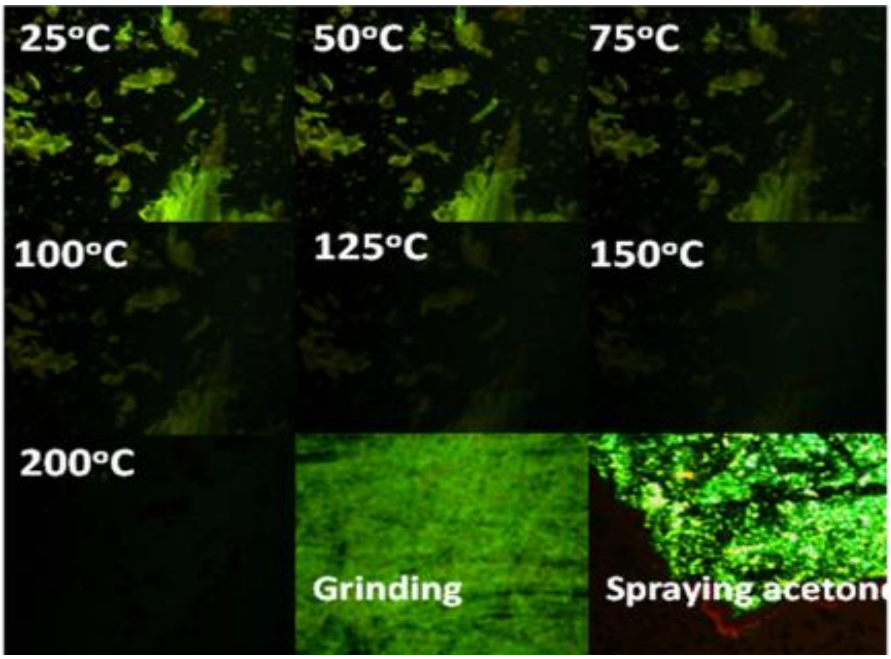

Figure 4.20 The fluoresence microscopeimages of the yellow form on heating from 25 °C to 200 °C and at various stages such as grinding and spraying acetone (λ_{ex}=380 nm).

To further get an insight of the mechanism behind the phenomenon of mechanochromism, Wide Angle X-ray Diffraction studies (WAXD) of both the red and yellow form of **DSB** was carried out. The XRD pattern of the red crystal consists of very sharp high intensity peaks which show the high crystalline character of the red form. This pattern completely disappears upon grinding (Figure 4.21). This throws light into the mechanism that molecular level grinding of the red crystal occurs by converting the highly crystalline red form to amorphous yellow powder form.

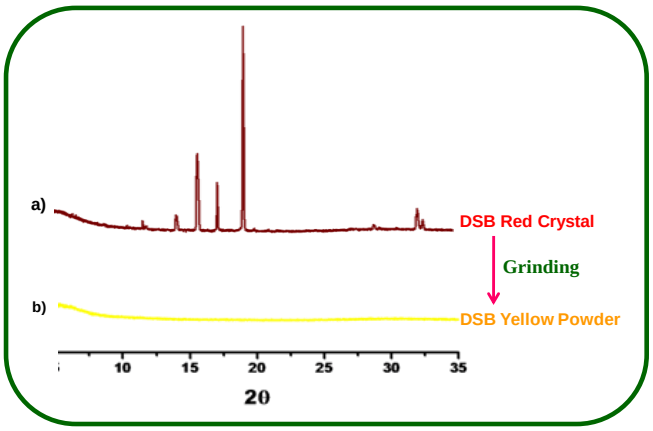

Figure 4.21 WAXD pattern of **DSB** (a) crystalline red sample and (b) ground yellow powder

To interpret the mechanochromism and thermochromism and get a clear insight about the mechanism, a variable temperature ^{1}H NMR studies was carried out. The ^{1}H NMR spectra of **DSB** in DMF (Figure 4.22) clearly visualises the presence of centre of symmetry of the ligand. Out of the two sets of pyrrolic NH, the peak corresponding to only one set of external pyrrolic NH is resonated at 10.43 ppm at room temperature. As the temperature is lowered the NH of the other pyrrolic ring which is directly bonded to the immine carbon begins to appear at 11.215 ppm. Similarly, the β-CH of the respective pyrrolic unit at room temperature resonated as a doublet is converted as singlet at low temperature. This may be due to the localisation of the NH proton at low temperature and also a kind of tautomerism, where the proton shuttles between the pyrrolic NH and Schiff base imine N as shown in Scheme 4.7 The interconversion between the tautomers is so rapid at high temperature which is reflected on

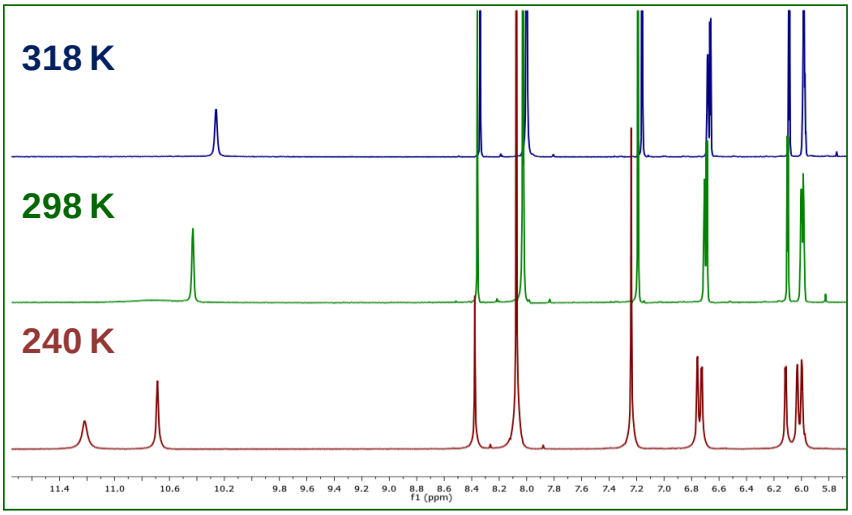

Figure 4.22 ^{1}H NMR spectra of **DSB** in DMF (Me_2NCHO-D_7**)** at various temperatures.

the NMR spectra recorded at high temperature. The aliphatic methylene protons which resonates as two separate quartets at low temperature, resonates as one single quartet due to the rapid interconversion between the tautomers at 318K. Several reports are there suggesting a similar intramolecular proton transfer mechanism for the thermochromism and photochromism existing in the keto and enol forms of anils [Hadjoudis *et. al* 2004].

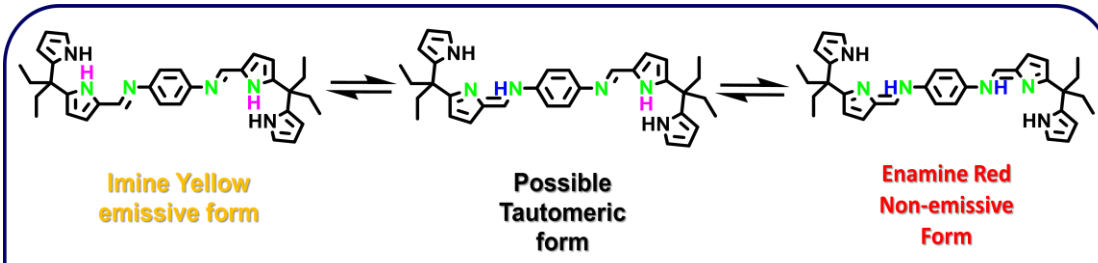

Scheme 4.7 Proposed mechanism for mechanochromism in **DSB**

Above studies suggest that **DSB** molecule exists as red non emissive enol isomer (crystalline) upon mechanical grinding converts into keto yellow emissive isomer (amorphous) which reverts back to the initial state on heating or recrystallisation.

4.4.6 Turn-on fluorescence Zn^{2+} ion sensing of DSB

The flexibility, temporal pre-organisation ability and combined with rich co-ordination chemistry of imine and pyrrolic NH- makes the ligand **DSB** well suited for the sequential binding of metal ions. In order to investigate the cation binding ability of **DSB**, a preliminary

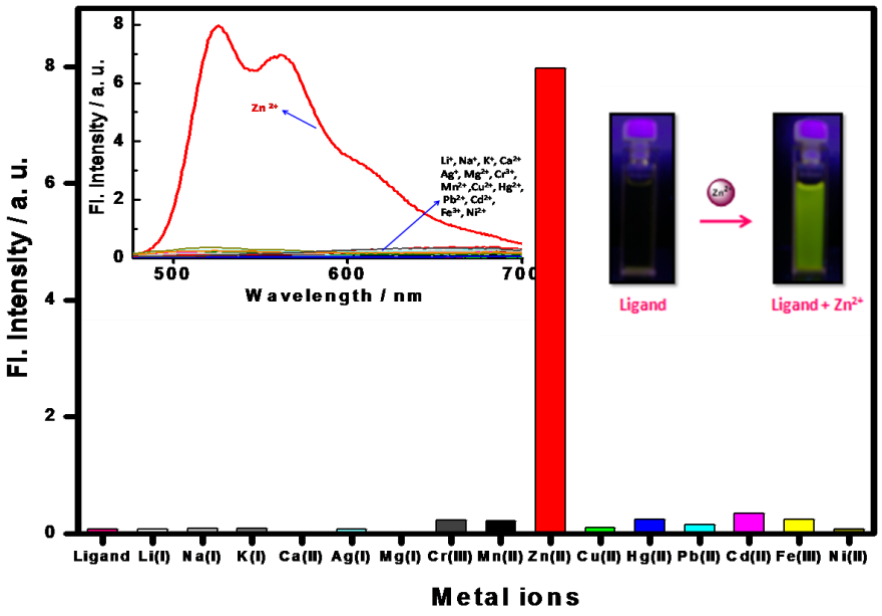

Figure 4.23 Fluorescence response of CH_3CN solution of **DSB** (10 μm) in the presence of 0.5 equiv. of various metal ions. The inset shows the fluorescence spectrum of the **DSB** in the presence of 0.5 equiv. of various metal ions.

qualitative experiment was performed by using a dilute CH_3CN solution of **DSB** (10μM) with 0.5 equiv. of various cations as perchlorate salts. To our surprise, change in emission was observed only in the case of zinc salt, where the ligand was practically not emissive became highly fluorescent upon treatment with 0.5 equiv. zinc perchlorate. Addition of various equiv. of Zn^{2+} ions resulted in the gradual decrease of ligand absorption peak at 380 nm with the simultaneous appearance of a new red shifted band at 435 nm through an isosbestic point at 404 nm accompanied by the visible color change from yellow to reddish orange (Figure 4.24). The **DSB** shows a greenish yellow fluorescence (Figure 4.23) upon binding with Zn^{2+} ions with the formation of an emission band at 530 nm shouldered at 560 nm. The quantum yield of respective complex is 0.12 with respect to fluorescin. This is ≈ 135 fold enhancement in emission intensity upon binding with 0.5 equiv. of Zn^{2+} ions, which provides an excellent

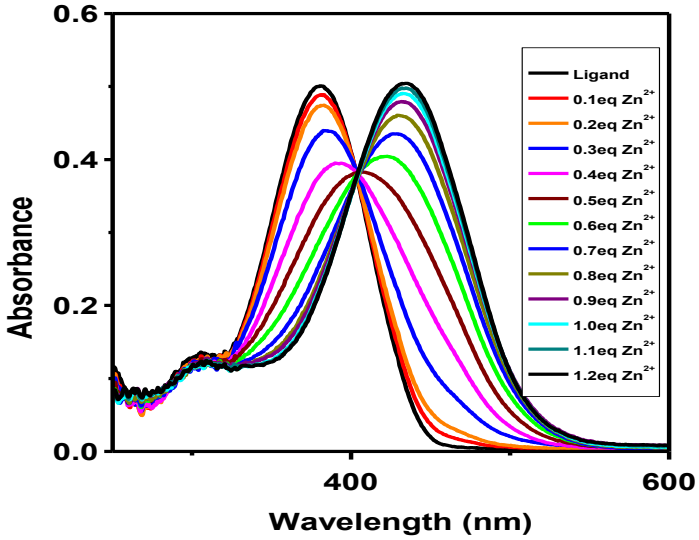

Figure 4.24 Changes in absorption spectra of **DSB** (15µM) upon titration with Zn^{2+} ions in acetonitrile.

'turn-on' ratio of zinc sensingTo test the sensing ability of **DSB**, it was treated with various biologically relevant mono, di and trivalent metal ions. Among the tested metal ions, only Zn^{2+} ions exhibited effective enhancement in fluorescence (Figure 4.23). The competitive recognition studies reveal that Zn^{2+} ions could be detected even in the presence of 100 equiv. of biologically relevant Na^{+}, K^{+}, Ca^{2+}, Mg^{2+} ions and other metal ions. The reversibility in binding was checked by titration with EDTA which resulted in quenching of fluorescence. The addition of 0.5 equiv of Zn^{2+} ions, resulted in the formation of $(\mathbf{DSB})_2Zn$ with the absorption maximum at 404 nm (Figure 4.24).

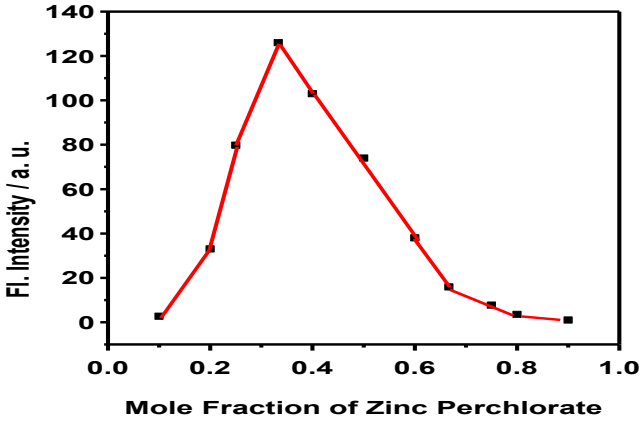

Figure 4.25 Job's plot for the complexation of **DSB** with Zn^{2+} ions in CH_3CN.

The stoichiometry of the complex was determined by jobs plot (Figure 4.25) and found to be 2:1 for ligand and Zn^{2+} ions. Upon increasing the Zn^{2+} concentration from 0.5 equiv. to 1 equiv, the absorption maximum is further shifted to 435 nm (Figure 4.24) and the emission band at 530 nm and 560 nm is gradually decreased and become 'turn-off' emission. It clearly suggest the formation of 2:2 complex, such as $(\mathbf{DSB})_2Zn_2$ (Figure 4.26 and 4.27). Overall, the dual fluorescence response of **DSB** with various equivalents of Zn^{2+} was observed.

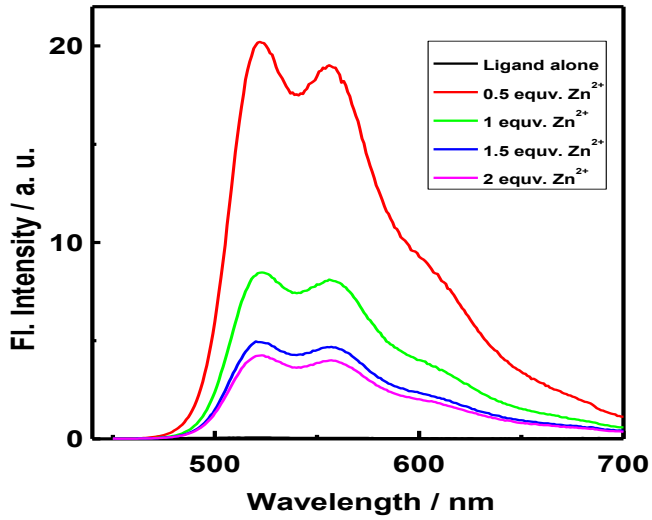

Figure 4.26 The changes in the emission spectrum of **DSB** (15µM) upon titration with Zn^{2+} ions in CH_3CN (λ_{ex}= 440 nm).

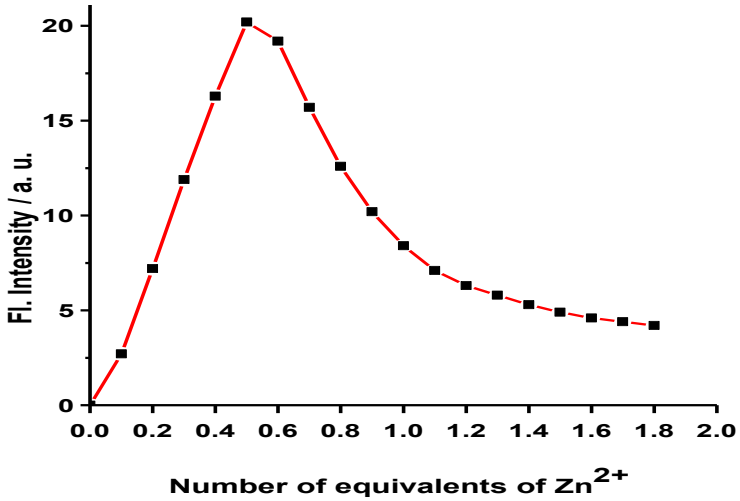

Figure 4.27 Fluorescence response of **DSB** (15 µm) in CH_3CN upon addition of various equiv. of Zn^{2+} with dual fluorescence response (λ_{ex}= 440 nm).

The dual fluorescence response was further confirmed by optical polarization microscopy. The fluorescence microscopy image was obtained *via* drop casting the CH_3CN solution containing **DSB** and 0.7 equiv. Zn^{2+} ions (Figure 4.28). It clearly shows that the greenish yellow fluorescent fibre like structures of the emissive 2:1 complex and the non-emissive red 2:2 complex which has spherical morphology.

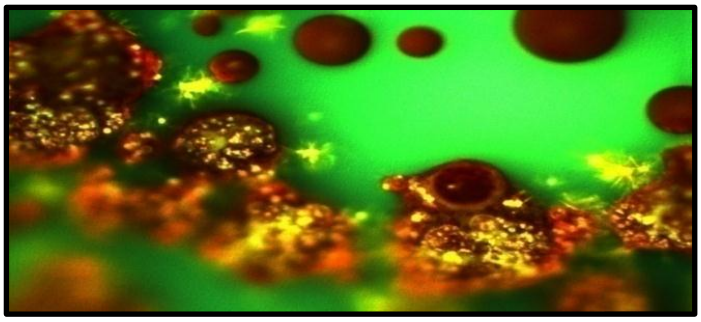

Figure 4.28 Fluorescence microscopic image of **DSB** with 0.7 equiv. of Zn^{2+} ions (λ_{ex}=380 nm).

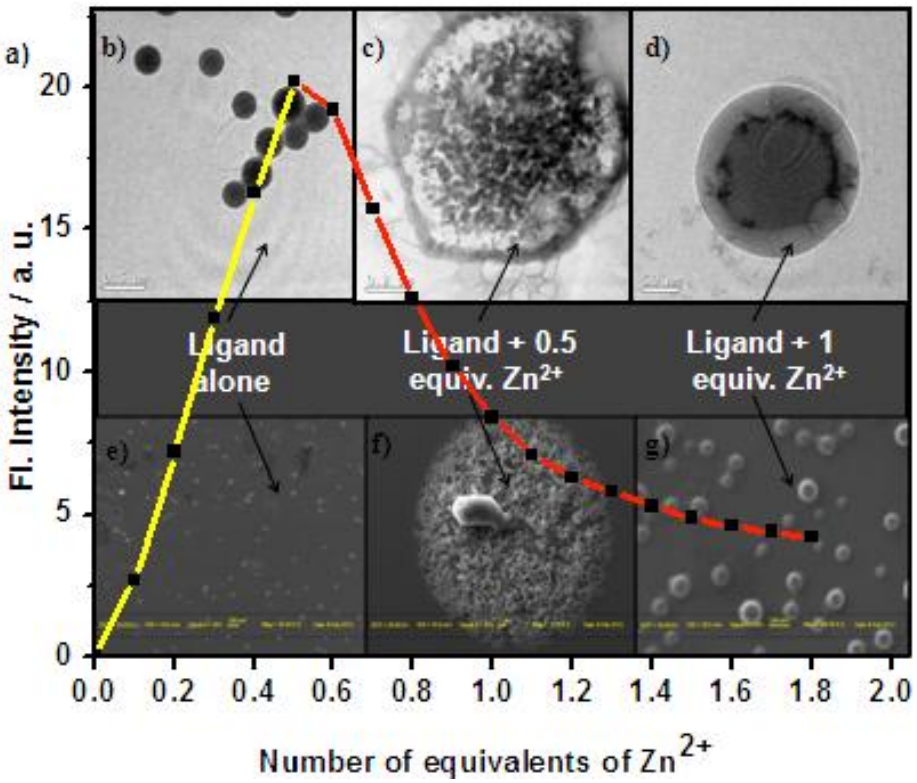

Figure 4.29 a) The dual fluorescence response of **DSB** (15 μm) in CH_3CN solution upon addition of various equivalents of Zn^{2+}. The TEM (b, c & d) and SEM (e, f & g) images of, **DSB** alone (b & e); **DSB** with 0.5 equiv. (c & f) and **DSB** with 1 equiv. (d & g) of Zn^{2+} ions.

The two type morphology of the complexes was again confirmed by the SEM and the TEM analysis (Figure 4.29 b-g). The ligand solution when mixed with 0.5 equiv. Zn^{2+} ion gave SEM image (Figure 4.29 e-g) with fibre like morphology and at 1 equiv. of Zn^{2+} ion concentration afforded nano spheres ranging from 100 to 250 nm in size. The size and morphology of the particles were also confirmed by the TEM analysis (Figure 4.29 b-d).

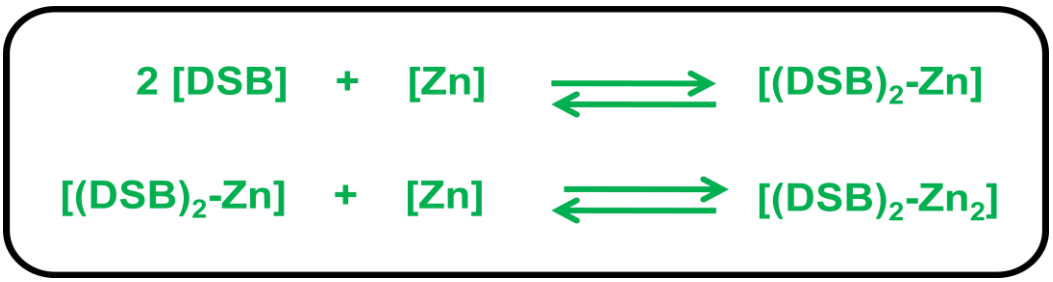

Figure 4.30 Proposed binding mechanisms for the **DSB** and Zn^{2+} ion complexation reaction.

The formation of these two different species (**DSB**)$_2$Zn and (**DSB**)$_2$Zn$_2$ was further confirmed by NMR titration and ITC technique. The ^{1}H NMR spectra of **DSB** in CD_3CN clearly visualises the presence of centre of symmetry of the ligand. As already discussed, out of the two sets of pyrrolic NH, one set of external pyrrolic NH is resonated at 8.59 ppm at room temperature. As discussed earlier when the temperature is lowered, the other two pyrrolic NH which is directly bonded to imine carbon begin to appear at 9.6 ppm which clearly shows the arresting of IMR at low temperature. During the NMR titration, different equivalents of $Zn(ClO_4)_2$ solution in CD_3CN were added to CD_3CN solution of **DSB** (Figure 4.31). As the concentration of Zn^{2+} ion increases, a new peak begins to appear at downfield region around 10 ppm. Till 0.5 equiv of Zn^{2+} ions, the NMR spectra became more and more complex due to the loss of centre of symmetry also suggests the formation of unsymmetric complex (**DSB**)$_2$Zn. When the concentration exceeds 0.5 equiv., the spectra became more and more clear. At 1 equiv. of Zn^{2+} ions, a neat symmetric NMR spectrum was obtained where the two sets of pyrrolic NH peaks were resonated at 9.0 and 10.4 ppm respectively and suggests

the formation of symmetric (**DSB**)$_2$Zn$_2$ species. The NMR titration study also confirms the fact that the pyrrolic NH protons are not deprotonated during binding with Zn^{2+} ions which shows only imine nitrogens are co-ordinated with Zn^{2+} ions. During NMR titration, the two pyrrolic NH protons that will appear only at low temperatures, slowly shows its presence at 10.8 ppm even at room temperature upon binding with Zn^{2+} ions. This is due to the fact that the pyrrole

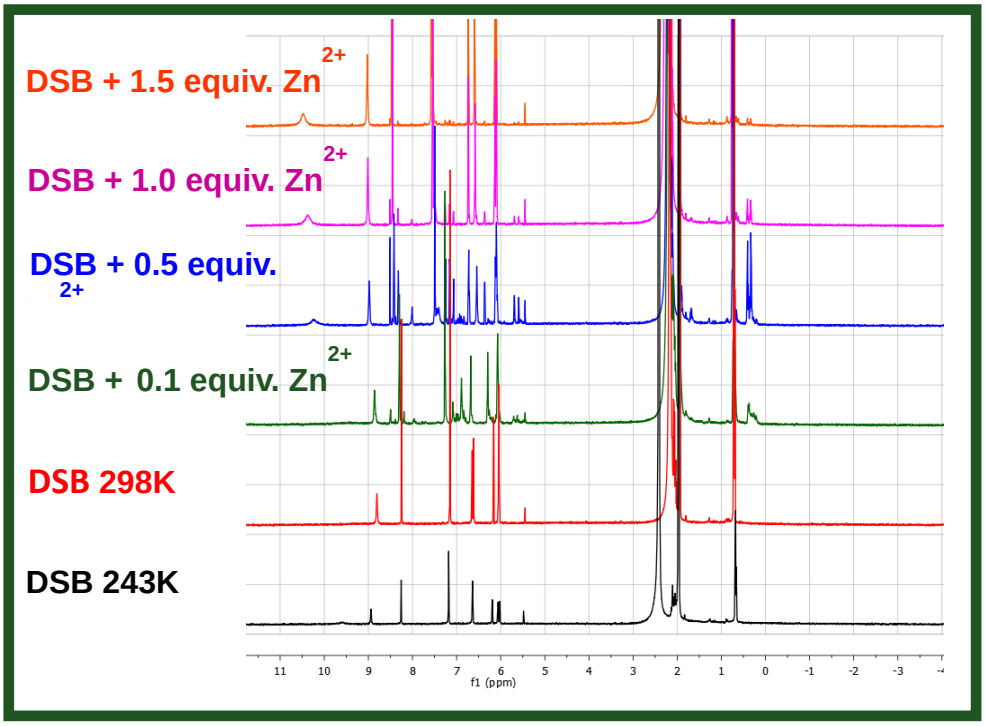

Figure 4.31 The stacked^{1}H NMR spectra of **DSB** with various equiv. of Zn^{2+} ions in CD_3CN.

rings which are free to move in metal free ligand is rigidified upon binding with Zn^{2+} ions. The cross linking of the Zn^{2+} ions in between the two ligands and the hydrogen bonding between the pyrrolic NH protons with the ClO_4^- ion in the (**DSB**)$_2$Zn and (**DSB**)$_2$Zn$_2$ complexes restricts the rotation of the pyrrole rings which is the reason for the appearance of the downfield shifted pyrrolic NH peaks.

The existence of two step binding mechanism for **DSB** with Zn^{2+} ions was further confirmed by isothermal titration calorimetry (ITC) (Figure 4.32). Aliquots of Zn(ClO_4)$_2$

solution in CH_3CN (20mM) is injected into the cell containing 2mM **DSB** solution in CH_3CN at 298 K and heat released upon their interaction is monitored over time. It is clear from the ITC data (Figure 4.33) that the binding of Zn^{2+} ions to **DSB** involves two thermally distinct processes. The first binding involves an exothermic process which occurs at a molar ratio of

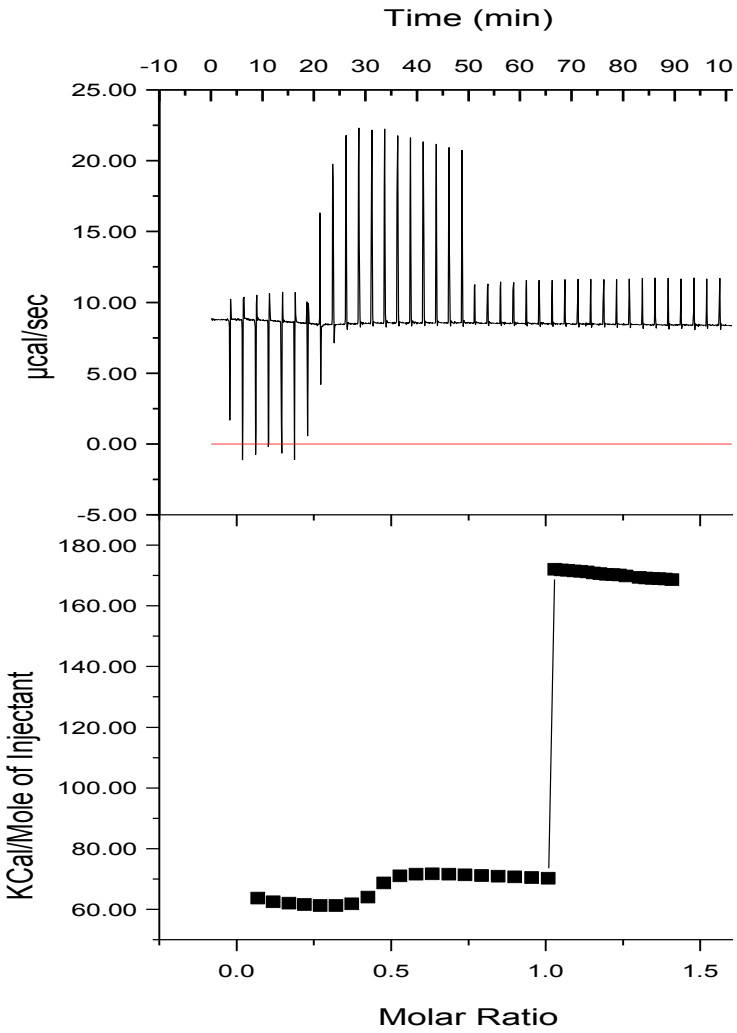

Figure 4.32 Isothermal titration curve for **DSB** upon titration with Zn^{2+} ions in CH_3CN.

0.5 equiv of Zn^{2+} ions reveals the formation of $(\mathbf{DSB})_2Zn$ type complex. The second binding process is a highly endothermic transition corresponding to 1:1 stoichiometry which is due to the formation of $(\mathbf{DSB})_2Zn_2$ complex as obtained from the spectral studies. In short, the ligand **DSB** shows a two-step binding process, first one corresponds to 2:1 complex which is exothermic and second step involves a 2:2 complex which is endothermic. The schematic

representation of the binding phenomenon of **DSB** is shown in the Figure 4.33. As reflected from the spectral analysis, the preliminary theoretical studies (Figure 4.34) indicate that the imine N-interaction with Zn^{2+} salt without deprotonating the dipyrromethane pyrrolic NH unit. The detailed studies are in progress in our lab.

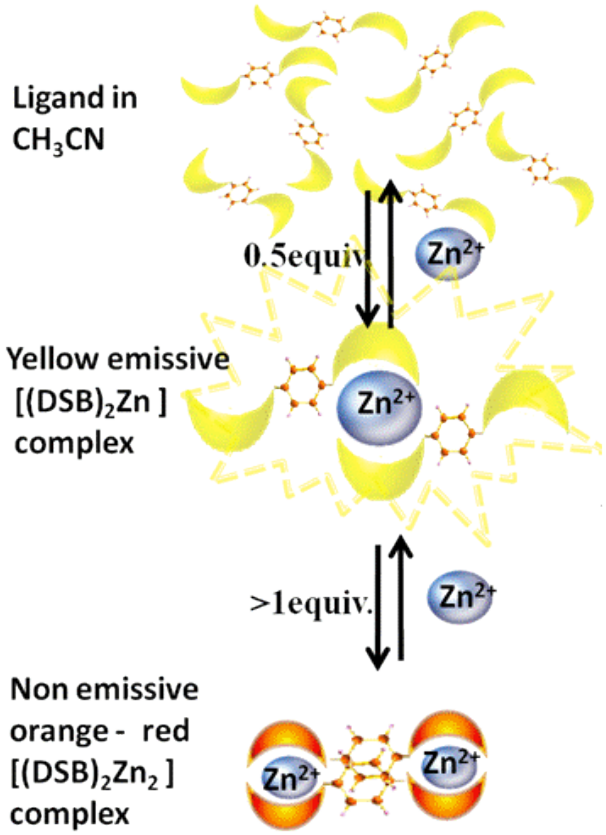

Figure 4.33 Schematic representation of the dual fluorescence response of **DSB** with 0.5 and 1 equiv. Zn^{2+} ions.

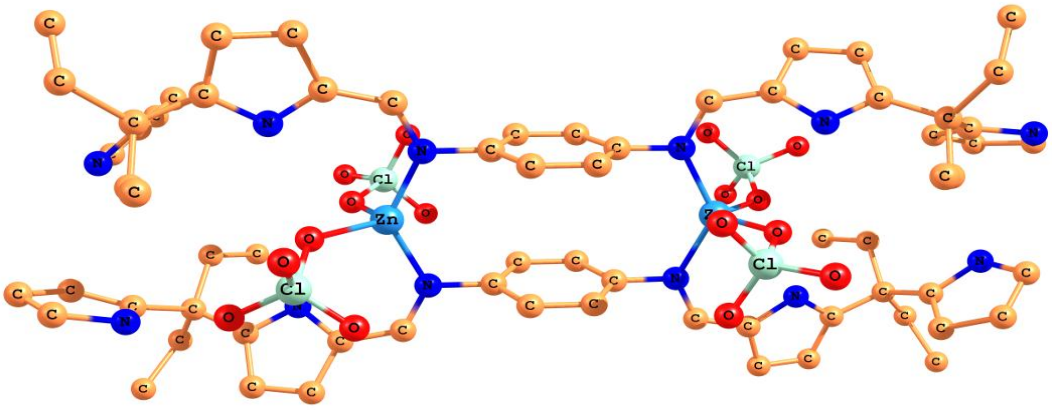

Figure 4.34 Optimized structure of (**DSB**)$_2$Zn$_2$ complex; Hydrogen atoms are omitted for clarity.

4.5 Conclusion

In summary, we have synthesised the *dragonesque* shaped acyclic *meso*-dialkyldipyrromethane based Schiff base (**DSB**). The single crystal X-ray analysis clearly reveals that the molecule forms strong intermolecular H-bonding interaction. The aggregation induced restriction of IMR and π…π interaction between the phenyl rings of the **DSB** molecule inturn forces the molecule to show interesting properties like AIEE in presence of water. Mechanochromic response of simple dipyrromethane based Schiff base ligand has been demonstrated external stimuli such as grinding, heating or spraying acetone. Such results in simple dipyrromethane Schiff base are hitherto unknown in the literature.

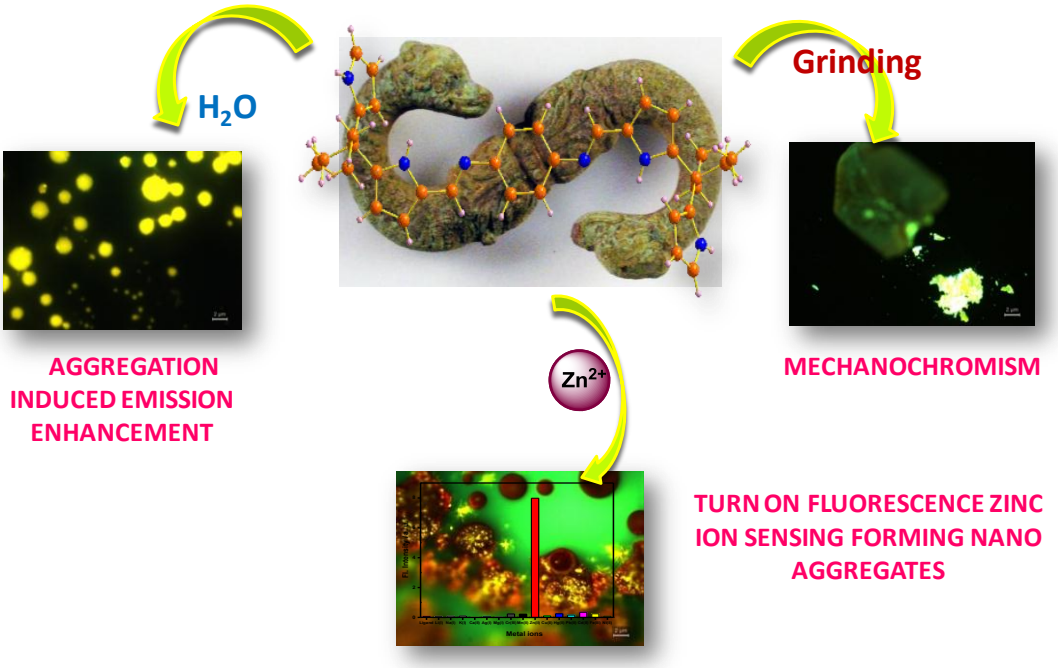

The aggregation and luminescence properties of **DSB** are also exploited for the selective detection of Zn^{2+} ions in CH_3CN solution. **DSB** exhibits dual fluorescence response to Zinc ions leading to the formation of emissive nano fiber like aggregates at lower concentration and non-emissive nano spheres like aggregates at higher concentration of Zinc ions. The results were unambiguously confirmed by NMR and ITC techniques and proved the

formation of 2:1 and 2:2 complexes in the presence of 0.5 and 1 equiv. of Zn^{2+} ions. Efforts to crystallize the Zn^{2+} complexes and biological imaging studies are currently in progress.

4.6 Experimental Section

4.6.1 General Information

The reagents and materials for synthesis were used as obtained from Sigma - Aldrich chemical suppliers. All solvents were purified and dried by standard methods prior to use. NMR solvents were used as received. NMR spectra were recorded with 500 MHz Bruker Advanced DPX Spectrometer with CD_3CN as solvent. Chemical shifts were expressed in parts per million (ppm) relative to TMS. FAB mass spectra were obtained on a JEOL SX-120/DA6000 spectrometer using argon (6 KV, 10 mA) as the FAB gas. The fluorescence spectra were recorded on a SPEX-Fluorolog F112X spectrofluorimeter. Solid state fluorescence and changes in fluorescence with temperature was observed using a LEICA DM 2500P polarized light optical microscope with a crossed polarizer configuration, equipped with Mettler Toledo FP900 Thermosystem heating/cooling stage. For SEM measurements, the samples were drop cast and air dried on one flat surface of cylindrical brass stubs and subjected for thin gold coating using JOEL JFC-1200 fine coater. The probing side was inserted into JEOL JSM-5600 LV Scanning electron microscope for taking photographs. FESEM images were recorded with an FEI-Nova NanoSEM600. TEM measurements were carried on an FEI-Technai 30G2 S-Twin, 300 kV HR-TEM microscope with an accelerating voltage of 100 kV. Samples were prepared by drop casting the solution on to a formvar coated copper grid (400 mesh) and allowing the excess solvent to evaporate under mild vaccum conditions. Electronic absorption spectra were recorded with Perkin Elmer – Lambda 25 UV-Visible spectrophotometer. Isothermal titration calorimetry was carried out using a Micro calorimeter (Microcal ITC 200) instrument. The single crystal X-ray diffraction data of **DSB** was collected on a Bruker AXS Kappa Apex 2 CCD diffractometer at 293(2) K. Good quality

single crystal was grown by slow evaporation of *n*-hepane into $CHCl_3$ solutions of **DSB**. Powder X–ray diffraction data were collected on a Bruker D8 Advance with DIVINCI design fitted with HTK 16 temperature chamber X-ray powder diffractometer using CuKα radiation (λ = 1.5418 Å). The Spectral grade *n*-hexane and doubly distilled water was used for all the experiments. All the metal perchlorates were purchased from Sigma Aldrich and used as received without any further purification. Fluorescence quantum yields were determined using fluorescein in 0.1M NaOH (Φ_f = 0.95) as a reference. All experiments were carried out at room temperature (25 ±1°C), unless otherwise mentioned.

4.6.2 Synthesis of the Schiff base DSB

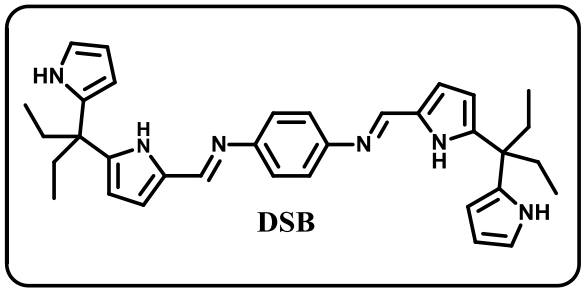

DSB

The syntheses of precursor **2** from diethyl dipyrromethaneis already discussed in chapter two. In the final step *p*-Phenylene-diamine (**3**) (0.47 g, 4.3 mmol) was added at room temperature to solution (2 g, 8 mmol) of 1-formyl-5,5-diethyldipyrromthane (**2)** in methanol. The reaction mixture was stirred for 48 hours and yellow precipitate was formed. The solid was filtered off, washed with cold methanol and dried in vacuum afforded 1.6 g of yellow crystalline solid of **DSB** in 35% yield. ^{1}H NMR ($CDCl_3$, 500 MHz) δ (ppm) 0.71-0.76 (S, 12H, CH_3), 1.97-2.05 (q, 8H, CH_2), 6.13-6.66 (10H, Pyrrolic CH),7.13 (s, 4H, phenyl CH), 7.85 (s, 2H, pyrrolic NH), 8.17 (s, 2H, imine CH), 9.24 (s, 2H, pyrrolic NH). ^{13}C ($CDCl_3$, 500 MHz), δ (ppm) 8.35, 29.34, 43.87, 76.77, 77.02, 77.28, 106.26, 107.70, 108.82, 116.72, 117.12, 121.64, 130.34, 135.55, 142.95, 148.45, 149.10; FAB mass (m/Z): calcd for $C_{34}H_{40}N_6$ is 532.3314 and found to be 533.68

4.6.2 ^{1}H NMR spectrum of Schiff base (DSB) in different deuterated solvents

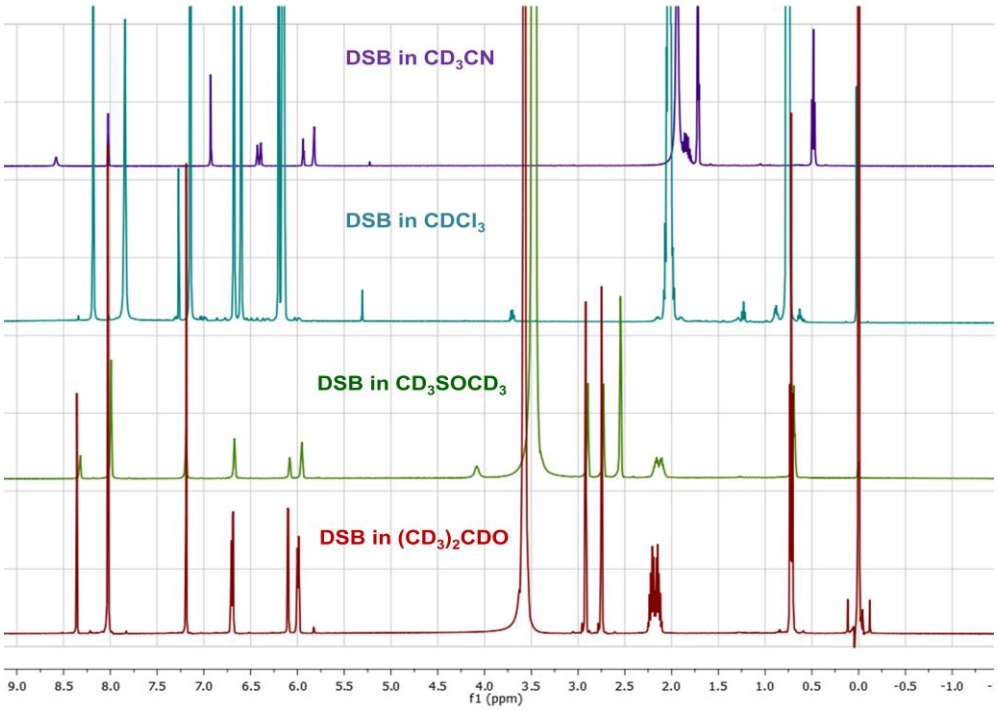

Figure 4.35 The stacked ^{1}H NMR spectra of **DSB** in various deuterated solvents.

4.7 Crystal data for DSB

	DSB ($CHCl_3$/*n*-Heptane)
Formula	$C_{34}H_{40}N_6$
M/g mol^{-1}	532.72
T/K	293(2)
Crystal dimensions/mm^3	0.20 x 0.05 x 0.05
Crystal system	Monoclinic
Space group	$P2_1/n$
a/Å	9.1417 (11)
b/Å	13.5350 (17)
c/Å	13.2294 (16)
α/°	90.00
β/°	107.511(2)
γ/°	90.00
V/$Å^3$	1561.1(3)
Z	2
ρ_{calcd}/mg m^{-3}	1.133
μ/mm^{-1}	0.068
F(000)	572
Reflns. Collected	2962
Indep.reflns.[*R*(int)]	8420[0.0517]
Max/min transmission	0.9912 and 0.9692
Data/restraints/parameters	3045/0/231
GOF on F^2	1.093
Final R indices[$I > 2\sigma(I)$]	R1 = 0.0826, wR2 = 0.1751
R indices (all data)	R1 = 0.0696, wR2 = 0.1672
$\Delta\rho$ [e $Å^{-3}$]	0.359 and -0.154

Table 4.1 Crystallographic data for **DSB**

SUMMARY

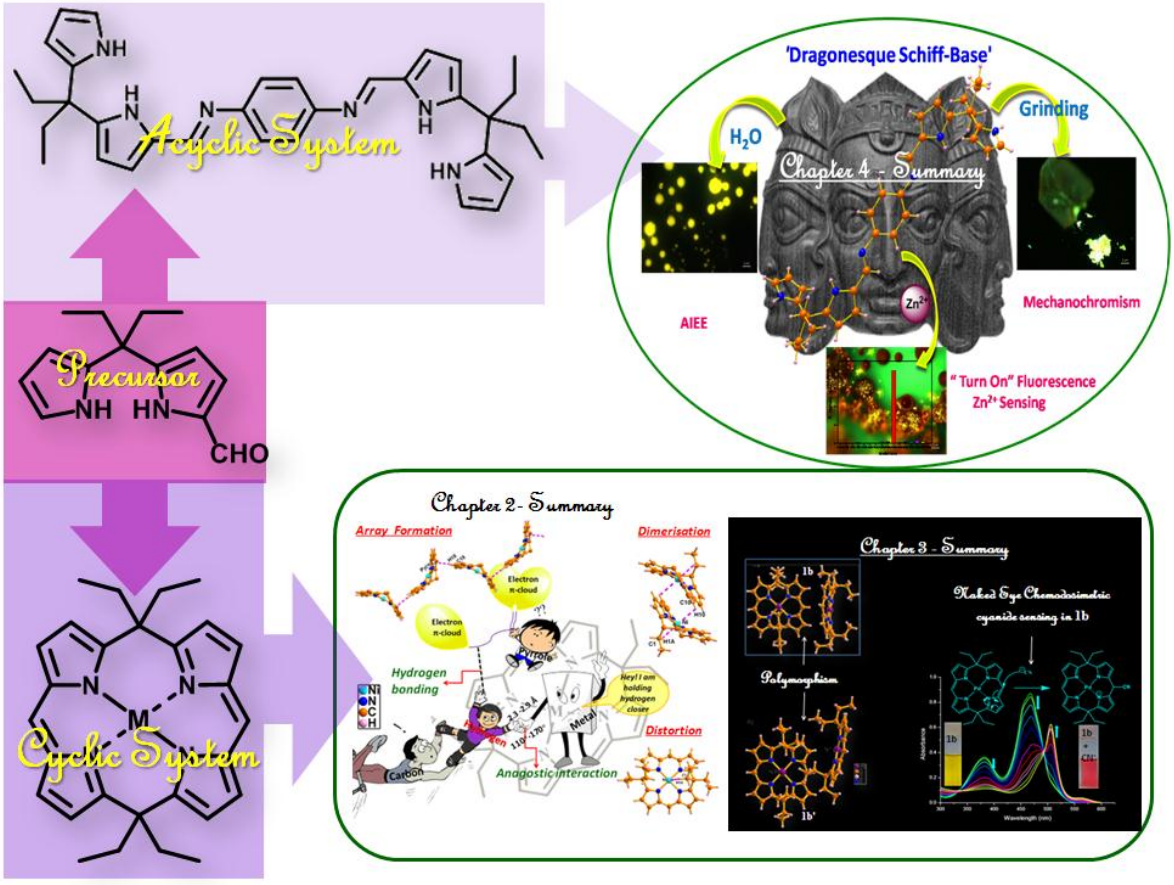
Acyclic System
Precursor
Cyclic System
'Dragonesque Schiff-Base'
Chapter 4 - Summary
Grinding
Mechanochromism
AIEE
"Turn On" Fluorescence
Chapter 2- Summary
Array Formation
Dimerisation
Hydrogen bonding
Distortion
Anagostic interaction
Chapter 3 - Summary
Naked Eye Chemodosimetric cyanide sensing in 1b
Polymorphism

List of Publications

1) *Chemodosimetric cyanide sensing in a 5,15-porphodimethene Pd(II) complex **Derry Holaday M. G.**, Gourav Tarafdar, B. Adinarayana, M. L. P. Reddy, and A. Srinivasan, *Chem. Commun*. **2014**, *50*, 10834-10836.
2) ***Exploring Anagostic Interactions in 5,15-Porphodimethene Metal Complexes. **Derry Holaday M. G.**, Gourav Tarafdar, Arun Kumar, M. L. P. Reddy, and A. Srinivasan, *Dalton Trans.* **2014**, *43*, 7699-7703.
3) Fluorine interaction controlled AIEE phenomenon in an expanded calixbenzophyrin and its vapoluminescent response: turn on emission with volatile ketones and esters. P. S. Salini, **Derry Holaday M. G.**, M. L. P. Reddy, C. H. Suresh and A. Srinivasan. *Chem. Commun.* **2013**, 49, 2213-2215.
4) 4,4,9,9-Tetraphenyl pyrroloindolizine: a structural analogue of calix[2]pyrrole. K. C. Gowri Sreedevi, Ajesh P Thomas, S. Ramakrishnan, P. S. Salini, **Derry Holaday M. G.**, M. L. P. Reddy, and A. Srinivasan, *Org. Biomol. Chem*. **2012**, *10(18)*, 3600-3605.
5) 5,5-Diaryldipyrromethanes: Syntheses and anion binding properties. K. C. Gowri Sreedevi, Ajesh P Thomas, P. S. Salini, S. Ramakrishnan, K. S. Anju, **Derry Holaday M. G.**, M. L. P. Reddy, C. H. Suresh, and A. Srinivasan, *Tetrahedron Letters* **2011**, *52*, 5995-5999.
6) ansa – Ferrocene - Incorporated Calixpyrroles and Calixphyrins: Syntheses and Spectral/ Structural Characterization. S. Ramakrishnan, K. S. Anju, Ajesh P. Thomas, K. C. Gowri Sreedevi, P. S. Salini, **Derry Holaday M. G.**, Eringathodi Suresh, and A. Srinivasan *Organometallics* **2012,** *31*, 4166-4173.
7) *Aggregation Induced Emission Enhancement and Luminescence Mechanochromism in Dragonesque Schiff Base. **Derry Holaday M. G.**, and A. Srinivasan, manuscript under preparation.
8) *Turn - On Fluorescence Zn^{2+} sensing via FON generation in a *dipyrrophen* Schiff Base. **Derry Holaday M. G.**, and A. Srinivasan, manuscript under preparation.

*pertaining to thesis

Papers/Posters presented in conference proceedings

1) International Conference on Materials for the Millenium (MATCON 2016), January 14-16, 2016 Organized by Cochin University of Science and Technology (CUSAT) Kalamaserry.
2) International Conference on Photonics and Solar Water Splitting (PSWS-2015), March 12-13, 2015, conducted by Department of Physics, St. Teresa's college, Ernakulam.
3) Seminar on Advances in Materials Chemistry (ADMAC 2014), October 15-16, 2014,, conducted by Department of Chemistry, Christian College, Chengannur.
4) Symposium on Recent Advances in Chemistry (2014), September 03-04, 2014. Organised by MES College, Ponnani and was awarded the **Best Paper Award**.

REFERENCES

Abe, T.; Itakura, T.; Ikeda, N.; Shinozaki, K. "Luminescence color change of a platinum (II) complex solid upon mechanical grinding" *Dalton Trans.*, **2014**, 711.

Aida, T.; Inoue, S. In The Porphyrin Handbook; Kadish, K. M., Smith, K. M., Guilard, R., Eds.; Vol. 6, Academic Press: San Diego, **1999**.

Akila, E.; Usharani, M.; Rajavel, R. "A review - general applications of Schiff base transition metal complexes derived from 2-aminophenol" *International Journal of Advanced Scientific and Technical Research.,* 5, **2013**, 457.

Assaf, S. Y.; Chung, S. -H. "Release of endogenous Zn^{2+} from brain tissue during activity" *Nature*, 308, **1984**, 734.

Banica, F. -G. Chemical Sensors and Biosensors: Fundamentals and Applications, Wiley, Chichester, UK, **2012**.

Barkigia, K. M.; Renner, M. W.; Xie, H.; Smith, K. M.; Fajer, J. "Structural consequences of porphyrin tautomerization, Molecular structure of a zinc isoporphyrin" *J. Am. Chem. Soc*., 115, **1993**, 7894.

Baskin, S. I.; Kelly, J. B.; Maliner, B. I.; Rockwood, G. A.; Zoltani, C. K. "Medicinal Aspects of Chemical Warfare" ed. D. T. Shirley, *TMM publications*, Washington DC, chapter 11, **2008**, 331.

Battersby, A. R.; Fookes, C. J. R.; Matcham, G. W. J.; McDonald, E. "Biosynthesis of the pigments of life: formation of the macrocycle" *Nature,* 285, **1980**, 17.

Beer, P. D. "*Chemical Sensors*, T. E. Edmonds; Chapman and Hall, New York, **1988**.

Belanzoni, P.; Rosi, M.; Sgamellotti, A.; Bonomo, L.; Floriani, C. "A theoretical analysis of the fundamental stepwise six-electron oxidation of porphyrinogen to porphyrins: the

energetics of porphodimethene and artificial porphyrin intermediates" *J. Chem. Soc., Dalton Trans*., **2001**, 1492.

Bhardwaj, V.; Gumber, D.; Abbot, V.; Dhimana, S.; Sharma, P. "Pyrrole: a resourceful small molecule in key medicinal hetero-aromatics" *RSC Adv.*, 5, **2015**, 15233.

Bhosale, S. V.; Bhosale, S. V.; Shitre, G. V.; Bobe, S. R.; Gupta, A. "Supramolecular Chemistry of Protoporphyrin IX and Its Derivatives" *Eur. J. Org. Chem.,* **2013**, 3939.

Bianchi, A.; Bowman-James, K.; García-Espana, E. "Supramolecular Chemistry of Anions" Eds.; Wiley-VCH: New York, **1997**.

Borisova, N. E.; Reshetova, M. D.; Ustynyuk, Y. A. "Metal-Free Methods in the Synthesis of Macrocyclic Schiff Bases" *Chem. Rev.*, 107, **2007**, 46.

Botulinski, A.; Buchler, J. W.; Lee, Y. J.; Scheidt, W. R.; Wicholas, M. "Metal Complexes with tetrapyrrole ligands, Solid-state and solution structures of iron(III) porphodimethenes, Effects of steric hindrance" *Inorg. Chem*., 27, **1988**, 927.

Brookhart, M.; Green, M. L. H.; Parkin, G. "Agostic interactions in transition metal compounds" *Proc. Natl. Acad. Sci., U. S. A.* 104, **2007**, 6908.

Bruckner, C.; Karunaratne, V.; Rettig, S. J.; Dolphin, D. "Synthesis of *meso*-phenyl-4,6-dipyrrins, preparation of their Cu(II), Ni(II), and Zn(II) chelates, and structural characterization of bis [*meso*-phenyl-4,6-dipyrrinato] Ni(II)" *Can. J. Chem*., 74, **1996**, 2182.

Bucher, C.; Seidel, D.; Lynch, V.; Král, V.; Sessler, J. L. "Novel Synthesis of Hybrid Calixphyrin Macrocycles" *Org. Lett*., 2, **2000**, 3103.

Buchler. J. W.; Puppe, L. "Metallkomplexe mit Tetrapyrrol-Liganden, II Metallchelate des α.γ-Dimethyl-α.γ-dihydro-octaäthylporphins durch reduzierende Methylierung von Octaäthylporphinato-zink" *Justus Liebigs Ann. Chem*., 740, **1970**, 142.

Cafeo, G.; Kohnke, F. H.; La Torre, G. L.; Parisi, M. F.; Nascone, R. P.; White, A. J. P.; Williams, D. J. "Calix[6]pyrrole and Hybrid Calix[n]furan[m]pyrroles (n+m=6): Syntheses and Host-Guest Chemistry" *Chem. Eur. J.*, 8, **2002**, 3148.

Caltagirone, C.; Gale, P. A. "Anion receptor chemistry: highlights from 2007" *Chem. Soc. Rev.*, 38, **2009**, 520.

Camiolo, S.; Gale, P. A.; Hursthouse, M. B.; Light, M. E. "Nitrophenyl derivatives of pyrrole 2,5-diamides: structural behaviour, anion binding and colour change signalled deprotonation" *Org. Biomol. Chem.*, 1, **2003**, 741.

Casiraghi, G.; Cornia, M.; Rassu, G.; Del Sante, C.; Spanu, P. "Synthesis and transformation of pyrrole *C*-glycoconjugate" *Tetrahedron.*, 48, **1992**, 5619.

Cavaleiro, J. A. S.; Rocha Gonsalves, A. M. d'A.; Kenner, G. W.; Smith, K. M. "Pyrroles and related compounds. Part XXII. Syntheses of pyrromethanes and a tripyrrane" *J. Chem. Soc., Perkin Trans.*, 1, **1973**, 2471.

Chang, G.-F.; Kumar, A.; Ching, W.-M.; Chu, H.-W.; Hung, C.-H. "Tetramethyl-*m* benziporphodimethene and Isomeric α,β-Unsaturated γ-Lactam Embedded N Confused Tetramethyl-*m*-benziporphodimethenes" *Chem.Asian J.*, 4, **2009**, 164.

Chauhan, S. M. S.; Bisht, T.; Garg, B. "1-Arylazo-5, 5-dimethyl dipyrromethanes: Versatile chromogenic probes for anions" *Sensors and Actuators B*, 141, **2009**, 116.

Chellappan, K.; Singh, N. J.; Hwang, I. C.; Lee, J. W.; Kim, K. S. "A Calix[4]imidazolium[2]pyridine as an Anion Receptor" *Angew. Chem. Int. Ed.*, 44, **2005**, 2899.

Chen, C.-T. "Evolution of Red Organic Light-Emitting Diodes: Materials and Devices" *Chem. Mater.*, 16, **2004**, 4389.

Chen, L. D.; Zou X. U.; Bühlmann, P. "Cyanide-Selective Electrode Based on Zn (II) Tetraphenylporphyrin as Ionophore" *Anal. Chem.*, 84, **2012**, 9192.

Cho, E. J.; Ryu, B. J.; Lee, Y. J.; Nam, K. C. "Visible Colorimetric Fluoride Ion Sensors" *Org. Lett*., 7, **2005**, 2607.

Chong, R.; Clezy, P. S.; Liepa, A. J.; Nichol, A. W. "The chemistry of pyrrolic compounds. VII. Synthesis of 5, 5'-diformyldipyrryl-methanes" *Aust. J. Chem.*, 22, **1969**, 229.

Clarke, O. J.; Boyle, R. W. "Selective Synthesis of Asymmetrically Substituted 5,15-Diphenylporphyrins" *Tetrahedron Lett*., 39, **1998**, 7167.

Clezy, P. S.; Smythe, G. A. "The chemistry of pyrrolic compounds. VIII. Dipyrrylthiones" *Aust. J. Chem.*, 22, **1969**, 239.

Coles, S. J.; Gale, P. A.; Hursthouse, M. B. "The first example of an anion-pyrrole complex" *CrystEngComm*., 3, **2001**, 259.

Coskun, A.; Deniz, E.; Akkaya E. U. "Effective PET and ICT Switching of Bora diaza indacene Emission: A Unimolecular, Emission-Mode, Molecular Half-Subtractor with Reconfigurable Logic Gates" *Org. Lett.*, 7, **2005**, 5187.

Cozzi, P. G. "Metal-Salen Schiff Base Complexes in Catalysis: Practical Aspects" *Chem. Soc. Rev*., 33, **2004**, 410.

Cuajungco, M. P.; Lees, G. J. "Zinc metabolism in the brain: relevance to human neurodegenerative disorders" *Neurobiol. Dis*., 4, **1997**, 137.

Deans, R.; Kim, J.; Machacek, M. R.; Swager, T. M. "A Poly(P-Phenyleneethynylene) with a Highly Emissive Aggregated Phase" *J. Am. Chem. Soc.*, 122, **2000**, 8565.

Depraetere, S.; Dehaen, W. "Electrophilic substitution reactions of dipyrroheptane" *Tetrahedron Lett*., 44, **2003**, 345.

Dolphin, D. "Porphyrinogens and porphodimethenes, intermediates in the synthesis of *meso*-tetraphenylporphins from pyrroles and benzaldehyde" *J. Heterocycl. Chem*., 7, **1970**, 275.

Domaile, D. W.; Que, E. L.; Chang, C. J. "Synthetic fluorescent sensors for studying the cell biology of metals" *Nat. Chem. Biol.*, 4, **2008**, 168.

Drewry, J. A.; Gunning, P. T. "Recent advances in biosensory and medicinal therapeutic applications of zinc(II) and copper(II) coordination complexes" *Coord. Chem. Rev.*, 255, **2011**, 459.

D'Souza, F.; Amin, A. N.; El-Khouly, M. E.; Subbaiyan, N. K.; Zandler, M. E.; Fukuzumi, S. "Control over Photoinduced Energy and Electron Transfer in Supramolecular Polyads of Covalently linked aza BODIPY-Bisporphyrin 'Molecular Clip' Hosting Fullerene" *J. Am. Chem. Soc.*, 134, **2012**, 654.

Dwyer, P. N.; Buchler, J. W.; Scheidt, W. R. "Crystal Structure and Molecular Stereochemistry of α, γ - Dimethyl - α, γ - dihydrooctaethylporphinatonickel(II)" *J. Am. Chem. Soc*., 96, **1974**, 2789.

Elsevier, C. J.; Reedijk, J.; Walton, P. H.; Ward, M. D. "Ligand design in coordination chemistry: approaches to new catalysts, new materials, and a more sustainable environment" *Dalton Trans.*, **2003**, 1869.

Eshghi, H.; Rahimizadeh, M.; Attaran, N.; Bakavoli, M. "Dipyrromethane as a new organic reagent for the synthesis of gold nanoparticles: preparation and application" *J. Iran. Chem. Soc.*, 10, **2013**, 1151.

Fan, D.; Taniguchi, M.; Yao, Z.; Dhanalekshmi, S.; Lindsey, J. S. "1, 9-Bis(N, N-dimethyl aminomethyl)dipyrromethanes in the synthesis of porphyrins bearing one or two *meso* substituents" *Tetrahedron*, 61, **2005**, 10291.

Fillaut, J. –L.; Kilig, H. A.; Dean, E.; Latouche, C.; Boucekkine, A. "Switching of Reverse Charge Transfers for a Rational Design of an OFF-ON Phosphorescent Chemodosimeter of Cyanide Anions" *Inorg. Chem.*, 52, **2013**, 4890.

Flint, D. L.; Fowler, R. L.; LeSaulnier, T. D.; Long, A. C.; O'Brien, A. Y.; Geier III, G. R. "Investigation of Complementary Reactions of a Dipyrromethane with a Dipyrromethanemonocarbinol Leading to a 5-Isocorrole" *J. Org. Chem.*, 75, **2010**, 553.

Fisher, H.; Orth, H. "*Die Chemie des Pyrrols*" Vol. I, Akademische Verlagsgesellschaft: Leipzig, **1934**, 332.

Gale, P. A.; Sessler, J. L.; Král, V.; Lynch, V. "Calix[4]pyrroles: Old Yet New Anion-Binding agents" *J. Am. Chem. Soc*., 118, **1996**, 5140.

Gale, P. A.; Anzenbacher, P. Jr.; Sessler, J. L. "Calixpyrroles II" *Coord. Chem. Rev*., 222, **2001**, 57.

Gale, P. A.; Navakhun, K.; Camiolo, S.; Light, M. E.; Hursthouse, M. B. "Anion-Anion Assembly: A New Class of Anionic Supramolecular Polymer Containing 3,4-Dichloro-2,5-diamido-substituted Pyrrole Anion Dimers" *J. Am. Chem. Soc*., 124, **2002**, 11228.

Gale, P. A. "Synthetic indole, carbazole, biindole and indolocarbazole-based receptors: applications in anion complexation and sensing" *Chem. Commun*., **2008**, 4525.

Gimeno, N.; Li, X.; Durrant, J. R.; Vilar, R. "Cyanide Sensing with Organic Dyes: Studies in Solution and on Nanostructured Al_2O_3 Surfaces" *Chem. Eur. J.*, 14, **2008**, 3006.

Giovannetti, R.; Uddin, J. (ed.); "The Use of Spectrophotometry UV-Vis for the Study of Porphyrins" Macro to Nano Spectroscopy, Chapter 6, INTECHOPEN, **2012**

Givaja, G.; Blake, A. J.; Wilson, C.; Schröder, M.; Love, J. B. "Macrocyclic diimino dipyrromethane complexes: structural analogues of Pac-Man porphyrins" *Chem. Commun.*, **2003**, 2508.

Givaja, G.; Blake, A. J.; Wilson, C.; Schröder, M.; Love, J. B. "Metal-directed ring-expansion in Schiff-base polypyrrolic macrocycles" *Chem. Commun.*, **2005**, 4423.

References

Gryko, D. T.; Tasior, M.; Koszarna, B. "Parallel synthesis of *meso*-substituted corroles and *meso*-substituted [22] pentaphyrins (1.1.1.0.0) from diacyldipyrromethanes" *J. Porphyrins Phthalocyanines*, 7, **2003**, 239.

Gryko, D. T.; Voloshchuk, R. "Synthesis and spectroscopic properties of 1-(acridin-9-yl)-dipyrranes and 1-(acridin-9-yl)-dipyrrins" *J. Porphyrins Phthalocyanines*, 13, **2009**, 390.

Gupta, K. C.; Sutar, A. K. "Catalytic Activities of Schiff Base Transition Metal Complexes" *Coord. Chem. Rev*. 252, **2008**, 1420.

Gupta, R. K.; Dubey, M.; Li, P. Z.; Xu, Q.; Pandey, D. S. "Size-Controlled Synthesis of Ag Nanoparticles Functionalized by Heteroleptic Dipyrrinato Complexes Having *meso*-Pyridyl Substituents and Their Catalytic Applications" *Inorg. Chem.*, 54, **2015**, 2500.

Hadjoudis, E.; Mavridis, I. M. "Photochromism and thermochromism of Schiff bases in the solid state: structural aspects" *Chem. Soc. Rev*., 33, **2004**, 579.

Hammel, D.; Erk, P.; Schuler, B.; Heinze, J.; Müllen, K. "Synthesis and reduction of 1,4-phenylene-bridged oligoporphyrins" *Adv. Mater.*, 4, **1992**, 737.

Haugland, R. P. "Handbook of fluorescent probes and research chemicals" *Molecular Probes Inc*., 9, **1996**, Eugene, OR.

Hayashi, T.; Dejima, H.; Matsuo, T.; Sato, H.; Murata, D.; Hisaeda, Y. "Blue Myoglobin Reconstituted with an Iron Porphycene Shows Extremely High Oxygen Affinity" *J. Am. Chem. Soc.*, 124, **2002**, 11226.

Hayes, A.; Kenner, G. W.; Williams, N. R. "Pyrroles and related compounds. Part I. Syntheses of some unsymmetrical pyrrolylmethylpyrroles (pyrromethanes)" *J. Chem. Soc.*, **1958**, 3779.

He, H.; Lo, P.-C; Yeung, S.-L.; Fong, W.-P.; Ng, D. K. P. "Preparation of Unsymmetrical Distyryl BODIPY Derivatives and Effects of the Styryl Substituents on their *In Vitro* Photodynamic Properties" *Chem. Commun.*, **2011**, 47, 4748.

Holliday, B. J.; Mirkin, C. A. "Strategies for the Construction of Supramolecular Compounds through Coordination Chemistry" *Angew. Chem. Int. Ed.*, 40, **2001**, 2022.

Hong, S. -J.; Lee, M. -H.; Lee, C. -H. "*meso*-Substituted Dipyrromethanes from Vinylogous Aromatic Heterocycles and Their Utilization to the Synthesis of *meso*-Functionalized Porphyrins" *Bull. Korean Chem. Soc*., 25, **2004**, 1545.

Hong, S. -J.; Yoo, J.; Kim, S. -H.; Kim, J. S.; Yoon, J.; Lee, C. -H. "β-Vinyl substituted calix[4]pyrrole as a selective ratiometric sensor for cyanide anion" *Chem. Commun.*, **2009**, 189.

Hong, Y.; Lam, J. W. Y.; Tang, B. Z. "Aggregation-Induced Emission: Phenomenon, Mechanism and Applications" *Chem. Commun.*, **2009**, 4332.

Hung, C. -H.; Chang, G. -F.; Kumar, A.; Lin, G. -F.; Luo, L. -Y.; Ching, W. -M.; Diau, E. W. -G. "*m*- Benziporphodimethene: a new porphyrin analogue fluorescence zinc(II) sensor" *Chem. Commun.*, **2008**, 978.

Inhoffen, H. H.; Buchler, J. W.; Jager. P. "Chemistry of chlorine and porphyrins [Chemie der Chlorine und Porphyrine]" *Fortschr. Chem. Org. Natur*., 26, **1968**, 284.

Jackson, A. H.; Kenner, G. W.; Warburton, D. "Pyrroles and related compounds, Part V, Syntheses of some pyrromethanes, tripyrranes and porphyrins" *J. Chem. Soc.*, **1965**, 1328.

Jakubiak, R.; Collison, C. J.; Wan, W. C.; Rothberg, L. J.; Hsieh, B. R. "Aggregation Quenching of Luminescence in Electroluminescent Conjugated Polymers" *J. Phys. Chem. A*, 103, **1999**, 2394.

Jasat, A.; Dolphin, D. "Expanded Porphyrins and Their Heterologs" *Chem. Rev*., 97, **1997**, 2267.

Jenekhe, S. A.; Osaheni, J. A. "Excimers and Exciplexes of Conjugated Polymers" *Science*, 265, **1994**, 765.

Jia, Y.; Li, J. "Molecular Assembly of Schiff Base Interactions: Construction and Application" *Chem. Rev.*, 115, **2015**, 1597.

Josefsen, L. B.; Boyle, R. W. "Photodynamic Therapy and the Development of Metal-Based Photosensitisers" *Metal-Based Drugs*, **2008**, 1.

Kadish, K. M.; Smith, K. M.; Guilard, R. In The Porphyrin Handbook, Vol. 6, Chapter 42, Academic Press: San Diego, **1999**.

Kang, S. O.; Begum, R. A.; Bowman-James, K. "Amide-Based Ligands for Anion Coordination" *Angew. Chem. Int. Ed*., 45, **2006**, 7882.

Katayev, E. A.; Severin, K.; Scopelliti, R.; Ustynyuk, Y. A. "Dioxygen Activation by Diiminodipyrromethane Complexes of Ni, Pd, and Pt" *Inorg. Chem.*, 46, **2007**, 5465.

Katayev, E. A.; Boev, N. V.; Khrustalev, V. N.; Ustynyuk, Y. A.; Tananaev, I. G.; Sessler, J. L. "Bipyrrole- and Dipyrromethane-Based Amido-imine Hybrid Macrocycles. New Receptors for Oxoanions" *J. Org. Chem.*, 72, **2007**, 2886.

Kim, S. H.; Hong, S. J.; Yoo, J.; Kim, S. K.; Sessler, J. L.; Lee, C. H. "Strapped Calix[4] pyrroles Bearing a 1,3-Indanedione at α - Pyrrolic Position: Chemodosimeters for the Cyanide Anion" *Org. Lett.*, 11, **2009**, 3626.

Kimura, E.; Koike, T. "Recent development of zinc - fluorophores" *Chem. Soc. Rev.*, 27, **1998**, 179.

Koshevoy, I. O.; Lin, C. L.; Karttunen, A. J.; Janis, J.; Haukka, M.; Tunik, S. P.; Chou, P. T.; Pakkanen, T. A. "Highly Luminescent Octanuclear Au^{I}–Cu^{I} Clusters Adopting

Two Structural Motifs: The Effect of Aliphatic Alkynyl Ligands" *Chem. Eur. J.*, 17, **2011**, 11456.

Král, V.; Sessler, J. L.; Zimmerman, R. S.; Seidel, D.; Lynch, V.; Andrioletti, B. "Calixphyrins: Novel Macrocycles at the Intersection between Porphyrins and Calixpyrroles" *Angew. Chem. Int. Ed*., 39, **2000**, 1055.

Krautler, B. "The Porphinoids - Versatile Biological Catalyst Molecules" *Chimia*, 41, **1987**, 277.

Krattinger, B.; Callot, H. J. "New routes from porphyrins to stable phlorins. *Meso*-alkylation and reduction of *meso*-tetraphenyl- and octaalkylporphyrins" *Tetrahedron Lett*., 37, **1996**, 7699.

Krattinger, B.; Callot, H. J. "Addition of sterically hindered organolithium compounds to *meso*-tetraphenylporphyrin" *Tetrahedron Lett*., 39, **1998**, 1165.

Kumar, S.; Dhar, D. N.; Saxeena, P.N. "Applications of metal complexes of Schiff bases - A review" *Journal of Scientific and Industrial Research.*, 68, **2009**, 181.

Lakowicz, J. R. (ed.), *Probe Design and Chemical Sensing, Topics in Fluorescence Spectroscopy*, Vol. 4, Plenum, New York, **1994**.

Langa, K.; Mosinger, J.; Wagnerova, D. M. "Photophysical properties of porphyrinoid sensitizers non-covalently bound to host molecules; models for photodynamic therapy" *Coord. Chem. Rev.*, 248, **2004**, 321.

Lee, C.-H.; Lindsey, J. S. "One-flask synthesis of *meso*-substituted dipyrromethanes and their application in the synthesis of *trans*-substituted porphyrin building blocks" *Tetrahedron*, 50, **1994**, 11427.

Lee, C. -H.; Miyaji, H.; Yoon, D. -W.; Sessler, J. L. "Strapped and other topographically nonplanar calixpyrrole analogues. Improved anion receptors" *Chem. Commun*., **2008**, 24.

Lee, C. -H.; Yoon, H. -J.; Shin, J. -S.; Jang, W. -D. "A Boradiazaindacene - Based Turn-On Fluorescent Probe for Cyanide Detection in Aqueous Media" *Chem. Eur. J.*, 18, **2012**, 4513.

Lee, D. A.; Smith, K. M. "Syntheses of symmetrically substituted 5-alkyl- and 5-aryl-dihydrodipyrrins and of porphyrins and bisporphyrins therefrom" *J. Chem. Soc., Perkin Trans.*, 1, **1997**, 1215.

Li, L. L.; Yang, C. J.; Chen, W. H.; Lin, K. J. "Towards the Development of Electrical Conduction and Lithium - Ion Transport in a Tetragonal Porphyrin Wire" *Angew. Chem. Int. Ed.*, 42, **2003**, *1505.*

Li, L. L.; Diau, E. W. G. "Porphyrin-sensitized solar cells" *Chem. Soc. Rev*., 42, **2013**, 291.

Lippard, S. J.; Berg, J. M. *Principles of Bioinorganic Chemistry*., University Science Books, Mill Valley, California, USA, **1994**, 139

Liu, W. X.; Jiang, Y. B. "Intramolecular Hydrogen Bonding and Anion Binding of *N*-Benzamido-*N*'-benzoylthioureas" *J. Org. Chem*., 73, **2008**, 1124.

Li, Y.; Dolphin, D. "Far-red absorbing azodipyrrin dyes-Synthesis, X-ray crystallographic, and spectral characterization of 1,9-diazodipyrrins and their metal complexes" *Can. J. Chem*., 89, **2011**, 481.

Luo, J.; Xie, Z.; Lam, J. W.; Cheng, L.; Chen, H.; Qiu, C.; Kwok, H. S.; Zhan, X.; Liu, Y.; Zhu, D.; Tang, B. Z. "Aggregation-Induced Emission of 1-Methyl-1,2,3,4,5-Pentaphenylsilole" *Chem. Commun.*, **2001**, 1740.

Lv, X.; Liu, J.; Liu, Y.; Zhao, Y.; Sun,Y. Q.; Wang, P.; Guo, W. "Ratiometric fluorescence detection of cyanide based on a hybrid coumarin-hemicyanine dye: the large emission shift and the high selectivity" *Chem. Commun.*, 47, **2011**, 12843.

Ma, J.; Dasgupta, P. K. "Recent developments in cyanide detection: A review" *Anal. Chim. Acta.*, 673, **2010**, 117.

Matano, Y.; Imahori, H. "Phosphole-Containing Calixpyrroles, Calixphyrins, and Porphyrins: Synthesis and Coordination Chemistry" *Acc. Chem. Res.*, 42, **2009**, 1193.

Matsumoto, T.; Urano, Y.; Shoda, T.; Kojima, H.; Nagano, T. "A Thiol-Reactive Fluorescence Probe Based on Donor-Excited Photoinduced Electron Transfer: Key Role of Ortho Substitution" *Org. Lett*., 9, **2007**, 3375.

Mauzerall, D.; Granick, S. "Porphyrin biosynthesis in erythrocytes: iii uroporphyrinogen and its decarboxylase" *J. Biol. Chem.*, 232, **1958**, 1141.

Mauzerall, D. "The photoreduction of porphyrins and the oxidation of amines by photo-excited dyes" *J. Am. Chem. Soc*., 82, **1960**, 1832.

Mei, J.; Hong, Y.; Lam, J. W. Y.; Qin, A.; Tang, Y.; Tang, B. Z. "Aggregation-Induced Emission: The Whole Is More Brilliant than the Parts" *Adv. Mater.*, 26, **2014**, 5429.

Mendes, A. C.; Baran, E. T.; Reis, R. L.; Azevedo, H. S. "Self-assembly in nature: using the principles of nature to create complex nanobiomaterials" *WIREs Nanomed. Nanobiotechnol.*, 5, **2013**, 582.

Müller-Dethlefs, K.; Hobza, P. "Noncovalent Interactions: A Challenge for Experiment and Theory" *Chem. Rev.*, 100, **2000**,143.

Murat-Onana, M. L.; Berini, C.; Minassian, F.; Pelloux-Léon, L.; Denis, J. -N. "An efficient method for the synthesis of unsymmetrical 2,2’-bis(pyrrolyl)alkanes" *Org. Biomol. Chem.*, 8, **2010**, 2204.

Nagarkatti, J. P.; Ashley, K. R. "Synthesis of Pyridyl *meso*-Substituted Dipyrrylmethanes" *Synthesis*, 3, **1974**, 186.

Nayar, P.; Brun, A. M.; Harriman, A.; Begley, T. P. "Mechanistic studies on proto chlorophyllide reductase: a model system for the enzymatic reaction" *J. Chem. Soc. Chem. Commun*., **1992**, 395.

Ni, J.; Zhang, X.; Qiu, N.; Wu, Y. H.; Zhang, L. Y.; Zhang, J.; Chen, Z. N. "Mechanochromic Luminescence Switch of Platinum(II) Complexes with 5-Trimethylsilyl ethynyl-2,20-bipyridine" *Inorg. Chem.*, 50, **2011**, 9090.

Onis, M. De.; Frongillo, E. A.; Blössner, M. "Is malnutrition declining? An analysis of changes in levels of child malnutrition since 1980" *Bull. W. H. O.*, 78, **2000**, 1222.

Orlewska, C.; Maes, W.; Toppet, S.; Dehaen, W. "5,5-Dialkyldipyrromethane as a precursor for the synthesis of calix[4]phyrins and pseudocorroles using MacDonald [2+2] condensations" *Tetrahedron Lett*., 46, **2005**, 6067.

Palomares, E.; Martínez-Díaz, M. V.; Torres, T.; Coronado, E. "A Highly Sensitive Hybrid Colorimetric and Fluorometric Molecular Probe for Cyanide Sensing Based on a Subphthalocyanine Dye" *Adv. Funct. Mater*., 16, **2006**, 1166.

Pandey, R. K. "Recent advances in photodynamic therapy" *J. Porphyrins Phthalocyanines*, 4, **2000,** 368.

Polo, L.; Segalla, A.; Bertoloni, G.; Jori, G.; Schaffner, K.; Reddi, E. "Polylysine–porphycene conjugates as efficient photosensitizers for the inactivation of microbial pathogens" *J. Photochem. Photobiol. B: Biology*., 59, **2000**, 152.

Ptaszek, M.; McDowell, B. E.; Lindsey, J. S. "Synthesis of 1-Formyldipyrromethanes" *J. Org. Chem*., 71, **2006**, 432.

Qin, W.; Long, S.; Panunzio, M.; Biondi, S. "Schiff Bases: A Short Survey on an Evergreen Chemistry Tool" *Molecules*, 18, **2013**, 12264.

Que, E. L.; Domaile, D. W.; Chang, C. J. "Metals in Neurobiology: Probing Their Chemistry and Biology with Molecular Imaging" *Chem. Rev.*, 108, **2008**, 1517.

Rambo, B. M.; Sessler J. L. "Oligopyrrole Macrocycles: Receptors and Chemosensors for Potentially Hazardous Materials" *Chem. Eur. J.*, 17, **2011**, 4946.

Rao, P. D.; Littler, B. J.; Geier III, G. R.; Lindsey, J. S. "Efficient Synthesis Of Monoacyl Dipyrromethanes and Their Use in the Preparation of Sterically Unhindered *trans*-Porphyrins" *J. Org. Chem*., 65, **2000**, 1084.

Rubio, N.; Prat, F.; Bou, N.; Borrell, J. I.; Teixidó, J.; Villanueva, A.; Juarranz, A.; Cañete, M.; Stockert, J. C.; Nonell, S. "A comparison between the photophysical and photosensitising properties of tetraphenyl porphycenes and porphyrins" *New J. Chem*., 29, **2005**, 378.

Sagara, Y.; Kato, T. "Mechanically induced luminescence changes in molecular assemblies" *Nature Chem.*, 1, **2009**, 605.

Salini, P. S.; Thomas, A. P.; Sabarinathan, R.; Ramakrishnan, S.; Sreedevi, K. C. G.; Reddy, M. L. P.; Srinivasan, A. "Calix[2]-m-benzo[4]phyrin with Aggregation-Induced Enhanced-Emission Characteristics: Application as a Hg^{II} Chemosensor" *Chem. Eur. J.*, 17, **2011**, 6598.

Salini, P. S.; Holaday, M. G. D.; Reddy, M. L. P.; Suresh C. H.; Srinivasan, A. "Fluorine interaction controlled AIEE phenomenon in an expanded calixbenzophyrin and its vapoluminescent response: turn on emission with volatile ketones and esters" *Chem. Commun.*, 49, **2013**, 2213.

Schmuck, C. "Side chain selective binding of N-acetyl-α-amino acid carboxylates by a 2-(guanidiniocarbonyl)pyrrole receptor in aqueous solvents" *Chem. Commun*., **1999**, 843.

Senge, M. O.; Runge, S.; Speck, M.; Ruhlandt-Senge, K. "Identification of Stable Porphomethenes and Porphodimethenes from the Reaction of Sterically Hindered Aldehydes with Pyrrole" *Tetrahedron*, 56, **2000**, 8927.

Sessler, J. L.; Cyr, M. J.; Lynch, V.; McGhee, E.; Ibers, J. A. "Synthetic and structural studies of sapphyrin, a 22-π-electron pentapyrrolic expanded porphyrin" *J. Am. Chem. Soc*., 112, **1990**, 2810.

Sessler, J. L.; Zimmerman, R. S.; Bucher, C.; Kŕal, V.; Andrioletti, B. "Calixphyrins: Hybrid macrocycles at the structural crossroads between porphyrins and calixpyrroles" *Pure. Appl. Chem.*, 73, **2001**, 1041.

Sessler, J. L.; Camiolo, S.; Gale, P. A. "Pyrrolic and polypyrrolic anion binding agents" *Coord. Chem. Rev*., 240, **2003**, 17.

Sessler, J. L.; Gale, P. A.; Cho, W. -S. "Anion Receptor Chemistry" *Monographs in supramolecular chemistry,* Royal Society of Chemistry, London, **2006**.

Sharada, D. S.; Muresan, A. Z.; Muthukumaran K.; Lindsey, J. S. "Direct Synthesis of Palladium Porphyrins from Acyldipyrromethanes" *J. Org. Chem.*, 70, **2005**, 3500.

Shinohara, H.; Honda, K.; Misaki, S.; Imoto, E. "Pyrrole Series. II. The Syntheses of *meso* (*p*-Substituted phenyl) dipyrrylmethenes and Their Copper Complexes" *Nippon Kagaku Zasshi*., 81, **1960**, 1740.

Shi, Y.; Hall, C.; Ciszewski, J. T.; Cao, C.; Odom, A. L. "Titanium dipyrrolylmethane derivatives: rapid intermolecular alkyne hydroamination" *Chem. Commun.*, **2003**, 586.

Siji, V. L.; Sudarsanakumar, M. R.; Suma, S. "Synthesis, Spectroscopic Characterization, and Antimicrobial Activity of Cobalt (II) Complexes of Acetone-*N*(4) Phenyl semicarbazone: Crystal Structure of $[Co(HL)_2(MeOH)_2](NO_3)_2$" *Transition Metal Chemistry*., 36, **2011**, 417.

Silva, A. P. De.; Gunaratne, H. Q. N.; Gunnlaugsson, T.; Huxley, A. J. M.; McCoy, C. P.; Rademacher, J. T.; Rice, T. E. "Signaling Recognition Events with Fluorescent Sensors and Switches" *Chem. Rev.*, 97, **1997**, 1515.

Sreedevi, K. C. G.; Thomas, A. P.; Salini, P. S.; Ramakrishnan, S.; Anju, K. S.; Holaday, D. M. G.; Reddy, M. L. P.; Suresh, C. H.; Srinivasan, A. "5,5-Diaryldipyrromethanes: syntheses and anion binding properties" *Tetrahedron Lett*., 52, **2011**, 5995.

Sreedevi, K. C. G.; Thomas, A. P.; Aparna, K. H.; Pradhan, R.; Reddy, M. L. P.; Lourderaj U.; Srinivasan, A. "Photoenolization via excited state double proton transfer induces ‘‘turn on’’ fluorescence in diformyl diaryl dipyrromethane" *Chem. Commun.*, 50, **2014**, 8667.

Steed, J. W.; Atwood, J. L. *Supramolecular Chemistry 2nd edition*. John Wiley & Sons, **2009**.

Stępień, M.; Latos-Grażyński, L.; Szterenberg, L.; Panek, J.; Latajka, Z. "Cadmium(II) and Nickel(II) Complexes of Benziporphyrins. A Study of Weak Intramolecular Metal−Arene Interactions" *J. Am. Chem. Soc*., 126, **2004**, 4566.

Sternberg, E. D.; Dolphin, D.; Bruckner, C. "Porphyrin-based photosensitizers for use in photodynamic therapy" *Tetrahedron*, 54, **1998**, 4151.

Takeda, N.; Inoue, S. "Polymerization of 1, 2- Epoxy propane and co-polymerization with carbon dioxide catalyzed by metallo porphyrins" *Makromol. Chem.*, 179, **1978**, 1377.

Tamaru, S. -i.; Yu, L.; Youngblood, W. J.; Muthukumaran, K.; Taniguchi, M.; Lindsey, J. S. "A Tin-Complexation Strategy for Use with Diverse Acylation Methods in the Preparation of 1,9-Diacyldipyrromethanes" *J. Org. Chem*., 69, **2004**, 765.

Tanaka, T.; Osuka, A. "Conjugated porphyrin arrays: synthesis, properties and applications for functional materials" *Chem. Soc. Rev*., 44, **2015**, 943.

Thiagarajan, V.; Ramamurthy, P. "Specific optical signalling of anions via intramolecular charge transfer pathway based on acridinedione fluorophore" *J. Lumin*., 126, **2007**, 886.

Thomas, S. W.; Joly, G. D.; Swager, T. M. "Chemical Sensors Based on Amplifying Fluorescent Conjugated Polymers" *Chem. Rev.*, 107, **2007**, 1339.

Tsuchimoto, T.; Hatanaka, K.; Shirakawa, E.; Kawakami, Y. "Indium triflate-catalysed double addition of heterocyclic arenes to alkynes." *Chem. Commun*., **2003**, 2454.

Turner, B.; Botoshansky, M; Eichen, Y. "Extended Calixpyrroles: *meso*-Substituted Calix[6]pyrroles" *Angew. Chem. Int. Ed*., 37, **1998**, 2475.

Veauthier, J. M.; Tomat, E.; Lynch, V. M.; Sessler, J. L.; Mirsaidov, J.; Markert, J. T. "Calix[4]pyrrole Schiff Base Macrocycles: Novel Binucleating Ligands for Cu(I) and Cu(II)" *Inorg. Chem.*, 44, **2005**, 6736.

Varughese, S. "Non-covalent routes to tune the optical properties of molecular materials" *J. Mater. Chem. C*, 2, **2014**, 3499.

Vennesland, B.; Comm, E. E.; Knownles, C. J.; Westly, J.; Wissing, F.; ed. "Cyanide in biology", *Academic Press*, London, **1981**.

Wagner, R. W.; Johnson, T. E.; Lindsey, J. S. "Soluble Synthetic Multiporphyrin Arrays. 1. Modular Design and Synthesis" *J. Am. Chem. Soc*., 118, **1996**, 11166.

Wagner, R. W.; Lindsey, J. S. "A molecular photonic wire" *J. Am. Chem. Soc*. 116, **1994**, 9759.

Wang, Q. M.; Bruce, D.W. "One-Step Synthesis of β, *meso*-Unsubstituted Dipyrromethane" *Synlett*., 12, **1995**, 1267.

Wang, Y.; Li, M.; Zhang, Y.; Yang, J.; Zhu, S.; Sheng, L.; Wang, X.; Yanga, B.; Zhang S. X. A. "Stress acidulated amphoteric molecules and mechanochromism via reversible intermolecular proton transfer" *Chem. Commun.*, 49, **2013**, 6587.

Wood, T. E.; Thompson, A. "Advances in the Chemistry of Dipyrrins and Their Complexes" *Chem. Rev*., 107, **2007**, 1831.

Woodward, R. B. "Total synthese des Chlorophylls" *Angew. Chem.*, 72, **1960**, 651.

Xu, Z.; Chen, X.; Kim, H. N.; Yoon, J. "Sensors for the optical detection of cyanide ion" *Chem. Soc. Rev.*, 39, **2010**, 127.

Xu, Z.; Yoon, J.; David R. S. "Fluorescent chemosensors for Zn^{2+}" *Chem. Soc. Rev.*, 39, **2010**, 1996.

Yadav, J. S.; Reddy, B. V. S.; Reddy, P. S. R.; Reddy, K. S.; Reddy, P. N. "A Novel Approach for the Synthesis of Dipyrrolyl Alkanols and Dipyrrolyl Alkylamines" *Synlett*., 3, **2003**, 417.

Yadav, M.; Singh, A. K.; Pandey, D. S. "First Examples of Heteroleptic Dipyrrin / *η5* Pentamethylcyclopentadienyl Rhodium / Iridium (III) Complexes and Their Catalytic Activity" *Organometallics*., 28, **2009**, 4713.

Yang, J. -S.; Yan, J. -L. "Central-ring functionalization and application of the rigid, aromatic, and H-shaped pentiptycene scaffold" *Chem. Commun*., **2008**, 1501.

Yang, L.; Li, X.; Yang, J.; Qu, Y.; Hua, J. "Colorimetric and Ratiometric Near-Infrared Fluorescent Cyanide Chemodosimeter Based on Phenazine Derivatives" *Appl. Mater. Interfaces* 5, **2013**, 1317.

Yang, L. -Y.; Chen, Q. -Q.; Yanga, G. -Q.; Ma, J. -S. "Self-assembly of bis(pyrrol-2-yl-methyleneamine)s bridged by flexible linear carbon chains" *Tetrahedron*, 59, **2003**, 10037.

Yang, Y.; Zhao, Q.; Feng, W.; Li, F. "Luminescent Chemodosimeters for Bioimaging" *Chem. Rev.*, 113, **2013**, 192.

Yin, Z.; Wang, W.; Guo, J.; Wang, J.; He, J.; Cheng, J. -P. "Quadruple hydrogen bonded self-assemblies of 5,5′-bisdiazo-dipyrromethane" *Chem. Commun*., **2008**, 957.

Young, C.; Tidwell, L.; Anderson, C.; Cyanide: Social, Industrial, and Economic Aspects, Minerals, Metals, and Materials Society, Warrendale, **2001**.

Zeng, L.; Miller, E. W.; Pralle, A.; Isacoff, E. Y.; Chang, C. J. "A Selective Turn-On Fluorescent Sensor for Imaging Copper in Living Cells" *J. Am. Chem. Soc*., 128, **2006**, 10.

Zoubi, W. A. "Biological Activities of Schiff Bases and Their Complexes: A Review of Recent Works" *Int. J. Org. Chem*, 3, **2013**, 73.